THE ELECTRICAL CONDUCTIVITY OF DOPED THORIA

IN THE TEMPERATURE RANGE

$500^{\circ} - 1450^{\circ}$ CENTIGRADE

by

Charles E. McGinley, B.Sc.

A Thesis submitted for the Degree of Doctor of Philosophy in the Faculty of Engineering of the University of Glasgow.

Engineering Laboratories
University of Glasgow
Glasgow, W.2.

October, 1968.

ProQuest LLC.
789 East Eisenhower Parkway
P.O. Box 1346
Ann Arbor, MI 48106 – 1346

ACKNOWLEDGEMENTS

The author wishes to thank Professor J.D. Robson, and his predecessor Professor G.D.S. MacLellan, for the provision of laboratory facilities, and the Science Research Council for financial support for part (28 months) of the duration of the research.

He would also like to thank Dr. P. Hancock, other members of the staff, and colleagues, of the Faculty of Engineering for encouragement and discussion.

Grateful acknowledgement is made of several helpful discussions with Dr. B.C.H. Steele of the Metallurgy Department, Imperial College, London, and Dr. C. Weaver of the Natural Philosophy Department, University of Strathclyde, Glasgow.

CONTENTS

CHAPTER PAGE

CHAPTER PAGE

CHAPTER 1

GENERAL INTRODUCTION

GENERAL INTRODUCTION

In recent years a great deal of interest has been aroused in the electrical conductivity of solid oxides at high temperatures. One of the main reasons is that it is believed high temperature fuel cells with solid oxygen ion conducting electrolytes of the type 0.85 ZrO_2-0.15 CaO* (1) may be economically worth developing. The possibility of fuel cell applications has stimulated the Westinghouse Electric Corporation, in particular, to carry out a great deal of research on the electrical properties of oxides possessing considerable oxygen ion conductivity.

Another possible commercial application is in magnetohydrodynamic (M.H.D.) power generation. Oxides may be used as insulators, and even electrodes, in M.H.D. generators at temperatures up to 2000°C (2). However, little work seems to have been done so far on the electrical conductivity side, as the more serious problems of corrosion, erosion and thermal shock have not yet been overcome.

The metallurgical applications of a knowledge of the electrical properties are also very important. From electromotive force measurements on high temperature galvanic cells (3) of the type A, A(O)/oxide electrolyte/B, B(O) where A(O) and B(O) are oxides of metals A and B, it is possible to calculate the free energy of formation of one of the metal oxides, say B(O), provided the free energy of formation of A(O) is known and the ionic transport number in the oxide electrolyte is unity. A small electronic contribution to the conductivity of the electrolyte may lead to erroneous results due to polarization of the electrodes. So it is important to ensure that the electronic transport number is close to zero for the conditions of temperature and oxygen partial pressure under which the thermodynamic studies are being carried out.

* cf. Page 3

Probably the most important metallurgical application of electrical conductivity studies is in the field of metallic corrosion. According to Wagner's theory (4,5) of high temperature parabolic oxidation the rate of growth of a compact protective oxide scale on a metal surface is determined by the rates of transport of cations, anions and electrons through this scale. The transport rates of the carriers are of course directly related to their partial conductivities. It follows that a knowledge of these partial conductivities will help greatly in elucidating the oxidation mechanism.

Other rate processes, as well as oxidation, are determined by ion mobilities and hence conductivities. Examples of these are sintering, solid state reactions and creep deformation.

From what has been said above it is clear that the study of the transport properties of oxides is of great commercial interest. The more detailed the knowledge we have of conductivity in oxides the greater will be our understanding of the many related properties and processes, such as those mentioned. For this reason and also for the intrinsic scientific interest involved the ultimate aim of electrical conductivity studies is not simply to tabulate electronic and ionic conductivity values but also to determine completely the mechanism by which the charges are transported i.e. we want to understand perfectly, on the atomic level, the behaviour of solid oxides in an applied electric field.

Much previous work on the conductivity of oxides has dealt with those in which the conductivity is predominantly electronic. The present research however is concerned with oxides possessing either mixed (electronic and ionic) or ionic conductivity. Since most of the previous research on this type of conductor has involved compounds other than oxides, for example, sulphides and alkali halides, in the next chapter the theory of the electrical conductivity of ionic solids in general,

rather than oxides in particular, will be reviewed. After this, the particular system chosen for the present investigation will be considered, the equipment used and experiments carried out will be described, the results obtained presented and their significance discussed.

* The numbers in a formula like $0.85ZrO_2$–0.15CaO give the mole fractions of the constituent oxides.

CHAPTER 2

REVIEW OF THE THEORY OF THE ELECTRICAL CONDUCTIVITY OF IONIC SOLIDS

2.1. Introduction

The electrical conductivity of most ionic solids is mixed i.e. partly electronic and partly ionic. However, usually one type of conductivity predominates and materials exhibiting pronounced mixed conduction are comparatively rare. Pohl, Stasiw, Smakula, Hilsch, Mollwo and their associates (6) have shown that, although stoichiometric alkali halides are ionic conductors, when an excess of metal or halogen is present appreciable electronic conduction also occurs. Other well known examples of mixed conductors are silver sulphide, cuprous sulphide and the cuprous halides. In these compounds, too, the ratio of electronic to ionic conductivity depends markedly on small deviations from stoichiometry (7). The simultaneous migration of both electrons and ions is necessary for the corrosion of metals exposed to oxygen, sulphur or halogens at high temperatures (4).

The conductivity of a mixed conductor can be expressed as the sum of the partial conductivities due to each mobile carrier i.e. the total conductivity σ is given by

$$\sigma = \sum_i \sigma_i$$

where σ_i is the partial conductivity due to charge carrier i which may be an electron, an electron hole or an ionic defect. σ_i in turn may be decomposed and expressed as

$$\sigma_i = n_i q_i \mu_i$$

where n_i, q_i and μ_i are the concentration, charge and mobility of charge carrier i. Thus the total conductivity is

$$\sigma = \sum_i n_i q_i \mu_i \qquad \ldots\ldots\ldots\ldots\ldots\ldots (1)$$

Ionic conductivity is caused by the movement of ion vacancies or interstitials. These may be present because of thermal effects (Schottky or Frenkel defects), non-stoichiometry, or doping with another ionic material one of whose ions has a

different valency from the corresponding ion in the host material. There may of course be a combination of these effects.

Electronic conductivity may be due either to electrons (n–type) or electron holes (p–type). Two models are used to describe electronic conductivity, the band model and , less frequently, the hopping electron model. On the band model n–type conductivity exists when there are free electrons in the conduction band, produced by thermal excitation from either the valence band (intrinsic) or from impurities or lattice defects with filled energy levels in the band gap (extrinsic). p–type conductivity is caused by the loss of electrons from the valence band to either the conduction band (intrinsic) or to impurities or lattice defects with empty energy levels in the band gap (extrinsic), leaving a mobile electron hole in the valence band. This model is applicable in cases where the electron mobility is high (30 to 10^4 cm^2 sec^{-1} V^{-1} at room temperature) and decreases with increasing temperature as the various scattering processes become more effective.

However, there are cases when the electron mobility is much lower ($\sim 10^{-2}$ cm^2 sec^{-1} V^{-1} or lower at room temperature) and increases exponentially with temperature. Under these conditions it no longer seems reasonable to consider the electrons and holes as moving freely in bands and instead they are described as jumping between neighbouring ions existing in different valence states. This is the hopping electron model (8).

In this chapter the variation of the electrical conductivity of an ionic solid with surrounding atmosphere, addition of aliovalent cations, temperature and measuring frequency will be discussed. Since the partial conductivity due to carrier i depends on both its concentration and mobility the variation of both these quantities must be considered. Electron energies

will be treated in terms of the band model.

The law of mass action is usually used to discuss electronic and ionic defect equilibria in ionic crystals. The defects are considered as solutes in the solid as a solvent. This approach is valid provided the defect concentrations are sufficiently small. This is usually true for intrinsic ionic defects and those produced by non-stoichiometry or a small concentration of impurity ($\leqslant$ a few mole $^{o}/o$). Any interactions of the defects are allowed for by the use of a constant activity coefficient, in accordance with Henry's law. For very large concentrations of electrons and holes Fermi-Dirac statistics may have to be used instead of Maxwell-Boltzmann statistics, and the law of mass action is no longer applicable.

We will assume in the examples to be considered that the law of mass action always holds and apply it in the following treatment as did Kroger and Vink (9).

Notation used to describe defects

In order to describe defects in solids we must adopt a system of notation. We will use that of Kroger and Vink (9). If MX is an ionic compound of metal M and non-metal X, the point defects are written

V_X	anion vacancy
V_M	cation vacancy
X_i	anion interstitial
M_i	cation interstitial
e^-	electron in conduction band
e^+	electron hole in valence band

Atoms on normal lattice positions are written M_M and X_X. A foreign atom F on a normal anion or cation site or in an interstitial position is written F_X, F_M and F_i respectively. A positive charge is represented by a superscript + and a

negative charge by a superscript $-$, these being charges relative to the perfect crystal. When no superscript is present the defect or foreign atom is considered to be neutral.

2.2. The effect of change of atmosphere on the conductivity of an undoped ionic solid

We will consider the case of the ionic solid MX in which M is a divalent metal and X a divalent non-metal which exists in the gaseous state as molecules X_2. Variation of the partial pressure p_{X_2} of the gas $X_2(g)$ in contact with MX will alter the extent of the non-stoichiometry of MX and so alter the concentrations of ionic defects. In order to preserve electrical neutrality complementary electronic defects will be created simultaneously.

If MX is non-stoichiometric with a deficit of X the reaction describing the interaction of MX with the gas $X_2(g)$ in the surrounding atmosphere may be written

$$MX = MX_{1-\delta} + \frac{\delta}{2} X_2(g) \quad \ldots\ldots\ldots\ldots\ldots\ldots\ldots\ldots (2)$$

From this equation it can be seen that decreasing the pressure p_{X_2} of $X_2(g)$ will increase the non-stoichiometry. On the other hand if MX is non-stoichiometric with an excess of X, decreasing p_{X_2} will decrease the non-stoichiometry.

As an example we will consider the case in which the defects in stoichiometric MX are Frenkel defects in the anion lattice. We will try to predict how the concentrations of defects, and so conductivity, will vary with the pressure of $X_2(g)$.

The formation of uncharged Frenkel defects can be described by the equation

$$nil = V_X + X_i \quad \ldots\ldots\ldots\ldots\ldots\ldots\ldots\ldots (3)$$

where nil represents the perfect crystal. Application of the

law of mass action to this equation yields

$$[V_x][X_i] = K_f^{\,1} \quad \ldots\ldots\ldots\ldots\ldots\ldots\ldots\ldots\ldots (4)$$

Square brackets represent concentrations and K's are mass action constants.

The interactions of $X_2(g)$ with MX to alter the concentrations of anion vacancies and interstitials are described by :

$$X_x = \tfrac{1}{2} X_2(g) + V_x \,, \quad [V_x]\, p_{X_2}^{\frac{1}{2}} = K_1 \quad \ldots\ldots\ldots\ldots\ldots (5)$$

$$\tfrac{1}{2} X_2(g) = X_i \,, \quad [X_i]\, p_{X_2}^{-\frac{1}{2}} = K_2 \quad \ldots\ldots\ldots\ldots\ldots (6)$$

The defects may be ionized either singly or doubly. These reactions give the following relations:

$$V_x = V_x^{+} + e^{-} \,, \quad [V_x^{+}][e^{-}] = K_a[V_x] \ldots\ldots\ldots\ldots\ldots\ldots (7)$$

$$V_x^{+} = V_x^{++} + e^{-} \,, \quad [V_x^{++}][e^{-}] = K_b[V_x^{+}] \ldots\ldots\ldots\ldots\ldots (8)$$

$$X_i = X_i^{-} + e^{+} \,, \quad [X_i^{-}][e^{+}] = K_c[X_i] \ldots\ldots\ldots\ldots\ldots\ldots (9)$$

$$X_i^{-} = X_i^{=} + e^{+} \,, \quad [X_i^{=}][e^{+}] = K_d[X_i^{-}] \ldots\ldots\ldots\ldots\ldots\ldots (10)$$

As well as being produced by ionization of defects, electrons may arise from intrinsic thermal excitation:

$$\text{nil} = e^{+} + e^{-} \,, \quad [e^{+}][e^{-}] = K_e \quad \ldots\ldots\ldots\ldots\ldots\ldots (11)$$

Combination of equations (4) to (11) yields the relation between the concentrations of doubly charged vacancies and interstitials:

$$[V_x^{++}][X_i^{=}] = K_a K_1 K_2 K_b K_c K_d K_e^{-2} = K_f \quad \ldots\ldots\ldots\ldots\ldots\ldots (12)$$

A condition which must hold under all circumstances is the neutrality condition. For the above situation this is

$$2[X_i^{=}] + [X_i^{-}] + [e^{-}] = 2[V_x^{++}] + [V_x^{+}] + [e^{+}] \ldots\ldots\ldots\ldots\ldots (13)$$

From the above equations it is possible to discover the variation of conductivity with p_{X_2}. Two extreme conditions of MX will be considered, (a) far from, and (b) close to, stoichiometry.

(a) <u>Far from stoichiometry</u>

At sufficiently large deviations from stoichiometry the intrinsic electronic and ionic disorder may be neglected.

At very low values of p_{X_2} the predominant ionic defects

will be anion vacancies and charge neutrality will be maintained by electrons. Equations (5), (7) and (8) give, for this case

$$\left[V_x^{+}\right]\left[e^{-}\right] = K_1 K_a p_{X_2}^{-\frac{1}{2}} \quad \text{.....(14)}$$

and

$$\left[V_x^{++}\right]\left[e^{-}\right]^2 = K_1 K_a K_b p_{X_2}^{-\frac{1}{2}} = K_v p_{X_2}^{-\frac{1}{2}} \quad \text{.....(15)}$$

When none of the vacancies are doubly ionized, $\left[V_x^{++}\right] = 0$ and equation (13) is

$$\left[e^{-}\right] = \left[V_x^{+}\right] \quad \text{.....(16)}$$

When all are doubly ionized $\left[V_x^{+}\right] = 0$ and

$$\left[e^{-}\right] = 2\left[V_x^{++}\right] \quad \text{.....(17)}$$

Substitution of equations (16) and (17) into (14) and (15) respectively yields

$$\left[V_x^{+}\right] = \left[e^{-}\right] = (K_1 K_a)^{\frac{1}{2}} p_{X_2}^{-\frac{1}{4}} \quad \text{.....(18)}$$

and

$$\left[V_x^{++}\right] = \tfrac{1}{2}\left[e^{-}\right] = (K_v/4)^{\frac{1}{3}} p_{X_2}^{-\frac{1}{6}} \quad \text{.....(19)}$$

Thus in a compound MX with a large deviation from stoichiometry due to anion vacancies, the concentration of electrons and hence the electronic conductivity (assuming the mobility of the electrons is independent of their concentration) will have a dependence on p_{X_2} ranging from $p_{X_2}^{-\frac{1}{4}}$ to $p_{X_2}^{-\frac{1}{6}}$ as none of the vacancies, or all of them, are doubly ionized.

When non-stoichiometry is due to a large excess of anion interstitials, neutralized by electron holes, a similar consideration of equations (6), (9), (10) and (13) yields

$$\left[X_i^{-}\right] = \left[e^{+}\right] = (K_2 K_c)^{\frac{1}{2}} p_{X_2}^{\frac{1}{4}} \quad \text{.....(20)}$$

and

$$\left[X_i^{=}\right] = \tfrac{1}{2}\left[e^{+}\right] = (K_i/4)^{\frac{1}{3}} p_{X_2}^{\frac{1}{6}} \quad \text{.....(21)}$$

where $K_i = K_2 K_c K_d$

Thus when non-stoichiometry in MX is due to a high concentration of anion interstitials, the electronic conductivity (if the electron hole mobility is independent of concentration) will have a dependence on p_{X_2} ranging from $p_{X_2}^{\frac{1}{4}}$ to $p_{X_2}^{\frac{1}{6}}$ as none of the interstitials, or all of them, are doubly ionized.

(b) Close to stoichiometry

Near stoichiometry the defect concentrations are controlled by the intrinsic electronic and ionic equilibria. For simplicity we will consider the situation in which the vacancies and interstitials are all doubly ionized. There are two extreme cases.

(i) $K_f \ll K_e$

In this case, from equations (11) and (12)

$$[e^-] = [e^+] = K_e^{\frac{1}{2}} \gg [V_x^{++}] \quad \text{and} \quad [X_i^=]$$

The concentration of electronic defects is determined by the intrinsic electronic equilibrium and is independent of p_{X_2}. The concentrations of ionic defects can be found from equations (15) and (12):-

$$[V_x^{++}] = (K_v/K_e)p_{X_2}^{-\frac{1}{2}} \qquad \ldots\ldots\ldots\ldots\ldots\ldots\ldots\ldots(22)$$

$$[X_i^=] = (K_i/K_e)p_{X_2}^{\frac{1}{2}} \qquad \ldots\ldots\ldots\ldots\ldots\ldots\ldots\ldots(23)$$

This situation will arise only if the band gap for intrinsic electronic equilibrium is much less than the energy of formation of anionic Frenkel defects.

(ii) $K_f \gg K_e$

In this case from equations (11) and (12)

$$[V_x^{++}] = [X_i^=] = K_f^{\frac{1}{2}} \gg [e^-] \text{ and } [e^+].$$

The concentration of ionic defects is determined by the intrinsic ionic equilibrium and is independent of p_{X_2}. The concentrations of electronic defects are found from equations (15) and (11):-

$$[e^-] = (K_v^{\frac{1}{2}}/K_f^{\frac{1}{4}})p_{X_2}^{-\frac{1}{4}} \qquad \ldots\ldots\ldots\ldots\ldots\ldots\ldots\ldots(24)$$

$$[e^+] = (K_i^{\frac{1}{2}}/K_f^{\frac{1}{4}})p_{X_2}^{\frac{1}{4}} \qquad \ldots\ldots\ldots\ldots\ldots\ldots\ldots\ldots(25)$$

This situation arises when the band gap is much larger than the energy of formation of anionic Frenkel defects.

The variation of defect concentrations with p_{X_2} for these two cases is shown in Figs a and b. The diagrams include the behaviour far from stoichiometry when the ionic defects

are all doubly ionized.

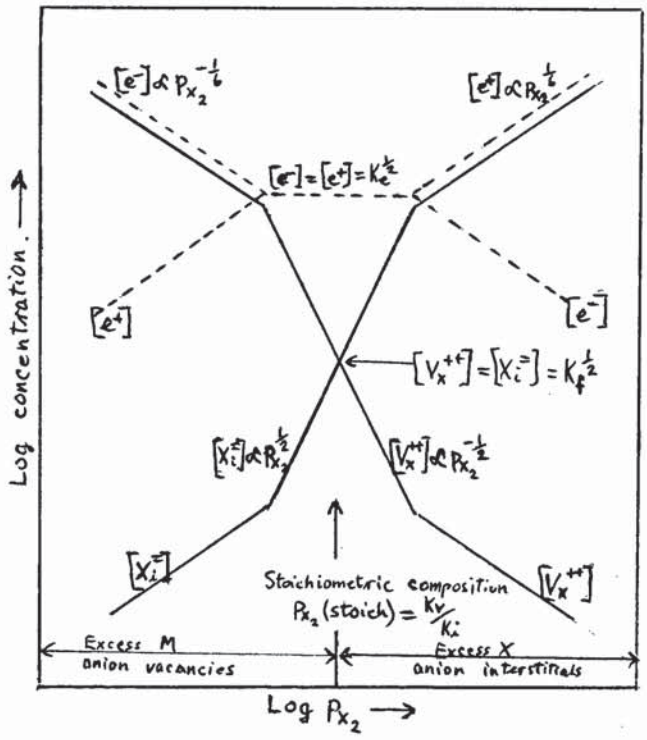

Case (i)

Fig a

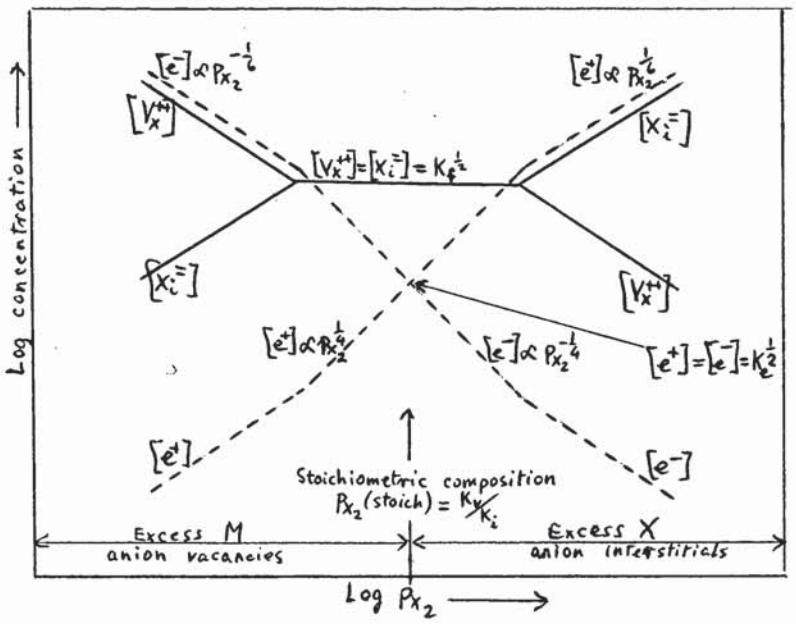

Case (ii)

Fig b

At the stoichiometric composition, $[V_x^{++}] = [X_i^{=}]$ and $[e^-] = [e^+]$. Hence it can be shown that the pressure of $X_2(g)$ at this composition is $p_{X_2}(stoich) = K_v/K_i$

When considering the variation of conductivity with the pressure of $X_2(g)$ it must be remembered that the mobility of electrons is much greater than that of ions.

So materials which behave as in case (i) will be predominantly electronic conductors at all values of p_{X_2} and the conductivity will vary with p_{X_2} in the same manner as the concentration of electrons or holes. Materials which behave as in case (ii) will have electronic conductivity at values of p_{X_2} much greater than, or much less than, $p_{X_2}(\text{stoich})$. This conductivity will vary with p_{X_2} in the same way as the concentration of electrons or holes and will be p-type at high p_{X_2} and n-type at low p_{X_2}. Close to stoichiometry the conductivity will be the sum of a p_{X_2}-independent ionic contribution and a p_{X_2}-dependent electronic contribution. The total conductivity may be almost completely ionic and then it will be independent of p_{X_2} over a range of values of p_{X_2} in the region of stoichiometry. If, however, the electronic conductivity is still appreciable at $p_{X_2}(\text{stoich})$ then no p_{X_2}-independent range of conductivity will be observed.

The variation of defect concentrations (and conductivity) with p_{X_2} for compound MX when the intrinsic ionic defects are of the cationic Frenkel or Schottky types can be treated in the same manner as was used above for anionic Frenkel defects.

2.3. The effect of doping on concentrations of defects and on conductivity

Doping of an ionic crystal is found to influence the defect concentrations and conductivity in various ways depending on the properties of the foreign atom and the particular state it assumes in the base crystal, the electronic and atomic imperfections present in the undoped base crystal (the native imperfections), the surrounding atmosphere, and the temperature.

A very general treatment of the effects of doping has been given by Kroger and Vink (9). They show that the equilibrium state of the crystal can be calculated by means of the law of mass action, as used earlier in this chapter, applied

to the following equations:

(1) all the equations which describe the electronic and ionic defects in the pure crystal, with the exception of the neutrality condition;

(2) equations describing the ionization of the foreign atoms;

(3) equations which describe the association of the foreign atoms with oppositely charged atomic defects;

(4) an equation which states that the total concentration of foreign atoms is the sum of the concentrations of the foreign atoms in all their various states, associated and unassociated, ionized and unionized;

(5) the complete neutrality condition, including the concentrations of the foreign atoms which are charged relative to the base lattice.

This set of equations is sufficient to calculate all the unknown concentrations.

We will deal with only a few simple cases. Let us consider a base crystal MX, composed of divalent cations and anions, in which the principal intrinsic atomic defects are doubly charged anionic Frenkel defects and in which the intrinsic electronic defect concentrations are negligibly small. We will also assume that association can be ignored, which is true at low dopant concentrations and high enough temperatures.

Consider adding the compound Me_2X to MX and suppose that the monovalent Me ions enter the crystal substitutionally on the normal cation sites, retaining their valency of one i.e. they exist in the crystal in the form Me_M^-. The neutrality condition is

$$[e^+] + 2[V_X^{++}] = [e^-] + [Me_M^-] + 2[X_i^=] \quad \ldots\ldots\ldots\ldots\ldots\ldots (26)$$

There are two extremes of behaviour, viz near stoichiometry and far from stoichiometry. (cf Page 11 case (ii))

Near stoichiometry

Near stoichiometry the concentrations of the electronic defects are negligible compared with those of the ionic defects and so the neutrality condition becomes

$$2\left[V_x^{++}\right] = \left[Me_M^{-}\right] + 2\left[X_i^{=}\right] \quad \ldots\ldots\ldots\ldots\ldots\ldots\ldots\ldots(27)$$

We know that

$$\left[V_x^{++}\right]\left[X_i^{=}\right] = K_f \quad \ldots\ldots\ldots\ldots\ldots\ldots\ldots\ldots\ldots\ldots(12)$$

Substituting equation (12) in equation (27) yields

$$2\left[V_x^{++}\right] = \frac{2K_f}{\left[V_x^{++}\right]} + \left[Me_M^{-}\right] \quad \ldots\ldots\ldots\ldots\ldots\ldots\ldots(28)$$

K_f increases exponentially with temperature and so there are two limiting conditions of equation (28) :

(i) At low temperatures

$$\frac{K_f}{\left[V_x^{++}\right]} \ll \left[Me_M^{-}\right]$$

and so $$\left[V_x^{++}\right] = \tfrac{1}{2}\left[Me_M^{-}\right] \quad \ldots\ldots\ldots\ldots\ldots\ldots\ldots(29)$$

Under these conditions the concentration of anion vacancies and the associated conductivity increase linearly with the amount of doping.

(ii) At high temperatures

$$\frac{K_f}{\left[V_x^{++}\right]} \gg \left[Me_M^{-}\right]$$

and so $$\left[V_x^{++}\right] = K_f^{\frac{1}{2}} = \left[X_i^{=}\right] \quad \ldots\ldots\ldots\ldots\ldots\ldots\ldots(30)$$

At high temperatures doping with Me_2X has no effect on the defect concentrations or on the conductivity.

The behaviour predicted above is shown (10) when $YO_{1.5}$ is added to stoichiometric ThO_2 (e.g. at 1000°C and p_{O_2} = 10^{-15}atm.) The conductivity, which is due almost solely to the oxygen vacancies increases linearly with $YO_{1.5}$ addition, at least for low concentrations of $YO_{1.5}$ (< 1 mole%) in agreement

with equation (29).

Similar treatments can be applied to the addition of aliovalent cations to a stoichiometric ionic compound in which the intrinsic defects are cationic Frenkel defects or Schottky defects. The results show that addition of a higher valent cation to a compound containing cationic Frenkel defects will lead to, at low temperatures, an increase in the concentration of cation vacancies. This behaviour has been observed for the addition of $CdBr_2$ to Ag Br (11)

For the addition of a higher valent cation to a compound containing Schottky defects we would expect the cation vacancy concentration to increase at low temperatures and to remain unchanged at high temperatures. This has been observed for KCl doped with $SrCl_2$ or $BaCl_2$ by means of conductivity measurements, the conductivity being determined by the cation vacancy concentration. (12)

Far from stoichiometry

Let us consider a large deviation from stoichiometry in MX due to a very high concentration of interstitial anions i.e. $[X_i^=] \gg K_f^{\frac{1}{2}}$. For the undoped MX the neutrality condition is

$$2[X_i^=] = [e^+] \quad \ldots\ldots(31)$$

and the defect equilibrium is described by the equations

$$[X_i^=][e^+]^2 = K_i p_{X_2}^{\frac{1}{2}} \quad \ldots\ldots(32)$$

and

$$[X_i^=] = \tfrac{1}{2}[e^+] = \left(\frac{K_i}{4}\right)^{\frac{1}{3}} p_{X_2}^{\frac{1}{6}} \quad \ldots\ldots(21)$$

When a small amount of Me_2X has been added the neutrality condition becomes

$$2[X_i^=] + [Me^-] = [e^+] \quad \ldots\ldots(33)$$

From equations (33) and (32), which still holds for the doped material, it can be seen that addition of monovalent Me decreases $[X_i^=]$ and increases $[e^+]$.

The equation describing the intrinsic anionic Frenkel defect equilibrium

$$\left[V_X^{++}\right] \cdot \left[X_i^{=}\right] = K_f \quad \ldots\ldots\ldots\ldots\ldots\ldots\ldots\ldots\ldots\ldots(12)$$

still holds, and as $\left[X_i^{=}\right]$ decreases this intrinsic equilibrium may have to be considered.

If enough Me_2X has been added to decrease the concentration of anion interstitials to the extent that $\left[Me_M^{-}\right] \gg \left[X_i^{=}\right]$, while $\left[V_X^{++}\right]$ as determined by equation (8) is still much less than $\left[X_i^{=}\right]$ (which is certainly possible provided p_{X_2} is sufficiently high) and so does not have to be included in the neutrality condition, then equation (33) reduces to

$$\left[e^{+}\right] = \left[Me_M^{-}\right] \quad \ldots\ldots\ldots\ldots\ldots\ldots\ldots\ldots\ldots\ldots(34)$$

i.e. the conductivity is completely electronic and the concentration of electronic defects is equal to the concentration of the foreign cation.

When equation (34) holds we can see by combining it with equations (32) and (12) that the concentrations of interstitial anions and anion vacancies are given by

$$\left[X_i^{=}\right] = \frac{K_i}{\left[Me_M^{-}\right]^2} p_{X_2}^{\frac{1}{2}} \quad \ldots\ldots\ldots\ldots\ldots\ldots\ldots\ldots\ldots\ldots(35)$$

$$\text{and } \left[V_X^{++}\right] = \frac{K_f}{K_i}\left[Me_M^{-}\right]^2 p_{X_2}^{-\frac{1}{2}} \quad \ldots\ldots\ldots\ldots\ldots\ldots\ldots\ldots\ldots\ldots(36)$$

We can again see from these equations that addition of Me_2X causes $\left[X_i^{=}\right]$ to decrease and $\left[V_X^{++}\right]$ to increase and so in principle it is possible for the predominant ionic defect to change from anion interstitials to anion vacancies as the concentration of Me_M^{-} increases.

This could explain what happens when $YO_{1.5}$ is added to ThO_2 at atmospheric pressure and 1000°C. The undoped ThO_2 has a large excess of interstitial oxygen and exhibits p-type electronic conductivity. Addition of $YO_{1.5}$ changes the

principle ionic defect type to oxygen vacancies and increases the p–type electronic conductivity (10).

If a lower valent cation is added to MX when it is non–stoichiometric due to the presence of metal vacancies the same behaviour may occur as when the non–stoichiometry is due to anion interstitials, treated above. Addition of Li_2O to NiO is an example of this situation, and it is found here that the conductivity, which is due entirely to electron holes, increases in direct proportion to the concentration of Li_2O added (13) in agreement with equation (34).

When MX is non–stoichiometric due to anion vacancies the addition of Me_2X gives a neutrality condition:

$$2\left[V_X^{++}\right] = \left[e^-\right] + \left[Me_M^-\right]$$

In this case an increase in concentration of the foreign atom means a decrease in $\left[e^-\right]$ and an increase in $\left[V_X^{++}\right]$. The decrease in $\left[e^-\right]$ may mean that eventually the intrinsic electronic equilibrium becomes important and the electronic conductivity changes from n–type to p–type.

Additions of higher valent cations to MX will produce similar effects. Thus if the non–stoichiometry is due to interstitial anions, doping will cause an increase in $\left[X_i^=\right]$, a decrease in $\left[e^+\right]$ and a possible change from p– to n–type conductivity. If non–stoichiometry is due to anion vacancies, doping will cause an increase in $\left[e^-\right]$, a decrease in $\left[V_X^{++}\right]$ and a possible change in the principal ionic defect from anion vacancies to anion interstitials.

The above theory has dealt with a very simple case viz. that in which the base crystal consists of anions and cations of the same valency of two, the intrinsic defects are completely ionized Frenkel defects and the foreign cation always goes onto a normal cation site of the base crystal. However, the same

general treatment can be used to deal with the other more complicated situation which arise.

2.4. Association of foreign ions and oppositely charged ionic defects

When an ionic compound MX is doped with aliovalent foreign cations (or anions), which exist in MX with an effective charge relative to the base crystal, these foreign cations (or anions) will attract the oppositely charged ionic defects present. We will consider as an example a foreign atom F on a normal cation site. If F exists in the base crystal in the form F_m^+ it will attract negatively charged cation vacancies, if it is in the form F_m^- it will attract positively charged anion vacancies. The energy of the vacancy is normally lowest when it is in a nearest neighbour position to the foreign atom. The equilibrium state at low temperatures is therefore that in which all the impurity ions have oppositely charged vacancies as nearest neighbours. These impurity vacancy pairs are known as associated pairs or complexes. As the temperature is increased the complexes will dissociate, the degree of dissociation depending on both temperature and impurity concentration. Evidence for the existence of such complexes has been found in NaCl + $CaCl_2$ ($Ca_{Na}^+ - V_{Na}^-$ pairs), (14) ThO_2 + CaO ($Ca_{Th}^= - V_o^{++}$ pairs) (15) and in many other systems.

Lidiard has discussed the thermodynamics of formation of such complexes (11, 16) for the example of KCl containing $CaCl_2$. The intrinsic defects in KCl are of the Schottky type and the electronic concentration is negligible. Calcium enters the lattice in the form Ca_K^+ and produces oppositely charged vacancies V_K^-. He assumes that the concentration of calcium ions c is large enough that the intrinsic thermal disorder can be neglected. The concentration of potassium vacancies is

therefore also equal to c. The degree of association is defined as p so that cp is the concentration of complexes. The association equilibrium can then be described by the equation

unassociated impurity ion + unassociated vacancy = impurity–vacancy complex

Application of the law of mass action then gives

$$\frac{cp}{c^2(1-p)^2} = K(T) \quad \ldots\ldots\ldots\ldots\ldots\ldots\ldots\ldots\ldots\ldots(37)$$

where the mass action constant K depends only on temperature T. In the simplest case when the impurity ion and the vacancy are regarded as associated only when they are nearest neighbours

$$\frac{p}{(1-p)^2} = Z_1 c \exp\left(\frac{g_a}{kT}\right) = Z_1 c \exp\left(\frac{h_a}{kT}\right) \exp\left(\frac{-s_a}{k}\right) \quad \ldots\ldots\ldots(38)$$

where Z_1 is the number of distinct orientations of the complex, g_a, h_a, and s_a are respectively the Gibbs free energy, enthalpy and entropy of association. On the assumption of zero thermal entropy of association Lidiard has calculated from equation (38) the dependence of p on c and T. This is discussed in reference (11).

Equation (38) can be rewritten in the form

$$1-p = \left(\frac{p}{Z_1 c}\right)^{\frac{1}{2}} \exp\left(\frac{s_a}{2k}\right) \exp\left(\frac{-h_a}{2kT}\right) \quad \ldots\ldots\ldots\ldots\ldots\ldots\ldots(39)$$

If, over a certain range of temperature, the value of p is always close to unity then the variation of p with temperature is negligible compared with that of 1–p. Under these conditions

$$1-p = \text{constant}.\exp\left(\frac{-h_a}{2kT}\right) \quad \ldots\ldots\ldots\ldots\ldots\ldots\ldots(40)$$

and the degree of dissociation, 1–p, and hence the concentration of free vacancies, varies as $\exp\left(\frac{-h_a}{2kT}\right)$

It is possible that the binding energy of the vacancies to the impurity ions at next nearest neighbour and even farther

separations may be appreciable. To allow for this (11) equation (38) is replaced by

$$\frac{p}{(1-p)^2} = c \sum_s z_s \exp\left(\frac{g_{as}}{kT}\right) \quad \ldots\ldots\ldots\ldots\ldots\ldots\ldots\ldots (41)$$

where z_s is the number of orientations of the complex in its S – th state with energy $g_{as} - g_{al}$ above that of the ground (nearest neighbour) state.

The existence of association effects must be realized in order to understand the behaviour of the ionic conductivity of doped materials. When NaCl is doped with sufficient $CdCl_2$ to allow the intrinsic thermal disorder to be neglected the concentration of cadmium ions is equal to that of sodium vacancies. Since all the current is carried by sodium vacancies, at least below 500°C (11), we would expect, ignoring association, that the conductivity would be directly proportional to the cadmium concentration. However, those sodium vacancies which are associated with cadmium ions in $V_{Na}^{-} - Cd_{Na}^{+}$ complexes are uncharged and so do not move under the influence of an applied electric field. So the formation of these uncharged complexes should cause the rate of increase of conductivity with doping to be less than the linear rate suggested above. This has been observed (17).

A similar effect has been observed for ThO_2 doped with CaO (18). At high enough CaO concentration the concentration of oxygen vacancies, which carry all the ionic current is equal to that of the calcium ions. However, the formation of $Ca_{Th}^{\prime\prime} - V_o^{++}$ neutral complexes is at least one of the factors which causes the rate of increase of ionic conductivity with doping to be less than linear.

A neutral impurity–vacancy complex will contribute to

the diffusion coefficient of the ion missing from the vacancy but will not contribute to the corresponding ionic conductivity. The measured diffusion coefficient of sodium in NaBr in the impurity controlled region is much larger than that calculated from the electrical conductivity, known to be due to sodium ions, by means of the Nernst–Einstein equation (19). This difference has been attributed to a contribution to the diffusion coefficient by neutral impurity ion – sodium vacancy complexes (11).

2.5. The effect of variation of temperature on electrical conductivity

As mentioned earlier (Page 4) the electrical conductivity of an ionic solid can be expressed as

$$\sigma = \sum_i n_i q_i \mu_i$$

where n_i, q_i, and μ_i are the concentration, charge and mobility of charge carriers i which may be electrons, holes, anions or cations. In general both n_i and μ_i will vary with temperature.

Ionic conductivity

For an undoped stoichiometric, ionic compound the equilibrium concentration n, at a fixed temperature T and pressure P, of intrinsic ionic defects can be obtained by writing down the Gibbs free energy G as a function of n and T and finding $\left(\frac{\partial G}{\partial n}\right)_{T,P}$ (11).

For the case of anionic Frenkel defects in the compound MX the result obtained is

$$\left[X_i^{=}\right]\left[V_x^{++}\right] = \text{constant}.\exp\left(\frac{-g_f}{kT}\right) \quad \ldots\ldots\ldots\ldots\ldots\ldots (42)$$

where g_f is the Gibbs free energy required to form a single doubly charged Frenkel defect. g_f can be expressed in terms of h_f and s_f, the enthalpy and entropy change in the formation of a Frenkel defect:

$$g_f = h_f - Ts_f$$

Substituting this in equation (42) yields

$$\left[X_i^{=}\right]\left[V_x^{++}\right] = \text{constant}.\exp\left(\frac{-h_f}{kT}\right) \quad \ldots\ldots\ldots\ldots\ldots\ldots\ldots(43)$$

This relationship is true whether $X_i^{=}$ and V_x^{++} are present because of thermal effects, or non-stoichiometry, or doping. If we are dealing with conditions in which intrinsic defects predominate then

$$\left[X_i^{=}\right] = \left[V_x^{++}\right] = \text{constant}.\exp\left(\frac{-h_f}{2kT}\right) \quad \ldots\ldots\ldots\ldots\ldots\ldots\ldots(44)$$

The dependence of the concentration of cationic Frenkel defects and Schottky defects on temperature can be found in the same way, or more simply by means of the law of mass action.

Lidiard (11) has shown that the mobility of ionic defects can be expressed as a function of temperature as

$$\mu = \text{constant}.\frac{1}{T}\exp\left(\frac{-\Delta h}{kT}\right) \quad \ldots\ldots\ldots\ldots\ldots\ldots\ldots\ldots\ldots(45)$$

where Δh is the enthalpy of motion of the defect.

Hence the intrinsic ionic conductivity due to a single type of charge carrier i varies with temperature as

$$\sigma T = \sigma_o \exp\left(\frac{h/2 + \Delta h}{kT}\right) \quad \ldots\ldots\ldots\ldots\ldots\ldots\ldots\ldots\ldots(46)$$

where σ_o is a constant (assuming Δs and s are independent of temperature).

From equation (46) it follows that

$$\frac{h}{2} + \Delta h = -\frac{\partial \log(\sigma T)}{\partial\left(\frac{1}{kT}\right)_p} \quad \ldots\ldots\ldots\ldots\ldots\ldots\ldots\ldots\ldots(47)$$

So a graph of $\log(\sigma T)$ against T^{-1} will be a straight line (if h and Δh are independent of temperature) of gradient $(\frac{1}{2}h + \Delta h)/k$.

In practice it is often $\log \sigma$ that is plotted against T^{-1} and this yields a straight line. This is because the term $\log T$ is not usually important enough to cause a deviation from

linearity, although its omission may give a slightly different gradient which does not have the full theoretical significance of $\frac{(\frac{1}{2}h + \Delta h)}{k}$.

If the compound MX is doped with an aliovalent ion, neutrality may be preserved by the formation of oppositely charged ionic defects. Energetic considerations show that these will be one of the intrinsic defects (11). For a high enough dopant concentration the neutralizing defect concentration will be independent of temperature. Under these conditions the temperature dependence of the conductivity due to the neutralizing defect will be that of the defect mobility only and a graph of log σT (or log σ) against T^{-1} will have a gradient of $\frac{\Delta h}{k}$.

These ideas have been verified many times in practice. For example the conductivity of KCl undoped and doped with $SrCl_2$ behaves as shown below (12).

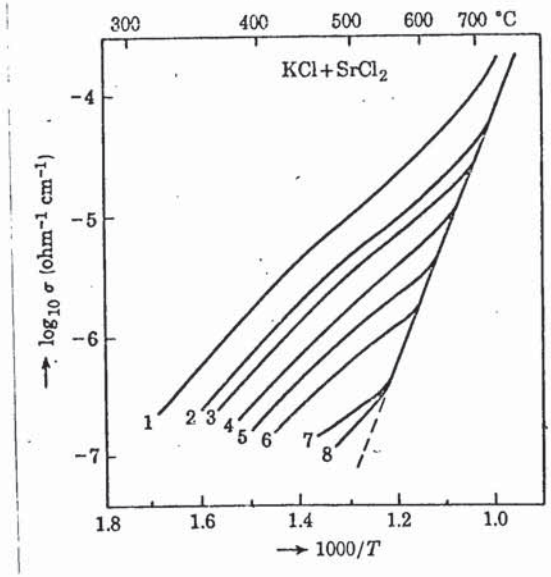

Fig. c.

The curves labelled 1 to 8 contain 19, 8.7, 6.1, 3.5, 1.9, 1.2, 0 and 0 respectively x 10^{-5} mole fraction of added $SrCl_2$. It is known that the intrinsic defects in KCl are Schottky defects and the conductivity is due almost entirely to the cations. Addition of $SrCl_2$ increases the concentration of cation vacancies above the intrinsic concentration provided enough $SrCl_2$ is added and the temperature is low enough.

From the figure the two types of conductivity behaviour can be clearly seen: the intrinsic behaviour at high temperatures where the slope depends on $\frac{1}{2}h + \Delta h$ and the magnitude of the conductivity is independent of the extent of doping; changing as the temperature is lowered to the extrinsic behaviour in which the slope is determined only by Δh and the magnitude of the conductivity increases as the doping increases.

For doped materials such as KCl + $SrCl_2$ impurity vacancy complexes are formed. When the concentration of dopant is very low and the temperature is very high the degree of association p will, according to equation (38), tend to its minimum value $\overline{z}c \exp\left(\frac{-\epsilon_a}{k}\right)$ and will be very small. Moreover this degree of association will not vary with temperature and so need not be considered in interpreting the variation of extrinsic conductivity with temperature. However, as the temperature falls and/or the dopant concentration increases the degree of association will increase and its rate of variation with temperature may become sufficiently large to affect the activation energy for extrinsic conductivity. In the extreme case of such a large dopant concentration and low temperatures that association is almost complete for all temperatures covered the degree of dissociation will vary with temperature as

$\exp\left(\frac{-h_a}{2kT}\right)$ as given by equation (40). The graph of log σ against T^{-1} will then have a slope of $\Delta h + \frac{1}{2} h_a$.

These considerations may explain the decrease in activation enthalpy observed for KCl + $SrCl_2$ for curve 1 in Fig c at 450°C. Below 450°C the activation enthalpy may contain a contribution $h_{a/2}$ due to dissociation of $Sr_K^+ - V_K^-$ complexes, which vanishes for higher temperatures when the degree of association is at its minimum and independent of temperature.

Electronic conductivity

The free electrons or holes contributing to the conductivity are produced by either intrinsic excitation or ionization of defects. The variation of their concentrations with temperature can be obtained by an application of the law of mass action.

The production of intrinsic electrons and holes is described by equation (7)

$$\text{nil} = e^+ + e^- \quad \text{.....(11)}$$

Applying the law of mass action to this equation yields

$$[e^+]\,[e^-] = K_e = \text{constant} \exp\left(\frac{-E_g}{kT}\right) \quad \text{.....(48)}$$

where E_g is the energy gap between the valence and conduction bands. (Strictly speaking since most of the experimental work is done under conditions of constant pressure, E_g should be the enthalpy gap. But for solids the difference between enthalpy and energy values is negligible, except perhaps at very high pressures).

So for intrinsic semiconductivity the temperature dependence of the electron concentration is given by

$$[e^+] = [e^-] = \text{constant.} \exp\left(\frac{-E_g}{2kT}\right) \quad \text{.....(49)}$$

Extrinsic semiconductivity is produced either by excitation of electrons from donor levels into the conduction band or from the valence band into acceptor levels. For

example the ionization of cation vacancies can be described by the equation

$$V_x = V_x^+ + e^- \quad \ldots\ldots\ldots\ldots\ldots\ldots\ldots\ldots (7)$$

The law of mass action yields

$$\frac{[V_x^+][e^-]}{[V_x]} = K_a = \text{constant} \exp\left(-\frac{E_a}{kT}\right) \ldots\ldots (50)$$

where E_a is the energy difference between an electron located at V_x and an electron at the bottom of the conduction band. The exact variation of $[e^-]$ with temperature will depend on the variation of $[V_x]$ and $[V_x^+]$. If $[V_x]$ is constant and $[e^-] = [V_x^+]$ then

$$[e^-] = \text{constant}.\exp\left(\frac{-E_a}{2kT}\right) \ldots\ldots\ldots\ldots (51)$$

If both $[V_x]$ and $[V_x^+]$ are constant then

$$[e^-] = \text{constant}.\exp\left(\frac{-E_a}{kT}\right) \ldots\ldots\ldots\ldots (52)$$

For non-stoichiometric compounds the temperature dependence of the electron concentration is usually determined by an energy which includes both the energy of oxidation or reduction and the ionization energy of the resulting defect. In the preceding example the anion vacancy may be produced by the reaction

$$X_x = \tfrac{1}{2} X_2(g) + V_x \quad \ldots\ldots\ldots\ldots\ldots\ldots (5)$$

If the energy required for this is E_1 then the law of mass action yields

$$[V_x] p_{X_2}^{\frac{1}{2}} = K_1 = \text{constant} \exp\left(\frac{-E_1}{kT}\right) \ldots\ldots\ldots\ldots (53)$$

Combination of equations (50) and (53) give

$$[e^-][V_x^+] = [V_x] K_a = K_1 K_a p_{X_2}^{-\frac{1}{2}} = \text{constant}\ p_{X_2}^{-\frac{1}{2}} \exp\left(-\frac{E_1 + E_a}{kT}\right) \quad (54)$$

If p_{X_2} is constant and $[e^-] = [V_x^+]$ then

$$[e^-] = \text{constant}.\exp\left(-\frac{E_1 + E_a}{2kT}\right) \quad \ldots\ldots\ldots\ldots\ldots\ldots\ldots\ldots(55)$$

and if p_{x_2} and $[V_x^+]$ are both constant then

$$[e^-] = \text{constant}.\exp\left(-\frac{E_1 + E_a}{kT}\right) \quad \ldots\ldots\ldots\ldots\ldots\ldots(56)$$

Since for most cases of semiconductivity the variation of the mobility of the electrons with temperature (usually as $T^{-3/2}$) is negligible compared to the variation of their concentration, the temperature dependence of the conductivity is simply that of the electron concentration. However, in those cases in which the hopping electron model is applicable the electron mobility increases exponentially with temperature. This has been observed for the transition metal oxides CoO, NiO, FeO and Cu_2O (20), and the activation energy is in the range 0.1 – 0.2 eV. In cases such as these the variation of mobility with temperature must be included in an estimate of the temperature dependence of the conductivity.

2.6. The variation of conductivity with measuring frequency

At frequencies below about 10^{10} c/s (above which atomic and electronic polarization effects may contribute to the conductivity) there are two main sources of variation of electrical conductivity of a solid material with measuring frequency. These are

(i) relaxation effects due to dipoles present in the material

and (ii) space charge, or interfacial, polarization effects. The dipole relaxation effects involve motion of the charge carriers over only a few atomic distances and so will be observed at higher frequencies than the space charge polarization effects (if the temperature is kept constant) as the latter require displacement of the carriers over many atomic distances. The changes in conductivity are accompanied by corresponding changes in the dielectric constant and the dielectric loss factor.

(i) The effects due to dipoles

As mentioned earlier when aliovalent ions are added to an ionic compound, these ions frequently combine with oppositely charged vacancies to form dipoles. Examples of these are $Cd_{Na}^{+} - V_{Na}^{-}$ and $Ca_{Th}^{=} - V_{O}^{++}$ dipoles in $NaCl + CdCl_2$ and $ThO_2 + CaO$ respectively. The effects of these dipoles are described by the well-known Debye equations. When there is d.c. conduction present along with these dipole effects, the behaviour in an alternating electric field is described by the relations

$$\varepsilon = \varepsilon_\infty + \frac{\varepsilon_s - \varepsilon_\infty}{1 + \omega^2\tau^2} \quad \text{.....(57)}$$

$$\sigma = \sigma_\infty - \frac{\sigma_\infty - \sigma_s}{1 + \omega^2\tau^2} \quad \text{.....(58)}$$

$$\tan\delta = \frac{\sigma_s}{\omega\varepsilon_s} + \frac{(\varepsilon_s - \varepsilon_\infty)\,\omega\tau}{\varepsilon_s + \varepsilon_\infty\omega^2\tau^2} \quad \text{.....(59)}$$

$$\tau = \tau_o \exp\left(\frac{\Delta H}{kT}\right) = \left(\frac{\varepsilon_s}{\varepsilon_\infty}\right)^{\frac{1}{2}}\omega_{max}^{-1} = \frac{\varepsilon_s - \varepsilon_\infty}{\sigma_\infty - \sigma_s} \quad \text{..(60)}$$

where ε, σ, τ and ω are the dielectric constant, conductivity, relaxation time and angular frequency respectively, the subscripts s and ∞ refer to low-frequency and high-frequency limiting values, τ_o is the intrinsic relaxation time, ΔH is the enthalpy change, or activation energy, for the activated jump mechanism, and ω_{max} is the value of ω at which the dissipation factor,

---

M.K.S. units are used throughout this discussion. The dielectric constant ε, as used here is given by $\varepsilon = K\varepsilon_o$ where K is the relative dielectric constant (compared to vacuum) and ε_o is the dielectric constant of vacuum, 8.85×10^{-12} F m^{-1}.

tan δ, passes through its maximum. The theory behind these equations is discussed in detail by Lidiard (11), von Hippel (21) and Frohlich (22).

For the temperature and frequency range in which these effects are operative the expected variations of ε, σ and tan δ with frequency at constant temperature are shown below.

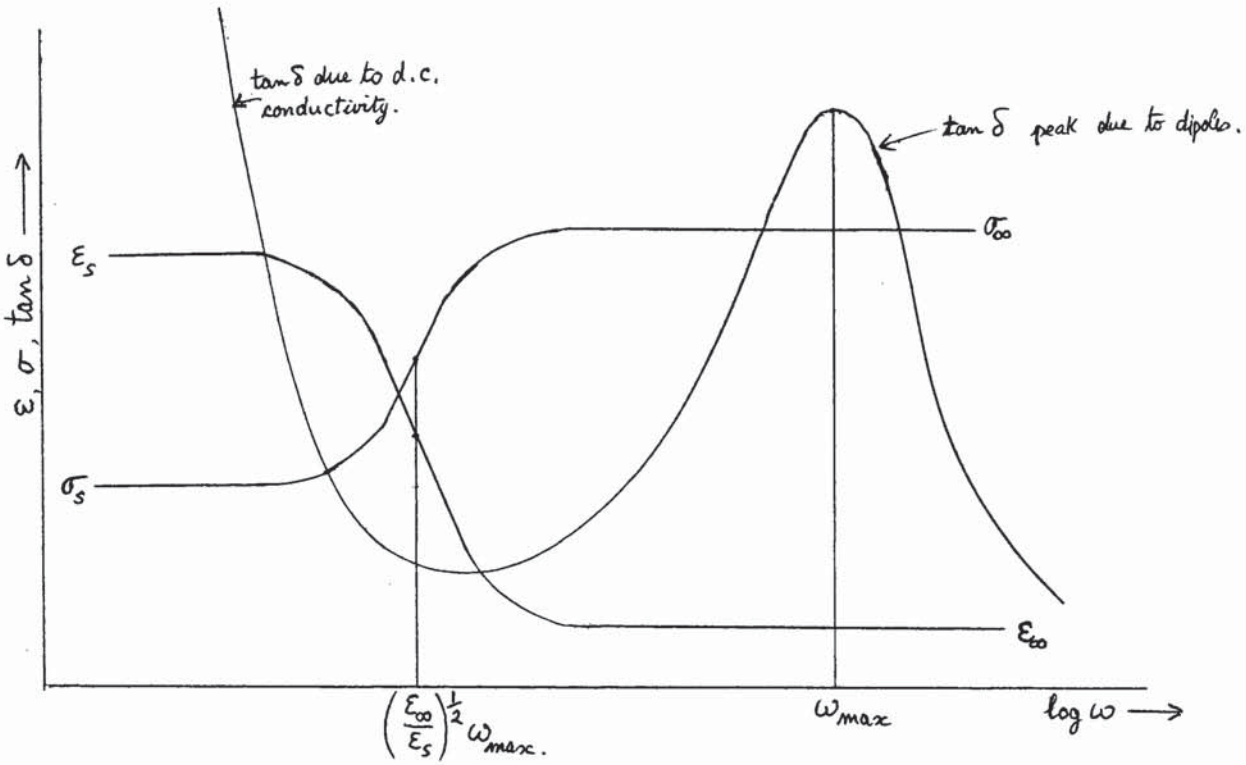

Fig. d.

If a.c. measurements are found to give this behaviour and it is known to be due to the presence of dipoles then σ_s is the conductivity due to free charge carriers and there is no contribution to σ_s from the charge carriers bound in the dipoles. The increase in σ_s in the region of $\omega = \left(\frac{\varepsilon_\infty}{\varepsilon_s}\right)^{\frac{1}{2}}\omega_{max}$ is due to a partial contribution from the dipoles and when $\sigma = \sigma_\infty$ the bound charge carriers in the dipoles are behaving as if they were completely dissociated. (21)

As the temperature increases, τ decreases and so ω_{max} moves to higher frequencies. The variation of conductivity with frequency for different temperatures is shown below

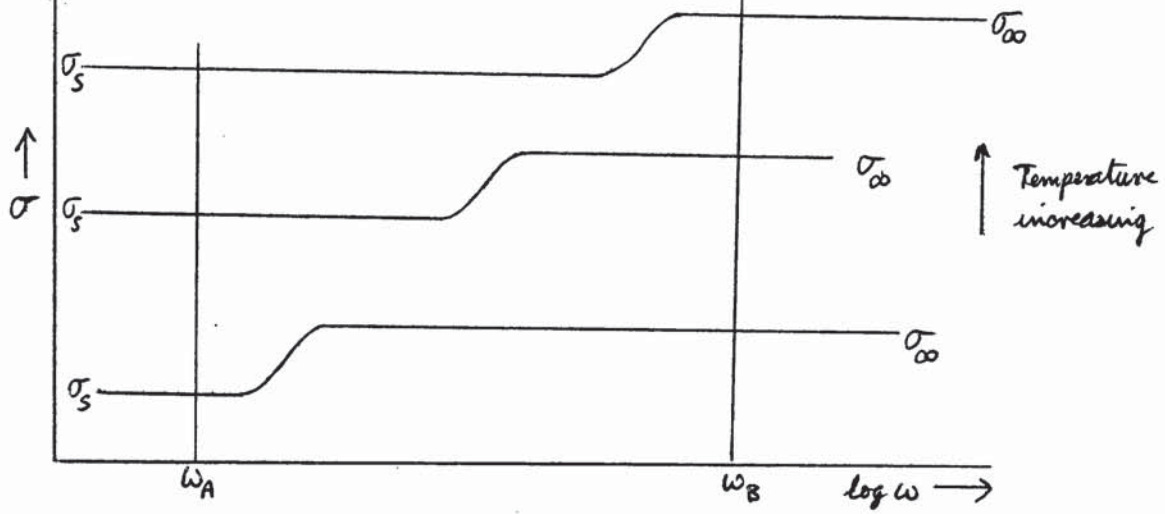

Fig e.

For a material in which the conductivity is completely ionic and is due only to defects introduced by doping, the conductivity for values of frequency less than ω_A will be due only to the motion of free defects. The associated defects will not contribute. The slope of the log σ against T^{-1} graph will be determined by the enthalpy of motion Δh plus a contribution from the enthalpy of association h_a (cf Page 19). The degree of association will depend on the temperature as given by equation (41).

The high frequency conductivity , σ_∞ , on the other hand is determined by the total concentration of defects, both free and bound, introduced by doping. When the frequency is so high that the dipoles cannot follow the alternating field the distinction between free and bound defects vanishes, and both contribute to the conductivity. (See Ref. (21) Page 177). So in this region, i.e. $\omega > \omega_B$, the slope of the log σ against T^{-1} graph is determined only by Δh.

It should be noted that the conductivity referred to in the earlier treatment of association was assumed to be that in the frequency range $\omega < \omega_A$.

From equation (60) it can be seen that if log ω_{max} is plotted against T^{-1} then, provided that $\log\left(\frac{\varepsilon_s}{\varepsilon_\infty}\right)$ is comparatively independent of T, the gradient of the line obtained should give

$\Delta H/K$. ε_∞ is due to atomic and electronic polarization effects both of which are almost independent of T. ε_s contains in addition only the effect obtained by aligning all the dipoles present in the field direction. At temperatures and concentrations at which association is nearly complete, ε_s is almost independent of temperature. So the value of ΔH obtained from the above mentioned plot should be quite accurate. This quantity is the energy required to move the mobile defect from one associated position to another.

These ideas have been verified for the case of CaF_2 doped with NaF (23). This doping produces $Na_{Ca}^- - V_F^+$ dipoles. When $\log \omega_{max}$ is plotted against T^{-1} an accurately linear straight line is obtained whose gradient gives the activation energy 0.53eV of motion of the fluorine vacancies. This activation energy agrees well with that of free fluorine vacancy diffusion which is reported as 0.55eV (24).

(ii) Space charge, or interfacial, polarization effects

In the preceding discussion of the conductivity of solids it was assumed that the unassociated charge carriers were, except for the normal bulk resistivity effects, completely free to move under the action of an applied field. In fact this is not always so. There may be present both internal and external barriers which hinder, or block completely, the flow of the charge carriers. The carriers pile up at these barriers and, by producing a back e.m.f., hinder the approach of further carriers. This effect is known as space-charge, or interfacial, polarization. The barriers in question may, for example, be electrodes which cannot supply or absorb the charge carriers (external barriers), or grain boundaries with a higher resistivity than that of the bulk grain (internal barriers).

When an alternating field of sufficiently low frequency is applied to the sample some space charge build-up will occur

at these barriers. As the frequency is increased this polarization will decrease and so the conductivity will increase. Eventually the frequency will be high enough that no appreciable space charge can build up in half a period of a.c. and the measured conductivity will then be that of the bulk material.

There have been two principal theoretical approaches to the problem of space charge polarization in solids: one deals with the polarization occurring at phase boundaries in a heterogeneous material; the other with the polarization due to blocking, or partly blocking, electrodes on a homogeneous sample.

The classical example of interfacial polarization in heterogeneous materials is the Maxwell–Wagner two–layer condenser, shown in Fig f below.

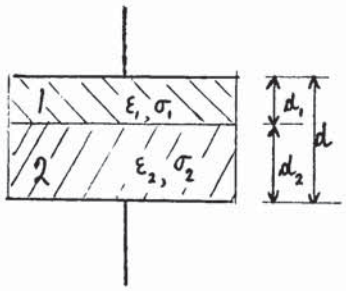

Fig. f.

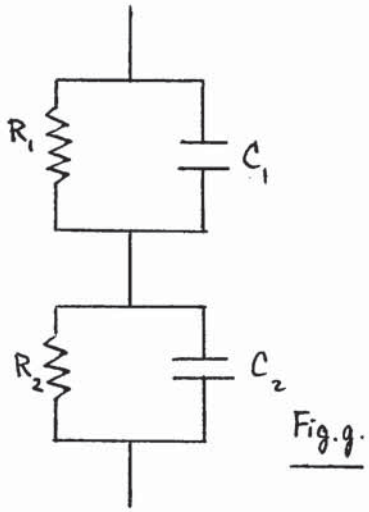

Fig. g.

The dielectric consists of two parallel layers , 1 and 2, of different materials having thicknesses d_1 and d_2, dielectric constants ε_1 and ε_2, and conductivities σ_1 and σ_2. If σ_1 and σ_2 are unequal there will be a build–up of space charge at the interface between the two layers when an electric field is applied.

This two layer condenser can be represented by the equivalent circuit shown beside it (Fig g). If A is the area of the condenser electrodes, then

$$R_1 = \frac{d_1}{A\sigma_1} \quad , \quad R_2 = \frac{d_2}{A\sigma_2} \quad , \quad C_1 = \frac{A\varepsilon_1}{d_1} \quad \text{and} \quad C_2 = \frac{A\varepsilon_2}{d_2}$$

By considering the application of an a.c. voltage to the equivalent circuit, it can be shown (21) that the two layer dielectric behaves as if it were a single dielectric material of thickness, $d = d_1 + d_2$ and whose electrical properties are given as a function of frequency by the following equations

$$\varepsilon = \varepsilon_\infty + \frac{\varepsilon_s - \varepsilon_\infty}{1 + \omega^2\tau^2} \quad \text{.....(61)}$$

$$\sigma = \sigma_\infty - \frac{\sigma_\infty - \sigma_s}{1 + \omega^2\tau^2} \quad \text{.....(62)}$$

$$\tan\delta = \frac{\sigma_s}{\omega} \frac{1}{\varepsilon_s + \varepsilon_\infty\omega^2\tau^2} + \sigma_\infty\tau \frac{\omega\tau}{\varepsilon_s + \varepsilon_\infty\omega^2\tau^2} \quad \text{.....(63)}$$

$$\tau = \frac{\varepsilon_1 d_2 + \varepsilon_2 d_1}{\sigma_1 d_2 + \sigma_2 d_1} = \frac{\varepsilon_s - \varepsilon_\infty}{\sigma_\infty - \sigma_s} = \tau_o \exp\left(\frac{\Delta H}{kT}\right) = \left(\frac{\varepsilon_s}{\varepsilon_\infty}\right)^{\frac{1}{2}} \omega_{max}^{-1} \quad (64)$$

It can be seen that equations (61) and (62) are identical with equations (57) and (58), and equations (63) and (64) are similar to equations (59) and (60). Symbols occurring in both sets of equations (57) to (60) and (61) to (64) have the same meaning in each case.

The first term in tan δ in equation (64) represents a background d.c. conductivity loss and the second term produces a Debye-type tan δ peak occurring at an angular frequency $\omega_{max} = \left(\frac{\varepsilon_s}{\varepsilon_\infty}\right)^{\frac{1}{2}} \tau^{-1}$ just as for the preceding case of dipole rotation plus d.c. conduction. In fact the variation of ε, σ and tan δ with frequency in this case can also be represented by Fig. d.

From equations (63) and (64) it follows that if tan δ is plotted as a function of temperature at fixed frequency ω a peak will be observed in the graph at the temperature at which

$$\omega\tau = \omega\tau_o \exp\left(\frac{\Delta H}{kT}\right) = \left(\frac{\varepsilon_s}{\varepsilon_\infty}\right)^{\frac{1}{2}} \quad \ldots\ldots\ldots\ldots\ldots\ldots\ldots\ldots (65)$$

This approach can be of use in verifying the existence of, and identifying, dielectric loss mechanisms.

If the two parallel layers 1 and 2 are each divided into many thinner parallel layers and these are then packed together in any order then, provided the total thicknesses of the two media are still d_1 and d_2, the electrical behaviour remains unaltered and is still described by equations (61) to (64).

This model has been used successfully by Koops (25) to explain the dispersion in conductivity and dielectric constant and the dissipation factor peak in nickel zinc ferrite. The material is assumed to consist of well conducting grains separated by layers of lower conductivity. It has also been used by Tallan and Graham to explain the similar behaviour of the electrical properties of single crystal sapphire (26). In this case it is assumed that the two layers consist of the bulk crystal and thin surface layers of a different conductivity. Florio (27) used the same model to discuss qualitatively his results on single crystal and polycrystalline alumina. He concluded that there is evidence of interfacial polarization both at grain boundaries and at a high resistance transition layer at the dielectric–electrode interface. Macfarlane and Weaver (28) explained the low-frequency dielectric losses they observed in thin films of NaCl and NaBr in terms of the Maxwell–Wagner model. Again in this case it is concluded that there is interfacial polarization both at grain boundaries and at the electrodes.

Because of the similarity in electrical behaviour predicted for the two types of polarization, interfacial and dipole relaxation, it may be difficult to distinguish between them. The best way may often be in terms of the values of

τ_o and ΔH (cf. equations (60) and (64)). For a dipole mechanism τ_o should be in the range 10^{-13} to 10^{-14} sec. and should be independent of sample treatment. ΔH in this case is simply the energy of motion as discussed on Page 24. In the interfacial polarization case τ_o may differ widely from the range 10^{-13} to 10^{-14} sec., and depends on, for example, grain size. ΔH in this case, being an energy for conduction, may contain formation, ionization and association contributions.

As was the case for dipole relaxation, ΔH for the interfacial polarization model can sometimes be obtained by plotting $\log \omega_{max}$ against T^{-1}. Again it is necessary for $\log\left(\frac{\varepsilon_s}{\varepsilon_\infty}\right)$ to vary with temperature much more slowly than $\frac{\Delta H}{kT}$. This will be the case for a material in which the charge carrier concentration is independent of temperature, possibly due to doping. In this case ε_∞ is due only to electronic and atomic polarization effects, and ε_s is due in addition to the static space charge which depends only on $T^{\frac{1}{2}}$, though its dependence on the Debye length l_D (defined on page 38). So $\log\left(\frac{\varepsilon_s}{\varepsilon_\infty}\right)$ is almost independent of temperature.

It is instructive to consider in more detail the case of grain boundary polarization as related to the Maxwell–Wagner model. Let us assume that region 1 is the grain boundary material and region 2 the bulk grain. Then $d_1 \ll d_2$. Since disorder on an atomic scale would be expected to alter the conductivity rather than the dielectric constant, it is reasonable to assume $\varepsilon_1 = \varepsilon_2$. If the grain boundaries are blocking then $R_1 \gg R_2$ i.e. $\frac{d_1}{\sigma_1} \gg \frac{d_2}{\sigma_2}$

Under these conditions the relaxation time τ is given by

$$\tau = \frac{\varepsilon_1 d_2 + \varepsilon_2 d_1}{\sigma_1 d_2 + \sigma_2 d_1}$$

$$= \frac{\varepsilon_2 (d_1 + d_2)}{\sigma_2 d_1} \qquad \text{since } \varepsilon_1 = \varepsilon_2 \text{ and } \sigma_2 d_1 \gg \sigma_1 d_2$$

$$= \frac{\varepsilon_2 d_2}{\sigma_2 d_1} \qquad \text{since } d_2 \gg d_1 \quad \ldots\ldots\ldots\ldots\ldots\ldots (66)$$

If ε_2 and d_1 are constant, then

$$\tau = \text{constant.}\ d_2/\sigma_2 \quad \ldots\ldots\ldots\ldots\ldots\ldots\ldots\ldots\ldots\ldots (67)$$

If, in addition, σ_2 is constant, then

$$\tau = \text{constant.}\ d_2 \quad \ldots\ldots\ldots\ldots\ldots\ldots\ldots\ldots (68)$$

i.e. under the conditions stated, the relaxation time is proportional to the grain size.

For the example considered above, as the frequency tends to zero the resistance tends to $R_1 + R_2 \approx R_1$. So the measured value of σ_s is determined by the conductivity σ_1 of the grain boundary material and in fact $\sigma_s = \frac{d}{d_1} \sigma_1$. On the other hand as the frequency becomes very high the measured resistance tends to R_2 and $\sigma_\infty = \sigma_2$ i.e. the conductivity measured in the high frequency region is the true value for the bulk material (25).

It seems reasonable to apply this two layer dielectric model to grain boundary polarization. In some cases the boundaries will have a much lower conductivity than the grains (25), as in the example above. It could also happen that the boundaries have the higher conductivity.

It also seems reasonable to apply this model to electrode polarization effects. In this case there will be a relatively low conductivity layer at the electrodes. For complete blocking of the charge carriers this layer will have zero conductivity. On the other hand if there is no blocking the conductivity of the layer will be the same as that of the bulk material.

The preceding treatment is a rather macroscopic approach to the problem of space charge polarization. A more fundamental approach is that adopted by Friauf (29) and Sutton (30), among others.

Friauf considered a material in which there were two types of carriers of equal charge, q , and opposite sign. The concentrations of the carriers varied due to diffusion, conduction and generation-recombination. For the case of plane parallel electrodes the differential equations relating the concentrations p of positive and n of negative carriers and the electric field E are

$$\frac{\partial p}{\partial t} = -\mu_p \frac{\partial (pE)}{\partial x} + D_p \frac{\partial^2 p}{\partial x^2} + k(c_o^2 - pn) \quad \text{.....(69)}$$

$$\frac{\partial n}{\partial t} = \mu_n \frac{\partial (nE)}{\partial x} + D_n \frac{\partial^2 n}{\partial x^2} + k(c_o^2 - pn) \quad \text{..... ...(70)}$$

$$\frac{\partial E}{\partial x} = \frac{(p - n)q}{\varepsilon} \quad \text{.....(71)}$$

In these equations t and x are time and position, D_p and D_n are the diffusion coefficients and μ_p and μ_n the mobilities of positive and negative carriers, ε is the dielectric constant of the material, k is a constant and c_o is the equilibrium concentration of positive and negative carriers.

By the use of two approximations: (a) for an applied voltage $V(t) = V_o + V_1 \exp(j\omega t)$ the dependent variables can be represented as

$$p(x,t) = p_o(x) + p_1(x)\exp(j\omega t)$$

and (b) the d.c. solution for zero external d.c. voltage is taken to be

$$p_o(x) = c_o \ , \ n_o(x) = c_o \text{ and } E_o(x) = 0$$

a set of linear homogeneous equations is obtained which can then be readily solved.

Approximation (a) holds as long as $eV_1 \ll kT$.

formation of the complementary defects are different from one another, space charges will arise near the crystal surfaces. However, the use of these approximations does allow a solution to be obtained which is expected to be capable of explaining, at least qualitatively, the experimental results.

One of the boundary conditions which must always be satisfied is $\int_{-\frac{1}{2}}^{\frac{1}{2}} E dx = V$ where the origin has been placed at the middle of the sample of length L. The other condition deals with the blocking of the carriers at the electrodes. If both carriers are completely blocked then the currents i_p and i_n are both zero at $x = \pm \frac{1}{2} L$. If only one, say the positive, is blocked then $i_p = 0$ at $x = \pm \frac{1}{2} L$ and there is no space charge build-up due to the other. In practice the transfer of ionic defects (charge carriers) from electrode to crystal or vice versa may be an activated process and partial blocking will occur.

For the particular case of both carriers blocked Friauf showed that the results for the parallel capacity C in excess of the geometrical capacity and the change in resistance are

$$C = \frac{C_o}{1 + \omega^2 \tau^2} \quad \text{.....(72)}$$

$$\Delta\left(\frac{1}{R}\right) = \frac{1}{R_o} \frac{1}{1 + \omega^2 \tau^2} \quad \text{.....(73)}$$

where $R_o = \frac{L}{q(\mu_p + \mu_n) c_o A}$ is the high-frequency bulk resistance

$C_o = \frac{A\varepsilon}{2 l_D}$ is the low-frequency limiting capacity,

$\tau = R_o C_o = \frac{L\, l_d}{D_p + D_n}$ is the Debye relaxation time, and

$l_D = \left(\frac{\varepsilon kT}{2q^2 c_o}\right)^{\frac{1}{2}}$ is the Debye length.

From equations (72) and (73) it can be seen that the

expressions for the total capacity and total conductance are the the same as those for ε and σ in equations (61) and (62). So this treatment, too, predicts an inflection in the graphs of conductance and capacity against frequency and also a dielectric loss tangent peak at a frequency defined by $\omega\tau = \left(\varepsilon_s/\varepsilon_\infty\right)^{\frac{1}{2}} = \left(C_s/C_\infty\right)^{\frac{1}{2}}$, where C_∞ is the high-frequency limiting capacity.

It has been shown by Sutton (32) that the same type of behaviour is found under suitable conditions when blocking electrodes are applied to a material containing mobile charge carriers of only one type. (Sutton's treatment began with the same equations as Friauf's (69) to (71). He obtained the case of a single mobile charge carrier simply by putting $\mu_n = D_n = 0$ in equation (70)).

So the behaviour predicted by the more fundamental approach for space charge polarization at blocking electrodes is similar to that found for the Maxwell-Wagner two layer dielectric. This is not really surprising as they are simply two different ways of dealing with the same phenomenon, interfacial polarization.

The Debye relaxation time for two charge carriers both of which are blocked at the electrodes is, according to Friauf,

$$\tau = \frac{L\, l_D}{D_p + D_n} \qquad \ldots\ldots\ldots\ldots\ldots\ldots\ldots\ldots\ldots\ldots (74)$$

as shown above. If there is only one charge carrier present, with diffusion coefficient D, we might expect the relaxation time to be

$$\tau = \frac{L\, l_D}{D} \qquad \ldots\ldots\ldots\ldots\ldots\ldots\ldots\ldots\ldots\ldots (75)$$

This compares reasonably well with Sutton's work which shows that, for a single type of charge carrier and blocking electrodes, when conditions are such as to give Debye type behaviour, the relaxation time can be written as

$$\tau = \text{constant}.\frac{L\, l_D}{D} \qquad \ldots\ldots\ldots\ldots\ldots\ldots\ldots\ldots (76)$$

where the constant depends on temperature and doping, but is

independent of frequency and specimen size.

Recalling now the Maxwell–Wagner treatment of grain boundary polarization, we see that according to equation (68), provided the concentration and mobility of charge carriers inside the grains remains constant, the Debye relaxation time is proportional to the grain size.

So all the above treatments agree in the prediction that, for constant conductivity in the high-conductivity region, the relaxation time is proportional to the length of the high-conductivity region.

This implies that, if in a particular sample there are high-conductivity regions of different lengths, there will be a corresponding number of relaxation times and the ratio of relaxation times will be equal to the ratio of the lengths of the high-conductivity regions. This can be applied to grain boundary polarization where the grains are of different sizes, or to the case of a polycrystalline material of uniform grain size with blocking electrodes and blocking grain boundaries.

Friauf's treatment predicted that the low-frequency limiting capacity for two carriers both of which are blocked at the electrodes is

$$C_o = \frac{A\varepsilon}{2\,l_D} \qquad \text{.....(77)}$$

This means that at low frequencies the sample behaves like two capacitors, of plate area A and separation l_D, in series. For the case of a single mobile carrier we would expect a low frequency capacity of similar size, perhaps the same size if there are two regions of space charge, one due to charge build-up and the other to charge depletion.

We can apply this result to the combined case of grain boundary polarization and electrode polarization. For the frequency region in which the electrode polarization effects are at their maximum we would expect a capacity given by equation (77).

If we are in a higher frequency region which corresponds to the low frequency limiting region for grain boundary polarization, we might expect the sample to behave like N capacitors in series, where N is the number of grain diameters in the inter-electrode gap. The limiting capacity in this case should have the value

$$C_o = \frac{1}{N} \cdot \frac{A\epsilon}{2l_D + d} \quad \text{.....(78)}$$

where d is the grain boundary thickness. The reason for the factor $2l_D + d$ in the denominator in equation (78) can be understood from the diagram below representing grain boundary polarization.

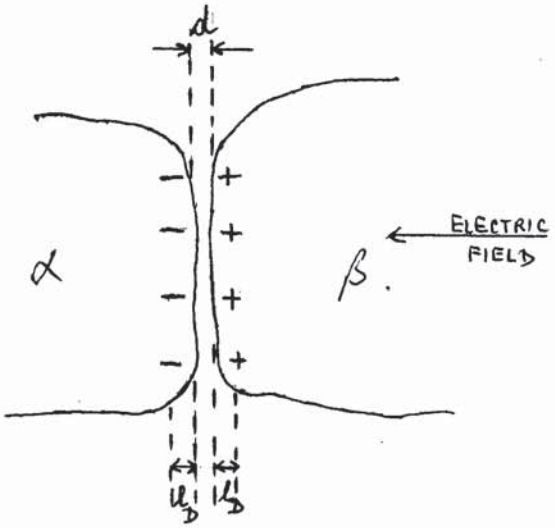

Fig h.

There will be a space charge layer in each grain α and β of thickness approximately l_D. The effective capacitor plate separation must also include the grain boundary thickness d and so is given by $2l_D + d$.

CHAPTER 3

DISCUSSION OF MATERIALS CHOSEN FOR INVESTIGATION

INTENDED PROGRAMME OF RESEARCH

DISCUSSION OF MATERIALS CHOSEN FOR INVESTIGATION INTENDED PROGRAMME OF RESEARCH

3.1. Reasons for investigating ThO_2, undoped and doped with the Group II oxides, CaO and SrO.

The particular system chosen for a study of electrical conductivity behaviour was thorium oxide doped with some Group II oxides, CaO and SrO, and also undoped for comparison purposes.

There were several reasons for this choice:-

(i) ThO_2 is a very refractory material (M.Pt. 3300°C) and its rate of weight loss in the conditions encountered in a magnetohydrodynamic generator is likely to be small (2). It is therefore a possible insulating material for this application, when pure. The presence of impurities may lower the resistivity, and hence its usefulness in insulation, and large enough quantities of impurities may even make it sufficiently highly conducting to consider it as an electrode material in M H D generation.

(ii) As mentioned on Page 1 galvanic cells with oxide electrolytes with an ionic transport number of one are useful for determining the free energies of formation of metal oxides. Kiukkola and Wagner (3) carried out measurements of this type successfully using the electrolyte 0.85 ZrO_2 – 0.15 CaO. However, the discovery by Peters and Mobius (31), confirmed by Schmalzried (32), that at low oxygen partial pressures ($\sim 10^{-21}$ atm. at 1000°C) this electrolyte exhibits appreciable electronic conductivity and so, under these conditions, cannot be used reliably in free energy determinations meant that new electrolytes had to be developed. Therefore, the electrical transport properties of some electrolytes based on thoria (which is more stable than zirconia) were investigated by, for example, Steele and Alcock (18) and Lasker and Rapp (10). The results

of these investigations show that thoria-based electrolytes are in fact suitable for free energy measurements down to lower oxygen partial pressures than those based on zirconia.

(iii) Because of its usefulness in galvanic cells and, possibly, in fuel cells there has been a great deal of work done on the electrical properties of zirconia with additions of oxides of lower valent cations. Most of this work has concentrated on the properties of ZrO_2 containing sufficient lower-valent cations to produce a fluorite lattice instead of the normal monoclinic or tetragonal lattice of undoped zirconia. This means that there is a large amount of data available with which results on the fluorite structure thoria-based electrolytes can be compared.

(iv) ZrO_2 has a fluorite lattice only when it is heavily doped. According to Tien and Subbarao (33), the lower limit of the fluorite phase for specimens of ZrO_2 doped with CaO and sintered at 2000°C is 12 to 13 mole °/o CaO. For lower CaO concentrations a two-phase mixture of cubic fluorite phase and monoclinic ZrO_2 is obtained (34). Undoped ThO_2, on the other hand, has a fluorite lattice (35). So with ThO_2 as the host material, it is possible to study the effects of small additions of lower valent cations to a fluorite lattice.

(v) Although, as mentioned in (ii) above, there has been some previous investigation into ThO_2 based electrolytes (10, 18) this has concentrated principally on those doped with oxides of trivalent cations such as Y_2O_3 or La_2O_3. Earlier work on ThO_2 doped with Group II oxides has been very limited in its scope.

3.2. Application of some of the previously discussed theory to thoria.

When CaO is added to ThO_2 previous workers' results (10,

18) suggest that the calcium will exist as $Ca_{Th}^{=}$ in a complete cation sublattice and charge neutrality will be preserved by the formation of an equal number of oxygen vacancies V_o^{++}.
Wachtman's work (15) shows that the calcium ions and oxygen vacancies combine to form dipoles, the degree of association depending on temperature and CaO concentration through equation (41). Wachtman's calculations give 0.71 eV and 0.37 eV as the energy required to free an oxygen vacancy from a calcium ion when the vacancy is in the nearest and next-nearest neighbour position respectively. So in calculating the degree of association it is obviously necessary to consider an oxygen vacancy in a next-nearest neighbour position to a calcium ion as associated with it.

Let us apply equation (41) to ThO_2 doped with CaO, regarding the oxygen vacancies as associated with the calcium ions only when in nearest and next-nearest neighbour positions. For the fluorite lattice of ThO_2 $Z_1 = 8$ and $Z_2 = 16$. Lidiard (16) has shown that the thermal entropy change in association can be taken as zero. Under the above conditions, application of equation (41) yields the following results:

Temperature	CaO content (mole %)	degree of association p
∞	5	0.41
1700°K	5	0.88
1200°K	5	0.95
700°K	5	0.995
∞	1	0.17
1700°K	1	0.75
1200°K	1	0.90
700°K	1	0.991

From the above we see that the degree of association for temperatures below 1700°K (1427°C) is very high, being always

greater than 0.88 for $0.95ThO_2 - 0.05CaO$, and 0.75 for $0.99ThO_2 - 0.01CaO$. For both these compositions, especially for $0.95ThO_2 - 0.05CaO$, the variation of the degree of association p with temperature is very small compared with that of $1 - p$, at least for temperatures below 1200°K. So for these lower temperatures we might reasonably expect equation (40) to be valid and the concentration of free oxygen vacancies to vary with temperature as $\exp\left(-\frac{ha}{2kT}\right)$, where in this case $h_a = 0.71$ eV.

For ThO_2 containing 100 p.p.m. CaO the degree of association varies from 0.91 to 0.10 as the temperature rises from 700° to 1700°K. In this case too the concentration of free oxygen vacancies will increase with temperature due to dissociation of dipoles. However, as equation (40) will not hold for values of p less than 0.9 the number of dipoles dissociated will increase with temperature at a lower rate than $\exp\left(-\frac{0.71}{2kT}\right)$, especially at the higher temperatures.

As for any other ionic compound the electrical conductivity of ThO_2, doped or undoped, will vary with the surrounding atmosphere. Let us consider first the case of pure ThO_2. As will be seen below the intrinsic ionic defects in pure ThO_2 are expected to be oxygen vacancies and interstitials. For a material such as ThO_2 with a large band gap the intrinsic electronic concentration will be negligible. For sufficiently high temperatures the oxygen vacancies and interstitials will be completely ionized. For this case the equilibrium between the oxide and the atmosphere at very low values of oxygen partial pressure p_{O_2} will be described by the equations

$$O_O = V_O^{++} + 2e^- + \tfrac{1}{2} O_2(g)$$

and

$$[e^-] = 2[V_O^{++}]$$

Application of the law of mass action yields

$$[e^-] = (2K_v)^{\frac{1}{3}} p_{O_2}^{-\frac{1}{6}}$$

(cf equation (19)).

At the other extreme of very high p_{O_2} where there will be a large concentration of oxygen interstitials, the following equations apply

$$1/2\ O_2(g) = O_i^{=} + 2e^+$$

$$[e^+] = 2[O_i^{=}]$$

Again the law of mass action yields

$$[e^+] = (2K_i)^{\frac{1}{3}} p_{O_2}^{\frac{1}{6}}$$

(cf equation (21)).

The behaviour at values of p_{O_2} at which the thoria is nearly stoichiometric will be that described in case (ii), page 10

i.e. $[O_i^{=}] = [V_O^{++}] = K_f^{\frac{1}{2}} \gg [e^-]$ and $[e^+]$.

The variation in concentration of all the defects present, electronic and ionic, will be as shown in Fig 5, Page 11.

Since the mobility of electrons is greater than that of ionic defects the total conductivity at high and low values of p_O will vary as the electronic concentration i.e. as $p_{O_2}^{\frac{1}{6}}$ and $p_O^{-\frac{1}{6}}$ respectively. Near stoichiometry the p_{O_2} – independent ionic conductivity will be added to the p_{O_2} –dependent electronic conductivity. A range of p_{O_2} in which the total conductivity is independent of the atmosphere implies almost complete ionic conductivity.

Now let us consider the case in which the ThO_2 is doped with the oxide of a lower valent metal such as CaO. For large enough additions of CaO the ionic equilibrium will be dominated by the CaO concentration for all values of p_{O_2} encountered.

Under these conditions

$$\left[V_O^{++}\right] = (1 - p)\left[CaO\right] \gg \left[O_i^{=}\right]$$

where $\left[V_O^{++}\right]$ refers to dissociated oxygen vacancies and p is the degree of association.

Since in this case we have a very high concentration of ionic defects we would expect to, and in fact do, find a large range of oxygen partial pressure in which the conductivity is completely ionic, independent of p_{O_2}, and determined by the amount of CaO added. For values of p_{O_2} beyond this range there will be, in addition, significant electronic conductivity.

The addition of oxygen at high values of p_{O_2} and its removal at low values of p_{O_2} can be described by the equations

$$1/2\ O_2(g) + V_O^{++} = O_O + 2e^+$$

and

$$O_O = 1/2\ O_2(g) + V_O^{++} + 2e^-$$

For large concentrations of dopant

$$\left[V_O^{++}\right] = \text{constant} = (1-p)\left[CaO\right]$$

and the law of mass action yields

$$\left[e^+\right] \alpha\ p_{O_2}^{\frac{1}{4}} \quad \text{at high } p_{O_2}$$

and

$$\left[e^-\right] \alpha\ p_{O_2}^{-\frac{1}{4}} \quad \text{at low } p_{O_2}$$

So at sufficiently high and low values of p_{O_2} there will be an electronic contribution to the conductivity varying as $p_{O_2}^{\frac{1}{4}}$ and $p_{O_2}^{-\frac{1}{4}}$ respectively.

3.3. Relevant previous work.

Lattice structure of undoped and doped thoria.

Pure thorium dioxide has a cubic fluorite lattice up to its melting point (3,300°C). The existence of the fluorite lattice was confirmed for both ThO_2 and UO_2 by the neutron diffraction studies of Willis (35). Further work by Willis (36) showed that in oxygen-excess non-stoichiometric UO_2 the point defects present are oxygen vacancies and interstitials, the

cation sub-lattice remaining undisturbed. As the UO_2 lattice constant is smaller than that of ThO_2, 5.479Å compared with 5.5972Å (37), it seems highly probable that oxygen ions can easily exist in ThO_2 in interstitial positions and the intrinsic ionic defects in ThO_2, as in UO_2, are oxygen vacancies and interstitials.

Further evidence of the existence of anion vacancies and interstitials in fluorite lattices is provided by the work of Ure (24). By means of transference number and electrical conductivity measurements on pure and doped crystals he showed that the predominant defect in CaF_2 is of the anti-Frenkel type involving equal numbers of fluorine vacancies and interstitials.

By a comparison of directly measured densities and those calculated from measured X-ray lattice parameters Hund and co-workers (38, 39, 40) have shown that when La_2O_3 or Y_2O_3 exists in solid solution in ThO_2 the trivalent ions replace the thorium ions and introduce an appropriate number of oxygen vacancies. This has been confirmed for the ThO_2–Y_2O_3 solid solutions, by the same method, by Subbarao, Sutter and Hrizo (41) and Wimmer, Bidwell and Tallan (42). Hund has also shown (43) that in the fluorite phase of the system ZrO_2–CaO the cation sub-lattice is complete with Ca^{2+} ions substituting for Zr^{4+} ions and there are vacancies in the oxygen sub-lattice equal in concentration to that of the calcium ions. It is reasonable to assume that the addition of CaO in solid solution in fluorite ThO_2 will also introduce anion vacancies.

Limit of Solubility of CaO and SrO in ThO_2

Curtis and Johnson (44) as a result of studying the densification of ThO_2 by additions of CaO concluded that the increased density observed was due to the production of oxygen vacancies when CaO went into solid solution in ThO_2. They

estimated that the maximum solubility of CaO in ThO_2 at 1800°C was at least 12.5 mole °/o. However, Mobius et al. (45) by studying the variation of lattice parameter with increased CaO concentration concluded that the maximum solubility at 1800°C to give the fluorite lattice is only 8 mole °/o.

Curtis and Johnson (44) noted that SrO, too, caused an increase in density of ThO_2 and suggest that this implies solution of the SrO. The results of Volchenkova and Pal'guev (46) of chemical phase analyses of specimens prepared at 1550°C from compacted mixtures of ThO_2 and SrO indicate that the maximum solubility of the SrO is about 2 – 3 mole °/o. Mobius et al. (45) put the limit of solubility at 1800°C in the range 3 to 5 mole °/o.

Electronic and ionic conductivity

Kiukkola and Wagner (3) observed that the conductivity of ThO_2 doped with La_2O_3 or CaO varied with the surrounding atmosphere and attributed this to the presence of electronic conduction. Foex (47) had earlier observed the same behaviour in undoped ThO_2. Pal'guev and Neuimin (48) measured the electronic and ionic transport numbers in several solid oxides and oxide mixtures by means of the galvanic cell emf. technique. Their results showed that for ThO_2 containing 15 mole °/o CaO there was considerable electronic conductivity at oxygen partial pressures in the region of 1 atmosphere, but that at the lower oxygen pressures defined by Fe, FeO and Cu, Cu_2O electrodes ($p_o < 10^{-6}$ atm. for temperatures below 1000°C) the ionic transport number between 800° and 1000°C was greater than 0.98. Steele and Alcock (18) found that the conductivity of ThO_2–based electrolytes increased with the oxygen partial pressure when this was greater than about 10^{-6} atm., indicating p–type electronic conductivity, but below 10^{-6} atm. the conductivity

was independent of p_{O_2}; emf measurements showed that this p_{O_2} -independent conductivity was due solely to the movement of ions, whereas the p_{O_2}-dependent conductivity had an appreciable electronic component. For undoped ThO_2 they found the same behaviour at high values of p_{O_2}, but the existence of a p_{O_2}-independent ionic conductivity region was rather uncertain. At very low values of p_{O_2} ($\sim 10^{-15}$ atm. at 1000°C) the conductivity of the undoped ThO_2 showed signs of increasing with decreasing oxygen pressure, suggesting the beginning of an n-type electronic contribution.

The findings of Steele and Alcock were confirmed for ThO_2-Y_2O_3 electrolytes by Lasker and Rapp (10). For undoped ThO_2 the latter observed a very definite p_{O_2} -independent conductivity region; emf measurements showed that in this region the conductivity was more than 90°/o ionic. Again there were signs of n-type electronic conductivity in undoped ThO_2 at very low values of p_{O_2} ($\sim 10^{-18}$ atm. at 1000°C). In the region of p-type conductivity the variation with oxygen pressure was as $p_{O_2}^{\frac{1}{4}}$ for the undoped ThO_2 suggesting that the concentration of oxygen vacancies was constant and determined by the impurities present. Bauerle (49) came to the same conclusion for his specimens of undoped ThO_2. He found that for both undoped ThO_2 and ThO_2 doped with $YO_{1.5}$ (1, 5 and 10 mole °/o $YO_{1.5}$) the variation of conductivity with oxygen partial pressure in the p-type electronic conductivity region accurately followed a $p_{O_2}^{\frac{1}{4}}$ dependence.

The results of other investigations (41, 42, 50) involving transport number determinations support the above views of the conductivity of ThO_2 and ThO_2-based electrolytes.

Much of the previous work has been concerned with the effect of dopant concentration on the conductivity. Hund and

co-workers (38, 39, 40) observed an increase in conductivity as Y_2O_3 and La_2O_3 were added in solid solution in ThO_2. Volchenkova and Pal'guev (46, 51) measured the variation of conductivity of ThO_2 with additions of oxides of the Group II metals over the whole range of compositions, 0-100°/o of Group II oxide doping. They, too, observed an increase in conductivity with doping at least for CaO, SrO and BaO in concentrations up to about 15 mole °/o. This increase may be interpreted in terms of the migration of oxygen ions via a vacancy mechanism, in analogy with the behaviour of the ZrO_2 - CaO system (33,34). But the conductivity of the ZrO_2-based electrolytes is completely ionic in air, whereas this is not the case for those based on ThO_2. Since the measurements of both Hund and co-workers and Volchenkova and Pal'guev were carried out in air, the validity of the analogy is somewhat suspect.

However, in more recent work in which measurements have been carried out in conditions in which the conductivity of the ThO_2-based electrolytes is known to be ionic, it is quite reasonable to make comparisons with ZrO_2-based electrolytes. It is found that the ionic condutivity in the ThO_2 systems increases linearly with concentration of dopant in the manner expected. The deviation from linear behaviour observed by Steele and Alcock (18) and Larker and Rapp (10) at the higher dopant concentrations, for ThO_2 doped with CaO, Y_2O_3 or La_2O_3, can be explained by the formation of neutral dopant ion - oxygen vacancy dipoles or, as in the system ZrO_2-CaO (33), by vacancy ordering.

Most of the previous investigations of the conductivity of ThO_2 containing La_2O_3, Y_2O_3 or Group II oxides in solid solution give an activation energy of ionic conduction of the order of 1.1 eV (18, 10, 42). The activation energy for the total conductivity when the measurements are carried out in air has also been found to have approximately the same value (18,

40, 41, 46, 51). The work of Edwards, Rosenberg and Bittel (52) on the diffusion of oxygen in ThO_2 yielded an activation energy of 2.85 eV; this was interpreted as the activation energy of intrinsic oxygen diffusion. This would imply that the activation energy of approximately 1.1 eV found for ionic conductivity in ThO_2–based electrolytes and also in undoped ThO_2 is that for impurity controlled, or extrinsic, conductivity. This value agrees reasonably well with that for extrinsic oxygen ion conductivity (1.26 eV) in the similar cubic fluorite solid solution, 0.85 ZrO_2–0.15CaO (53).

The effect of measuring frequency on conductivity

In the high temperature electrical conductivity studies of previous workers on ZrO_2 or ThO_2 or oxide electrolytes like 0.87 ThO_2–0.13$YO_{1.5}$ or 0.85ZrO_2–0.15CaO the frequency at which the measurements were carried out does not appear to have been regarded as an important variable. Usually the only information given is the frequency at which the measurements were carried out, which is usually about 1000 c/s. Sometimes all that is said is that alternating current was used (54). Direct current measurements have generally been avoided, presumably because of a realization of the possibility of space charge polarization effects.

Some previous workers (55) have measured the conductivity using an a.c. four terminal method. This method eliminates the possibility of electrode polarization effects, but still leaves the possibility of grain boundary polarization in polycrystalline specimens. In some cases it was found that the results of two and four terminal methods were the same (56, 57). This implies that, even for the two terminal measurements, electrode polarization is unimportant. Dixon et al. (58) found that their four terminal measurements on stabilized zirconia

were independent of frequency for the temperatures at which this was checked. This means that in this case there was neither electrode nor grain boundary polarization effects of any significance, unless their spot checks happened to be carried out under conditions in which a constant grain boundary polarization contribution, independent of frequency, existed.

The general picture that emerges is that for a.c. measurements there are no polarization effects: where these effects are looked for, they are found not to exist; and even when no attempt is made to avoid them the linearity of most of the graphs of the logarithm of the conductivity against the inverse absolute temperature makes it reasonable to assume that there are no complicating effects due to polarization.

However, both the work of Danforth and Bodine (59,60) on ThO_2 single crystals and Vest and Tallan (61) on polycrystalline $0.85ZrO_2$–$0.15CaO$ show the existence of long–time polarization effects due to blocking of ions at the electrodes. So in principle the a.c. conductivity may be affected by this. In practice the effects would be expected to be most noticeable at high temperatures and low frequencies. Wimmer, Bidwell and Tallan (42) found that, to obtain conductivity values for $0.13YO_{1.5}$–$0.87ThO_2$ at 900°C to 1600°C which were independent of frequency they had to carry out their measurements at 50 kc/s, above which the conductivity was independent of frequency. This confirms that in some cases polarization effects will affect the a.c. conductivity value.

The work of Wachtman (15) is also of some relevance to the present investigation. For ThO_2 doped with 1.5 mole °/o CaO Wachtman observed an internal friction peak and a dielectric

loss peak due to the movement of oxygen vacancies around substitutional Ca ions, to which they were bound to form neutral dipoles. The dielectric loss peak occurred at 695 c/s at 246°C and 6950 c/s at 310°C. From the variation with temperature of the frequency at which this peak, and that due to internal friction, occurred Wachtman estimated that the energy to move an oxygen vacancy from one nearest neighbour position of a Ca ion to another was 0.93 eV. For conductivity measurements at temperatures above 500°C it is unlikely that the effect of this dipolar dielectric relaxation will be noticeable at frequencies below 20 kc/s; 20 kc/s will correspond to an angular frequency less than ω_A in Fig e on Page 30.

3.4. Programme of research

Previous work (18,46,51) suggests that when CaO or SrO is added to ThO_2 in concentrations of less than 1 mole °/o, the conductivity increases linearly with doping. The initial intention was to investigate this behaviour. The conductivity was to be examined as a function of oxygen partial pressure, temperature (over the range 500° – 1450°C), and concentration of dopant (< 1 mole °/o). The effect of measurement frequency was also to be examined to confirm that, above a few hundred cycles per second, the conductivity was independent of frequency.

However, it was found that addition of 1 mole °/o CaO produced an increase in conductivity in air of only 60°/o. This was smaller than expected and considered too small to enable an accurate determination of the variation of conductivity with concentration of CaO, at concentrations less than 1 mole °/o, to be obtained. Also it had been found that the conductivity of undoped thoria and of thoria containing 1 mole °/o CaO was strongly dependent on frequency, behaviour which had not previously been reported. So it was decided to examine the

the conductivity of thoria doped with concentrations of CaO and SrO greater than 1 mole %, looking particularly closely at the frequency dependence of the conductivity.

Ideally, conductivity mechanisms in solids should be investigated using single crystals. As single crystals of ThO_2 are virtually unobtainable commercially and an attempt at producing them in the laboratory would be a major project in itself, it was necessary to use polycrystalline specimens. These were to be prepared by the method of cold compacting and sintering.

As this was a completely new field of research in the Engineering Department at Glasgow University, all the required equipment had to be either bought or constructed before any conductivity measurements could be made. A great deal of time was spent on this preparatory work, which is described in detail in the next chapter.

CHAPTER 4

EXPERIMENTAL EQUIPMENT

EXPERIMENTAL EQUIPMENT

4.1. Sintering furnace

An essential piece of equipment for producing dense polycrystalline specimens of a refractory material is a high temperature sintering furnace. When this research was started there were none available commercially which would suit all the requirements and so it was decided to build one. The design finally chosen was a modified version of a furnace described by Arthur and Priest (62).

This furnace is shown in Figs 1 and 2. The casing consists of a double walled copper cylinder with both ends of the annular region closed by brass flanges. In operation cooling water is passed between the cylinders. Brass end-plates, with copper cooling coils soldered to their outside surfaces, are fitted to the top and bottom by means of O-ring seals. A quartz window at the end of a copper tube is fitted to the top plate for temperature measurement with an optical pyrometer. The window is kept clean by means of a steel shutter under the top end-plate. This shutter is fitted to one end of a brass rod which passes through the top plate to a knurled knob outside the furnace. An O-ring in a machined groove in the rod provides a vacuum tight seal even on rotation of the rod. At high temperatures the rod tends to become very hot and so it is essential to water-cool it in case the O-ring deteriorates.

The power leads are internally water-cooled circular copper rods, brought into the furnace by means of the arrangement (63) shown in Fig 3. The brass collar B is brazed to the furnace base-plate A to get a leak-proof join. When C, also of brass, is screwed into B the rubber tubing is compressed and vacuum

tightness is obtained. The pieces of Tufnol ensure that the leads are electrically insulated from each other and from the casing, and also help to keep the leads firmly in position. The channels for the cooling water, are shown by dashed lines. They are produced by drilling two holes 1/4in. diameter to 5/16in. from the bottom of the solid copper bar. These are connected to the tubes D by drilling in from the side. Another hole 3/5in. dia and 3/8in. deep is then drilled out of the centre of the top of the bar. When a plug 3/16in. deep is soldered into this hole a continuous channel for the cooling water is obtained.

The furnace chamber is connected to diffusion and backing pumps through a water cooled side tube, a baffle valve and a cold trap. A Penning gauge on the side tube gives the pressure reading.

The slit cylindrical heating element shown in Fig 4 is made completely of tantalum. Parts **A** are 0.010in. thick sheet formed into half cylinders. These are encircled at the top by a ring B of .020in. thick metal to leave two diametrically opposite slits about 1/8in. wide. To obtain a reasonably uniform hot zone .020in. sheet C is also added to the bottom of the element. The legs are made from five 1/2in. wide strips of tantalum, four of which are 0.020in. thick and the fifth, 1/2in. shorter than the others, 0.030in. thick. These are joined together to form 0.110in. thick leads, the shorter strip placed in the middle forming a .030in. wide slot. The tops of the leads are bent to 3/4in. radius and the element is then fitted into the slots left by the shorter strips. The pieces of metal are joined either by rivetting or spot-welding. Both methods proved satisfactory.

The radiation shielding rests on a .020in. molybdenum plate raised 4in. from the base-plate by three steel legs. The

side shielding consists of two concentric cylinders, the inner of tantalum 3.3in. dia and 7.5in. high, the outer of stainless steel 4in. dia and 8in. high with 8 turns of molybdenum sheet (not in diagram) dimpled to minimise contact between turns, between the two. The shielding above and below the element is composed of six discs, again dimpled, the inner four of tantalum, the outer two of molybdenum. The top shields have a hole 1/4in. dia to allow temperature measurement and the bottom shields have holes to allow passage of the legs of the heating element and the tungsten specimen support stand. Great care must be taken in assembly to ensure that the heating element legs do not touch the bottom shields. All the shielding is made from .005in. sheet.

Initial temperature measurements were made using a W5%Re-W26%Re thermocouple passing through the top plate into the hot zones. However, it was very difficult to produce a satisfactory hot junction and even more difficult to position the thermocouple without breaking it at the hot junction so an optical pyrometer was adopted as the means of measuring temperature.

Power was obtained from the 13 Amp, 240 Volt mains supply through a continuously variable autotransformer (Variac), with a maximum output current of 20 Amp, and a 23:1 step down transformer.

The furnace has a very small heat capacity so any increase in input voltage produces an almost immediate rise in temperature to the temperature corresponding to the new voltage setting. A slow average increase in temperature produced by a series of finite voltage increments in fact subjects any ceramics in the furnace to a series of thermal shocks, as some shattered crucibles

showed. Driving the Variac with a motor overcame this problem as well as saving time. By using a slow speed motor and three sets of very high reduction ratio gear wheels it was possible to obtain an almost constant heating rate of 400°C/hour over the range 0 – 2000°C. The furnace could be cooled overnight by use of a micro-switch arranged to switch off the motor, operating in reverse, when the input voltage dropped to zero. With use at high temperature the element became thinner due to volatilization. So, although a power input of 3.1 K watts could produce a temperature of 2000°C with an element which had been heated for some time, when a new one was substituted the maximum temperature obtainable with this power was only 1875°C.

The pressure inside seldom rose to above 3×10^{-5} mm Hg even when the furnace was at 2000°C.

4.2. Compacting equipment

Before being sintered the oxide powders were cold compacted at high pressure into discs.

The first compacting die used consisted of a cylinder of Stubs steel 3ins. long, 1.1ins. outside diameter with a hole down centre of diameter 0.45in. The pressure was applied by two opposing plungers also of Stubs steel. The abrasion resistance of the internal surface of the die and of the surfaces of the plungers was improved by hardening to about 900 V.P.N. by quenching in a solution of salt from 770°C. According to Timoshenko (64) the maximum pressure P which can be applied before yielding of the inner surface begins is given by

$$P = \frac{Y}{2} \frac{b^2 - a^2}{b^2}$$

where Y is the yield point and a and b are the inner and outer radii.

Taking the yield point of Stubs steel as 36 tons/in , it can

be seen that for the above die the maximum compacting pressure permissible is 15 tons / in^2. The pressure actually used was 10 tons / in^2.

Specimens were prepared by dry-pressing ThO_2 powder in this die at 10 tons / in^2 and heating them for 2 1/2 hours in the sintering furnace at 1600°C. However, this method had serious limitations: the specimens were badly cracked due to the absence of an uniform compacting pressure throughout the powder; the outside of the specimens were seen to have picked up some steel contamination from the inside of the die; and the density obtained was only 79% of theoretical.

An attempt was made to overcome these limitations by applying hydrostatic pressure to the powder through an organic medium. The organic material used was a proprietary polyvinyl chloride gel, ''Vinamold'' , which under high pressure behaves substantially as though it were a liquid (65). The use of hydrostatic pressure did in fact eliminate cracking and any P.V.C. contamination was removed by heating in air.

The arrangement used for compacting[66] is shown in Fig 5. The die and plungers are made from EN 24 steel heat-treated to have a yield point of 55 tons/in^2. The Vinamold pieces A and B are made by heating the Vinamold to about 150°C and casting the resulting liquid into moulds designed to produce the desired shape and dimensions. When it has cooled the Vinamold remains firm and retains the shape of the moulds. To stop the Vinamold extruding past the plungers under pressure hard rubber discs 1/4 in. thick are placed between the plunger faces and the P.V.C. gel as shown. When the rubber is compressed it expands laterally and provides a tight seal which contains the Vinamold. Using this arrangement it is possible to have fairly large clearances ($\sim$ .005 in.) between the outside of the plunger and

the inside wall of the die. Applying to this die the previously quoted formula it appears that plastic yielding of the inner surface should begin at 26 tons/in^2. In fact pressures of 30 tons/in^2 were employed without any noticeable deformation. This may be because the radial pressure on the inner wall of the die is exerted only on that area in contact with the Vinamold, which is only about 1/3 of the total internal surface. The quoted formula assumes pressure on the entire inner surface.

As noted by Steele (66), a difficulty sometimes encountered with this method was the embedding of the oxide powders in the walls of the mould with the resultant pulling apart of the compacts on releasing the pressure. However, it was found that using a poly-methyl methacrylate binder, as suggested by Steele, did not help at all when preparing specimens in a mould containing a cavity for the powder of depth 0.24 in. and diameter 0.65in. As much deeper cavities of the same diameter had been found in preliminary work to give perfectly good compacts without any binder, it was decided to increase the depth from 0.24 to 0.30in. Using cavities of this increased depth there was no difficulty in producing good compacts with or without the addition of binder.

4.3. Furnace and specimen holder used in conductivity measurements

The furnace constructed for use in the electrical conductivity measurements is shown in Figs 7 and 8.

It consists of a Purox recrystallized alumina tube, 2.55 in. O.D. x 2.16 in. I.D. x 31 in. long, wound over the middle 12in. with 20 s.w.g. Pt/10% Rh alloy wire. The central 2lin. of the tube are enclosed in a dural cylindrical case, 12in. diameter, with Sindanyo end-plates. The insulation is pure alumina powder for 2in. out from the windings and Morgan M.I. 28 firebrick for the remaining volume. Inside this tube fits another also of recrystallized alumina and with dimensions 1.81in. O.D.

x 1.5in. I.D. x 35in. long. The specimen whose conductivity is to be measured is placed within the inner tube. In the first measurements of conductivity an earthed molybdenum sheet was wrapped round the inner tube, the molybdenum being protected by forming gas ($90^{o}/_{o}N_2$ + $10^{o}/_{o}H_2$) flowing through the annular region between the two tubes. In subsequent measurements the molybdenum sheet was dispensed with as experimental results showed that it did not affect the results obtained.

To protect the Mo sheet by forming gas it was necessary to make the annular region gas-tight. As conductivity measurements were to be made in different atmospheres it was also necessary to make the inner tube gas-tight. This was achieved by means of O-ring seals, the O-rings being compressed against the tubes by brass end-piece as shown. It was found that the tubes used were not accurately circular in cross-section and the brass pieces fitting over them had therefore to have an internal diameter slightly greater than the maximum tube diameter. Despite this it was possible to get vacuum tight sealing, although in some cases it was necessary to smooth the outside of the alumina tube with SiC paper and then rub in some vacuum grease. To lessen the chance of problems arising associated with the differential thermal expansion of brass and alumina, viz. cracking of the alumina tubes or loss of vacuum tightness in the O-ring seals, it was necessary to maintain the ends of the tubes as close as possible to room temperature. So alumina radiation shields were used inside the inner alumina tube; the parts of the outer tube outside the furnace casing were cooled by water flowing in copper coils wound tightly round the tube on top of aluminium foil; and the brass end-pieces were also water cooled. The radiation shields were made by cutting slices, 1/10in. thick, off a rod of machinable alumina. Six were used at the top and

bottom of the furnace and they were positioned approximately at the same level as the ends of the furnace casing. The top ones were suspended by a nichrome wire and separated by alumina beads. The bottom ones were supported on an alumina tube, which encircled the tube supporting the specimen, and were separated by other pieces of alumina tube (see Fig 10).

The disc specimen on which measurements are to be made is positioned in the hot zone by means of the spring-loaded holder shown in Figs 8, 9 and 10. The central alumina tube is positioned firmly in the bottom brass piece. A channel 1/16in. diameter is drilled in this brass piece parallel to and just outside the central tube to ensure easy flow of gas into the furnace. The specimen, with 0.005in. Pt foil electrodes on either side in contact with the Pt paste previously baked onto its flat surfaces, is placed between two alumina discs on top of the central tube and held there ~~by means of the pressure exerted~~ by means of the pressure exerted by the springs. A Pt - Pt 13$^{o}/_{o}$Rh thermocouple is spot welded to the bottom electrode. This enables the temperature of the specimen to be measured and also provides a lead (the alloy wire) for conductivity measurements. The thermocouple wires pass inside the central tube, as shown, down the tube, insulated from each other by small twin bore alumina insulators, and out at the bottom through a Tufnol plug. The other lead is a Pt 13$^{o}/_{o}$Rh wire spot-welded to the top electrode. This passes down a thin alumina tube and out of the bottom in the same way as the thermocouple. The three wires are brought through the wall of the brass end-piece by means of a vacuum seal consisting of rubber compressed between two pieces of Tufnol (Fig 8).

The weight of the alumina tubing , specimen holder and brass end-pieces is supported on a steel ring connected to the

stand on which the furnace sits by means of steel strips.

The temperature of the furnace was controlled by means of an Ether Proportional Controller in conjunction with a saturable reactor. The Pt – Pt 13% Rh control thermocouple was placed in the annular region just inside the tube holding the furnace winding and positioned so that its hot junction was about 2in. short of the centre of the hot zone. This enabled the temperature to be controlled to within ± 1°C over a period of several hours and up to the maximum operating temperature, 1450°C.

4.4. Atmospheres used in conductivity measurements

The conductivity was measured in different atmospheres in order to find out how it varied with oxygen partial pressure, p_{O_2}. The atmospheres used and the corresponding p_{O_2} are shown below:–

Atmosphere	p_{O_2} (atmospheres)
vacuum produced by rotary pump	Estimated to be in the range 10^{-4} to 10^{-6}
B.O.C. argon, containing < 10 ppm O_2	estimated to be in the range 10^{-4} to 4×10^{-6} (depending on flow rate)
Air Products argon containing < 4 ppm O_2	estimated to be in the range 10^{-4} to 2×10^{-6} (depending on flow rate)
argon containing 0.1% O_2	10^{-3}
wet forming gas	1.6×10^{-11} at 1500°C to 2.3×10^{-30} at 500°C.

The pressure produced by the rotary pump was measured by means of two widely separated Pirani gauges, one near the pump and the other at the far end of the furnace from the pump. The pressure readings were not the same so it was not possible to estimate accurately the oxygen partial pressure at the specimen. Instead the expected range of p_{O_2} at the specimen is quoted above.

The gases were passed from cylinders through polythene tubing of 1/8in. wall thickness, then through a Platon flowmeter and into the furnace. On leaving the furnace they were bubbled through dibutyl phthallate to prevent any backstreaming of air. The low vapour pressure of dibutyl phthallate meant that it was unlikely to contaminate the furnace atmosphere. The whole system of tubing, flowmeter and furnace was leak tested before experiments, using a Leybold leak detector and 'Freon' gas (CCl_2F_2). Polythene tubing of 1/8in. wall thickness was found to be vacuum tight, unlike that of 1/16in. wall thickness or rubber tubing. Inside the furnace the total gas pressure was always atmospheric (except when vacuum was used).

The conductivity in argon containing only a few ppm O_2 was found to be dependent on the flow rate. This is discussed in Chapter 6 and is the reason why a range of p_{O_2} rather than a specific value is given above.

No attempt was made to dry the argon as a calculation, similar to the one given below for wet forming gas, shows that for the B.O.C. argon, which contains < 8ppm H_2O (Manufacturer's specifications), the p_{O_2} due to dissociation of the water present at 1400°C is $< 10^{-8}$ atmospheres, which is much less than the lowest estimated value due to the free O_2 present (4×10^{-6}atm.) Similarly for the other sources of argon traces of water present do not have an appreciable effect on the oxygen partial pressure. The same holds for the dissociation of traces of CO_2. Therefore, for the argon supplies used the oxygen partial pressure is due solely to the free oxygen present and is independent of temperature.

The forming gas, consisting of 90°/o N_2 and 10°/o H_2 (by volume), was passed through a bottle of water immersed in ice in a Thermos flask, and then into the furnace. The dew point

of the wet forming gas was measured as 4.5°C and hence the value of p_{O_2} as a function of temperature could be calculated.

p_{O_2} due to forming gas (90°/o N_2 + 10°/o H_2) saturated with water vapour at 4.5°C.

Consider 10 moles of forming gas saturated with water vapour at 4.5°C.

We have 9 moles N_2 + 1 mole H_2 + n moles H_2O.

We know that $p_{N_2} + p_{H_2} + p_{H_2O} = 1$ atm.

Assume all components i behave as ideal gases. Then

$$\frac{p_i}{n_i} = \frac{RT}{V}$$

where p_i = partial pressure of component i
n_i = no. of moles of component i
R = gas constant
V = volume occupied by the gases
T = Absolute temperature

$$\therefore \frac{p_{H_2}}{n_{H_2}} = \frac{p_{N_2}}{n_{N_2}} = \frac{p_{H_2O}}{n} = \frac{\text{total pressure}}{\text{total no. of moles}}$$

p_{H_2O} = saturated vapour pressure of H_2O at 4.5°C = .00828atm.

$p_{H_2} + p_{N_2} = 1 - 0.0083 = 0.9917$atm.

$$p_{N_2} = \frac{n_{N_2}}{n_{H_2}} p_{H_2} = 9\, p_{H_2}$$

$\therefore p_{H_2} = 0.09917$atm.

$$n = n_{H_2} \cdot \frac{p_{H_2O}}{p_{H_2}} = \frac{0.00828}{0.09917} = 0.0834 \text{ moles}$$

Now consider this wet gas going into a furnace at temperature T. Assume the fraction of H_2O dissociated is x. The dissociation reaction is

$$H_2 + 1/2\, O_2 = H_2O$$, with equilibrium constant K

We now have
(1 + nx)moles H_2 + 9 moles N_2 + (1/2)nx moles O_2 + (1 − x)n moles H_2O

$$\therefore p_{H_2O} = \frac{n(1-x)}{10 + n + (1/2)nx} \quad ; \quad p_{H_2} = \frac{1 + nx}{10 + n + (1/2)nx} \quad ;$$

$$p_{O_2} = \frac{(1/2)nx}{10 + n + (1/2)nx}$$

From the law of mass action

$$p_{O_2} = \left(\frac{p_{H_2O}}{p_{H_2}}\right)^2 \frac{1}{K^2}$$

$$= \left(\frac{n(1-x)}{1+nx}\right)^2 \frac{1}{K^2}$$

$$= \frac{n^2}{K^2} \qquad \text{since } x \ll 1 \quad (\text{At } 1400^\circ C,\ x \approx 10^{-10})$$

$$\therefore \quad p_{O_2} = \frac{7 \times 10^{-3}}{K^2}$$

We also know that $\Delta G^\circ = -RT \ln K$

where ΔG° is the standards Gibbs free energy change.

In the reaction $H_2 + 1/2 O_2 = H_2O$

$$\Delta G^\circ = -59{,}000 + 13.38T$$

$$\therefore \quad K = \exp\left(-\frac{\Delta G^\circ}{RT}\right) = \exp\left(\frac{59{,}000}{1.9872\ T}\right) \exp\left(\frac{-13.38}{1.9872}\right)$$

So we have

Temp. ($^\circ C$)	K	$p_{O_2} = \frac{n^2}{K^2}$ (atm.)	$\log_{10} p_{O_2}$
500	5.5×10^{13}	2.315×10^{-30}	−29.6355
600	7.762×10^{11}	1.16×10^{-26}	−25.9355
700	2.147×10^{10}	1.52×10^{-23}	−22.8182
800	1.18×10^{9}	5.03×10^{-21}	−20.2984
1000	1.53×10^{7}	2.99×10^{-17}	−16.5243
1400	5.9×10^{4}	2.01×10^{-12}	−11.6968

These data are shown graphically in Fig 15.

4.5 Electrical conductivity measuring equipment

The electrical conductivity of metal oxides is very dependent on temperature, usually exponentially. So when measuring their conductivity as a function of temperature it is necessary to use a technique which will cover a wide impedance range. A bridge using the transformer ratio-arm principle satisfies this requirement and in this investigation a commercially available model, Wayne-Kerr B 221, was used (the impedance range covered by this bridge is 10^{-4} ohm and 10 farad to 10^{11} ohm and 10^{-15} farad). This bridge in its basic form operates at a fixed frequency of 1592 c/s. To investigate the variation of conductivity with frequency additional signal generating and detecting equipment was required, and this too was obtained from the Wayne-Kerr Company (S121 Audio Signal Generator and A 321 Waveform Analyser). With this equipment measurements of conductance G and capacitance C can be made over the range 30c/s to 20kc/s with an accuracy of $\pm$ 0.1%. From the measured values of G and C the dielectric loss tangent $\tan\delta$ can be calculated using the relation $\tan\delta = \frac{G}{\omega C}$, where ω is the measuring frequency in radians/sec.

CHAPTER 5

EXPERIMENTAL WORK

EXPERIMENTAL WORK

5.1 Preparation of specimens for conductivity measurements

The method used to prepare specimens was similar to that used by Steele (66). An outline of this is given below:

(i) The quantities of nitrates required to give the desired composition were calculated. Solutions of the nitrates in distilled water were prepared and mixed. (All nitrates are soluble in water; liquids mix more readily than powders).

(ii) The nitrate solution was evaporated to dryness by slow heating over a bunsen, with continuous stirring to avoid fractional crystallization. The flame was turned up and heating was continued until the nitrates had decomposed to the oxides.

(iii) The oxides were ground in an agate mortar and then calcined in air for 24 hours at 1000°C inside a closed thoria crucible.

(iv) The oxide powders were again ground and then compressed in the Vinamold at 30 tons/in^2, to produce approximately disc-shaped pellets.

(v) The compacted pellets were heated to about 1100°C to remove any contamination by the P.V.C. gel (and binder if it was used).

(vi) The pellets were now sintered in the vacuum furnace at 2000°C for 2 – 6 hours inside a closed thoria crucible.

(vii) The sintered pellets were heated in air at 1150°C for 12 hours to restore stoichiometry.

(viii) The pellets were now ground down to give discs with accurate geometrical dimensions.

(ix) The discs were placed in 50% nitric acid for one minute

to remove metallic impurities from the surface, washed in water, then acetone and heated to 1000°C to remove any surface organic contamination.

(x) To obtain good electrical contacts platinum paste (Johnson-Matthey N 758) was painted on the flat surfaces. The paste was allowed to dry in air and then baked on at 1000°C.

The specimens were now ready to be used for conductivity measurements.

Kantan et al. (67) found that , for a maximum sintering temperature of 1700°C, undoped thoria pellets prepared from the oxalate were denser than those prepared from the nitrate. But Steele showed that, if the above procedure was followed, the nitrate gave as high a density as the oxalate and also involved less risk of having two phases present in the doped materials. Kantan et al. agree with Steele that the optimum calcining temperature of thoria prepared from the nitrate is about 1000°C and the optimum compacting pressure is 30 tons/in^2. They showed that the density increased up to this pressure, but not significantly beyond it. The densities obtained by Steele were 95°/o of theoretical for undoped, and above 99°/o for ~~the~~ doped, thoria. So Steele's preparation method was used in the present work.

The grinding of the sintered pellets was done in several stages. First the pellet was placed in the recess a in the brass device shown in Fig 6 and ground down on SiC paper until the lower face was smooth. The pellet was then reversed, level AA^1 was lowered, and the other face was also ground smooth. Repetition of this process produced accurately parallel faces. The pellet was now put in a lathe between Tufnol pressure pads and ground to a circular cross-section using emery paper over the blunt end of a cutting tool. The flat faces were then reground as before to remove any chipped edges produced in the

lathe grinding. The final grinding of the flat faces was on 600 grit SiC paper.

The dimensions of the specimens were measured with a micrometer. The values for those used in conductivity measurements were:

specimen	diameter (cm.)	thickness (cm.)
undoped ThO_2, T.4.	1.252 ± 0.005	0.510 ± 0.001
undoped ThO_2, T.5.	1.236 ± 0.005	0.484 ± 0.001
0.99 ThO_2 – 0.01 CaO	1.242 ± 0.004	0.2915± 0.0002
0.95 ThO_2 – 0.05 CaO	1.143 ± 0.004	0.2624± 0.0002
0.95 ThO_2 – 0.05 SrO	1.191 ± 0.004	0.3056± 0.0002

5.2 Measurement of specimen densities

The densities of the specimens were calculated from measured values of the mass and geometrical dimensions. The results for the compositions whose electrical properties were examined are:

100% of theoretical for 0.95 ThO_2 – 0.05 CaO
89% of theoretical for 0.99 ThO_2 – 0.01 CaO
88% of theoretical for 0.95 ThO_2 – 0.05 SrO
83% of theoretical for undoped ThO_2

The error in the densities is within ± 1.5%

The low density of the undoped ThO_2 specimens may be due to the shorter calcination time (10 hours) and lower sintering temperature (1850°C) used in their preparation compared to the other specimens (24 hours and 2000°C). An attempt was made to increase the density of the SrO–doped pellets by repeating the sintering treatment they had received (6 hours at 2000°C), but no change in density resulted.

5.3. Polishing and microscopic examination of specimens

The microstructure of samples of the compositions used for electrical conductivity studies was examined.

Specimens were mounted in a thermosetting plastic and then polished, first on several grades of SiC paper (220, 320, 400 and 600 grit), and then on Selvyt polishing cloth impregnated with diamond powder. Four sizes of diamond were used – 30, 6, 1 and 1/4 micron. The polished specimens were then etched in hot phosphoric acid for between 5 and 25 minutes.

The polished specimens, etched and unetched, were photographed through a microscope. So also was a calibrated grating, at the same magnifications. All the photographs were enlarged by the same amount and so, by comparing the specimen photographs with those of the grating, the grain size could be estimated.

Some of these photographs are shown in Figs 11 – 13. Measurements of grain size yielded the following results:–

Specimen	Range of grain diameters (micron)	Approximate average grain diameter (micron)
ThO_2	4 to 27	15
0.99 ThO_2.0.01 CaO	5 to 35	20
0.95 ThO_2.0.05 CaO	7 to 50	30
0.95 ThO_2.0.05 SrO	14 to 40	30

The porosity of the specimens can be clearly seen on the unetched surfaces. Although examination of polished sections has been used to measure porosity quantitatively (68), it is not believed that this could be done in this instance without a much closer investigation of the progress of the polishing. However, these photographs certainly give a qualitative idea of the specimens' porosity and these are in agreement with the measured density value.

It can be seen from the photographs that the porosity is

confined entirely to the grain boundaries.

5.4. Measurement of leakage resistance

To obtain accurate values of the resistance of a specimen care must be taken to ensure that any resistance in parallel with the specimen (the leakage resistance) is comparatively large. The specimen holder described in Chapter 4.3. is designed so that the leakage path is through rubber and Tufnol at room temperature, and alumina at temperatures low in comparison with that of the sample. So the leakage resistance is expected to be high.

To verify this the specimen holder was inserted in the furnace as in Figs 9 and 10 except that the top platinum foil was removed from beneath the top alumina disc and allowed to hang beside the alumina tube containing the top electrode lead. The furnace was now heated and the leakage resistance measured as a function of temperature. It was found that this resistance was indeed very high, being much larger than that expected for the thoria specimens. The resistance of a thoria specimen in forming gas (the highest resistance encountered in this work) was found to be less than 0.1°/o of the leakage resistance at all temperatures investigated. The error introduced by the leakage resistance will therefore be of this order and so will be unimportant.

Some values are given below:-

Temperature (°C)	Conductance of ThO_2 specimen in forming gas (Mho)	Leakage conductance (Mho)	$\frac{\text{specimen resistance}}{\text{Leakage resistance}} \times 100$
1400	6×10^{-3} (estimated)	3×10^{-6}	0.05
1164	10	1.8×10^{-7}	0.02
925	6×10^{-5}	10^{-8}	0.016
630	3.4×10^{-6}	2.4×10^{-9}	0.07

The conductance of the ThO_2 specimen at 1400° C had to be estimated

from the graph of log (conductivity) against T^{-1} since the highest temperature at which it was measured was 1300°C.

5.5. Measurement of lead resistance.

As the temperature rises the increase in resistance of the electrode leads, i.e. the alloy leg of the thermocouple and another single Pt 13°/o Rh wire, each of 0.020. in diameter, is accompanied by a marked decrease in the resistance of the oxide specimens. In case the resistances became comparable at high temperatures, the lead resistance was measured (using the Wayne Kerr Low Impedance Adaptor Q221) as a function of temperature by short-circuiting the leads at the specimen. The results are shown in Fig. 14. In some cases the lead resistance is about 19°/o of the specimen resistance and would introduce an appreciable error if not allowed for.

5.6. Measurement of stray capacity

Using the same arrangement as that for measuring leakage resistance the stray capacity was measured as a function of frequency (300 – 20,000 c/s) and temperature (400°C – 1400°C) while the furnace power was on. The stray capacity was found to be independent of frequency and to increase slightly with temperature. The value was always in the range 6 to 10 pF.

The geometrical capacity of the electrodes when separated by a vacuum gap and arranged as for measurements of specimen capacitance and conductance was calculated to be about 0.5 pF.

5.7. Measurement of the conductivity and capacitance of oxide specimens

The electrical conductance of specimens of undoped ThO_2, ThO_2 doped with CaO (1 and 5 mole °/o) and ThO_2 doped with SrO (5 mole °/o), prepared as described in Section 5.1, was

was determined as a function of temperature (500°C – 1450°C), frequency (30 – 20,000 c/s), and oxygen partial pressure (using the atmospheres described in Section 4.4.). To measure conductance with the Wayne Kerr Bridge it is necessary to balance the bridge for both capacitance and conductance. The capacitance of the specimens was also noted. In interpreting the complex conductivity behaviour observed, this capacitance reading was of great importance both in itself and because, when combined with the conductance, it enabled the dielectric loss tangent to be determined.

The specimen on which measurements were to be made was inserted in the furnace as shown in Figs 9 and 10. Values of conductance G and capacitance C were taken at 1592 c/s over one or two heating and cooling cycles in the atmospheres of interest. At temperature intervals of 100 – 200°C the variation of G and C with frequency was noted. Values of G and C agreed within 10°/o for increasing and decreasing temperatures and for successive cycles. The specimen was left at the measuring temperature until steady conductance and capacitance values were obtained. The time required for equilibration after a change in either temperature or oxygen partial pressure varied from about 1/2 to about 3 hours depending on the temperature. The effect of furnace temperature drift, which, because of the associated conductance drift, could hide the fact that equilibrium had been reached, was allowed for by estimating the change in conductance due to a given change in temperature. The conductance can always be related to the Absolute temperature T, at least for small temperature intervals, by the relation

$$G = \text{constant} \cdot \exp(-\varepsilon/kT)$$

where ε is the empirical activation energy and k is Boltzmann's constant. By differentiating this expression the percentage

change in conductance due to a change δT in temperature is found to be given by

$$100 \frac{\delta G}{G} = \frac{\varepsilon}{kT^2} \delta T.$$

A similar expression holds for a change δC in capacitance with temperature.

Errors in conductance and capacitance are introduced through errors in temperature measurement and in balancing the bridge. Another worker (69) in the same laboratory as the author calibrated a large number of Pt – Pt 13°/o Rh thermocouples against a standard thermocouple obtained from the National Physical Laboratory and accurate to $\pm$ 0.3C°. Since all the thermocouples calibrated gave a reading within the accuracy of the standard, it seems reasonable to assume that the thermocouples used in the electrical conductivity measurements, which were not calibrated, were also accurate to within this limit of $\pm$ 0.3C°. From the relation above between δG and δT, it follows that if, for example, ε = 1 eV, T = 1000°K, $\delta T = \pm$ 0.3C° then the error in G is $\pm$ 0.36°/o. In the present investigation it is estimated that the errors in G and C due to temperature inaccuracies were always within $\pm$ 1°/o.

The error in reading the scale values of G and C is $\pm$ 0.1°/o. But as there is also some difficulty in knowing precisely when the bridge is balanced, the error in the bridge measurements is higher, about $\pm$ 0.5°/o. So the total error in G and C is $\pm$ 1.5°/o. The dielectric loss tangent, $\tan \delta = \frac{G}{\omega C}$, has in addition an error due to frequency ω of $\pm$ 1°/o. So $\tan \delta$ is expected to be accurate to within $\pm$ 4°/o.

The above errors quoted for C and $\tan \delta$ do not include the effects of stray capacity, which is not allowed for in the values plotted in the results (Figs16-56). However the C and

and tan δ results are required for a discussion which is essentially qualitative and the effect of stray capacity can easily be allowed for when required (when the total capacity is less than about 80pF). In fact a close examination of the results shows that the presence of stray capacity does not significantly affect the general behaviour of graphs containing C and tan δ as one of the variables.

There were some occasions when it was found impossible to balance the bridge at all accurately, usually at low frequencies and/or low temperatures. In these cases the error may be as high as 50°/o. Any such results, if plotted, are indicated as being doubtful.

Specific conductivity values, σ, were obtained from the measured conductance G by means of the relation

$$\sigma = \frac{tG}{A}$$

where A is the area of the flat face of the specimen and t is its thickness. The error in conductivity values due to those in measuring the specimen dimensions is ± 1°/o. In estimating σ the lead resistance is subtracted from the total measured resistance.

So the total error in specific conductivity due to errors in measurement of temperature and specimen dimensions, and in balancing the bridge, are estimated to be ± 2.5°/o. No allowance has been made for any contact resistance effects or for specimen porosity.

The results of the electrical measurements are presented in Figs 16 - 56 and discussed in the following chapters.

CHAPTER 6

THE ELECTRICAL CONDUCTIVITY OF UNDOPED THORIA

DISCUSSION OF RESULTS

THE ELECTRICAL CONDUCTIVITY OF UNDOPED THORIA

DISCUSSION OF RESULTS

6.1. Introduction

The results of electrical conductivity measurements at 1592 c/s on undoped thoria are shown in Fig 16 as a function of temperature. Measurements were carried out on two specimens and the results agreed closely (for example, in air the conductivity values agreed within 1°/o at 1300°C and 10°/o at 700°C). The atmospheres used were air, B.O.C. argon, wet forming gas and vacuum. The results in vacuum are not shown in Fig 16, as they were very close to those in forming gas, and their inclusion would have confused the graph. However, they are shown in Fig 17. For this specimen composition the maximum temperature reached was only 1300°C, due to difficulties (later rectified) in controlling the furnace at higher temperatures.

The results of Fig 16 are replotted in Fig 17 to show the variation of the conductivity at 1592 c/s with oxygen partial pressure.

It was found that the conductivity in argon was dependent on the flow rate. This effect was present at all temperatures. It was measured at only one temperature, approx. 765°C, and the results are shown as a graph of conductance against flow rate in Fig. 18. The flow rates plotted are those of the argon as measured on a Platon flowmeter calibrated for air. As the specimen temperature did not remain constant, the temperature is noted beside each experimental point. The temperature drift cannot explain the changes in conductance observed (see Chapter 5.7.) It can be seen from Fig 18 that the conductance decreases as the flow rate increases to 1000 cc/min. For higher flow rates the conductance is comparatively constant. However, it was decided that the lack of reproducibility in these high

high flow rate results did not justify the use of so much argon and all subsequent measurements in argon, for both undoped and doped samples, were made at a constant flow rate of 200 cc/min.

The reason for this dependence of conductivity on argon flow rate is not known. However, it is known that conductivity decreases with decreasing oxygen partial pressure, p_{O_2}, so it seems reasonable to suggest that high flow rates correspond to lower p_{O_2} than low flow rates. Also as it is difficult to see how the gas can produce a lower p_{O_2} than that due to the oxygen content (in the case of B.O.C. argon $\leqslant$ 10 p.p.m.) it is suggested that the flat region in Fig 18 corresponds approximately to this minimum p_{O_2}, approximately 10^{-5} atm., and the lower flow rates give higher p_{O_2}. This idea is confirmed by the fact that at approximately 765°C the minimum observed conductivity in argon is within 10°/o of the value in vacuum, where p_{O_2} is expected to be about 10^{-5} atm., whereas the value in argon at 200 cc/min. is considerably higher.

No similar dependence of conductivity on gas flow rate has been described for two-terminal conductivity measurements. But Bauerle (49) found that the conductivity of ThO_2 and $ThO_2 - Y_2O_3$ samples measured using a four-terminal method was independent of gas flow rate only for flow rates above a certain value. He gave no explanation of the flow rate dependence at lower flow rates but assumed, as suggested above, that the oxygen partial pressure in the flow rate-independent region was that due to the oxygen content of the gas.

In the present investigation the conductivity in forming gas was independent of the flow rate.

6.2. Variation of conductivity with oxygen partial pressure

The conductivity of undoped thoria decreases with decreasing oxygen partial pressure (Fig 17) indicating the

presence of considerable p–type conductivity at high p_{O_2}, as found by other workers (10,18,47,55) and appears to become almost independent of p_{O_2} below about 10^{-8} atmospheres. On Fig 17 are also plotted the results of Lasker and Rapp (10) and Steele and Alcock (18). It can be seen that, although the conductivity values obtained in the present work are higher than those of the other investigators the slopes of the curves are very similar. However, it is not possible to get an accurate value of the slope obtained in the present work due partly to the uncertainty about the value of p_{O_2} in vacuum and argon, and partly to the lack of experimental points.

The occurrence of p_{O_2} –independent conductivity in a wide band gap material such as ThO_2 normally means that the conductivity is ionic (18). Lasker and Rapp, by means of galvanic cell emf measurements, showed that in the p_{O_2} –independent region the conductivity of their undoped thoria was predominantly ionic (the ionic transport number was greater than 0.9). Although the absolute values of conductivity of thoria prepared by different methods from starting materials of different impurity content vary considerably (Fig 19), transport numbers are more reproducible. For example at 1000°C in air the conductivity obtained by Subbarao et al. (41) (at 1000 c/s) is a factor 4 greater than that obtained by Lasker and Rapp (10) (at 1592 C/S), yet the average ionic transference number between p_{O_2} = 0.21 and 1 atm. is approximately 0.05 in both cases. Also the average ionic transport number of 0.70 obtained by Pal'guev and Neuimin (48) at 1000°C between Fe,FeO and Cu,Cu_2O electrodes agrees well with that of 0.78 obtained by Lasker and Rapp at the same temperature between Co,CoO and Cu,Cu_2O electrodes. As the p_{O_2} due to both Co,CoO and Fe,FeO lie in the p_{O_2} –independent region of conductivity the same transport number is expected for

these two cells. So it seems likely that in the present work too the region of p_{O_2} below about 10^{-8} atm. represents chiefly ionic transport.

The results of both Steele and Alcock (18) and Lasker and Rapp (10) indicate the appearance of n-type conductivity at very low p_{O_2}. This is also observed in the present work. As the temperature falls the oxygen partial pressure in the wet forming gas also falls (see Fig 15). As can be seen from Fig 16 when the temperature is 514°C ($10^4/T = 12.7$) the conductivity in forming gas (in which p_{O_2} is now 10^{-29}atm.) becomes larger than that in argon in which the conductivity is either purely ionic or ionic plus p-type electronic. This increase in the conductivity in forming gas at low p_{O_2} above that of the p_{O_2} -independent ionic conductivity can be attributed to n-type electronic conductivity.

Some idea of the ionic transport number t_i in atmospheres other than forming gas, in which t_i is assumed to be very close to unity, can be obtained from the ratio $t_i = \frac{\sigma_{ionic}}{\sigma_{total}}$ where σ_{ionic} is the conductivity in forming gas and σ_{total} is the conductivity in the atmosphere under consideration. This calculation shows that in air at all temperatures in the range 550° – 1300°C the conductivity is predominantly (> 70°/o) electronic. However, as will be shown later, little reliance can be put on the quantitative values obtained because of the dependence of the conductivity on the measuring frequency.

6.3. Variation of conductivity with temperature

Over limited ranges of temperature (sometimes hundreds of degrees) the conductivity of undoped thoria in all of the atmospheres used obeys the relation $\sigma = A \exp(-\varepsilon/kT)$ where A is a constant and ε is an activation energy or enthalpy (eV).

The results obtained at 1592 c/s are shown in Fig 16. Some other people's results are superimposed on these in Fig 19 for the purpose of comparison.

The results of the present investigation may be compared with those of other people under similar conditions e.g. two-terminal measurements on polycrystalline specimens at 1000°C and p_{O_2} = 0.21 atm. Under these conditions the present results are a factor 1.6 less than those of Subbarao et al. (41) at 1000 c/s, a factor 2 greater than those of Lasker and Rapp (10) at 1592 c/s and Volchenkova and Pal'guev (46) at 3000 c/s, a factor 5.6 greater than those of Steele and Alcock (18) at 1500 c/s and a factor 50 greater than those of Hund and Mezger (40) at 1000 c/s.

The slopes of the curves are in better agreement as can be seen from Fig 19. In air the slopes obtained by Subbarao et al., Hund and Mezger and Lasker and Rapp are almost identical with the present results. The results obtained in the present work in forming gas agree quite closely in slope with those obtained by Lasker and Rapp at the same oxygen partial pressures. However, neither the present results nor those of Lasker and Rapp give a straight line over the temperature range 800°–1100°C, despite Lasker and Rapp's claim that they do. These workers may have overlooked the non-linearity of their results because of the much smaller temperature range covered compared with that of the present investigation, because they took measurements at only four temperatures 800°, 900°, 1000° and 1100°C and because the investigation of the temperature dependence of the conductivity was not the main object of their research.

Considerable variation in the conductivity behaviour of the same ''pure'' oxides investigated by different workers is commonly found. For example Pappis and Kingery (70) collected

the results of many investigations on Al_2O_3 and found that '' "values for the conductivity reported by different investigators vary over several orders of magnitude and experimental activation energies of 1.5 to 4.0 eV have been reported for reasonably pure single crystals. A much wider range of values has been found for polycrystalline specimens''. So it is to be expected that there will also be some variation in results obtained for ''pure'' (i.e. undoped) thoria.

The precise reasons for these differences are not known although suggestions can be made. For example it is known that increasing impurity contents often increase the conductivity of ionic crystals (see Chapter 2.3.) The higher impurity content of the thoria used in the present work may explain its increased conductivity compared to the purer material used by Steele and Alcock. But it is often difficult to explain differences in this way as few investigators give details of the impurity contents of their materials. Other possible explanations are differences in density and contact resistance.

Edwards, Rosenberg and Bittel (52) measured the diffusion coefficient of oxygen in ThO_2 over the temperature range 800°–1500°C. They obtained an activation energy of 2.85 eV which they attributed to intrinsic, as opposed to impurity–controlled, diffusion. Since the activation energy of ionic conductivity (i.e. in forming gas) obtained in this investigation never exceeds 1.9 eV (the value of ε between 980° and 1160°C) it would appear that the ionic conductivity is controlled by the impurities present (see Appendix) up to the maximum temperature investigated. Any suspicion that the increase in slope at about 900°C is due to an extrinsic–intrinsic transition is shown to be false by ~~the fact that if the measurements are carried out at 20 kc/s this increase in slope vanishes (see Fig 20), and also by~~ the similar behaviour exhibited by the highly doped (5 mole%)

samples (see Figs 24 and 30). In fact the dip in the log σ vs. T^{-1} graph observed in forming gas is shown in Chapter 9 to be produced by space charge polarization at the grain boundaries.

The conclusion that the ionic conductivity is impurity controlled leads the author to suggest that in forming gas the difference between his results and those of Lasker and Rapp (Fig 19) is due to a higher purity of Lasker and Rapp's sample, which gives it a lower extrinsic ionic conductivity. Lasker and Rapp do not make clear what the concentrations of the impurities in their sample are, but do state that they are cations of valency less than four, Mg, Li, Na and K i.e. the type which will introduce oxygen ion vacancies. The slopes of the graphs of log σ vs T^{-1} in forming gas are similar in the two cases. This must mean that the blocking effects of the grain boundaries are similar and that the grains are approximately the same size (see Chapter 9).

At the highest temperatures reached it is thought that the conductivity may be close to that of bulk ThO_2 with little error introduced by interfacial polarization effects (see Chapter 9). If this is so the activation energy in forming gas between 1160° and 1300°C, 1.39 $\pm$ 0.14 eV, is the energy to move an oxygen vacancy plus, perhaps, a contribution to dissociate the vacancy from a mono-, di-, or tri-valent impurity ion, in accordance with the discussion of Chapters 2.4. and 3.2. However the lower activation energies found for ionic conduction in higher temperature ranges in 0.95 ThO_2 – 0.05 CaO and 0.95 ThO_2 – 0.05 SrO indicate that this value of 1.39 eV probably does in fact contain some effects of grain boundary polarization. This is confirmed by the work of Danforth and Bodine (59,60) on ThO_2 single crystals, with similar impurity content to the ThO_2 used in the present work, in vacuum. They stated that their

observed conductivity was >99°/o ionic and, over the temperature range 900° – 1300°C, they obtained an activation energy of 1.1 eV.

Over the temperature range 950° – 1360°C (it was found possible on one occasion to control the furnace temperature at 1360°C and a conductivity reading was obtained at this temperature in air) the log σ vs T^{-1} graph in air is accurately linear and the activation energy is 1.07 ± 0.05 eV in agreement with the value of Subbarao et al. This will be due to an ionic contribution, as discussed above, and an electronic contribution. The electronic activation energy will be half the energy to introduce an oxygen atom into an oxygen ion vacancy, V_o^{++}, and then doubly ionize it (see Chapters 2.5. and 3.2.), plus the energy to move a positive hole, if the hopping electron model applies to ThO_2, as it probably does to ZrO_2 (71).

6.4. Variation of conductivity with frequency

The conductivity of undoped thoria was measured as a function of frequency over the range 30 c/s to 20,000 c/s at different temperatures and in the two atmospheres air and B.O.C. argon. The results are shown in Figs. 33 and 35. A marked dependence of conductivity on frequency is observed at low temperatures, the conductivity in air at 504°C increasing by a factor 10 when the frequency is changed from 30 c/s to 20,000 c/s. At high temperatures (above 900°C in air and above 1160°C in B.O.C. argon) the conductivity is almost independent of frequency in the frequency range employed.

The increase in conductivity with frequency observed at low temperatures is due to a diminishing effect of space charge polarization with increasing frequency. So the higher the frequency the closer the measured conductivity is to the bulk conductivity of thoria. The conductivity at high temperatures which is almost independent of frequency is that of a specimen

which contains some space charge polarization. However it appears that it is likely that at high enough temperatures the polarization present does not have a marked effect on the conductivity, which is expected to be approximately that of the bulk material. This is discussed in Chapter 9.

No other workers investigating the conductivity of undoped thoria mention finding such pronounced frequency effects. There are certainly long time polarization effects, as found by Danforth and Bodine (59,60) for thoria single crystals in vacuum. Steele and Alcock (18) found no frequency dependence above 1000 c/s, but neither does the author at sufficiently high temperatures. Rudolph (55) used four terminal measurements at 5 to 100 c/s '' to overcome polarization effects '' , the inference being that he succeeded but he gives no further details. Others (10,41,47,48,40) simply state that they used alternating current at a fixed frequency. However, at least in the cases of Subbarao et al (41) and Lasker and Rapp (10) it is difficult to believe, when one notes the close agreement between their conductivity results and those of this investigation, that they would not have observed the same frequency dependence had they looked for it.

This dependence of conductivity on frequency means that the slopes of the log σ vs T^{-1} and log σ vs log p_{O_2} curves also vary with the frequency of measurements. In Fig. 20 log σ vs T^{-1} is plotted for 290, 1592 and 20,000 c/s in the frequency dependent range of temperature. The variation produced by these different measuring frequencies can be clearly seen. Unfortunately at the time the conductivity of undoped thoria was investigated the importance of the variation of conductivity with frequency was not fully appreciated and measurements in forming gas were made at only one frequency, 1592 c/s. However, as the

frequency dependence for the doped (Figs 27 and 32) and undoped (Fig 20) samples is similar both in air and in argon, the same is expected to hold for forming gas. This means that in forming gas the frequency dependence for the undoped ThO_2 will be even more pronounced than in argon. So it appears that, when comparing the slopes of log σ vs T^{-1} curves, frequency is a variable which must be specified. Also activation energies measured from the slopes of log σ vs T^{-1} curves must be regarded as of doubtful value unless it has been verified that there are no interfering space charge polarization effects present.

The effect of different measuring frequencies on the slopes of log σ vs log p_{O_2} curves is shown in Fig 21. But the value of this gradient is a quantity very often used in determining the defects producing conductivity in oxides. For example Vest et al (71) relied heavily on the measured gradient of their log σ vs log p_{O_2} graph to support their belief that the conductivity of monoclinic zirconia at high p_{O_2} was due to completely ionized zirconium vacancies. Their conclusion may be correct, but the present investigation casts some doubt on the value of their evidence. Lasker and Rapp (10) believe that the 1/4 power dependence they obtained for log σ vs. log p_{O_2} for their undoped thoria at high oxygen partial pressures was due to the presence of impurities, and had their material been much purer they would have obtained a 1/6 power dependence. The author agrees that their observed conductivity is strongly influenced by, and in the p_{O_2} -independent region determined by, the impurity content of their samples, but the present work shows that if they had made their measurements at say 20,000 c/s instead of 1592 c/s, the gradients of their graphs might have been considerably altered.

The dependence of the slope of the log σ vs. log p_{O_2}

curves on frequency means that the ratio of conductivities in two different atmospheres also depends on frequency. So, if the ionic transport number at any particular p_{O_2} is defined by $t_i = \frac{\sigma_{ionic}}{\sigma_{total}}$ the value obtained will depend on the frequency at which the measurements are made.

6.5. Summary

The electrical conductivity of undoped thoria has been examined as a function of the three variables, oxygen partial pressure, temperature and frequency.

The observed variation of conductivity with p_{O_2} showed that the undoped thoria was a mixed conductor, p-type electronic plus ionic, at values of p_{O_2} greater than about 10^{-8}atm. Below 10^{-8}atm. the p_{O_2} -independence of the conductivity strongly suggests that it is predominantly ionic. At very low values of p_{O_2} (10^{-29}atm. at 514°C) there is evidence of the existence of some n-type conductivity. These findings agree with those of previous workers (10,18).

Despite agreement under certain conditions with the results of other investigations (10, 18, 40, 41) it was found that at 1592 c/s the log σ vs T^{-1} curve in forming gas was not accurately linear over the temperature range 550°-1300°C. There was a pronounced dip in the middle which has not previously been reported for ionic conductivity in ThO_2 or ZrO_2, either doped or undoped. It was stated that this dip was caused by space charge polarization at the grain boundaries.

An examination of the present results in forming gas compared with measurements of the extrinsic oxygen diffusion coefficient showed that the ionic conductivity of the undoped ThO_2 samples investigated was impurity controlled at all temperatures up to 1300°C. This belief was confirmed by the similarity in the results at 1592 c/s for doped and undoped

samples, ~~and by the comparative behaviour of the log σ vs T^{-1} curves for undoped ThO_2 at different frequencies.~~

At 1592 c/s the activation energies in air, over the temperature range 950°–1360°C, and forming gas, over the temperature range 1160°–1300°C, were found to be 1.07 ± 0.05 eV and 1.39 ± 0.14 eV respectively. It is believed the value in forming gas may be higher than that of bulk ThO_2 because of grain boundary polarization effects.

Over the range 30–20,000 c/s it was found that the conductivity, at low temperatures, was strongly dependent on frequency in the atmospheres, air and B.O.C. argon, in which this phenomenon was examined. At high temperatures, above 900°C in air and 1160°C in B.O.C. argon, the conductivity was almost independent of frequency.

This frequency dependence of the conductivity was shown to cause a variation in the slopes of the graphs of log σ vs T^{-1} and log σ vs log p_{O_2} with the frequency of measurement. Therefore, any theoretical interpretation of these slopes, without first ensuring that there are no interfering space charge polarization effects, the cause of the frequency dependence of the conductivity, is certainly liable to error.

CHAPTER 7

THE ELECTRICAL CONDUCTIVITY OF THORIA DOPED WITH CaO

DISCUSSION OF RESULTS

THE ELECTRICAL CONDUCTIVITY OF THORIA DOPED WITH CaO

DISCUSSION OF RESULTS

7.1. Introduction

Previous work (44,45) has shown that at 1800°C the solubility of CaO in ThO_2 to form a single phase fluorite solid solution is well above 5 mole °/o, so it is expected that the two compositions, 0.99 ThO_2–0.01 CaO and 0.95ThO_2–0.05 CaO, studied in this investigation will each consist of only one phase. Microscopic examination revealed no evidence of the presence of a second phase.

The conductivity of thoria is known to increase with addition of CaO (18,51). The results of this investigation showed that addition of 1 mole °/o CaO produced an increase of only about 60°/o in the conductivity in air, so measurements on this composition were made in only two atmospheres, air and vacuum. The addition of 5 mole °/o CaO produced a much greater increase in conductivity, to about three times that of undoped thoria, and conductivity measurements on this composition were made in air, argon containing 0.1°/o O_2, Air Products argon, vacuum and wet forming gas.

It was found that in Air Products argon, which has almost the same oxygen content as B.O.C. argon ($\leqslant$ 4 p.p.m. and $\leqslant$ 10 p.p.m. respectively) the conductivity of the 0.95 ThO_2 –0.05 CaO sample was again dependent on the flow rate, the conductivity decreasing with increasing flow rate. The measurements in this atmosphere were therefore made at a fixed flow rate of 200cc/min as in the case of undoped ThO_2. However, in argon containing 0.1°/o O_2 and in forming gas no flow rate dependence of the conductivity was observed. A spot check on the conductivity of 0.99 ThO_2 – 0.01 CaO revealed that it too

was dependent on (B.O.C.) argon flow rate.

The results of electrical conductivity measurements at 1592 c/s are shown as graphs of log σ vs T^{-1} over the temperature range 550°C to 1450°C in Fig 23 for 0.99 ThO_2–0.01 CaO in air and vacuum and in Fig 24 for 0.95 ThO_2–0.05 CaO in the atmospheres mentioned above with the exception of vacuum. The conductivity of 0.95ThO_2–0.05CaO in vacuum is greater than in Air Products argon by between 0 and 20°/o and so the vacuum results are omitted from Fig 24 to avoid making it too confusing.

These results are replotted in Fig 25 for the composition 0.95 ThO_2–0.05 CaO (including the vacuum results) to show the variation of conductivity (at 1592 c/s) with oxygen partial pressure.

7.2. Variation of conductivity with oxygen partial pressure

As can be seen from Fig 25 the conductivity of the sample 0.95 ThO_2–0.05 CaO decreases with decreasing partial pressure of oxygen down to about 10^{-8}atm. and then becomes independent of p_{O_2} . This behaviour, similar to that found for the undoped thoria, again indicates significant p–type electronic conduction at high p_{O_2} ($> 10^{-8}$atm.) and predominant ionic conduction at lower oxygen pressures.

Both Kiukkola and Wagner (3) for 0.85 ThO_2–0.15 CaO and Carter (reported by Wachtman (15)) for 0.90 ThO_2–0.10 CaO observed a change in conductivity with surrounding atmosphere which they ascribed to the presence of electronic conductivity. Pal'guev and Neuimin (48) by means of electromotive force measurements showed that the electrolyte 0.85 ThO_2–0.15 CaO possessed appreciable electronic conductivity for oxygen partial pressures of the order of 10^{-2} atmospheres but that at lower oxygen pressures ($\sim 10^{-7}$ to 10^{-25} atmosph.) the conductivity was almost wholly ionic. Steele and Alcock (18) carried out emf measurements on the electrolyte 0.95 ThO_2 –0.05 CaO at 1000°C

between electrodes of Cu, Cu_2O and Ni, NiO in one cell and Ni, NiO and Fe, FeO in another. They found that in the former cell, the electrodes of which corresponded to oxygen partial pressures of $10^{-6.3}$ and $10^{-10.4}$ atm. the electrolyte possessed a little ($\sim 3^{o}/o$) electronic conductivity but in the latter with oxygen partial pressures of $10^{-10.4}$ and $10^{-14.4}$atm. at the electrodes the conductivity was $> 99^{o}/o$ ionic. They also measured the conductivity at 1500 c/s as a function of temperature and oxygen partial pressure and their results for 800°C and 1000°C are superimposed on the log σ vs. log p_{O_2} graphs of the present investigation for the purpose of comparison. It can be seen that the general shape of the curves is the same in each case: at high oxygen partial pressures the conductivity decreases rapidly with decreasing p_{O_2} , whereas at lower oxygen pressures the conductivity is independent of p_{O_2} .

Taking into account the results of other investigators quoted above and the levelling-off of the log σ vs log p_{O_2} curves it seems reasonable to assume, although this was not verified in this investigation by transport number determinations, that the conductivity values for 0.95 ThO_2-0.05 CaO in the p_{O_2}-independent region correspond to approximately $100^{o}/o$ ionic transport.

For the 0.99 ThO_2-0.01 CaO composition the conductivity decreases by a factor of 4 on going from air (p_{O_2} = 0.21 atm) to vacuum ($p_{O_2} \sim 10^{-5}$atm) indicating a high proportion of p-type electronic conductivity in air (see Fig 23). No measurements were carried out on this sample in forming gas.

From the log σ vs log p_{O_2} curves in Fig 25 a rough estimate can be made of the transport numbers of 0.95 ThO_2-0.05 CaO assuming the conductivity in forming gas is ionic. For example in air (p_{O_2}=0.21 atm.) the ionic transport number (from the relation

$t_{ion} = \frac{\sigma_{in\ air}}{\sigma_{in\ air}}$) is 0.34 at 1400°C, 0.15 at 1000°C and 0.23 at 600°C. These values are lower than those obtained from the results of Steele and Alcock (18,66) using the same method. These workers results yield a value of 0.4 for the ionic transport number in oxygen (p_{O_2} = 1 atm.) for all temperatures in the range 700° – 1100°C, and an extrapolation of their results up to 1400°C and down to 600°C would still give the same value. The difference is possibly due, at least in part, to polarization effects which are certainly present in this investigation but apparently not in the work of Steele and Alcock.

The gradient of the graph of log σ vs. log p_{O_2} for 0.95 ThO_2–0.05 CaO in air at 1400°C is less than the value of 1/4 suggested by the theory in Chapter 3. At 1400°C it is believed that polarization effects are negligible so this is not the explanation. The reason for the discrepancy is probably simply that 0.21 atm. O_2 is not a high enough p_{O_2} to give a conductivity completely controlled by the concentration of positive holes, which should be proportional to $p_{O_2}^{1/4}$. The transport number results given above show that at 1400°C 34°/o of the conductivity in air is due to ions.

7.3. Variation of conductivity with temperature

The variation of conductivity at 1592 c/s with temperature for the CaO–doped samples is shown in Figs. 23 and 24 for the different atmospheres used. There is a striking similarity between the shapes of the graphs of the doped and undoped samples, the principal effect of addition of 1 and 5 mole °/o CaO being to shift the conductivity over the entire temperature range covered to higher values.

The results of other workers for 0.95 ThO_2–0.05 CaO are also shown in Fig 24. In air Volchenkova and Pal'guev (51) obtained lower conductivity values but a similar slope over the

temperature range 700°C to 1100°C for measurements carried out at 3000 c/s. The lower conductivity values may be due to the lower density of their samples. The results of Steele and Alcock (18) at 1500 c/s over the range 700° to 1100°C and at an oxygen partial pressure of 1 atm. are slightly lower than the results of the present investigation in air but have almost the same activation energy. But they obtained a linear graph of log σ vs T^{-1} for their measurements in argon and forming gas and their conductivity values in these two atmospheres differed by only about 20°/o. These results do not agree with the present work in which, over the temperature range 700° – 1100°C, there was a much larger difference between conductivity values in argon and forming gas, there was a pronounced dip in the log σ vs T^{-1} results in forming gas, and although a straight line could be obtained in this temperature range for the log σ vs T^{-1} results in argon the activation energy deduced from it (1.34 eV) was larger than that obtained by Steele and Alcock (1.09 eV). Also, Steele and Alcock observed no dependence of conductivity on argon flow rate or on frequency contrary to the present investigation.

However, examination of the results obtained in the present work in the ranges of temperature where the conductivity is almost frequency independent (above 750°C in air and above 1200°C in forming gas) shows that the slopes of the log σ vs T^{-1} graphs in these regions agree reasonably well with the slopes of Steele and Alcock's graphs in the 700°C – 1100°C region and moreover the conductivity in argon is almost identical to that in forming gas, again in agreement with the findings of Steele and Alcock.

The high temperature activation energies obtained in the present investigation for 0.95 ThO_2–0.05 CaO were 0.99 ± 0.01 eV in forming gas for the temperature range 1270° – 1440°C and 1.02 ± 0.05 eV in air for the temperature range 975° – 1465°C. The lower activation energy found for ionic conduction compared with

that in the undoped ThO_2 (1.39 eV) may be explained by the higher temperature range in which this activation energy was measured in the doped material. At these higher temperatures the effect of grain boundary polarization is expected to be less and the conductivity, and so activation energy, closer to that of the bulk material. It is possible that at the highest temperatures employed (above 1350°C) electrode polarization becomes important and lowers the conductivity and the activation energy to below that of the bulk material. These ideas are discussed in Chapter 9.

The high temperature activation energy in air is very similar to that of the undoped ThO_2 (1.07 ± 0.05 eV).

7.4. Variation of conductivity with addition of CaO

The conductivity of thoria was found to increase with addition of CaO. The behaviour at 1000°C is shown in Fig 26. Although this conductivity increase was smaller than that observed by Steele and Alcock (18) the results obtained agree in their general trend with those of other workers whose results are also shown in Fig. 26. The decrease in gradient of the log σ vs composition curve above about 1 mole °/o CaO, believed to be due to association of Ca^{2+} ions and oxygen vacancies (11), or possibly oxygen vacancy ordering (72), was observed, but doping was not increased to a sufficiently high concentration to observe the conductivity maximum and subsequent decrease obtained in other investigations (18,51).

7.5. Variation of conductivity with frequency

To find out if the conductivity of the CaO–doped samples varied with frequency, measurements were carried out over the range 30 c/s to 20,000 c/s. As with the undoped samples a marked frequency dependence was found in the lower temperature

ranges used, i.e. below about 750°C in air and about 1200°C in the other atmospheres. At higher temperatures the conductivity was almost independent of frequency in the range covered. The results obtained for 0.95 ThO_2–0.05 CaO in air and forming gas are shown in Figs 41 and 43 as graphs of log (conductance) vs log (frequency).

For these CaO–doped samples, too, it is believed that this frequency dependence is due to decreasing effects of polarization as the frequency is increased. In some cases, e.g. for the 0.95 ThO_2–0.05 CaO specimen in forming gas at 575°C (and also at lower temperatures) it appears that 1592 c/s is a high enough frequency to overcome polarization effects and the measured conductivity is the true bulk conductivity of the material. However, for all higher temperatures it is believed that at 1592 c/s there is some space charge polarization present, even at the highest temperatures investigated where the conductivity is almost independent of frequency. These effects are examined in more detail in Chapter 9.

This frequency dependence again implies that the shapes of the log σ vs. log p_{O_2} and log σ vs T^{-1} graphs will change as the measuring frequency is changed. In Fig. 22 log (conductance, G) is plotted against log p_{O_2} for the 0.95 ThO_2–0.05 CaO specimen, for the frequencies 290, 1592 and 20,000 c/s at the three temperatures 680°, 840° and 1010°C. It can be clearly seen that the gradients of these curves in the p–type conductivity region i.e. $p_{O_2} > 10^{-8}$ atm. change with frequency so it is obviously impossible to use these gradients as evidence regarding the identity and degree of ionization of the defect producing the electronic conductivity. In the low oxygen pressure region, where the conductivity is completely ionic and where the number of oxygen vacancies is fixed by the composition, the conductivity will be independent of p_{O_2} regardless of the extent of polarization

and hence regardless of the frequency of measurement. However, as can be seen from Fig 22 different ionic conductivity values will be obtained for different frequencies.

The effect of measuring frequency on the log σ vs T^{-1} curves can be seen in Fig 27 where results are presented for the conductance of the 0.95 ThO_2–0.05 CaO specimen at 290, 1592 and 20,000 c/s. It can be seen at a glance that the activation energy calculated from the gradient of these curves will depend strongly on the frequency of measurement.

From the log G vs log (frequency) graphs for 0.95 ThO_2–0.05 CaO in forming gas (Fig. 43) it appears that for temperatures under 711°C measurements taken at 20,000 c/s may contain no polarization effects. Therefore log G vs T^{-1} at 20,000 c/s below 711°C should give the activation energy of ionic conductivity. Measurements at 20,000 c/s were taken at only three temperatures in this range (711°C, 575°C, and 503°C) and the results can be seen in Fig 27. The three points lie on a straight line whose gradient gives an activation energy of 1.33 eV. This value agrees well with that of 1.285 eV calculated from Wachtman's results (15) taking the activation energy for conduction as the sum of that for motion of an oxygen ion vacancy and one half the energy of association, h_a, of a Ca ion–oxygen vacancy pair. It was shown in Chapter 3.2. that in 0.95 ThO_2–0.05 CaO the degree of association of these pairs is greater than 0.95 below 1200°K and under these conditions the activation energy for conduction will contain a contribution $h_a/2$ (see also Chapter 2.5.) Wachtman calculated the association energy as approximately 0.71 eV and measured the energy of motion as 0.93 eV, using results of experiments on internal friction and dielectric loss due to rotation of $Ca_{Th}^{=} - V_o^{++}$ dipoles, techniques which are unaffected by space charge polarization effects.

7.6. Summary

The electrical conductivity of ThO_2 doped with 1 and 5 mole °/o CaO has been examined as a function of oxygen partial pressure, temperature and frequency. The maximum temperature reached (1465°C) is well above that (1100°C) of previous investigators (18,51).

The variation of conductivity with p_{O_2} supports the results of other workers (18) that the conductivity of these solid solutions is mixed at high p_{O_2} and becomes purely ionic when the value of p_{O_2} drops below about 10^{-8} atm.

The conductivity of ThO_2 increased with CaO doping, the effect of the doping on the log σ vs. T^{-1} curves at 1592 c/s being to raise them to higher conductivity values with little alteration in their slopes. The dip noticed in the log σ vs T^{-1} curve in forming gas for undoped thoria was still present after addition of 5 mole °/o CaO.

As was the case for the undoped ThO_2, the CaO-doped specimens exhibited a strong dependence of conductivity on frequency at the lower temperatures investigated, and it was shown that this means that the slopes of the log σ vs log p_{O_2} and log σ vs T^{-1} curves alter considerably with frequency.

The values of the high-temperature activation energies were found to be 0.99 $\pm$ 0.10 eV in forming gas over the temperature range 1270° – 1440°C and 1.02 $\pm$ 0.05 eV in air over the temperature range 975° – 1465°C.

The value of the activation energy at temperatures in the range 503°–711°C was measured approximately under conditions in which it was believed the conductivity was purely ionic and was not affected by space charge polarization effects. The value obtained was in reasonable agreement with that calculated from results of experiments known to be free from space charge polarization effects.

CHAPTER 8

THE ELECTRICAL CONDUCTIVITY OF THORIA DOPED WITH SrO

DISCUSSION OF RESULTS

THE ELECTRICAL CONDUCTIVITY OF THORIA DOPED WITH SrO

DISCUSSION OF RESULTS

8.1. Introduction

Having examined some of the electrical properties of thoria doped with CaO the investigation was continued to look at the effect of doping with SrO. As strontium is the alkaline earth immediately below calcium in the periodic table and both metals have, therefore, similar properties, doping with either oxide would be expected to produce similar behaviour.

The only previous electrical conductivity measurements on thoria doped with SrO are those of Volchenkova and Pal'guev (46) who measured the conductivity over the whole range of composition of the ThO_2–SrO system. However, their measurements were carried out in only one atmosphere (air), at a fixed frequency of 3000 c/s, and up to a maximum temperature of only 1000°C. In this investigation only one composition was examined (0.95 ThO_2–0.05 SrO), but the temperature range was extended to 1450°C and the effects of altering the oxygen partial pressure and the measurement frequency were also examined.

Previous work (45,46) indicates that the maximum solubility of SrO in ThO_2 to give a single phase fluorite solid solution is about 2 – 3 mole °/o at 1550°C and 3 – 5 mole °/o at 1800°C. The present samples, which were prepared at 2000°C, contain 5 mole °/o SrO, so it is possible that there is not complete solution of the SrO. However, microscopic examination of polished and etched sections revealed no trace of a second phase.

Volchenkova and Pal'guev found that even small additions of SrO to ThO_2 produced brown specimens. The 0.95 ThO_2–0.05 SrO specimens prepared in the present work were white. This

discrepancy may be due to differing impurity contents of the starting materials, but it is impossible to be sure of this as Volchenkova and Pal'guev did not give an analysis of their chemicals.

8.2. Variation of conductivity with oxygen partial pressure

The conductivity of 0.95 ThO_2–0.05 SrO was found to vary with oxygen partial pressure p_{O_2} in the same manner as 0.95 ThO_2–0.05 CaO. At high p_{O_2} ($> 10^{-8}$ atm.) the conductivity decreased rapidly as p_{O_2} decreased showing the presence of p–type electronic conductivity, while at lower oxygen partial pressures the pressure independence of the conductivity indicated an ionic transport number of one. The results obtained at 1592 c/s are shown in Fig 29 as a plot of log σ vs log p_{O_2} for temperatures in the range 600° to 1400°C.

The ionic transport numbers t_i in air calculated from the ratio $t_i = \frac{\sigma_{\text{in forming gas}}}{\sigma_{\text{in air}}}$ at 600°, 1000° and 1400°C are 0.18, 0.05 and 0.24 respectively. The corresponding transport numbers for 0.95 ThO_2–0.05 CaO are 0.23, 0.15 and 0.34. In fact, it is found that in air for all temperatures in the range 550°–1400°C the percentage electronic conductivity for the 0.95 ThO_2–0.05SrO composition is appreciably greater than for 0.95 ThO_2–0.05 CaO.

The slope of the log σ vs log p_{O_2} curve at 1400°C is less than 1/4 as was found for 0.95 ThO_2–0.05 CaO, and presumably for the same reason.

8.3. Variation of conductivity with temperature

The variation of the conductivity at 1592 c/s of 0.95 ThO_2–0.05 SrO with temperature over the range 500°C to 1450°C and in the three atmospheres air, Air Products argon and forming gas is shown in Fig 30 as a graph of log σ vs T^{-1}. Once again there is a striking resemblance between the shapes of these

graphs and those corresponding to the previously discussed specimens. The results obtained in air on 0.98 ThO_2–0.02 SrO at 3000 c/s by Volchenkova and Pal'guev (46) are plotted on the same graph. It can be seen that the results obtained by these workers by doping with 2 mole °/o SrO are similar in magnitude and activation energy to the present results on a sample doped with 5 mole °/o SrO.

The present results give high temperature activation energies of 1.16 ± 0.12 eV in forming gas over the range 1315°–1450°C and 0.91 ± 0.05 eV in air over the range 1155°–1450°C. The higher activation energy of ionic conduction compared with that in 0.95 ThO_2–0.05CaO is believed to be partly a real property of the bulk oxide (see next section 8.4.) and partly due to the fact that electrode polarization effects are relatively unimportant for the SrO–doped sample compared with the CaO–doped sample.

8.4. Variation of conductivity with addition of SrO

Addition of 5 mole °/o SrO to ThO_2 had very little effect on the conductivity. In Fig 31 the log σ vs T^{-1} graphs at 1592 c/s for 0.95 ThO_2–0.05 SrO and undoped ThO_2 are drawn together for ease of comparison. In air the doped material has a conductivity which is greater than that of the undoped thoria for all temperatures covered, the increase being between 10°/o and 58°/o. In argon and forming gas doping produced at some temperatures an increase and at others a decrease in conductivity but the change was always less than 25°/o. These results disagree with those of Volchenkova and Pal'guev who, as can be seen from Fig 30 found that addition of 2 mole °/o SrO to ThO_2 produced, in air, a marked increase in the conductivity both in magnitude, by a factor 3 or more, and in the slope of the log σ vs T^{-1} curve.

The addition of 5 mole °/o SrO would be expected to produce a large number of oxygen ion vacancies and so a large increase in ionic conductivity. The difference in density between the SrO–doped and undoped specimens is not the explanation of the low conductivity of the doped specimen, as this has the higher density, which would tend to give it the higher conductivity. Nor does the presence of a second phase, due to the solubility limit of Sr in ThO_2 having been exceeded, seem a plausible explanation. Microscopic examination revealed no sign of a second phase and, moreover, Volchenkova and Pal'guev found that the conductivity, in air, of ThO_2 continued to increase with addition of SrO up to 15 mole °/o by which concentration a second phase was certainly present.

Some understanding of the low conductivity of the SrO–doped ThO_2 may be gained by comparing its behaviour with that of the 0.95 ThO_2–0.05 CaO specimen which has a much higher conductivity. Part of the explanation of this higher conductivity is the lower porosity of the CaO–doped specimen. Part is due to the lower energy of association of a $Ca_{Th}^{=} - V_o^{++}$ pair compared to a $Sr_{Th}^{=} - V_o^{++}$ pair, which means there are more free vacancies transporting charge in the CaO–doped specimen at any given temperature. This is stated in analogy with the systems KCl + $CaCl_2$ and KCl + $SrCl_2$. Bassani and Fumi (73) calculated the energy of association in these systems as 0.32 eV and 0.39 eV, respectively, in qualitative agreement with the higher conductivity observed when KCl is doped with $CaCl_2$ rather than $SrCl_2$.

In Fig 51 the increase in conductivity at the high end of the frequency range at 596°C is produced by the movement of oxygen vacancies around Sr ions in a $Sr_{Th}^{=} - V_o^{++}$ dipole (see Chapter 9.3.). In the 0.95 ThO_2–0.05 CaO specimen this effect does not appear until below 503°C (Fig 43). This means that

the energy to move an oxygen vacancy around a Ca ion in 0.95 ThO_2 –0.05 CaO is lower than round a Sr ion in 0.95 ThO_2–0.05 SrO (see Chapter 2.6.) It seems very probable that when the oxygen vacancies are freed from the divalent impurities the energies of motion are not altered much. This means that in the CaO–doped samples the energy of motion of a free oxygen vacancy is less than in the SrO–doped samples and so the mobility is higher. This is another factor which contributes to the relatively high conductivity of the 0.95 ThO_2–0.05 CaO specimen.

If the above ideas are correct the high temperature activation energy for conduction in forming gas, determined by both the energy of motion of an oxygen vacancy and the dissociation energy of the dipoles, should be larger for 0.95ThO_2 –0.05 SrO than for 0.95 ThO_2–0.05 CaO. This is in fact what is found in this investigation (1.16 eV compared with 0.99 eV), though part of this difference is probably due to electrode polarization effects in the 0.95 ThO_2–0.05 CaO specimen.

The above discussion explains why addition of 5 mole °/o SrO to ThO_2 should not give such a large increase in conductivity as addition of 5 mole °/o CaO. However, it does not explain why there was never any significant increase, and in some cases actually a decrease, in the conductivity of ThO_2 on addition of 5 mole °/o SrO.

8.5. Variation of conductivity with frequency.

For ThO_2 doped with 5 mole °/o SrO a similar dependence of conductivity on frequency was found as for undoped thoria and that doped with 1 and 5 mole °/o CaO. The results are shown in Figs 49 and 51 as graphs of log G vs log (frequency) in air and forming gas over the frequency range 30 c/s to 20,000 c/s.

As with the previous specimens the conductivity at the

lower temperatures is strongly dependent on frequency because of a marked variation in space charge polarization with frequency. At higher temperatures (above about 800°C in air and about 1200°C in argon and forming gas) the conductivity is almost independent of frequency.

This frequency dependence again must be taken into account when considering the variation of conductivity with oxygen partial pressure and temperature. Graphs of log G vs log p_{O_2} for the frequencies 290, 1592 and 20,000 c/s are shown in Fig 28. At all frequencies the graphs exhibit the same general behaviour: at oxygen partial pressure above about 10^{-8} atm. the conductivity decreases rapidly with decreasing p_{O_2} indicating p-type electronic conductivity; at lower oxygen partial pressures the conductivity is independent of p_{O_2} indicating ionic conductivity. However, any attempt to use the gradients of these graphs to identify the defects present and their state of ionization seems futile due to the large variation of gradient with frequency.

Fig 32 shows log G vs T^{-1} graphs in air, argon and forming gas for the frequencies 290, 1592 and 20,000 c/s. The frequency employed obviously has a considerable effect on the activation energy obtained, and so care must be taken in interpreting these activation energies. However, below 792°C in forming gas it appears that at 20,000 c/s space charge polarization may no longer affect the conductivity (cf. Fig 51) so it may be possible, for lower temperatures, to estimate the true activation energy of ionic conduction in 0.95 ThO_2–0.05 SrO. To do this we must subtract any contributions to the conductivity due to rotation of oxygen vacancies in $Sr_{Th}^{=} - V_O^{++}$ dipoles. Reasonable estimates of conductance values free from space charge polarization and dipole effects are those at 792°C and 20 k c/s, 596°C and 10k c/s, and 470°C and 290 c/s. We

find that these three points lie on a straight line (Fig 32) which gives an activation energy of 1.24 eV. This is slightly smaller than the value found at about the same temperatures for 0.95 ThO_2–0.05 CaO (1.33 eV), whereas according to the discussion in the preceding section, it should be slightly larger. This discrepancy can be explained by the fact that the values of conductance used to obtain the activation energy could only be estimated approximately.

8.6. Summary

The electrical conductivity of 0.95 ThO_2–0.05 SrO has been examined as a function of oxygen partial pressure, temperature and frequency. In the one previous investigation (46) of this system the only variable was temperature (up to 1000°C).

From the change in conductivity with p_{O_2} it was seen that this material is a mixed conductor at $p_{O_2} > 10^{-8}$ atm. and an ionic conductor at the lower oxygen pressures used. This behaviour is identical with that of other thoria-based electrolytes (10, 18, Chapter 7).

The shapes of the log σ vs T^{-1} curves for 0.95ThO_2–0.05SrO at 1592 c/s were very similar to those obtained for undoped ThO_2 and ThO_2 doped with CaO. In particular, the dip in the curve in forming gas was still present.

Addition of 5 mole °/o SrO to ThO_2 had little effect on the magnitude of the conductivity. This behaviour was explained, at least in part, by comparison with 0.95ThO_2–0.05CaO: the activation energies of movement of an oxygen vacancy and of dissociation of a divalent cation–oxygen vacancy dipole are greater for the SrO–doped than the CaO–doped ThO_2.

The conductivity of the 0.95ThO_2–0.05SrO specimen was very dependent on frequency at the lower temperatures. This

produced a variation in the slopes of the log σ vs log p_{O_2} and log σ vs T^{-1} curves with frequency.

The values obtained for the high temperature activation energies were 1.16 $\pm$ 0.12 eV in forming gas over the range 1315°–1450°C and 0.91 $\pm$ 0.05 eV in air over the range 1155°–1450°C.

The activation energy for ionic conduction in the temperature range 470°–792°C was calculated approximately under conditions free from polarization effects. The result obtained was in reasonable agreement with that obtained under similar conditions for $0.95ThO_2$–0.05CaO.

CHAPTER 9

INVESTIGATION OF THE CAUSES OF THE FREQUENCY DEPENDENCE OF THE ELECTRICAL PROPERTIES

INVESTIGATION OF THE CAUSES OF THE FREQUENCY DEPENDENCE OF THE ELECTRICAL PROPERTIES

9.1. Introduction

It has been seen in the previous three chapters that the conductivity of all the specimens examined varied considerably with the measuring frequency, indicating the existence of polarization effects. To gain some understanding of these effects, to try to estimate the importance of their influence on the conductivity values and to find the temperature and frequency ranges in which they were operative, it was decided to examine the capacities and dielectric loss tangents of the specimens as a function of frequency at constant temperature, and temperature at constant (1592 c/s) frequency. The theory in Chapter 2.6. shows that variations in conductivity with frequency, if caused by either dipole or space-charge polarization effects, will be accompanied by corresponding changes in capacity and dielectric loss tangent. Previous work (29) has demonstrated that the presence of polarization affects the capacity much more than the conductivity; and dielectric loss peaks are much easier to identify than inflections in graphs of conductivity or capacity against frequency.

Figs 33 to 56 show some of the results obtained. Omitted are results for 0.99 ThO_2–0.01 CaO, as its behaviour is what would be expected for a sample intermediate in composition between undoped ThO_2 and 0.95 ThO_2–0.05 CaO. Also omitted are results, for the doped specimens, of capacity and tan δ as a function of frequency in atmospheres other than air and forming gas as here too the behaviour can be inferred from that in the two extremes of oxygen partial pressure presented. For the undoped thoria no results were obtained in forming gas for

capacity and tan σ as a function of frequency, so results in B.O.C. argon are presented instead.

9.2. Proposed explanation of the frequency dependence of the electrical properties.

It is suggested that the frequency dependence of the electrical properties can be explained in terms of four space charge polarization effects, with some signs of dipole relaxation at the lowest temperatures investigated for the 0.95 ThO_2–0.05SrO sample. The space charge polarization is produced by the blocking of both oxygen ion vacancies and electron holes at both the grain boundaries and the electrodes. It will be shown by a discussion of the results obtained in this investigation how they support this proposal.

9.3. Discussion of results in terms of this proposed explanation

(a) Dipole relaxation effects

Wachtman (15) observed a dielectric loss peak in 0.985 ThO_2–0.015 CaO due to reorientation of $Ca_{Th}^{2-} - V_o^{++}$ dipoles. At 246°C the peak was at 695 c/s, at 310°C it had moved to 690 c/s. From equation (60) it follows that

$$\nu_{max} = \frac{1}{2\pi}\left(\frac{C_s}{C_\infty}\right)^{\frac{1}{2}} \frac{1}{\tau_o} \exp\left(-\frac{\Delta H}{kT}\right)$$

where ν_{max} is the frequency corresponding to the angular frequency ω_{max}, and C_s/C_∞, the ratio of the static and high frequency limiting capacities, is equal to $\epsilon_s/\epsilon_\infty$. C_∞ is due only to atomic and electronic polarization and hence is independent of temperature. C_s is due, in addition, to the aligning of the dipoles with the electric field. Since the degree of association is greater than 0.99 below 700°K (see Chapter 3.2.), the concentration of dipoles, and so C_s, is independent of temperature below this value. Therefore

$$\nu_{max} = \text{constant} \cdot \exp\left(-\frac{\Delta H}{kT}\right).$$

From Wachtman's results, and using his value of $\Delta H = 0.93$ eV, it follows that the dielectric loss peak due to the dipoles will occur at a frequency of 20,000 c/s when the temperature is 347°C. So for higher temperatures any dielectric loss peak in the frequency range below 20k c/s must, for the CaO–doped specimens, be caused by some other polarization effect...

The results obtained for the 0.95 ThO_2–0.05 CaO specimen at the lowest temperature investigated (503°C) show no effects which could possibly be attributed to dipole relaxation. However, for the 0.95ThO_2–0.05SrO specimen there is an increase in the ionic conductivity at 470°C and 596°C at the high end of the frequency range (Fig 51) which is due to dipole effects. Wachtman's results show that a $Ca_{Th}^{=} - V_o^{++}$ dipole will produce a loss peak at 470°C and 100k c/s. Taking account of the factor C_s/C_∞ , and assuming, in accordance with Wachtman's results, that it has a value of about 2, it is found that the point of inflection due to dipoles in the log σ vs. log ν graph should occur at 71 k c/s. So it is not unlikely that at 470°C this dipole effect will produce a noticeable change in conductivity with frequency over the range 1 – 20 kc/s. This is in fact what is observed for the 0.95ThO_2–0.05SrO specimen, the dipole in this case being $Sr_{Th}^{=} - V_o^{++}$. The effects of the rotation of this dipole can still be seen at 596°C for frequencies above 5k c/s.

The fact that dipole relaxation effects can be seen for 0.95ThO_2–0.05SrO (Fig 51) but not for 0.95ThO_2–0.05CaO (Fig 43), at temperatures in the 500°–600°C range means that the activation energy of movement, ΔH in equation (60), of oxygen vacancies is greater in the specimens doped with SrO than in the one doped with CaO. This is part of the explanation of the higher conductivity observed when ThO_2 is doped with 5 mole °/o CaO rather than 5 mole °/o SrO.

(b) Ionic space charge polarization effects

It has been seen in Chapters 6–8 that in forming gas the conductivity of the doped specimens is completely ionic and that of the undoped specimens is predominantly (probably at least 90%) ionic.

(i) $0.95ThO_2$–0.05CaO in forming gas

Looking first at the results for tan δ as a function of T^{-1} at 1592 c/s (Fig 48) two loss peaks can be clearly seen. One occurs at 560°C and the other at 1160°C. It is believed that these are due to two interfacial space charge polarization effects, the blocking of oxygen ion vacancies at the grain boundaries at lower temperatures and at the electrodes at higher temperatures. The increase in tan δ at the highest temperatures used may be due to free carrier conductivity, when tan δ is proportional to the conductivity σ_s (equation (63)), which increases exponentially with the temperature.

These loss peaks should be present in the graphs of log (tan δ) against log (frequency ν) (Fig 46). The low temperature peak can be seen at 575°C and 3000 c/s. As the above temperature rises this peak should, according to the theory of Chapter 2.6, move towards higher frequencies. At 711°C it occurs at a frequency just above 20k c/s, the maximum used in this investigation. At 847°C this peak has moved to still higher frequencies and another peak is beginning to make its appearance at the low frequency end of the range. At 974°C and 1158°C this second peak is at approximately 290 c/s and 6000 c/s respectively. The 6000 c/s, 1158°C peak is believed to be the same as the high temperature peak in Fig 48, and so to be due to ion blocking at the electrodes. The peak in the 1388°C isotherm at 5000 c/s should appear at a lower temperature in the tan δ vs T^{-1} (at 1592 c/s) graph. Since there is no sign of it, either in

this graph or in any of the others (e.g. for 0.95 ThO_2–0.05SrO) it will be assumed to be spurious and ignored.

Looking now at the graphs of capacity as a function of frequency (Fig 44) it can be seen that very large values of capacity, indicative of space charge polarization are in general obtained. At the lowest temperatures used, 575°C and 503°C, the capacity levels off at high frequencies to a low limiting value of about 20 pF. The geometrical capacity, calculated using the value of 18.4 obtained by Wachtman for the relative dielectric constant of pure ThO_2 at 25°C, is about 6 pF. Wachtman's results also show that the aligning of the $Ca_{Th}^{2-} - V_o^{2+}$ dipoles will, at most, double this capacity. The measured value of stray capacity was found (Chapter 5.6) to be always in the range 6 to 10 pF. So the total capacity expected for the $0.95ThO_2$–0.05CaO specimen when there is no space charge polarization is in the range 18 to 22 pF. The close agreement between this value and that actually observed provides strong evidence that for temperatures below 575°C there is no space charge polarization present at frequencies greater than 10k c/s.

The rapid increase in capacity with decreasing frequency at 503°C, 575°C and 711°C is attributed to build–up of ionic space charge at the grain boundaries. As the temperature rises the inflection in the graphs moves to higher frequencies as expected. At 711°C there is a low frequency levelling–off of the capacity due to the presence of maximum grain boundary polarization. At 847°C and 974°C there are still signs of this limiting polarization region, though at higher frequencies.

A grain boundary can be considered as a capacitor in parallel with a finite resistance. As the temperature rises the grain boundary blocking resistance will decrease, the leakage of charge across the boundaries will become easier and so the space

charge polarization effects due to the boundaries will be marked. This will explain why at 1592 c/s the capacity at 974°C is less than that at 847°C, and at 20,000 c/s the capacity at 1158°C is less than that at 974°C. This idea of partially blocking grain boundaries has been used by Macfarlane and Weaver (28) to explain their results on thin films of alkali halides at temperatures of 24°C to 119°C.

For temperatures of 1158°C and higher there is little evidence of grain boundary polarization effects at frequencies below 20 kc/s. However, there is a rapid increase in capacity with decreasing frequency at these temperatures, indicating the presence of another space charge polarization effect. This is due to blocking at the electrodes. The low frequency limiting capacity due to this polarization mechanism has not been reached in this investigation but it is obviously somewhat greater than 1 μF. The theoretical value of this low frequency limiting capacity for the case of completely blocking electrodes can be calculated from equation (77). The result obtained is 16 μF, which agrees reasonably well with the experimental results and confirms the existence of electrode polarization effects.

It is also possible to calculate the theoretical value of the capacity due to complete grain boundary polarization. Substituting $d = 10$ Å (approx. twice the lattice constant) and $N = 87 = \frac{\text{specimen thickness}}{\text{average grain diameter}}$ in equation (78) the capacity obtained is 9×10^{-2} μF. This is somewhat larger than the experimental value at 711°C, which is slightly above 10^{-2} μF. The smallness of the observed value may be explained by leakage of charge across the grain boundaries.

The explanation put forward is confirmed by the results shown in Fig 47 of log C as a function of T^{-1} at 1592 c/s. At the lowest temperatures there is a rapid increase in capacity

with rising temperature, due to the increase in ionic defect mobility with temperature. The breakdown in ionic blocking at the grain boundaries causes the capacity to decrease as the temperature is raised above 890°C. The effect of electrode polarization becomes apparent above 1045°C where once again the capacity increases rapidly with temperature. At the highest temperature reached (1440°C) there is no sign of either a breakdown in blocking at the electrodes or a levelling-off of the capacity due to the maximum electrode space charge polarization having been reached.

In the light of the preceding discussion the results for conductivity as a function of frequency can be explained. At 503°C, 575°C and 711°C the graphs (Fig 43) have the expected shape corresponding to the behaviour of capacity and dielectric loss with frequency at these temperatures, and as predicted for interfacial polarization (Chapter 2.6, Fig d). At these low temperatures 20,000 c/s is a high enough frequency to overcome polarization at the grain boundaries and give the true bulk conductivity. (At 503°C it was impossible to obtain a clear balance point on the bridge and the results for capacity and conductance are approximate. Tan δ is determined by the quotient of these uncertain capacitance and conductance values and is therefore liable to very large errors. So the results for tan δ are not presented at this temperature.) At 847°C and 974°C there are obvious signs of grain boundary polarization even at 20,000 c/s. At 974°C there is in addition a drop in conductivity at the low end of the frequency range, corresponding to the increase in capacity and the appearance of a tan δ peak. These lower frequency effedts are due to space charge polarization at the electrodes.

Confirmation of the belief that the frequency dependence

of the conductivity is caused by blocking of oxygen vacancies at the electrodes and the grain boundaries comes from an application of equations (68), (75) and (76). These equations predict that, if the only variable is frequency, the relaxation time corresponding to blocking of a charge carrier at the end of a conducting region is proportional to the length of the conducting region. If τ_1 and τ_2 are the relaxation times for the polarization effects causing the changes in conductivity at 974°C at the high and low frequency ends of the range covered, and ν_1 and ν_2 are the frequencies at the points of inflection, then if the polarization effects are blocking of oxygen vacancies at the electrodes and the grain boundaries, the following relation should hold:

$$\frac{\tau_1}{\tau_2} = \frac{\nu_2}{\nu_1} = \frac{\text{grain diameter}}{\text{specimen thickness}}$$

The grain diameter is 30 μ and the specimen thickness is 2.6 mm. (see Chapter 5.3 and 5.1) So their ratio is 1.1×10^{-2}. The values of ν_2 and ν_1 are estimated at approximately 30 c/s and 30 kc/s. So ν_2/ν_1 is 10^{-3}. Considering the uncertainty in the values of ν_2 and ν_1 this agreement is good enough to be regarded as confirmation of the interpretation of the observed behaviour.

At 1158°C and 1388°C the change in conductivity with frequency caused by electrode polarization is still noticeable, although the variation is small. At 1388°C both the slope of the log C against log ν graph and the value of the capacity (greater than that at 1158°C) show quite clearly that there is electrode polarization present even at 20 kc/s. Moreover a close examination of the frequency dependence of the conductivity at 1388°C (on a larger scale than Fig43) shows that there is no sign of any change in conductivity due to grain boundary polarization below 20 kc/s.

The effect of electrode polarization on the conductivity value at frequencies of 1592 c/s and above seems to be small.

At 1388°C the conductivity at 20 kc/s is larger than that at 1592 c/s by only 1.8 °/o of the value at 1592 c/s. This difference is caused by electrode polarization alone. At 1158°C and 974°C the figures are 3°/o and 35 °/o respectively, the larger values at the lower temperatures being due to the increasing effect of grain boundary, not electrode, polarization. In fact as the temperature falls the effect of electrode polarization on the a.c. conductivity decreases. So the results of this investigation show that for 0.95ThO_2–0.05 CaO the maximum error observed (at 1388°C) due to electrode polarization in taking the conductivity at 1592 c/s to be the true bulk conductivity is of the order of 2°/o. At higher temperatures this error will increase. So the activation energy, 0.99 eV, of ionic conduction for 0.95 ThO_2–0.05 CaO over the range 1270° – 1440°C found from the graph of log σ against T^{-1} at 1592 c/s may be slightly low.

These results agree with those of Danforth and Bodine (59) (60) who found that single crystals of ThO_2 exhibited a polarization effect due to blocking of ions at the electrodes. Since the impurity content of their ThO_2 was similar to that of the undoped thoria used in this work and their measurements were carried out in vacuum it would be expected that the conductivity they measured was predominantly impurity controlled ionic conductivity. They measured the d.c. conductivity at zero time over the range 900°–1300°C. When plotted as log σ vs T^{-1} they obtained an accurate straight line which yielded an activation energy of 1.1 eV. The linearity of their graph and the value of activation energy obtained show that their results were not affected by the observed polarization. I.e. over the range 900°–1300°C d.c. conductivity values at zero time, equivalent to a.c. values at about 1000 c/s, are not in appreciable error due to

ionic space charge polarization at the electrodes for a specimen of the thickness (2 mm.) used by Danforth and Bodine.

Electrode polarization may also explain why, in their investigation of specimens 1–2 mm. thick of 0.87 ThO_2–0.13 $YO_{1.5}$, Wimmer, Bidwell and Tallan (42) found that over the temperature range 900°C–1600°C the conductivity was independent of frequency only above 50k c/s.

The conductivity behaviour is believed to be like that shown schematically below

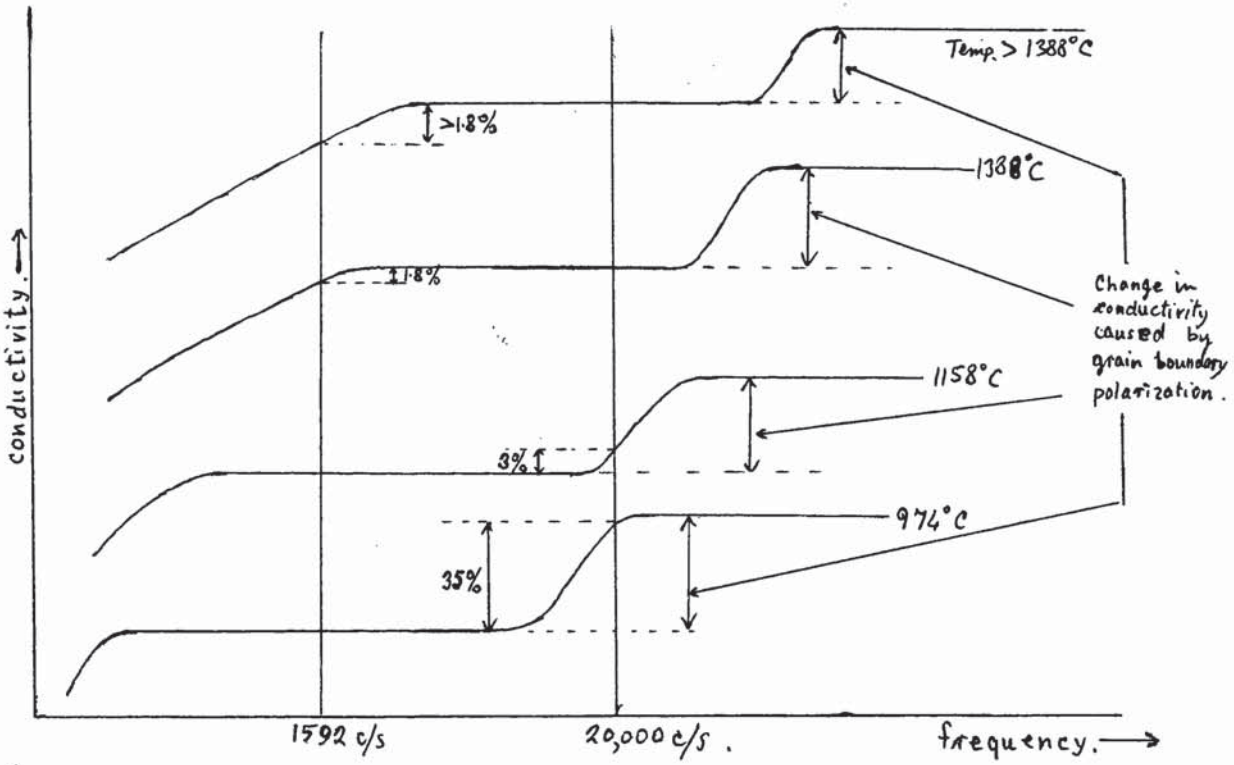

Fig i.

At 1388°C the conductivity at 20,000 c/s is less than the true bulk conductivity because of grain boundary polarization. The magnitude of the difference is unknown. The only direct measure of this is supplied by the log σ vs log ν curve for 0.95ThO_2–0.05CaO at 711°C (Fig 43). At this temperature grain boundary blocking decreases the conductivity by a factor 5. However the rapid decrease in capacity with increasing temperature for temperatures in the range 880°C to 1050°C (Fig 47), attributed to the breakdown of grain boundary blocking, strongly suggests that at high enough

temperatures, above about 1200°C, the grain boundaries have a negligible blocking effect and so their presence will not influence the conductivity value obtained. If this is so the measured conductivity at 1592 c/s between 1200°C and 1388°C is the true bulk conductivity of the material.

It is now possible to explain the shape of the log σ vs T^{-1} graph for 0.95 ThO_2–0.05 CaO in forming gas (Fig 24). At temperatures between about 500° and 640°C the graph is linear, there is no space charge polarization at 1592 c/s and the activation energy (about 1.3 eV) is the sum of the energy to move an oxygen vacancy and one half the energy of dissociation of a $Ca_{Th}^{=} - V_o^{++}$ dipole. At temperatures above 640°C the oxygen vacancies pile up at the grain boundaries and the conductivity is thereby reduced; this produces the dip in the curve between 640°C and 840°C. At 840°C the blocking effect of the boundaries begins to break down, as can be seen from the capacity vs T^{-1} graph (Fig 47) and the conductivity increases with temperature more rapidly than it would for a single crystal i.e. for a material with no internal blocking. For temperatures above about 1200°C the conductivity, as suggested above, appears to be that of the bulk material, except for some small effect of electrode polarization for temperatures higher than 1380°C.

If the dip in the log σ vs T^{-1} graph in forming gas (Fig 24) is produced only by the presence of grain boundaries, as appears to be the case, then the expected shape of this curve for single crystals can be guessed as being like the dashed line in Fig. j below. This line also assumes there is no electrode polarization. Thefull line represents the experimental results.

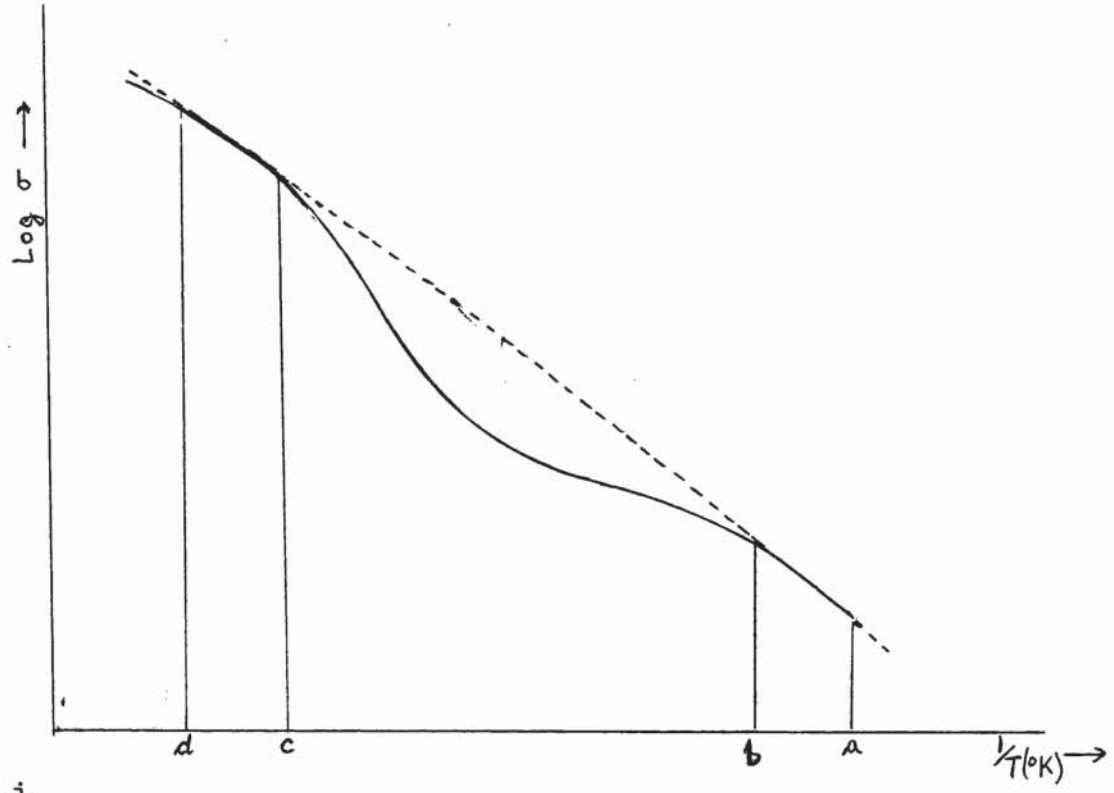

Fig. j.

In the region ab there is no space charge polarization. In bc the effect of grain boundary blocking is seen. cd is thought to be a region in which there are no electrode pplarization effects, and the grain boundary polarization has a negligible influence on the conductivity. The temperature at c is in the region of 1200°C. The decrease in conductivity observed for temperatures above d is attributed to electrode polarization. The slight decrease in slope of the dashed line as the temperature rises, and so the lower activation energy at dc as compared with ba, can be explained by dipole dissociation.

(ii) <u>0.95 ThO_2–0.05 SrO in forming gas</u>

The behaviour of this composition was similar to that of 0.95 ThO_2–0.05 CaO.

The graph of tan δ against T^{-1} again showed two peaks due to grain boundary and electrode blocking (Fig 56). These occurred at higher temperatures (600°C and 1340°C) than in the 0.95 ThO_2–0.05 CaO specimen and as both specimens had the same grain size and approximately the same thickness this indicated that the

activation energy for ionic conduction was greater in the SrO–doped specimen than in that doped with CaO, as previously noted. (Chapters 8.4. and 9.3.(a)).

The tan δ vs frequency graphs (Fig 54) are very similar to those for CaO doping, except that in this case there is no peak corresponding to that at 1388°C and 5000 c/s in 0.95 ThO_2–0.05CaO. The peak at 1266°C and 1592 c/s in 0.95 ThO_2–0.05 SrO sppears at 1400°C at a frequency greater than 20,000 c/s.

The variation of capacity with temperature (Fig 55) is similar to that for 0.95 ThO_2–0.05 CaO. Higher temperatures are required to produce the same degree of polarization, again indicating that a greater energy is required to free and move the oxygen vacancies. The lesser electrode polarization at higher temperatures, compared with the results for 0.95 ThO_2–0.05 CaO implies that the error in conductivity due to this effect will be smaller for the 0.95 ThO_2–0.05 SrO specimen. In fact there are no indications that electrode polarization introduces any error into the conductivity at 1592 c/s below the maximum temperature (1450°C) reached. The higher temperature (compared with that for 0.95 ThO_2–0.05 CaO) required to produce the decrease in capacity attributed to the breakdown of grain boundary blocking means that a higher temperature (about 1300°C compared with 1200°C) must be reached before this blocking ceases to affect the conductivity at 1592 c/s.

The importance of grain boundary blocking at a higher temperature than for 0.95 ThO_2–0.05 CaO can be seen from the C vs ν (Fig 52) and σ vs ν (Fig 51) graphs. At 969°C there is a much greater grain boundary effect for 0.95 ThO_2–0.05 SrO than at 974°C for the CaO–doped specimen, yet the temperatures are almost the same. The σ vs ν graphs at 596°C and 470°C also show quite clearly the effects of the $Sr_{Th}^{2-} - V_o^{2+}$ dipoles, as mentioned earlier.

The shape of the log σ vs T^{-1} graph (Fig 30) can be explained in a similar way as for the 0.95 ThO_2–0.05 CaO specimen. If we compare it with Fig j, the temperature at c in this case appears to be of the order of 1300°C and the region ba has a lower slope because of the increasing effect of the dipoles on the conductivity with decreasing temperature.

(iii) Undoped ThO_2 in forming gas or B.O.C. argon

It was shown in Chapter 6 that the ionic conductivity of the undoped ThO_2 was controlled by the presence of impurities. So the electrical behaviour due to ionic movement is expected to be similar to that of the doped samples.

The dependences of conductivity, capacity and dielectric loss on frequency were not examined in forming gas, so these dependences have to be inferred from those in B.O.C. argon in which the conductivity is intermediate between that in air (predominantly electronic) and forming gas (predominantly ionic) and also from results of conductivity, capacity and tan δ as a function of temperature at 1592 c/s in forming gas.

A plot of tan δ against T^{-1} in forming gas at 1592 c/s has only one peak in the temperature range 490° – 1300°C (Fig 40). This is at about 550°C and is due to blocking of oxygen vacancies at the grain boundaries. There is no sign of a peak due to electrode blocking though, in analogy with the doped specimens, this would be expected to appear at some higher temperature. A factor which helps to put this peak outside the temperature range covered is that the undoped specimens are about twice as thick as the doped specimens, and so the relaxation time for electrode polarization is doubled, according to equation (75). Had the undoped specimens been only half as thick as they were, this peak may have appeared below 1300°C.

This low temperature peak can be seen (Fig 38) in the

tan δ against frequency graphs in B.O.C. argon. It appears at 200 c/s at 524°C and 6,000 c/s at 619°C. The peak just visible at 880°C and 1592 c/s is believed to be produced by electronic effects. 1026°C was not a high enough temperature to show the effect of blocking of ions at the electrodes.

The graphs of capacity against frequency in B.O.C. argon (Fig 36) show evidence of the ionic behaviour observed in the doped specimens: at 524°C the frequency independent capacity ~~independent capacity~~ indicates that there is no space charge polarization at the higher frequencies (this frequency independent capacity is half that observed for the doped specimens because their thickness was half that of the undoped specimen); the rapid increase of capacity with decreasing frequency at 524°, 619° and 768°C, and the levelling-off of the capacity at low frequencies at 768° and 880°C, indicate grain boundary polarization; and the steeper slope at low frequencies of the curve at 1026° compared with that at 880°C is evidence of electrode polarization.

Variation of capacity with temperature at 1592 c/s in forming gas (Fig 39) confirms the ionic behaviour discussed above. The curve is similar to those obtained for the doped specimens. There are the same indications of grain boundary polarization, breakdown of grain boundary blocking and electrode polarization. A comparison of this graph with those (Figs 47 and 55) for the doped samples suggests that the temperature at which grain boundary polarization ceases to affect the conductivity is approximately the same as for the 0.95 ThO_2–0.05 SrO (1300°C) rather than the 0.95 ThO_2–0.05 CaO sample (1200°C). This may explain the high activation energy (1.39 eV) obtained in forming gas over the temperature range 1160°–1300°C for undoped ThO_2 at 1592 c/s (see Chapter 6.4.)

The variation of conductivity with frequency in B.O.C. argon (Fig 35) is similar to that for the doped specimens in forming gas. At 524°C there is free charge (frequency-independent) conductivity above about 4k c/s. (This is confirmed by the capacity vs frequency, and the gradient (-1) of the tan δ vs frequency, isotherms for the same values of frequency and temperature.) For all temperatures in the range investigated 524°-1026°C there is evidence of grain boundary polarization. 1026°C was not a high enough temperature to demonstrate the effect of electrode polarization on the conductivity.

The shape of the log σ vs T^{-1} curve in forming gas (Fig 16) can be explained in a similar way as for the doped specimens. Comparing Fig 16 with Fig j, there is a noticeable contribution from n-type conductivity at low temperatures which increases the conductivity in region ba, and it seems reasonable to suggest that the point c corresponds to approximately 1300°C.

If the explanation of the dip in the log σ vs T^{-1} curves in forming gas is grain boundary blocking it would be expected that when the temperature is high enough to overcome this, the activation energy should be 1.1 eV in agreement with the value found by Danforth and Bodine for single crystals in vacuum. The activation energy found in this investigation for undoped ThO_2 in forming gas was 1.39 eV over the temperature range 1155°-1300°C. But the graph is slightly curved in this temperature interval, the activation energy decreasing with increasing temperature. Over the range 1240°-1300°C the activation energy is 1.25 eV and it seems quite possible that at temperatures abvoe 1300°C, when it is suggested grain boundary blocking is no longer effective, the value of the activation energy will be 1.1 eV. However, this cannot be known from the present results as 1300°C was the maximum temperature investigated.

If the activation energy of ionic conduction in ThO2

containing 100 p.p.m. divalent impurities (which is approximately equivalent to the impurity content of both Danforth and Bodine's samples and those used in the present work) is really 1.1 eV at 1300°C, there is the problem of explaining why the activation energy in ThO_2 doped with 5 mole °/o SrO or CaO is not considerably higher than this at 1300°C due to a much larger contribution from the energy of association of the divalent ion–oxygen vacancy dipoles.

(c) Space charge polarization effects in air

From the preceding chapters it is known that in air the conductivity of all the compositions investigated is due to two charge carriers: oxygen ion vacancies which contribute about 25°/o of the total conductivity; and positive electron holes which contribute the remaining 75°/o. Since space charge polarization due to one carrier will affect the conductivity and other electrical properties due to the second carrier, the resultant electrical properties are not simply the sum of the two contributions. Because of this the interpretation of the electrical properties in air is more difficult than in forming gas, where there is only one charge carrier.

(i) $0.95\ ThO_2$–0.05 CaO in air

Tan δ plotted against T^{-1} in air (Fig 48) has only one peak at about 800°C. Since there is no trace of this peak when the conductivity is due solely to ions (in forming gas), it is attributed to space charge polarization by the positive electrons. Since electronic space charge polarization at grain boundaries is not uncommon (74), at least at room temperature, and platinum electrodes are normally regarded as reversible to electrons, there is a temptation to ascribe this peak to grain boundary blocking. But the position of it (800°C) relative to the position of the peak due to blocking of ions at the grain boundaries (560°C) argues against this.

a single charge carrier is given by $\tau = \frac{L^2}{D}$, as in equation (75), and this is combined with the Nernst–Einstein equation and the expression for l_D on page 38, it follows that

$$\tau^2 = \frac{L^2 \varepsilon}{2kTc_o\mu^2}$$

where the symbols have the same meanings as in Chapter 2.6. For constant temperature T and thickness L (of grain or specimen), and assuming equation (75) can be applied to electrons and ions separately (ignoring any interactions between the two carriers)

$$\left(\frac{\tau_i}{\tau_e}\right)^2 = \frac{q_i \sigma_e \mu_e}{q_e \sigma_i \mu_i}$$

where the subscripts i and e refer to ions and electrons. Since $q_i = 2q_e$, $\sigma_e \approx 3\sigma_i$ and we would expect μ_e to be larger than μ_i, it follows that $\tau_i > \tau_e$. Therefore, the angular frequency at which the conductivity and capacity vs. log (frequency) isotherms inflect is greater for electrons than for ions i.e. $\omega_e > \omega_i$.

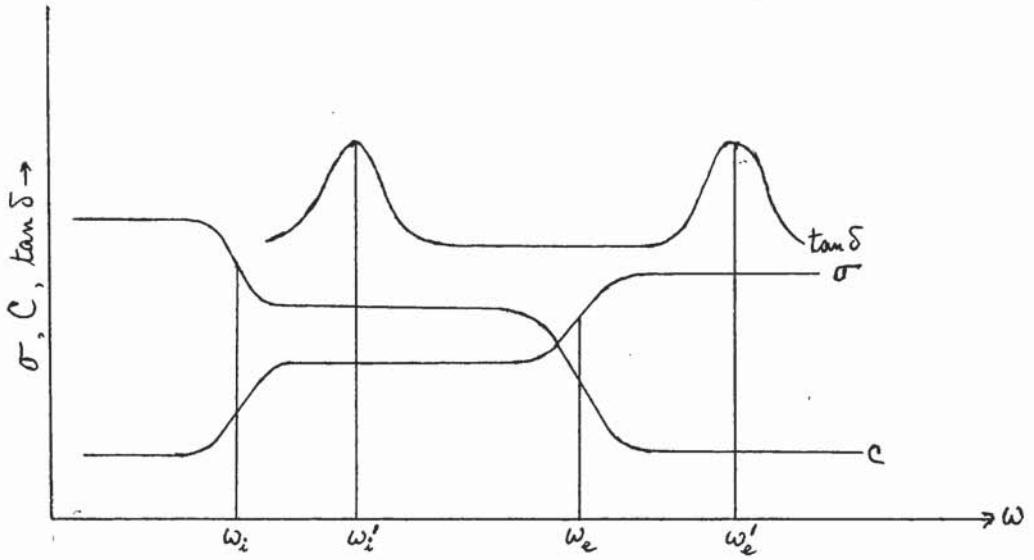

Fig. k.

The frequencies corresponding to the tan δ peaks, $\omega_i^{\,1}$ and $\omega_e^{\,1}$ are related to ω_i and ω_e by the relations (cf. Fig d, Page 29)

$$\omega_i^{\,1} = \left(\frac{C_{si}}{C_{\infty i}}\right)^{\frac{1}{2}} \omega_i \text{ and } \omega_e^{\,1} = \left(\frac{C_{se}}{C_{\infty e}}\right)^{\frac{1}{2}} \omega_e$$

There is not sufficient experimental data supplied by the present work to enable an accurate evaluation of the capacity ratios to be made. However, since it would require an extremely large

ionic capacity ratio relative to the electronic capacity ratio to make ω_i^{-1} greater than ω_e^{-1}, it will be assumed this does not happen. This means that the temperature at which the loss peak due to electronic grain boundary polarization occurs must be below that corresponding to ionic grain boundary polarization (at fixed frequency). So the observed loss peak in air cannot be due to blocking at the grain boundaries, but is ascribed instead to blocking at the electrodes. The loss peak due to grain boundary blocking of the electrons must be at a temperature below 550°C. There is no sign of it for this composition as low enough temperatures were not used but it can just be seen for the 0.95 ThO_2–0.05 SrO sample (Fig 56).

The 800°C, 1592 c/s peak discussed above can be seen in Fig 45 in the 868°C isotherm of tan δ against frequency at 4000 c/s. The same peak is at 1000 c/s at 734°C and approximately 50 c/s at 601°C. There are signs of another peak at 1067°C and about 2000 c/s, 1266°C and 8000 c/s, and 1407°C and a frequency above 20k c/s. This second peak is probably caused by ionic blocking at the electrodes.

The graph of capacity as a function of T^{-1} is shown in Fig. 47. Since the electrons have a greater mobility than the ions, at 1592 c/s and a given temperature they will reach the grain boundaries, or the electrodes, before the ions. As the temperature rises from 550°C the capacity, which is much greater than that due to ions alone, increases. This increase can be interpreted as being caused by blocking of electrons at the grain boundaries. The levelling–off of the curve at about 700°C may indicate maximum grain boundary electronic polarization. The subsequent rapid increase in capacity with rising temperature can be explained by a breakdown in grain boundary blocking and a build up of electronic space charge at the electrodes. The

lower capacity in air in the temperature range 680°C – 850°C compared with that in forming gas may be explained by the presence of electronic space charge at the grain boundaries which, by repelling oxygen vacancies, tends to prevent their build–up at the grain boundaries and makes the ionic effects appear at higher temperatures than when ionic defects alone are present. Also at temperatures above 700°C the rapid increase in capacity attributed to electronic polarization at the electrodes hides any effects of grain boundary ionic polarization. Presumably at higher temperatures than the maximum (1465°C) investigated the capacity in air will again increase because of ion blocking at the electrodes.

The graphs of capacity as a function of frequency (Fig 42) show the presence of space charge polarization effects. At 601°C the loss peak due to grain boundary electronic polarization occurs at a frequency greater than 20k c/s whereas that due to electrode electronic polarization occurs at about 50 c/s. So we might expect in the range 50 c/s – 20k c/s the complete absence of space charge due to electrons at the electrodes, but not at the grain boundaries. The shape of the 601°C capacity against frequency curve may therefore be attributed to build–up of electronic space charge at the grain boundaries. The slope of the 734°C curve may be attributed to electronic polarization at the grain boundaries for frequencies above 1000 c/s and at the electrodes for lower frequencies. Above 868°C there will be no noticeable effect on the slope of the curve of electrons at grain boundaries. The behaviour above 1000°C is due to a combination of electronic and ionic effects.

At 601°C the results discussed above indicate that there will be the maximum electronic space charge at the grain boundaries for low frequencies, and less as the frequency increases. This explains the increase in conductivity with frequency (Fig 41)

at this temperature. At 734°C the frequency dependence of the conductivity at the high and low ends of the frequency range is possibly due to blocking of electrons at the grain boundaries and electrodes respectively. At 868° and 1067°C the frequency dependence can be explained in terms of blocking of electrons at the electrodes. For higher temperatures blocking of ions at the electrodes may be the major cause of the slight dependence of conductivity on frequency. Since above 734°C the frequency dependence, attributed at least partly to electron blocking at the electrodes, is very small (certainly in comparison with that at 601°C), it appears that the build-up of electronic space charge at the electrodes does not produce a significant change in the conductivity and so the presence of this space charge at the electrodes probably does not introduce an important error into the conductivity value.

After examining the frequency dependence of the conductivity, capacity and dielectric loss tangent, and the temperature dependence of the capacity and loss tangent of 0.95 ThO_2–0.05CaO in forming gas it was possible to explain the reason for the unusual shape of the graph of log σ vs T^{-1}, and to identify two temperature ranges where the conductivity and activation energy might reasonably be assumed to be that of the bulk material. This was because at the highest temperatures employed the effect of ionic space charge polarization at the electrodes was not yet large enough to affect the conductivity by more than a few °/o and the ionic grain boundary polarization had disappeared because of a decrease in blocking with rise in temperature. At the lowest temperatures there were no ionic space charge polarization effects at 1592 c/s as the ionic mobility was not large enough to cause charge build-up even at the grain boundaries. But in air polarization caused by blocking of electrons at the electrodes is

noticeable at temperatures well below the maximum employed, and the effect of grain boundary electronic polarization is significant to much lower temperature values than ionic. As a result there are electronic polarization effects present over the entire temperature range covered (550°–1465°C). To make matters worse there are also present ionic polarization effects, the importance of which is unknown, as the effect on the ionic space charges of interaction with the electronic space charges is unknown.

However, although it is difficult to analyse the various polarization effects in air it is probable that here too the high-temperature (above about 1000°C) conductivity values are reasonably close to those of the bulk material: the presence of electronic space charge at the electrodes appears not to have much effect on the conductivity; the results in forming gas show that the blocking of ions at the electrodes will not be important; grain boundary blocking of electrons appears, from the variation of capacity with temperature (Fig 47), to break down at about 200C° lower than that of ions; and the partial blocking of the ionic component should not introduce an error of more than a few °/o. In any case, whatever space charge polarization effects are operative, they do not produce an appreciable variation of conductivity with frequency over the range 100–20,000 c/s at temperatures between 1067°C and 1407°C; nor do they prevent an exponential increase in conductivity with temperature between 1000°C and 1465°C.

On the other hand at temperatures in the range 734°–550°C the conductivity is noticeably dependent on frequency and it is impossible to obtain accurate values for the bulk material. The activation energy at 1592 c/s in this temperature range (Fig 24) obviously cannot be given any theoretical significance.

(ii) $0.95ThO_2$–0.05SrO in air

The variation of tan δ with T^{-1} at 1592 c/s is shown in Fig. 56. Again there is a very pronounced loss peak not found in forming gas. This occurs at a temperature of 830°C, and is attributed to blocking of electrons at the electrodes. Below 500°C there is an increase in tan δ with decreasing temperature as a peak is approached caused by blocking of electrons at the grain boundaries.

The graphs of tan δ against frequency (Fig 53) show the peak due to the electrodes' blocking of electrons, and, as for the CaO–doped specimen, at the highest temperature (1407°C) there are signs of a peak at a frequency above 20k c/s which may be attributed to blocking of ions at the electrodes.. The existence of the peak attributed to grain boundary blocking of electrons can be clearly seen at 515°C and 10,000 c/s.

The graphs of capacity against T^{-1} (Fig. 55) and against frequency (Fig. 50) show similar behaviour to that of the $0.95ThO_2$–0.05 CaO specimen. The lowest temperature measurements on the SrO–doped sample (Fig. 50) show the presence at the highest frequencies of a capacity free from all space charge polarization effects.

The results for conductivity against frequency (Fig. 49) are similar to those of the $0.95\ ThO_2$–0.05 CaO specimen at 623°C and above. At 515°C and 456°C the high–frequency results give a conductivity value unaffected by grain boundary polarization effects, as expected from the position of the tan δ peak attributed to electronic grain boundary polarization (Fig 53). At 456°C the increase in conductivity at frequencies above 5k c/s is due to a contribution from the dipoles.

The behaviour of the conductivity as a function of temperature is much the same as was found for $0.95\ ThO_2$–0.05 CaO.

Here again at high temperatures (above 1000°C) the conductivity may well be reasonably close to that of the bulk material. However, the frequency dependence at temperatures below 750°C is greater than for 0.95 ThO_2–0.05 CaO and in general it is not possible to obtain meaningful values of conductivity and activation energy.

(iii) Undoped ThO_2 in air

The peak produced by the blocking of electrons at the electrodes can be seen in the graph of tan δ against T^{-1} at about 890°C (Fig. 40). It is, however, much less pronounced than for the doped specimens. Part of the explanation of this is that the background dielectric loss is greater for the undoped, than for the doped specimens. Another factor is that the undoped specimens were about twice as thick as the doped specimens and so the peak is displaced to higher temperatures, into the temperature region of large background loss. The displacement of the peak with specimen thickness provides another piece of evidence for the belief that it is produced by electrode, as opposed to grain boundary, effects. Had this peak been produced by grain boundary blocking it would have occurred at a lower temperature than in the doped specimens as the grain size in the undoped specimens (15μ) is half that in the doped specimens. No peak due to grain boundary blocking of electrons was observed as measurements were not carried out at a low enough temperature.

The peak observed in the tan δ vs. T^{-1} plot can just be seen in the graph of tan δ against frequency (Fig 37) at 884°C and about 3000 c/s. At the lower temperatures there is no peak which can be attributed to grain boundary polarization, but the slopes of the graphs show that there is some polarization mechanism operative.

The graph of log C against T^{-1} (Fig 39) shows the same behaviour as for the doped specimens. As discussed for the doped

specimens there is evidence for both grain boundary and electrode blocking of electrons. The decrease in capacity at the highest temperatures may indicate that, in this case, the blocking of electrons at the electrodes is breaking down.

The graphs of capacity (Fig 34) and conductivity (Fig 33) as a function of frequency can be interpreted in terms of blocking of electrons at electrodes and grain boundaries, as for the doped specimens, at temperatures below 884°C. No readings of capacity and conductivity as a function of frequency were taken at temperatures above 884°C, but it was noted that the frequency dependence of the conductivity was negligible.

The low temperature ($<$ 884°C) frequency dependent conductivity is obviously unreliable because of the effect of polarization. However, the high temperature conductivity values and so activation energy may be reasonably accurate, in analogy with the doped specimens.

(d) Space charge polarization effects in atmospheres intermediate in p_{O_2} between air and forming gas

The only results which will be commented on here are those in Fig. 48, which show the variation of tan δ with T^{-1} in different atmospheres. In the argon with a low oxygen content ($<$ 4p.p.m.) three dielectric loss peaks can be seen, at 1115°C, 850°C and approximately 560°C. These are the peaks previously attributed to blocking of oxygen ion vacancies at the electrodes, electron holes at the electrodes and oxygen ion vacancies at the grain boundaries. The appearance at the same value of p_O of peaks believed to be caused by electronic and ionic effects separately, confirms this belief and tends to argue against the interpretation of the peaks in air as ionic peaks, displaced by interaction with electron holes to lower temperatures than those at which they occurred in forming gas.

9.4. Summary

In this chapter the variation of capacity and dielectric loss tangent of each of the specimens discussed in Chapters 6–8 was examined as a function of temperature (at 1592 c/s) and frequency. With the information so obtained an attempt was made to explain the previously noted behaviour of the electrical conductivity of the samples.

It was suggested that the frequency dependence of the electrical properties was caused by blocking of both oxygen ion vacancies and electron holes at both grain boundaries and electrodes and also, for the SrO–doped specimen at the lowest temperatures investigated, by dipolar relaxation.

It was shown that Wachtman's results imply that any dielectric loss peak observed for CaO–doped ThO_2 at frequencies below 20k c/s and temperatures above 350°C must have some cause other than dipole relaxation. In fact, no effects of dipoles were observed for CaO–doped ThO_2 down to the lowest temperature (503°C) investigated. However, for the SrO–doped specimen a variation of conductivity with frequency caused by the Sr_{Th}^{2-}–V_o^{2+} dipoles was found below 600°C. The occurrence of dipole effects in the SrO–doped specimen at higher temperatures than in that doped with CaO means that the activation energy of motion of an oxygen vacancy is greater in 0.95 ThO_2–0.05 SrO than in 0.95 ThO_2–0.05 CaO.

The electrical effects due to ionic motion were examined for the doped ThO_2 in forming gas, and for the undoped ThO_2 in argon when the frequency was being varied and in forming gas at fixed frequency (1592 c/s) when the temperature was being varied. It was concluded that there was interfacial polarization present due to blocking of oxygen ion vacancies at both grain boundaries and electrodes. Grain boundary polarization was the cause of the marked (up to 600%) variation of ionic conductivity

with frequency over the temperature range from about 1100°C to about 550°C and the frequency range 100 c/s – 20 kc/s. The grain boundary blocking and its decrease as the temperature rose produced the dip observed in the log σ vs T^{-1} curves at 1592 c/s in forming gas for all the specimens examined. Electrode polarization caused the measured conductivity of the 0.95ThO_2–0.05 CaO specimen at 1592 c/s to be slightly lower than that of the bulk material at the highest temperatures investigated (about 2°/o lower at 1388°C). Electrode polarization was not observed to affect the conductivity of the other specimens.

It was suggested that the activation energy for ionic conduction could be obtained from the log σ vs T^{-1} curves, at 1592 c/s, in forming gas, when the temperature was high enough to make grain boundary blocking negligible (above about 1300°C, 1200°C and 1300°C for undoped ThO_2, 0.95 ThO_2–0.05 CaO and 0.95 ThO_2–0.05 SrO respectively), provided there was no error introduced by electrode polarization. It was also possible to obtain this activation energy from the same curves when the temperature was low enough that grain boundary polarization introduced no error, provided there were no effects on the conductivity from dipole relaxation or the appearance of n–type electronic conductivity.

In air the conductivity of the specimens was predominantly ($\sim$ 75°/o) electronic. When tan δ was plotted against T^{-1}, peaks were observed which were not present when the conductivity was ionic (i.e. in forming gas). It is believed these peaks showed the presence of electronic space charge polarization produced by blocking at both grain boundaries and electrodes. It was tentatively suggested that electronic polarization effects may explain many of the observed features of the behaviour of the electrical properties in air. Blocking of electrons at the electrodes did not appear to have much effect on the conductivity,

unlike that at grain boundaries which was proposed as the explanation of the pronounced frequency dependence of the conductivity at the lower temperatures (below 700°–900°C). It was suggested that the activation energies obtained from the log σ vs T^{-1} graphs at 1592 c/s may be reasonably accurate at temperatures above about 1000°C, but at low temperatures, where the conductivity is very dependent on frequency, they cannot be regarded as giving the energy of conduction in the bulk material. The analysis of the experimental results in air is necessarily more uncertain than in forming gas, because of the presence in air of two charge carriers and their unknown mutual interaction.

Finally it was pointed out that, in the graph of tan δ against T^{-1} for 0.95 ThO_2–0.05 CaO in argon containing less than 4 p.p.m. O_2, there were two peaks which had been found in forming gas and were produced by blocking of oxygen ion vacancies, and another peak which had been found in air and attributed to blocking of electrons at the electrodes. The appearance of this latter peak in the same atmosphere as the two ionic peaks confirmed that it was produced by electrons.

CHAPTER 10

CONCLUSIONS AND SUGGESTIONS FOR FURTHER WORK

CONCLUSIONS AND SUGGESTIONS FOR FURTHER WORK

10.1 Conclusions

The conclusions which can be drawn from this work are contained in the summaries at the ends of the four preceding chapters, so only those which are thought to extend or contradict previous investigations are reviewed briefly here.

It has been found that the electrical conductivity of polycrystalline specimens of undoped thoria containing the equivalent of about 100 p.p.m. divalent impurities, and thoria doped with small quantities ($\leqslant 5$ mole %) of CaO or SrO is very dependent on the measurement frequency for wide ranges of temperature and oxygen partial pressure.

When the conductivity is purely ionic the cause of this frequency dependence over the temperature range from about 1100°C to about 550°C is grain boundary blocking of oxygen ion vacancies. In addition for the 0.95 ThO_2–0.05 CaO specimen there was a variation between 1380°C and 1440°C caused by blocking of the oxygen vacancies at the electrodes, and for the 0.95 ThO_2–0.05 SrO specimen a variation between 500° and 600°C caused by the presence of Sr_{Th}^{2-}–V_O^{2+} dipoles. It appears from this investigation that the values of ionic conductivity obtained at 1592 c/s in the temperature range of approximately 1250°–1450°C are the true values for the bulk material with an error due to polarization effects of no more than a few percent. At the lower temperatures (about 500°–700°C) too, it is possible to choose frequency values in the range 30 c/s – 20 kc/s at which the ionic conductivity is independent of space charge and dipole polarization effects. However it appears that, at no frequency in the range 30 c/s – 20 kc/s, for temperatures between about 700°C and 1100°C, is the ionic conductivity value that of the bulk material.

In air, where the conductivity is predominantly (about

75%) electronic, it was suggested that the explanation of the frequency dependence at the lower temperatures (about 800°–500°C) might be blocking of electron holes at the grain boundaries. The effects of ion blocking at the grain boundaries could not be clearly distinguished in air, though they presumably play some part in the observed behaviour. At these low temperatures no conductivity value in the frequency range 30 c/s – 20kc/s could be definitely identified as that of the bulk material. At high temperatures (above about 1000°C) it seems plausible, though there is no conclusive proof of this, that the conductivity values are reasonably close to those of the bulk material. At these high temperatures the conductivity is almost independent of frequency.

An important consequence of this frequency dependence of the conductivity is that in general an activation energy obtained from the slope of a graph of log (conductivity) against reciprocal absolute temperature at a fixed frequency cannot be regarded as the activation energy of conduction in the bulk oxide, independent of the presence and properties of grain boundaries and electrodes. Another consequence is that the slopes of graphs of log (conductivity) against log (oxygen partial pressure) may depart drastically from those expected theoretically, or agreement between experiment and theory may be fortuitous. Before these graphs can be used to elucidate the conductivity behaviour, care must be taken to ensure that there are no interfering polarization effects present.

From the appearance of dipole relaxation effects in SrO–doped ThO_2 at higher temperatures than in CaO–doped ThO_2, it is known that the activation energy of motion of an oxygen ion vacancy is higher in the SrO–doped material. This is at least part of the explanation of the lower ionic conductivity of

0.95 ThO_2–0.05 SrO compared with 0.95 ThO_2–0.05 CaO.

10.2. Suggestions for further work.

The present investigation could be extended in various ways which would yield useful information on the properties of ThO_2–based systems:–

(i) Measurements carried out at higher temperatures would yield further information on the electrode polarization observed.

(ii) If higher frequencies were used it should be possible to measure directly the change in conductivity produced by grain boundary blocking over a range of temperatures. Hence it might be possible to estimate accurately the temperature at which grain boundary blocking becomes negligible. It might even be possible to observe this temperature.

(iii) The use of purer samples of undoped ThO_2, or of other compositions of ThO_2–CaO or ThO_2–SrO solid solutions, might yield materials with a greater proportion of electronic conductivity than those investigated. This would enable the electronic polarization effects to be examined in greater detail.

(iv) The use of specimens of different thicknesses and grain sizes would show if the relaxation time for interfacial polarization varied with the length of the conducting region as predicted by equations (68), (75) and) (76).

(v) Four terminal measurements should make the variation of conductivity with frequency attributed to electrode polarization vanish.

(vi) The use of single crystals should make all the effects, on conductivity, capacity and tan δ, attributed to grain boundary blocking vanish.

(vii) Four terminal conductivity measurements on single crystals would yield values of conductivity and activation energy known to be free from all space charge polarization effects.

Comparison of these results with those of the present investigation would show whether or not the temperature regions thought, in the case of the polycrystalline samples, to give values of conductivity and activation energy characteristic of the bulk material, did in fact do so.

Four terminal measurements on single crystals would also make possible an accurate examination of the variation of the activation energy of conduction with temperature and extent of doping. These results would shed a great deal of light on the association behaviour of divalent cations and oxygen vacancies in ThO_2.

An important problem raised by this work is why there has been no previous mention of pronounced grain boundary polarization effects in ThO_2-based electrolytes. The author has no reason to doubt the accuracy of his experimental observations. The results of the measurements of conductivity, capacity and dielectric loss tangent are self-consistent for each specimen, and the same behaviour is observed for all the compositions investigated. Moreover in some preliminary work, not described in this thesis, the conductivity of another undoped ThO_2 specimen was examined in air and the same type of frequency dependence of the conductivity was observed. This specimen was prepared from a different source of ThO_2 and compacted in the Stubs steel die described in Chapter 4.2. The conductivity measurements were carried out in a different furnace. The only similarity in the treatment of this specimen and the ones discussed in detail was that they were all sintered in the same furnace, though at different temperatures. However, it is difficult to believe that this sintering furnace can produce grain boundaries which block the flow of charge more efficiently than those produced in other furnaces.

The author does not know the solution to this problem. Perhaps the grain boundaries in the specimens he examined were, in fact, more highly blocking than those in most other investigations. Perhaps the same frequency dependent behaviour would have been observed by some other workers, as mentioned in the discussion of Lasker and Rapp's results on undoped ThO_2, had they looked for it. It seems that the answer will come only from an accumulation of data from many experiments like those carried out in this investigation.

APPENDIX

Results of Spectrographic Analysis

Samples of sintered pellets of the compositions on which conductivity measurements were carried out, as well as some of the thorium nitrate starting material, were sent to Johnson Matthey for spectrographic analysis. The results are shown below.

Element found	Materials analysed				
	A	B	C	D	E
Al	30	400	60	40	20
Ca	50	50			50
Fe	30	10	8	20	10
Mg	2	1	2	2	3
Si	30	20	60	200	80
Na	10	10	10	20	50

The numbers are the concentrations of the elements found in ppm. A,B,C and D are samples of undoped ThO_2, 0.95 ThO_2 – 0.05 SrO, 0.95 ThO_2 – 0.05 CaO and 0.99 ThO_2 – 0.01 CaO. E is the thorium nitrate starting material.

1. J. Weissbart and R.J. Ruka — J.Electrochem. Soc., 109,p.723(1962
2. M.A. Hepworth and G. Arthur — Symposium on Magnetoplasmadynamic Electrical Power Generation, University of Durham, 1962.
3. K. Kiukkola and C. Wagner — J. Electrochem. Soc.,104,p.379(1957
4. C. Wagner — Z. phys. Chem.(Leipzig), B21,p.25 (1933).
5. C. Wagner — Atom Movements,p.153. Amer. Soc. Metals, Cleveland, 1951.
6. R.W. Pohl — Phys.Z., 35,p.107(1934); 39,p.36 (1938). Proc. phys.Soc., 49(extra part), p.3(1937).
7. C. Tubandt — Handbuch der Experimentalphysik, Vol.12, Part 1, p.412. Akademische Verlagsgesselschaft, Leipzig, 1933.
8. F.A. Kroger — The Chemistry of Imperfect Crystals North-Holland, Amsterdam, 1964.
9. F.A. Kroger and H.J. Vink — Solid State Physics,Vol.3. Academic Press, New York, 1956.
10. M.F. Lasker and R.A. Rapp — Z.phys.Chem.(Frankfurt), 49,p.198 (1966).
11. A.B. Lidiard — Handbuch der Physik, Vol.20, edited by S. Flugge. Springer-Verlag, Berlin, 1956.
12. H. Kelting and H. Witt — Z. Physik, 126,p.697 (1949).
13. E.J.W. Verwey, P.W. Hoayman and F.C. Romeyn — Chem. Weekblad, 44,p.705 (1948).
14. Y. Haven — J. Chem.Phys., 21,p.171 (1953).
15. J.B. Wachtman — Phys. Rev., 131,p.517 (1963).
16. A.B. Lidiard — Phys. Rev., 94, p.29 (1954).
17. H.W. Etzel and R.J. Maurer — J.Chem.Phys., 18,p.1003 (1950).
18. B.C.H. Steele and C.B. Alcock Trans. AIME, 233,p.1359 (1965).

19.	D. Mapother, H.N. Crooks and R.J. Maurer	J.Chem.Phys., 18,p.1231 (1950).
20.	P. Kofstad	High-Temperature Oxidation of Metals, Wiley, 1966.
21.	A.R. von Hippel	Dielectrics and Waves, Wiley, 1954.
22.	H. Frohlich	Theory of Dielectrics, Oxford University Press, 1949.
23.	H.B. Johnson, N.J. Tolar, G.R. Miller and J.B. Cutler	J.Amer.Ceram.Soc., 49,p.458(1966).
24.	R.W. Ure	J.Chem.Phys., 26, p.1363 (1957).
25.	C.G. Koops	Phys. Rev., 83,p.121 (1951).
26.	N.M. Tallan and H.C. Graham	J.Amer.Ceram.Soc., 48,p.512 (1965).
27.	J.V. Florio	J.Amer.Ceram.Soc., 43,p.262 (1960).
28.	J.C. Macfarlane and C. Weaver	Phil.Mag., 13, p.671 (1966).
29.	R.J. Friauf	J.Chem.Phys., 22, p.1329 (1954).
30.	P.M. Sutton	J.Amer.Ceram.Soc., 47,p.188 and p.219 (1964).
31.	H. Peters and H.H. Mobius	Z.phys.Chem.(Leipzig)209p.298 (1958)
32.	H. Schmalzried	Z. Elektrochem., 66,p.572 (1962).
33.	T.Y. Tien and E.C. Subbarao	J.Chem.Phys., 39,p.1041 (1963).
34.	T.Y. Tien	J.Amer.Ceram.Soc., 47,p.430(1964).
35.	B.T.M. Willis	Proc.Roy.Soc.A, 274,p.122 (1963).
36.	B.T.M. Willis	Proc.Brit.Ceram.Soc., 1,p.9(1964).
37.	F. Hund	Ber. dtsch.keram.Ges., 42,p.251 (1965).
38.	F. Hund	Z. anorg.allgem.Chem., 274,p.105 (1953).
39.	F. Hund and W. Durrwachter	Z. anorg.allgem.Chem., 265,p.67 (1951).
40.	F. Hund and R. Mezger	Z. phys.Chem.(Leipzig), 201,p.268 (1952).

41. E.C. Subbarao, P.H. Sutter and J. Hrizo — J.Amer.Ceram.Soc., 48,p.443 (1965).

42. J.M. Wimmer,L.R. Bidwell and N.M. Tallan — J.Amer.Ceram.Soc., 50,p.198 (1967).

43. F. Hund — Z.phys.Chem.(Leipzig),199,p.142(1952)

44. C.E. Curtis and J.R. Johnson — J.Amer.Ceram.Soc., 40,p.63 (1957).

45. H.H. Mobius, H. Witzmann and W. Witte — Z.Chem., 4, p.152 (1964).

46. Z.S. Volchenkova and S.F. Pal'guev — Trans.Inst.Electrochem. USSR, (English Transl.) 4, p.53 (1964).

47. M. Foex — Comptes Rendus, 215,p.534 (1942).

48. S.F. Pal'guev and A.D. Neuimin — Trans.Inst.Electrochem.USSR,(English Transl.), 1, p.90 (1961).

49. J.E. Bauerle — J.Chem.Phys., 45, p.4162 (1966).

50. J.W. Patterson, E.C. Bogren and R.A. Rapp — J.Electrochem.Soc., 114,p.752(1967).

51. Z.S. Volchenkova and S.F. Pal'guev — Trans.Inst.Electrochem.USSR(English Transl.), 1, p.104 (1961).

52. H.S. Edwards, A.F. Rosenberg and J.T. Bittel — Report No. ASD-TDR-63-635, Wright-Patterson Air Force Base, Ohio (July, 1963).

53. W.D. Kingery, J. Pappis, M.E. Doty and D.C. Hill — J.Amer.Ceram.Soc., 42,p.393 (1959).

54. H.A. Johansen and J.G. Cleary — J.Electrochem.Soc., 111,p.100(1964).

55. J. Rudolph — Z.Naturforsch., 14a,p.727 (1959).

56. T.Y. Tien — J.Appl.Phys., 35,p.122 (1964).

57. D.W. Strickler and W.G. Carlson — J.Amer.Ceram.Soc., 47,p.122 (1964).

58. J.M. Dixon, L.D. La Grange, U. Merten, C.F. Miller and J.T. Porter — J.Electrochem.Soc., 110,p.276 (1963).

59. W.E. Danforth and J.H. Bodine — J.Franklin Inst., 260,p.467 (1955).

60. W.E. Danforth — J.Franklin Inst., 266,p.483 (1958).

61. R.W. Vest and N.M.Tallan — J.Appl.Phys., 36,p.543 (1965).

62. G. Arthur and J.H.Priest — J.Sci.Insts., 38, p.80 (1961).

63. J.H. Rendall — J.Sci.Insts., 29,p.248 (1952).

64. S.P. Timoshenko — Strength of Materials, Part 2, 2nd Edition. Van Nostrand, New York, 1953.

65. T.W. Penrice — Powder Metallurgy, 1/2,p.79 (1958).

66. B.C.H. Steele — Ph.D. Thesis, University of London, (1965).

67. S.K. Kantan, R.V. Raghaven and G.S. Tendolkhar — 2nd U.N. International Conference on the Peaceful Uses of Atomic Energy, Vol.6, p.134 (1958).

68. G.M. Fryer and J.P. Roberts — Trans.Brit.Ceram.Soc. 62,p.537(1963).

69. C.A. Walker — Ph.D. Thesis, University of Glasgow, 1967.

70. J. Pappis and W.D. Kingery — J.Amer.Ceram.Soc., 44,p.459 (1961).

71. R.W. Vest, N.M. Tallan and W.C. Tripp — J.Amer.Ceram.Soc., 47,p.635 (1964).

72. Z.S. Volchenkova and S.F. Pal'guev — Trans.Inst.Electrochem.USSR,(English Transl.) 1, p.97 (1961).

73. F. Bassani and F.G. Fumi — Nuovo Cim., 11, p.274 (1954)

74. J. Volger — Progress in Semiconductors, Vol. 4, edited by A.F. Gibson. Heywood and Co.Ltd., London, 1960.

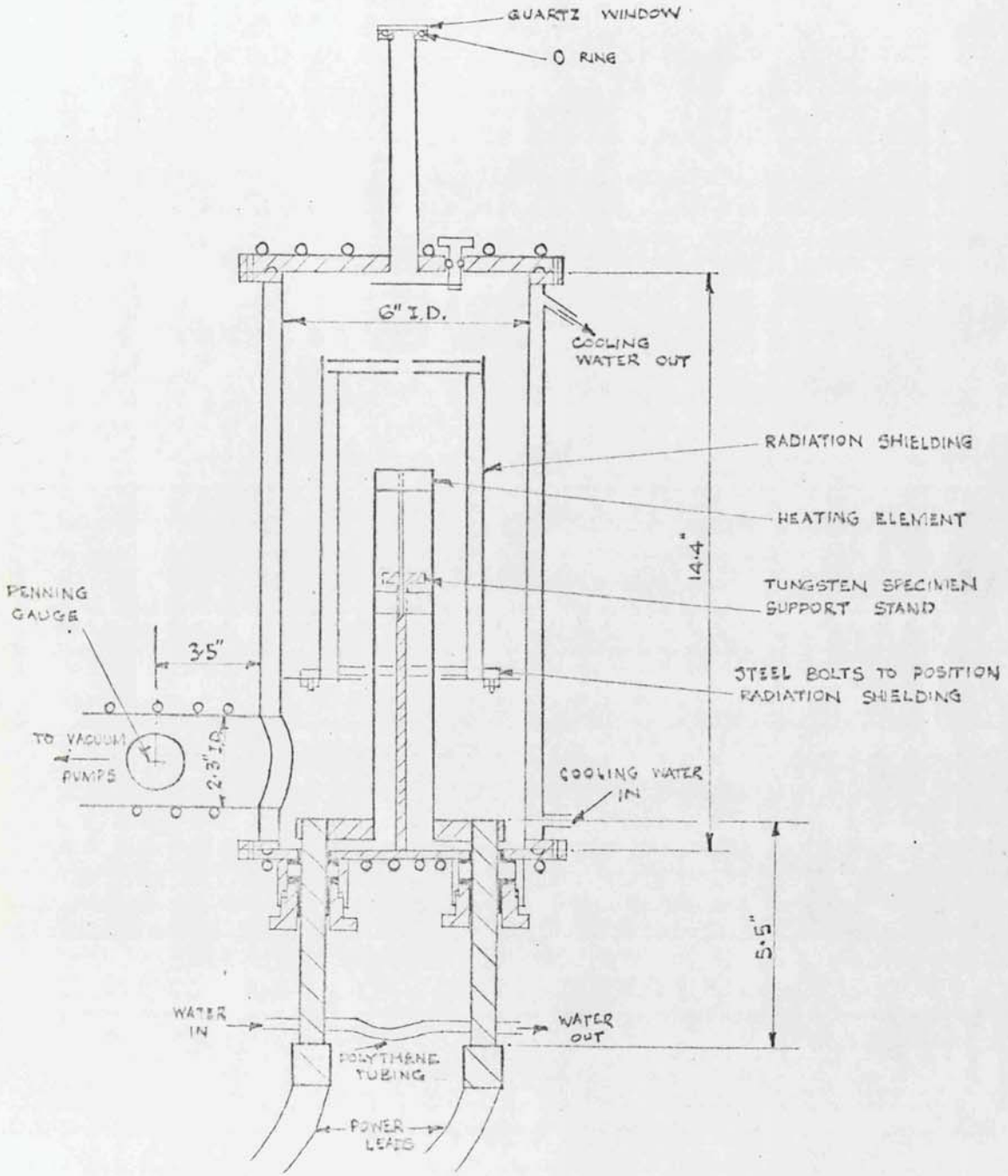
QUARTZ WINDOW
O RING
6" I.D.
COOLING WATER OUT
RADIATION SHIELDING
HEATING ELEMENT
14.4"
TUNGSTEN SPECIMEN SUPPORT STAND
PENNING GAUGE
3.5"
STEEL BOLTS TO POSITION RADIATION SHIELDING
TO VACUUM PUMPS
2.3" I.D.
COOLING WATER IN
5.5"
WATER IN
WATER OUT
POLYTHENE TUBING
POWER LEADS

FIG. 1.

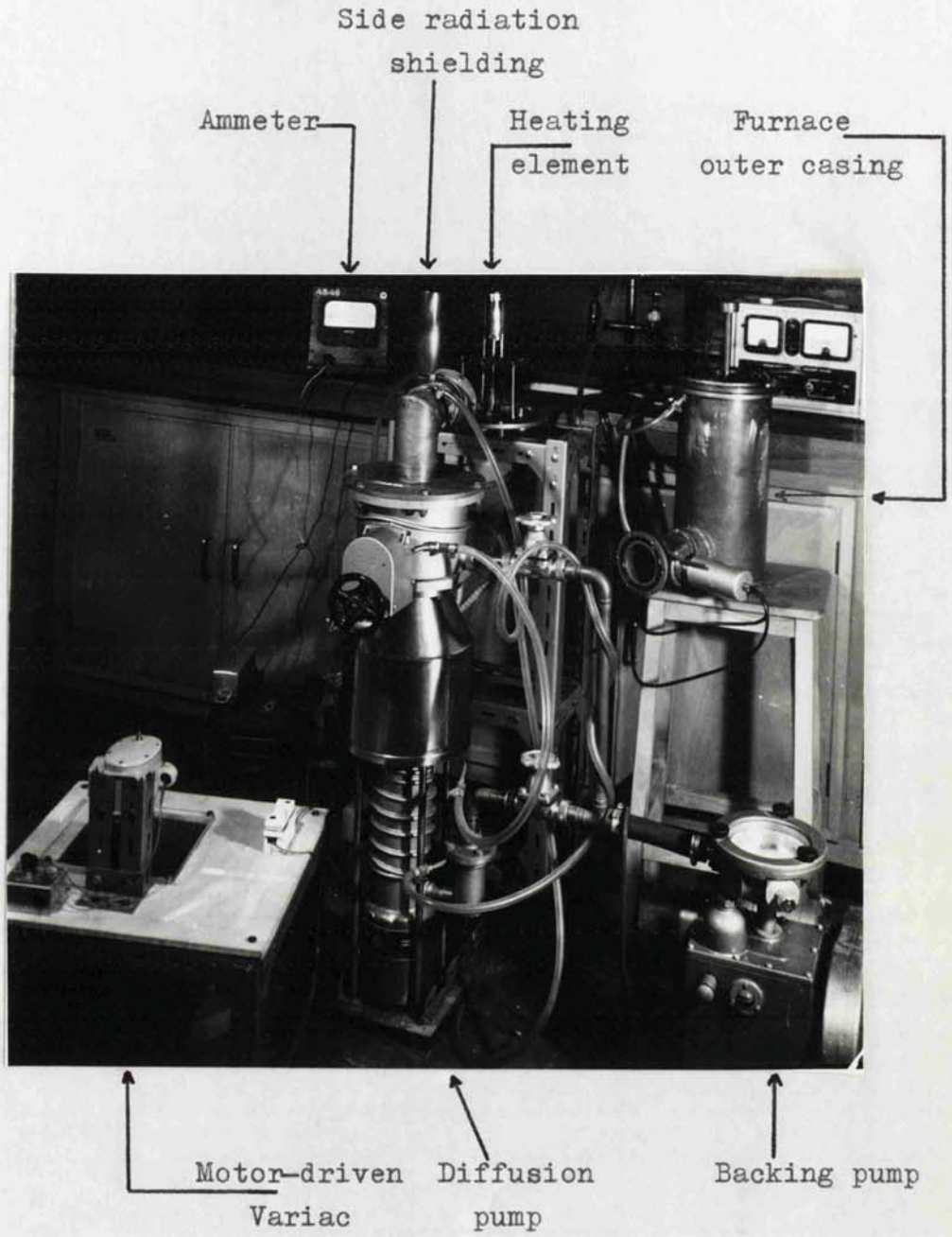

Fig 2. Sintering furnace

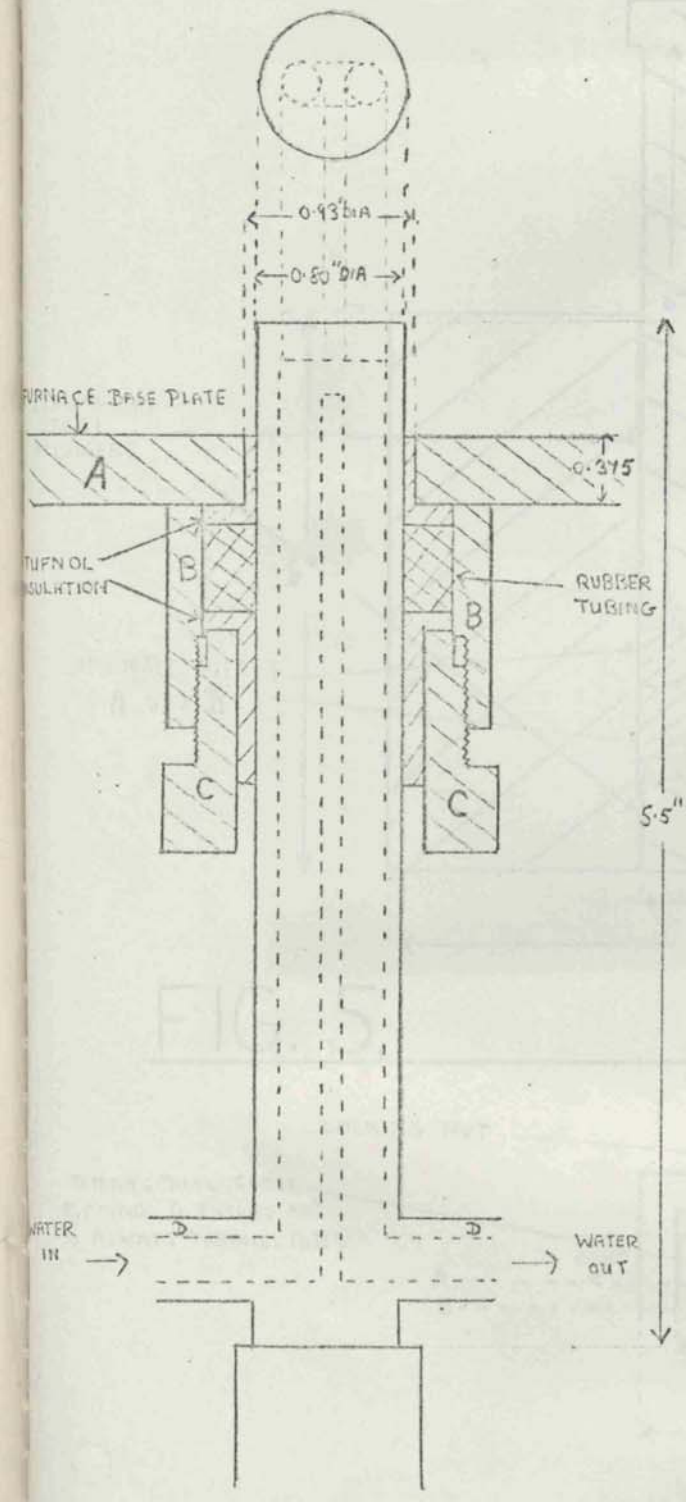
0·93" DIA
0·80" DIA
FURNACE BASE PLATE
A
0·375
TUFNOL INSULATION
B
RUBBER TUBING
B
C
C
5·5"
WATER IN
WATER OUT

FIG. 3.

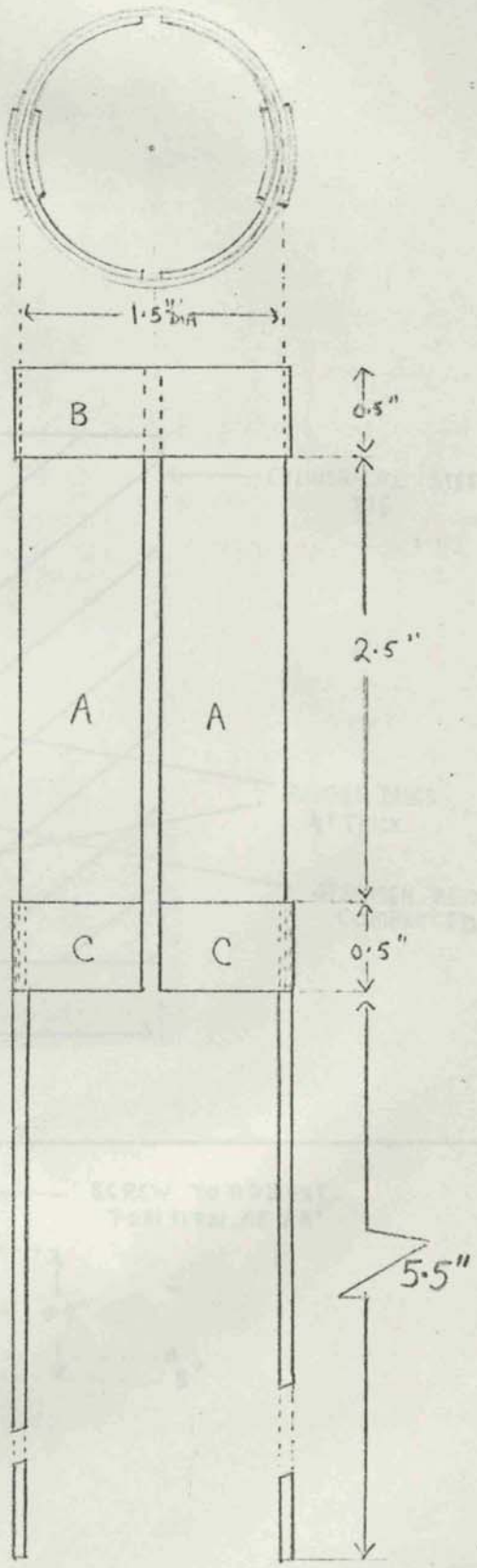
1·5" DIA
B
0·5"
2·5"
A
A
C
C
0·5"
5·5"

FIG. 4.

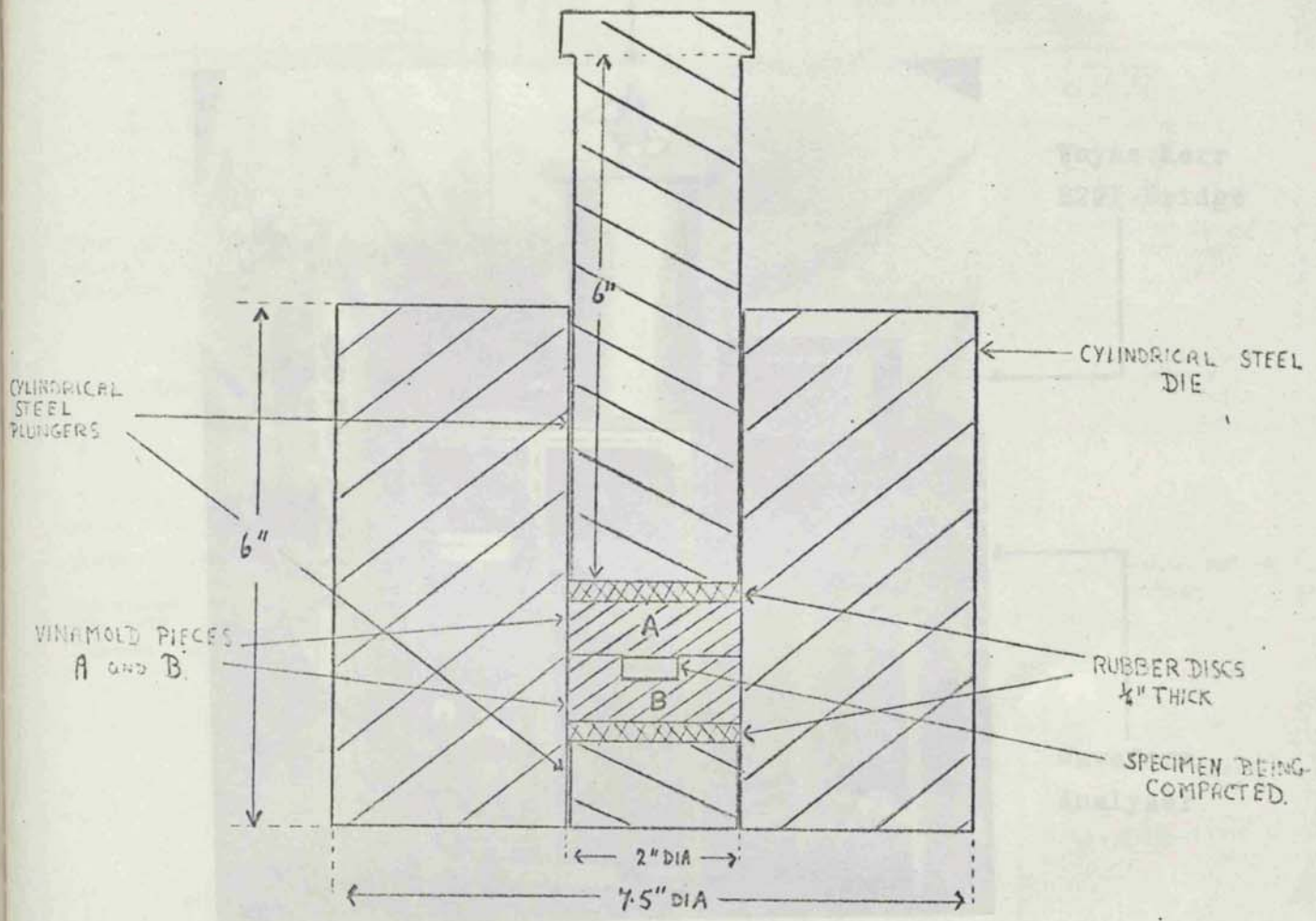
6"
CYLINDRICAL STEEL DIE
CYLINDRICAL STEEL PLUNGERS
6"
VINAMOLD PIECES A AND B
A
B
RUBBER DISCS ¼" THICK
SPECIMEN BEING COMPACTED.
2" DIA
7·5" DIA

FIG. 5.

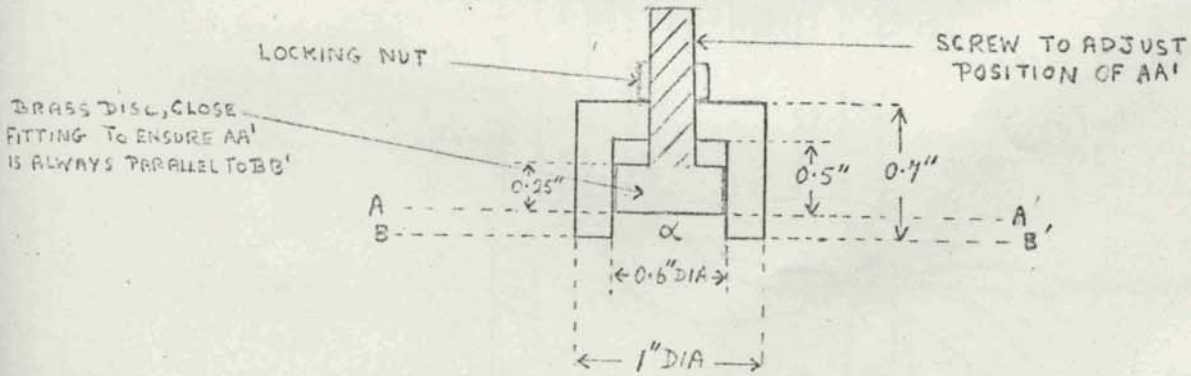
LOCKING NUT
SCREW TO ADJUST POSITION OF AA'
BRASS DISC, CLOSE FITTING TO ENSURE AA' IS ALWAYS PARALLEL TO BB'
0·25"
0·5"
0·7"
A
B
α
A'
B'
0·6" DIA
1" DIA

FIG. 6.

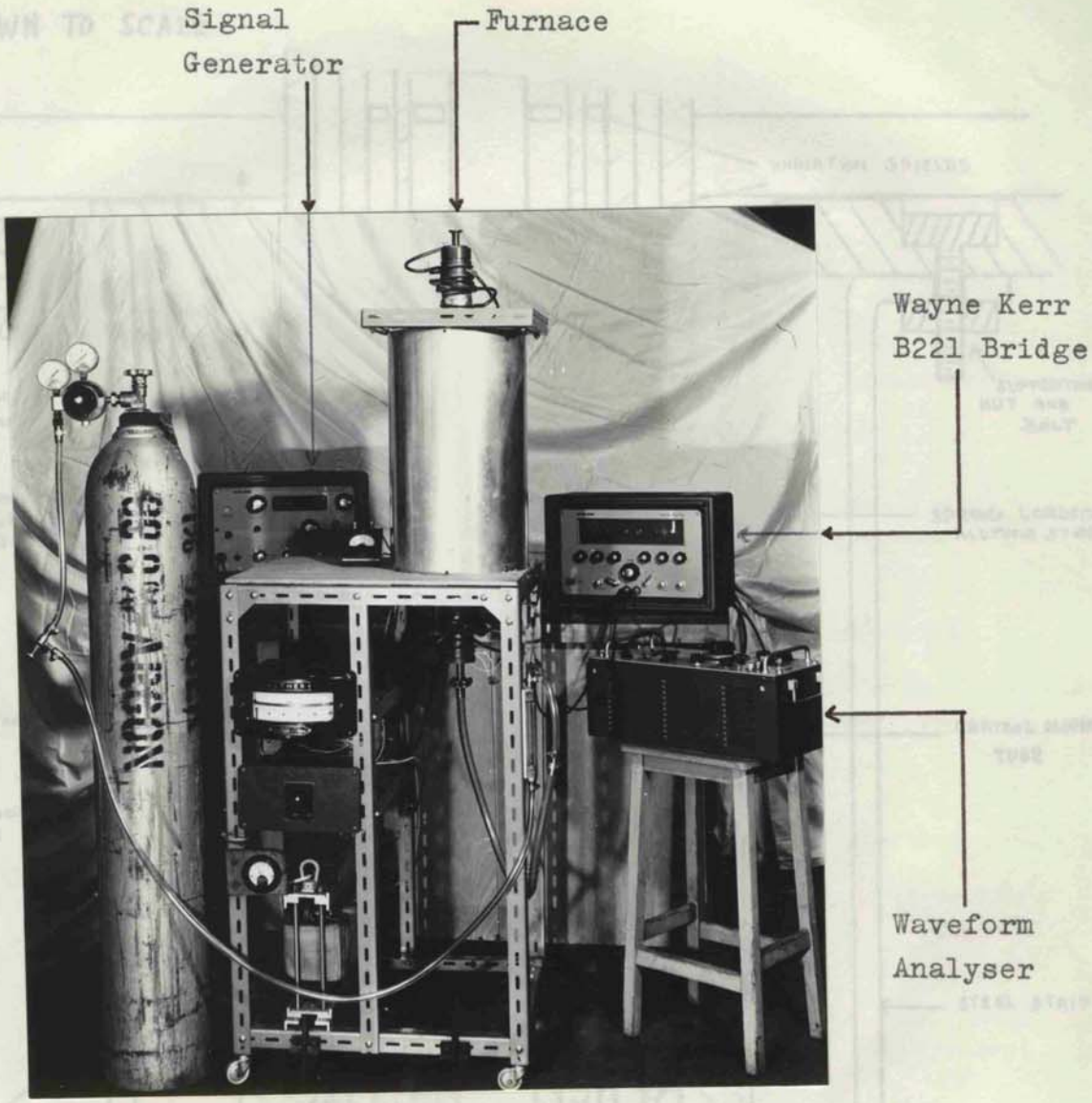

Fig 7 Furnace and associated equipment for carrying out electrical conductivity measurements.

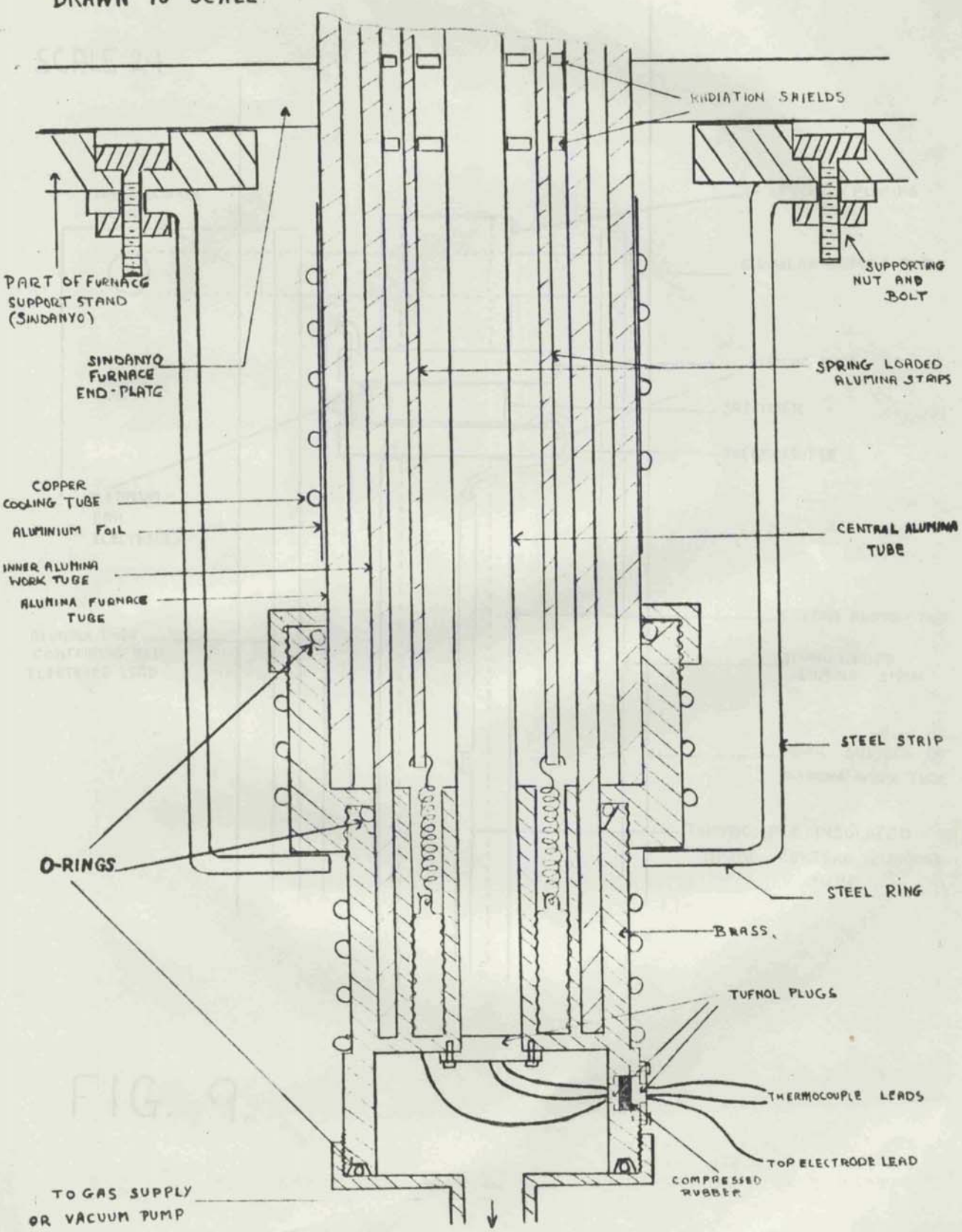
DRAWN TO SCALE
RADIATION SHIELDS
PART OF FURNACE SUPPORT STAND (SINDANYO)
SUPPORTING NUT AND BOLT
SINDANYO FURNACE END-PLATE
SPRING LOADED ALUMINA STRIPS
COPPER COOLING TUBE
ALUMINIUM FOIL
CENTRAL ALUMINA TUBE
INNER ALUMINA WORK TUBE
ALUMINA FURNACE TUBE
STEEL STRIP
O-RINGS
STEEL RING
BRASS
TUFNOL PLUGS
THERMOCOUPLE LEADS
TOP ELECTRODE LEAD
COMPRESSED RUBBER
TO GAS SUPPLY OR VACUUM PUMP

FIG. 8.

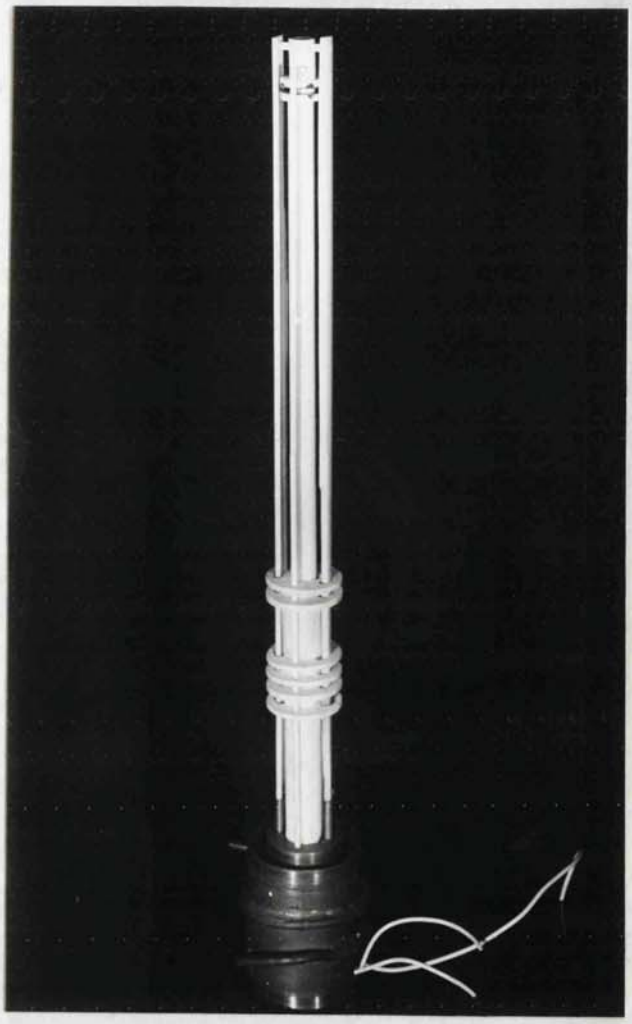

Fig 10 Specimen holder for electrical conductivity measurements.

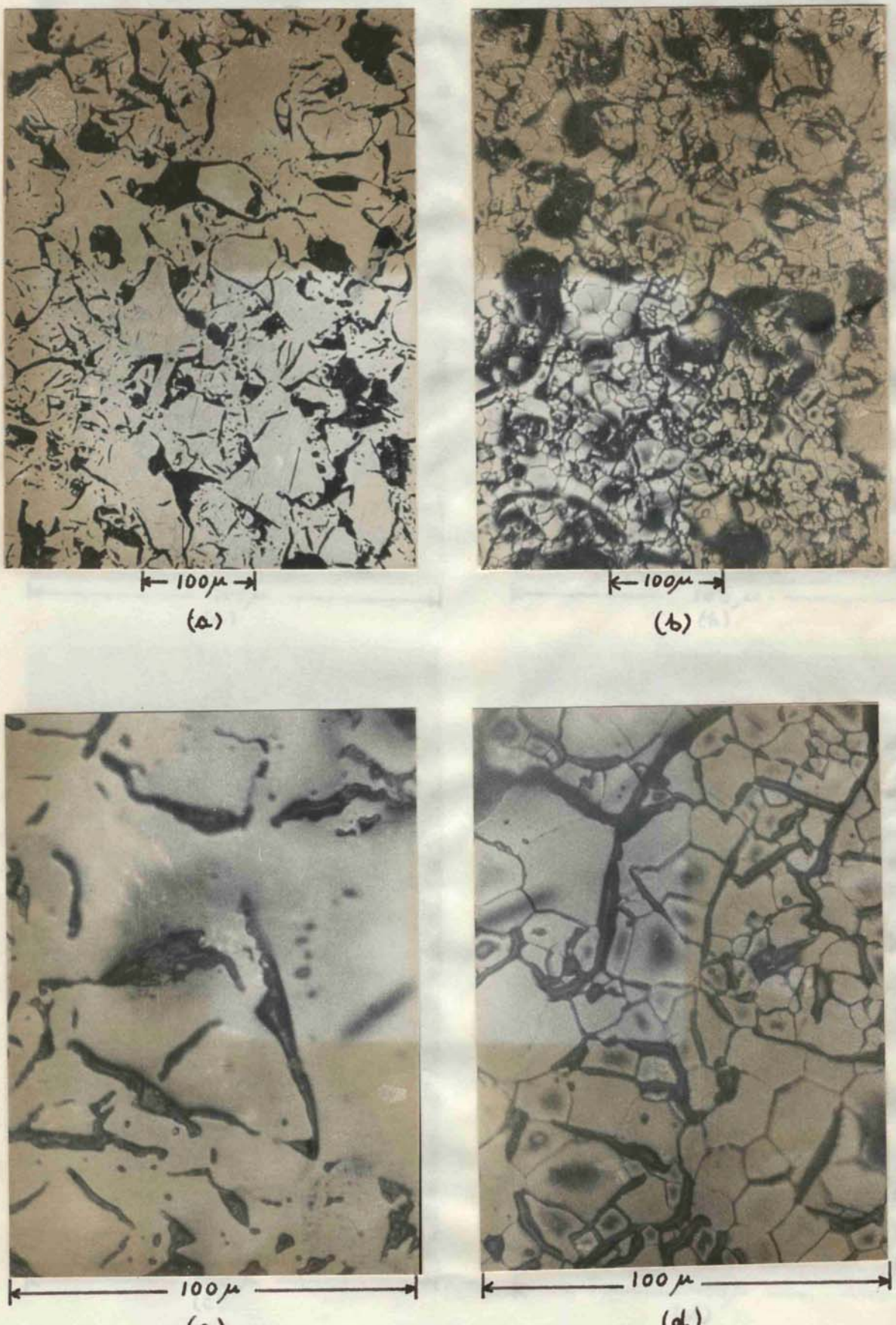

Fig. 11. Undoped ThO_2. (a) and (c) unetched; (b) and (d) etched for 6 minutes.

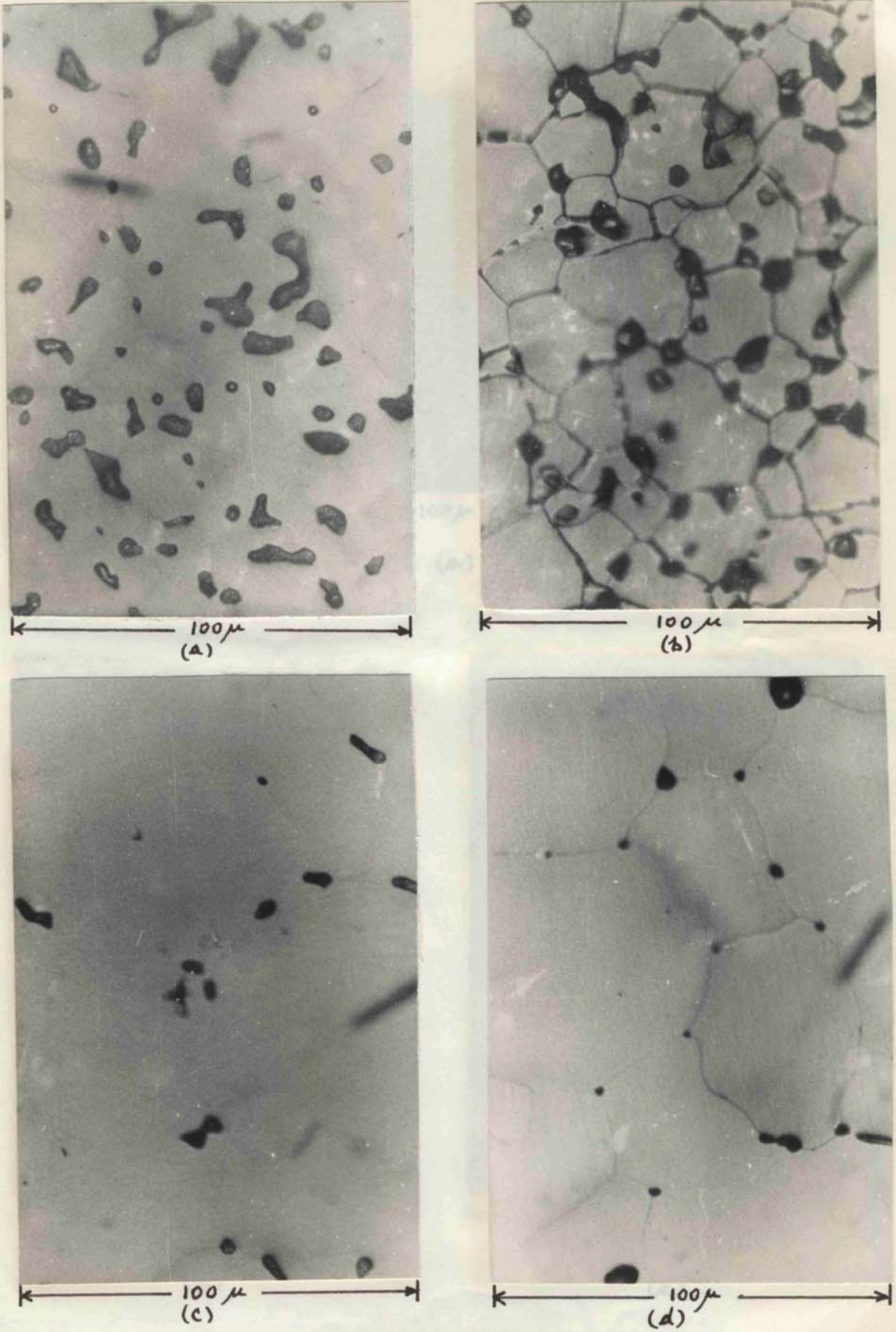

Fig. 12. (a) 0.99ThO_2–0.01CaO unetched; (b) 0.99ThO_2–0.01CaO etched 25 minutes
(c) 0.95ThO_2–0.05CaO unetched; (d) 0.95ThO_2–0.05CaO etched 5 minutes

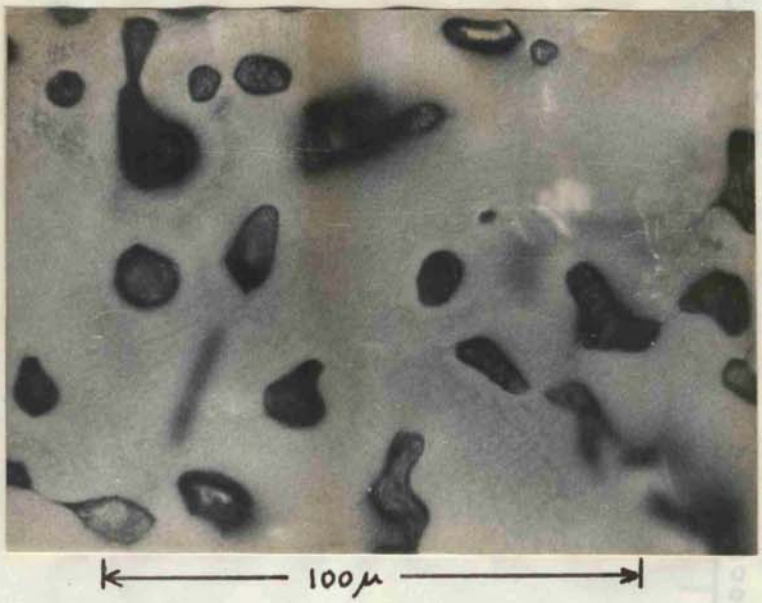

(a)

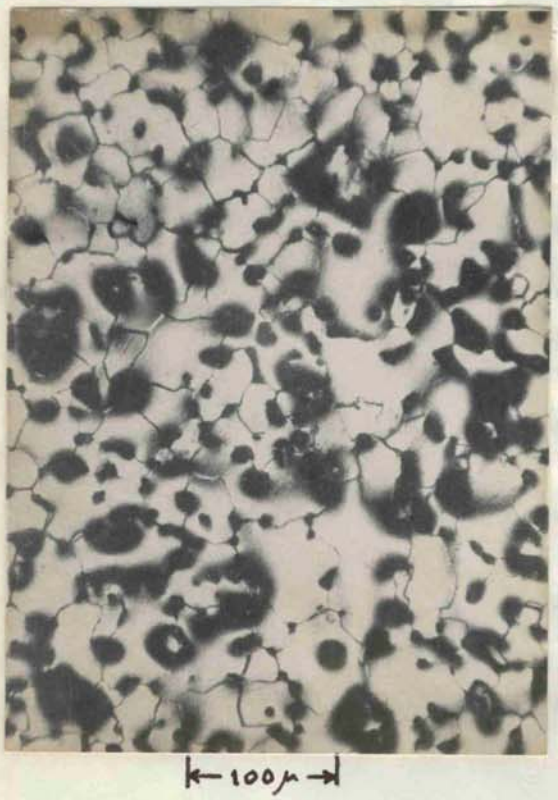

(b)

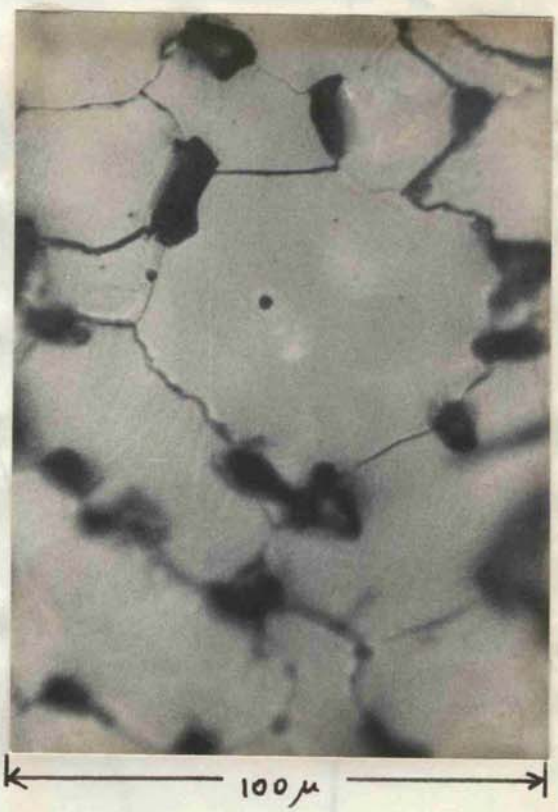

(c)

Fig. 13. $0.95ThO_2$–0.05SrO (a) unetched; (b) and (c) etched for 25 minutes.

Fig. 14 Variation of lead resistance with temperature

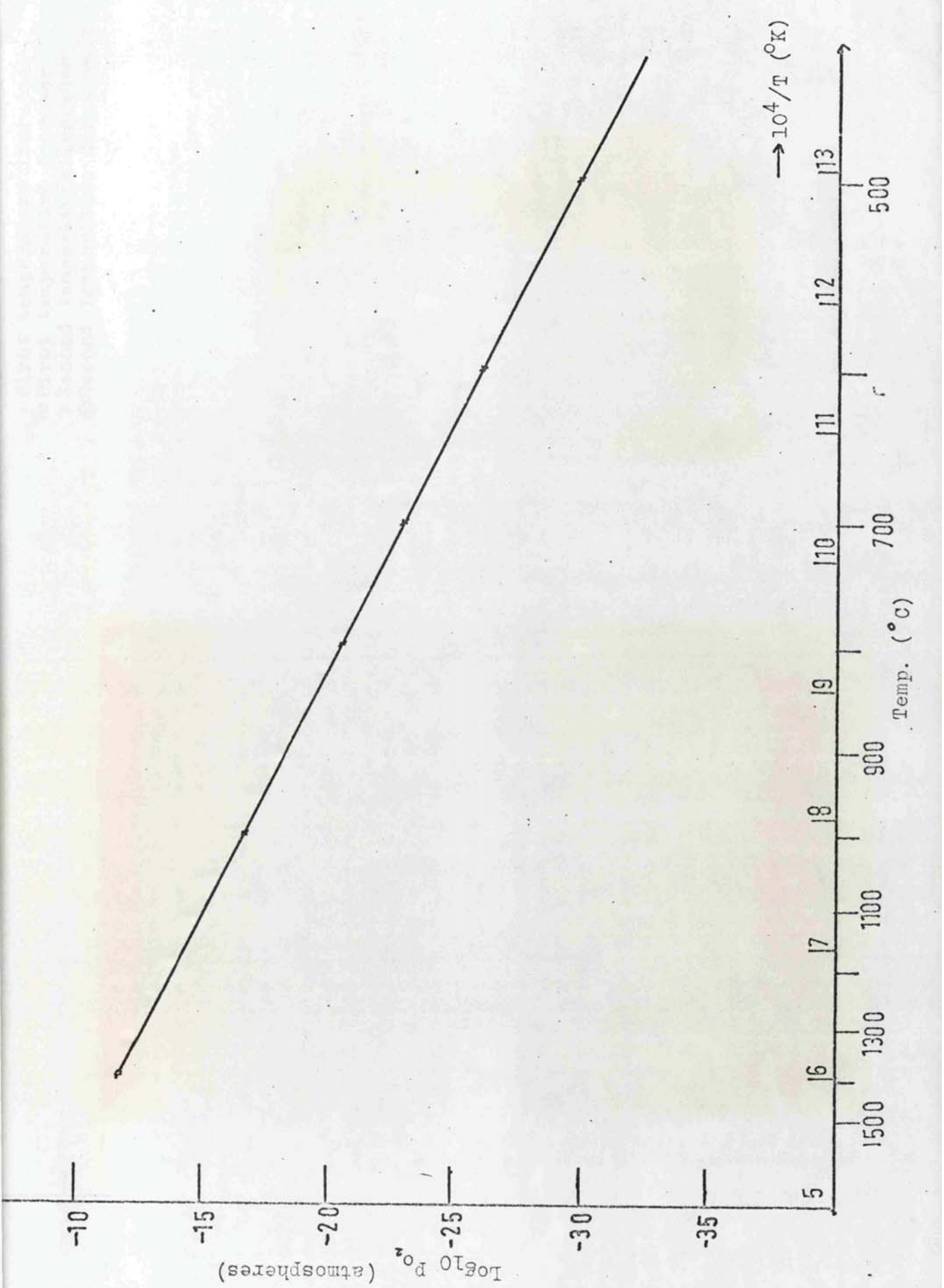

Fig. 15 Variation with temperature T of oxygen partial pressure P_{O_2} in wet forming gas.

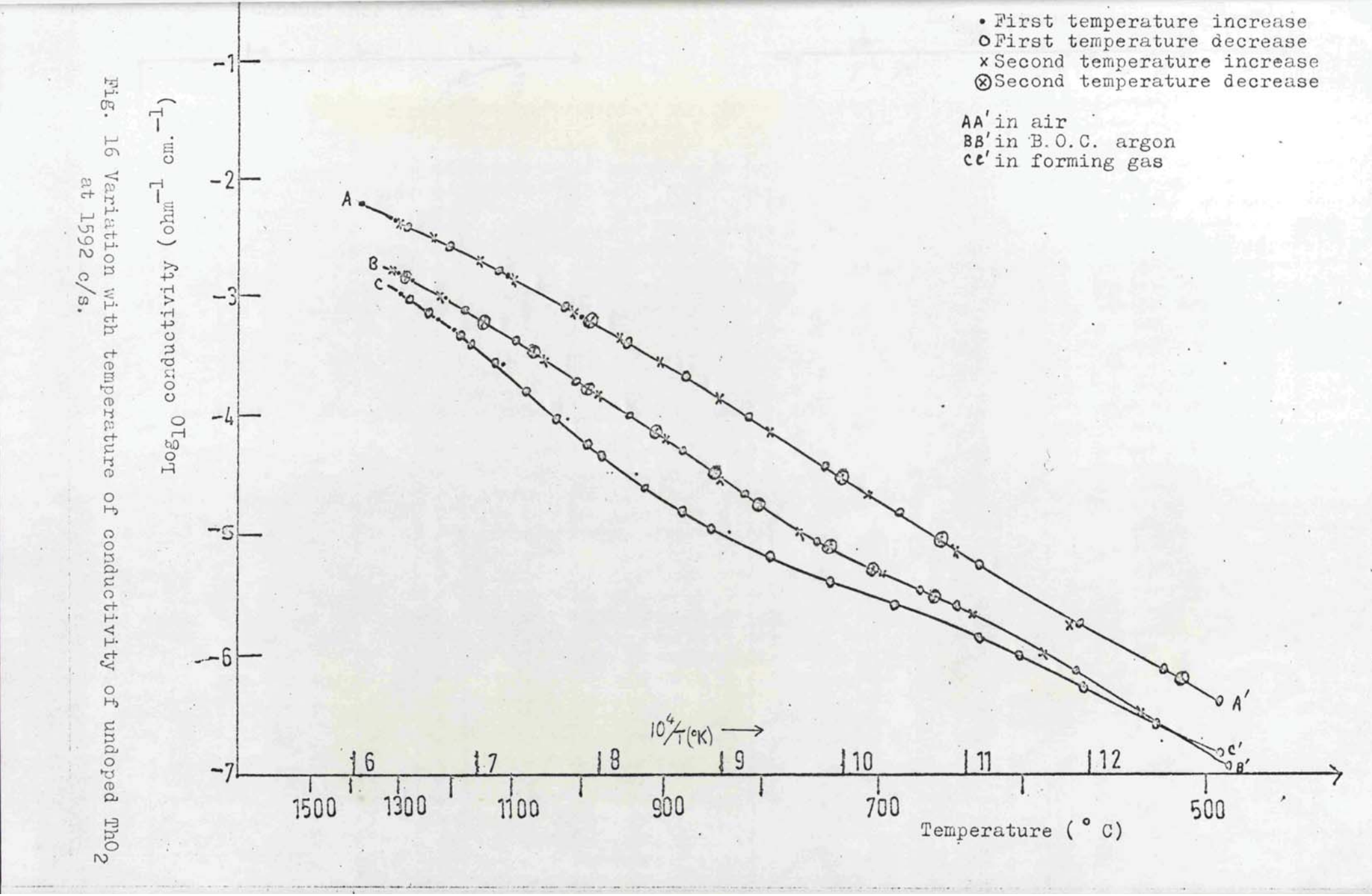

Fig. 16 Variation with temperature of conductivity of undoped ThO_2 at 1592 c/s.

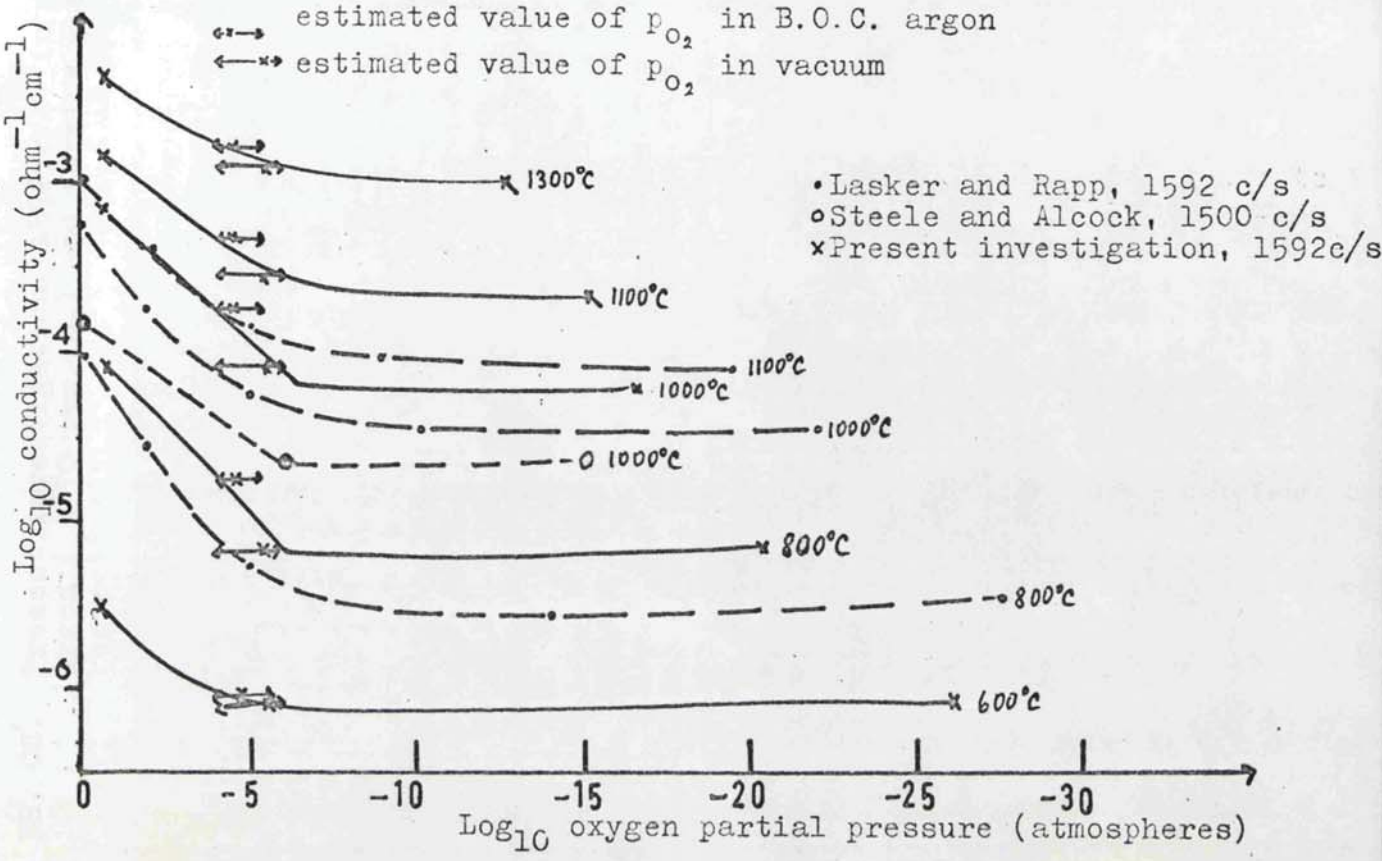

Fig. 17. Variation of conductivity at 1592 c/s of undoped ThO_2 with oxygen partial pressure.

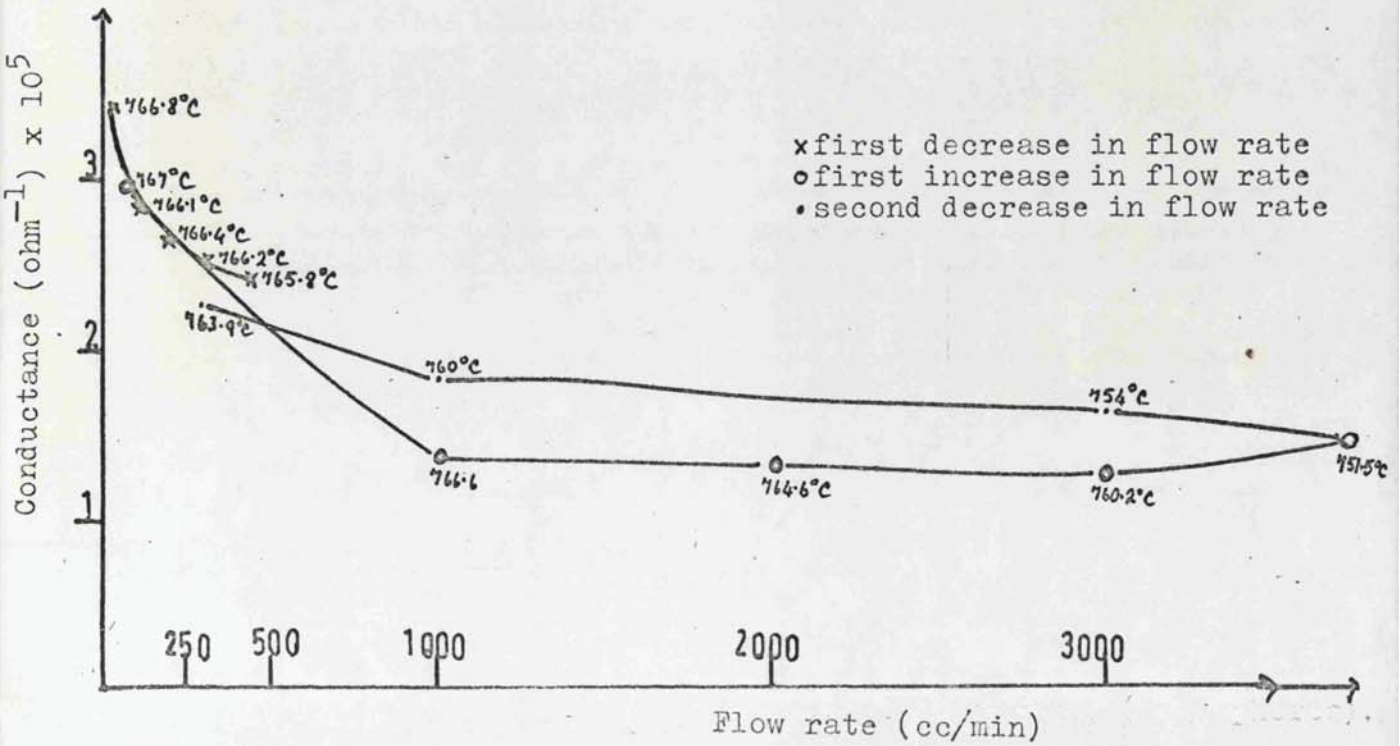

Fig. 18. Variation of conductance at 1592 c/s with flow rate of B.O.C. argon for undoped ThO_2

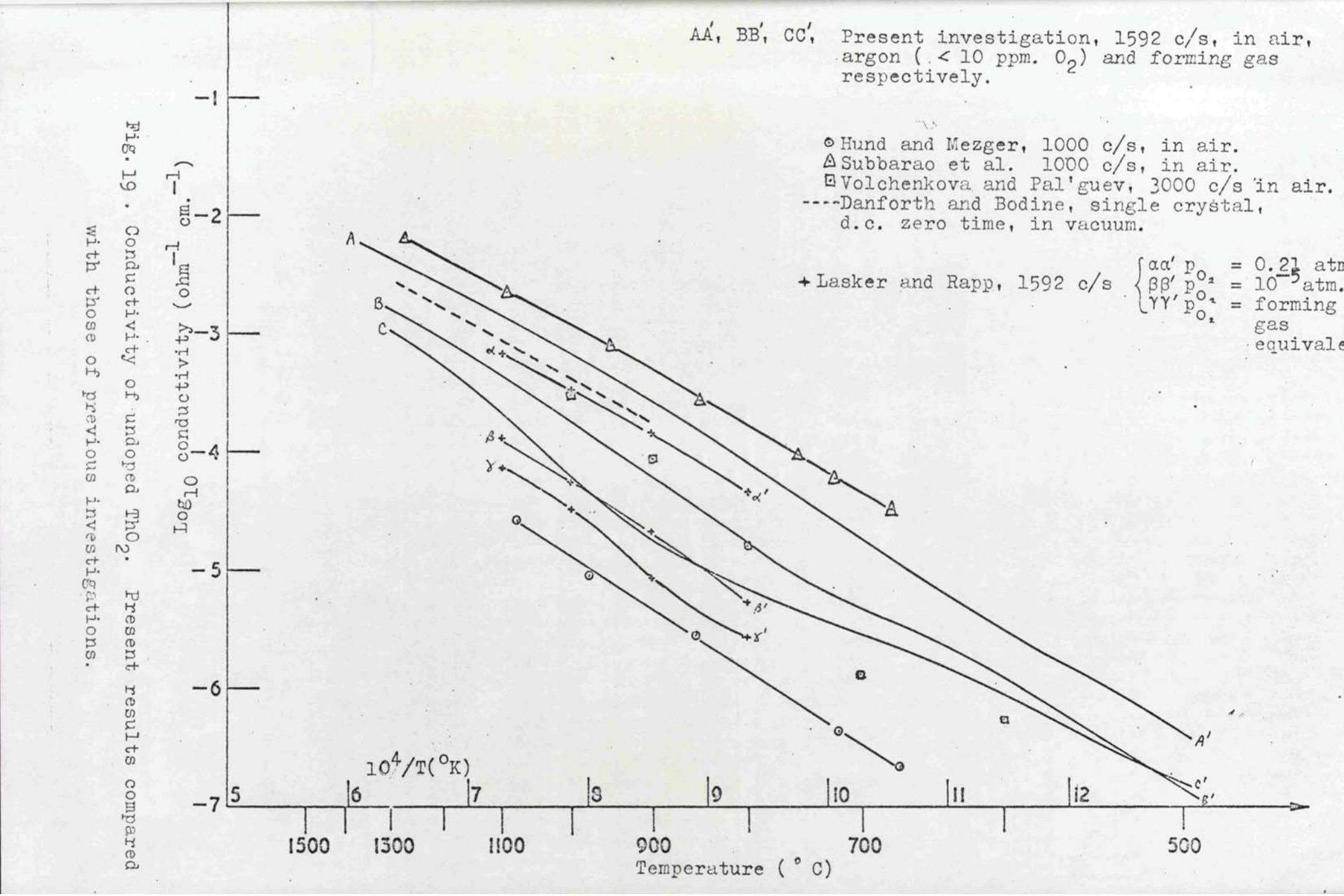

Fig. 19 . Conductivity of undoped ThO_2. Present results compared with those of previous investigations.

Fig. 20. The effect of different measuring frequencies on the variation of conductivity with temperature for undoped ThO_2

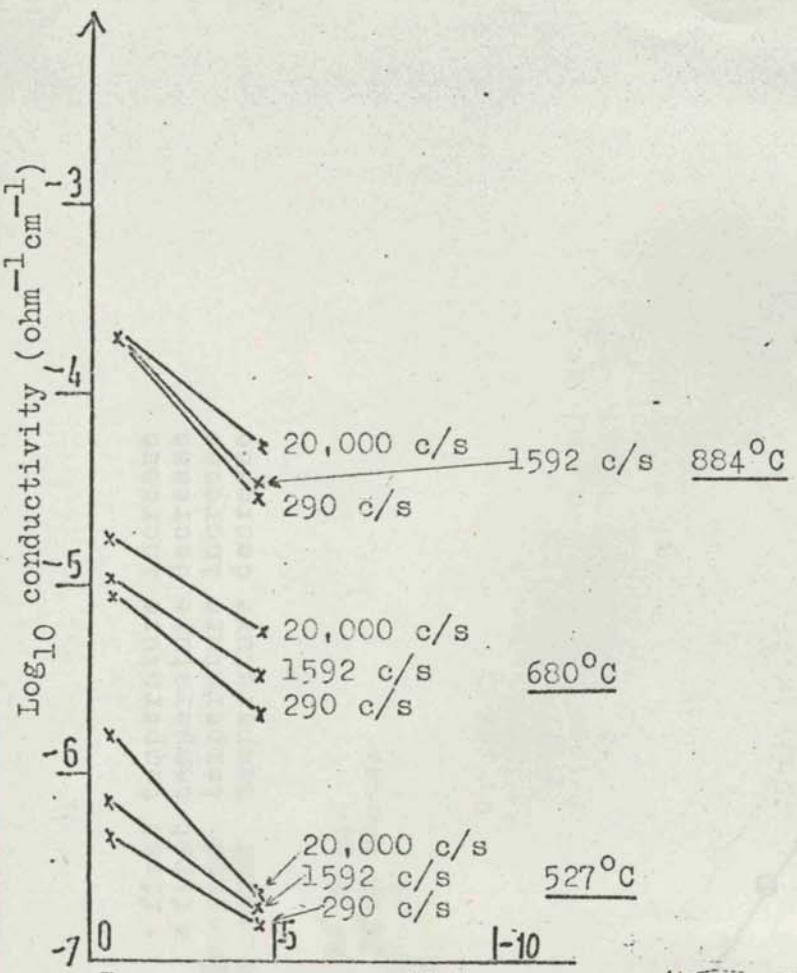

Fig. 21. Effect of measuring frequency on the variation of conductivity with oxygen pressure for undoped ThO_2

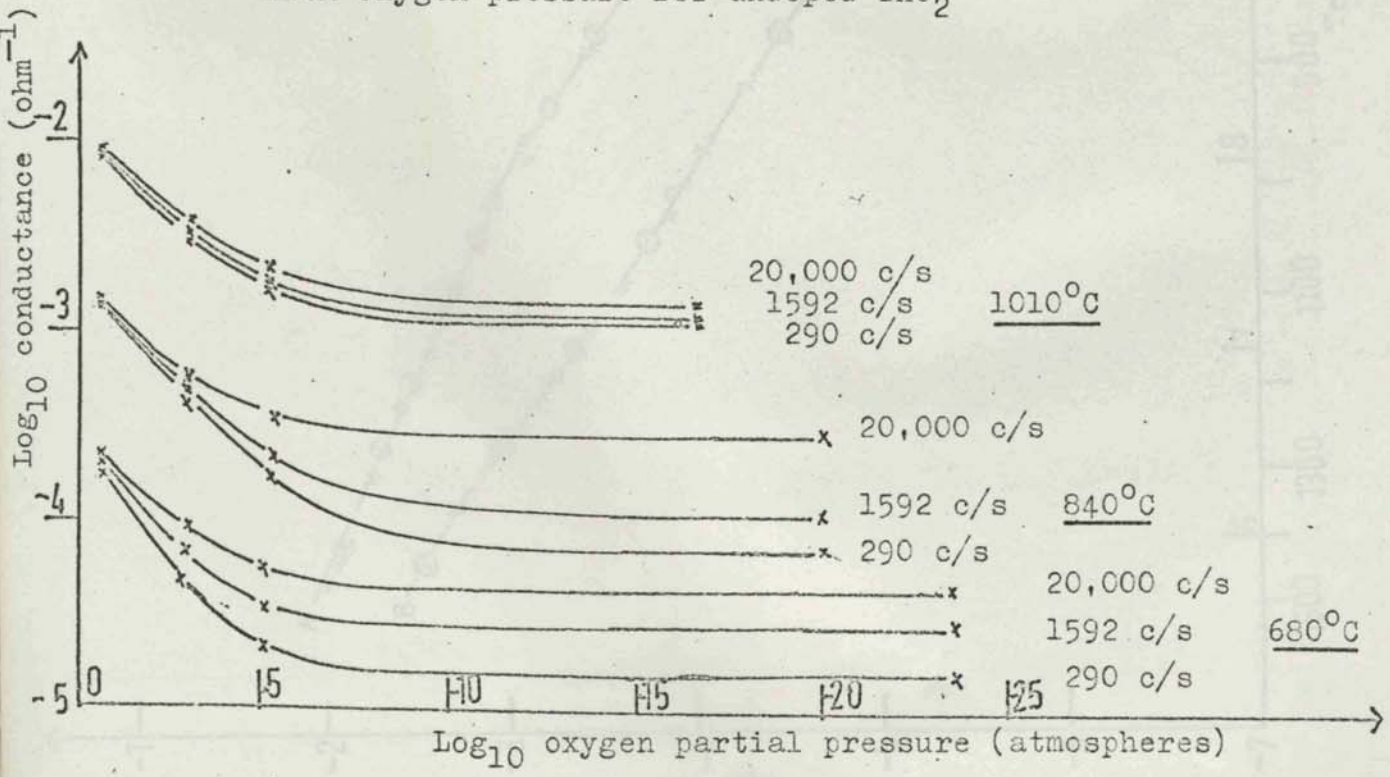

Fig. 22. Effect of measuring frequency on the variation of conductance with oxygen pressure for 0.95 ThO_2 –0.05 CaO

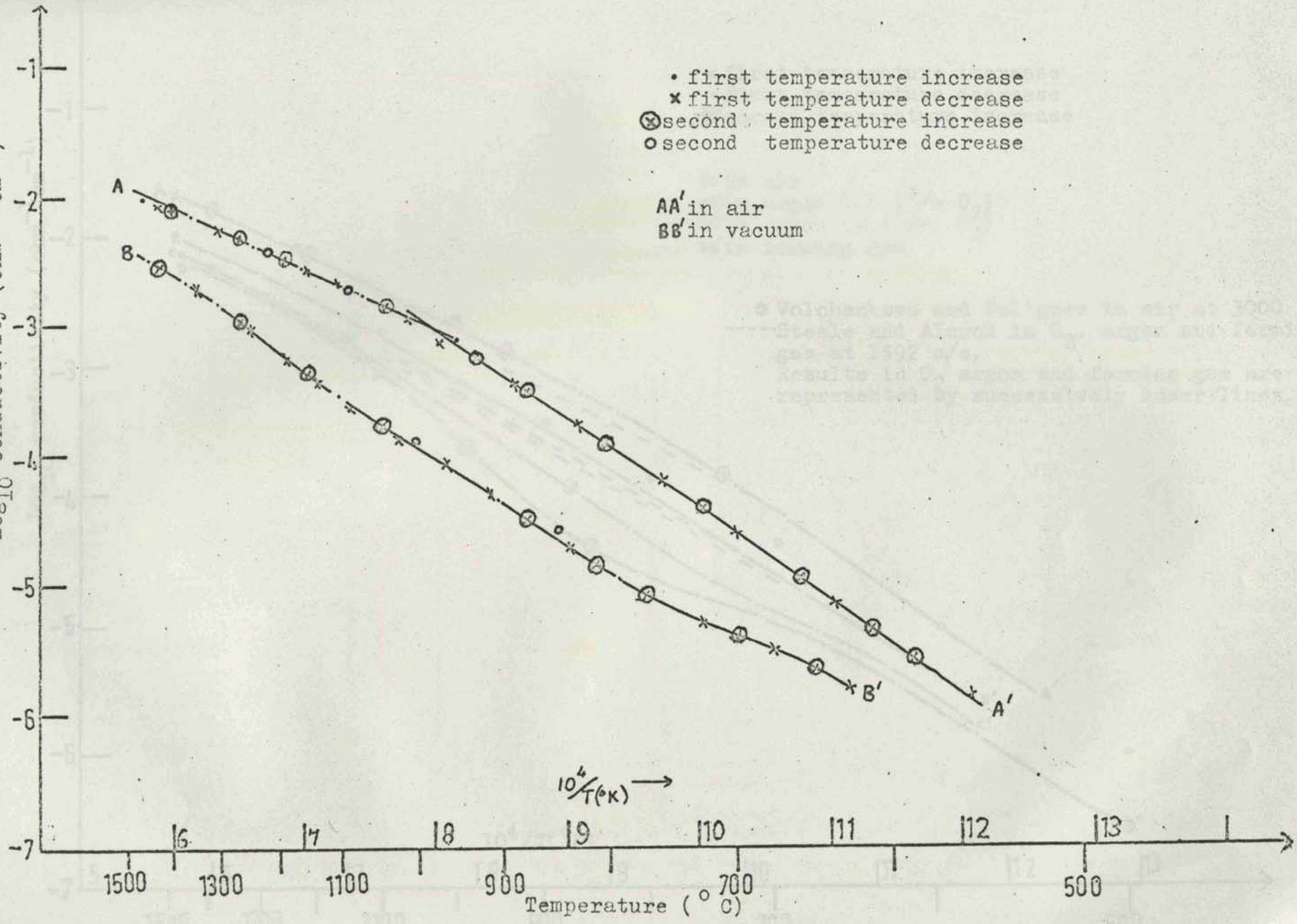

Fig. 23. Variation with temperature of conductivity of 0.99 ThO_2 –0.01 CaO at 1592 c/s.

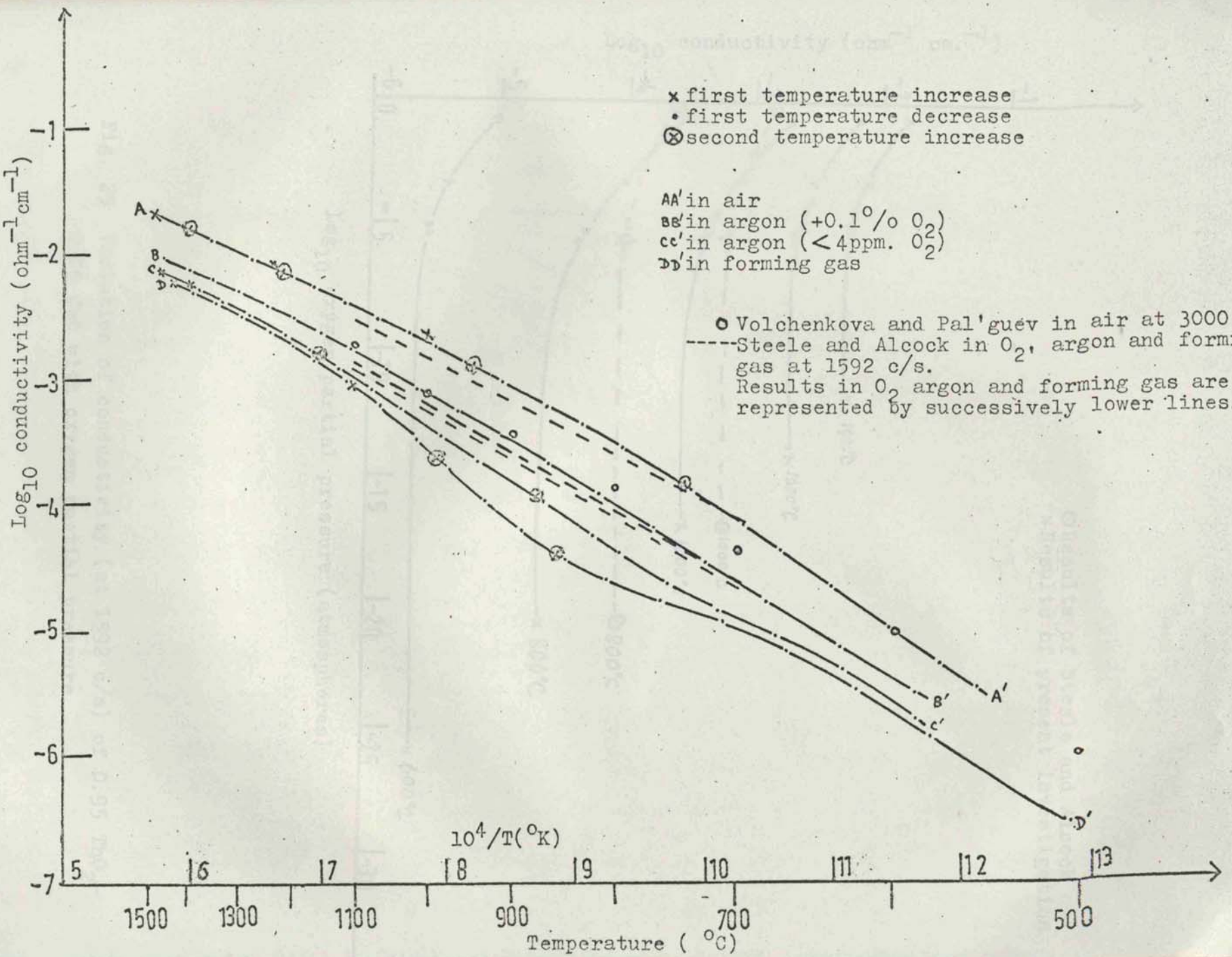

Fig. 24. Variation with temperature of the conductivity of 0.95 ThO_2 —0.05 CaO at 1592 c/s.

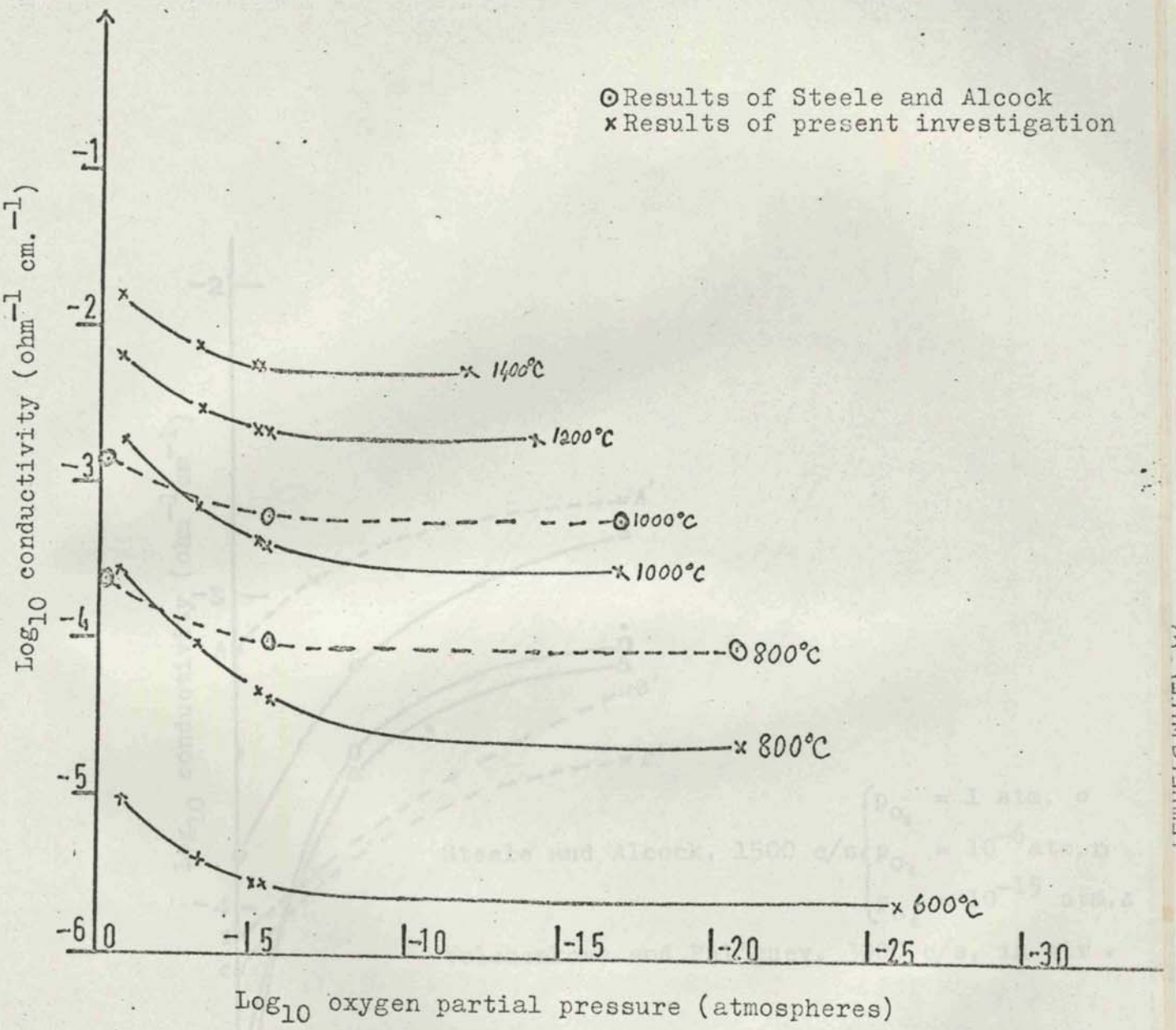

Fig. 25 Variation of conductivity (at 1592 c/s) of 0.95 ThO_2–0.05 CaO with oxygen partial pressure.

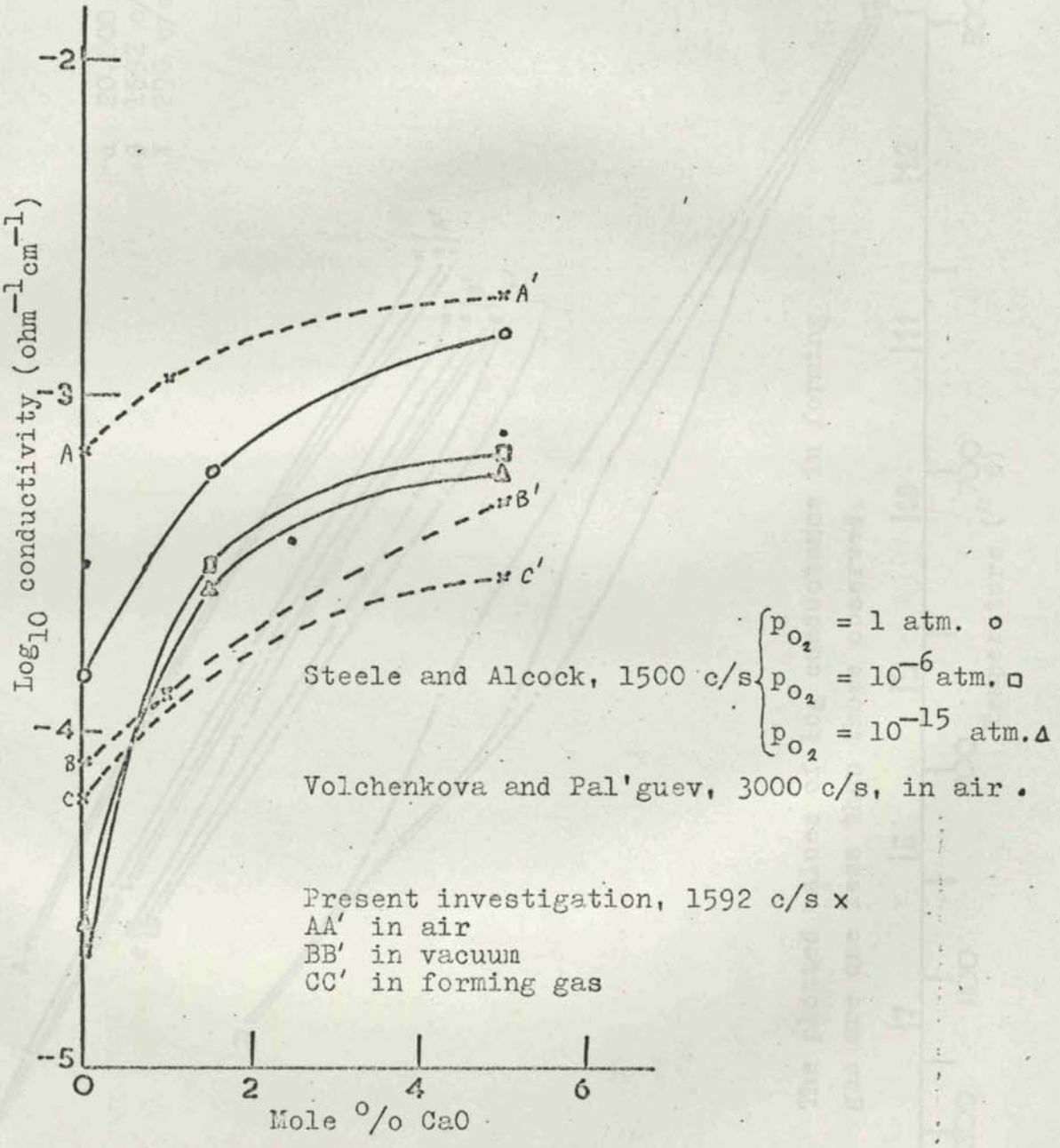

Fig. 26. Variation of conductivity of ThO_2 with addition of CaO at 1000°C.

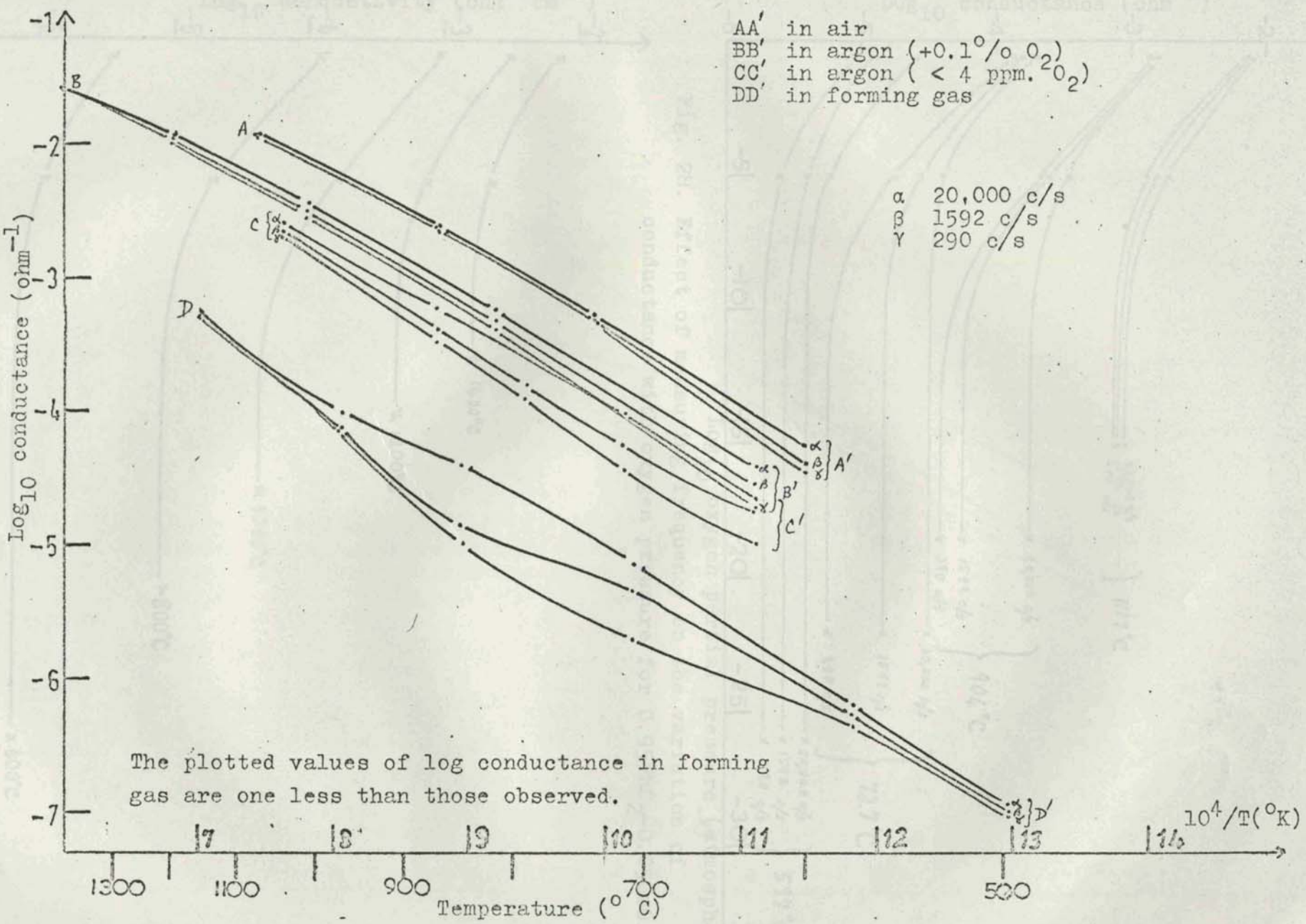

Fig. 27. The effect of different measuring frequencies on the variation ofconductance with temperature for 0.95 ThO2 –0.05 CaO.

Temperature(°C)

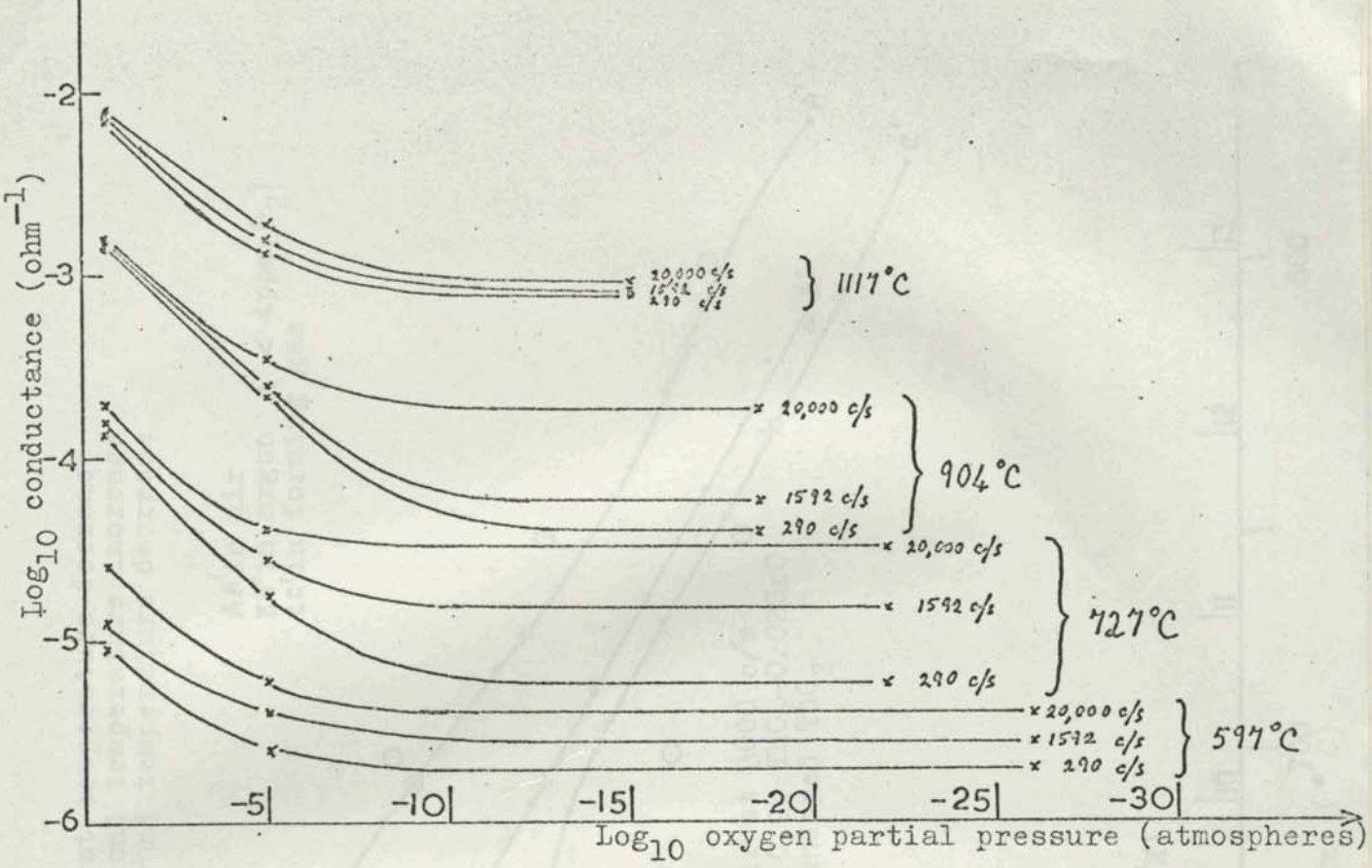

Fig. 28. Effect of measuring frequency on the variation of conductance with oxygen pressure for $0.95ThO_2$–0.05SrO.

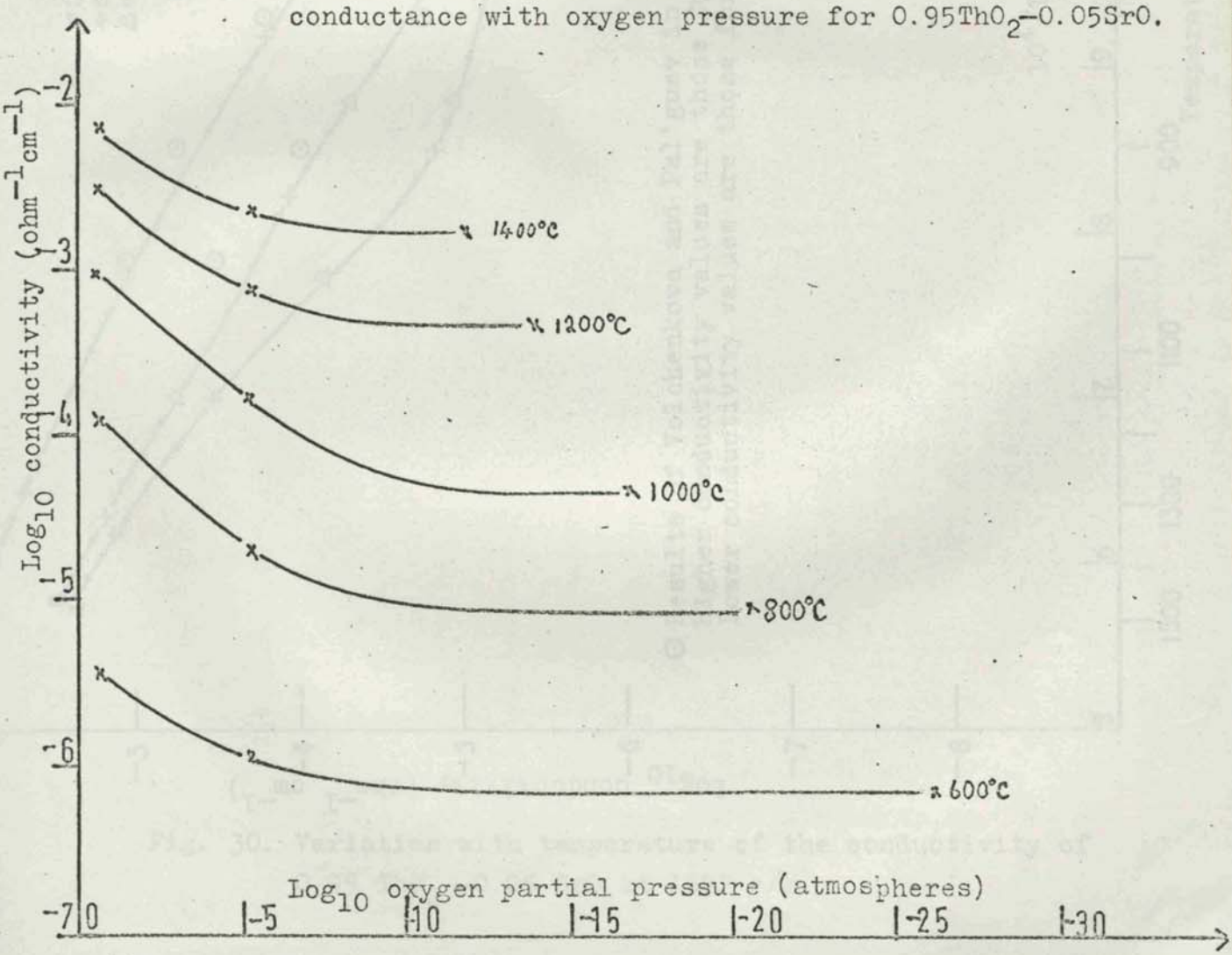

Fig. 29. Variation ofconductivity (at 1592 c/s) of $0.95ThO_2$ –0.05SrO with oxygen pressure.

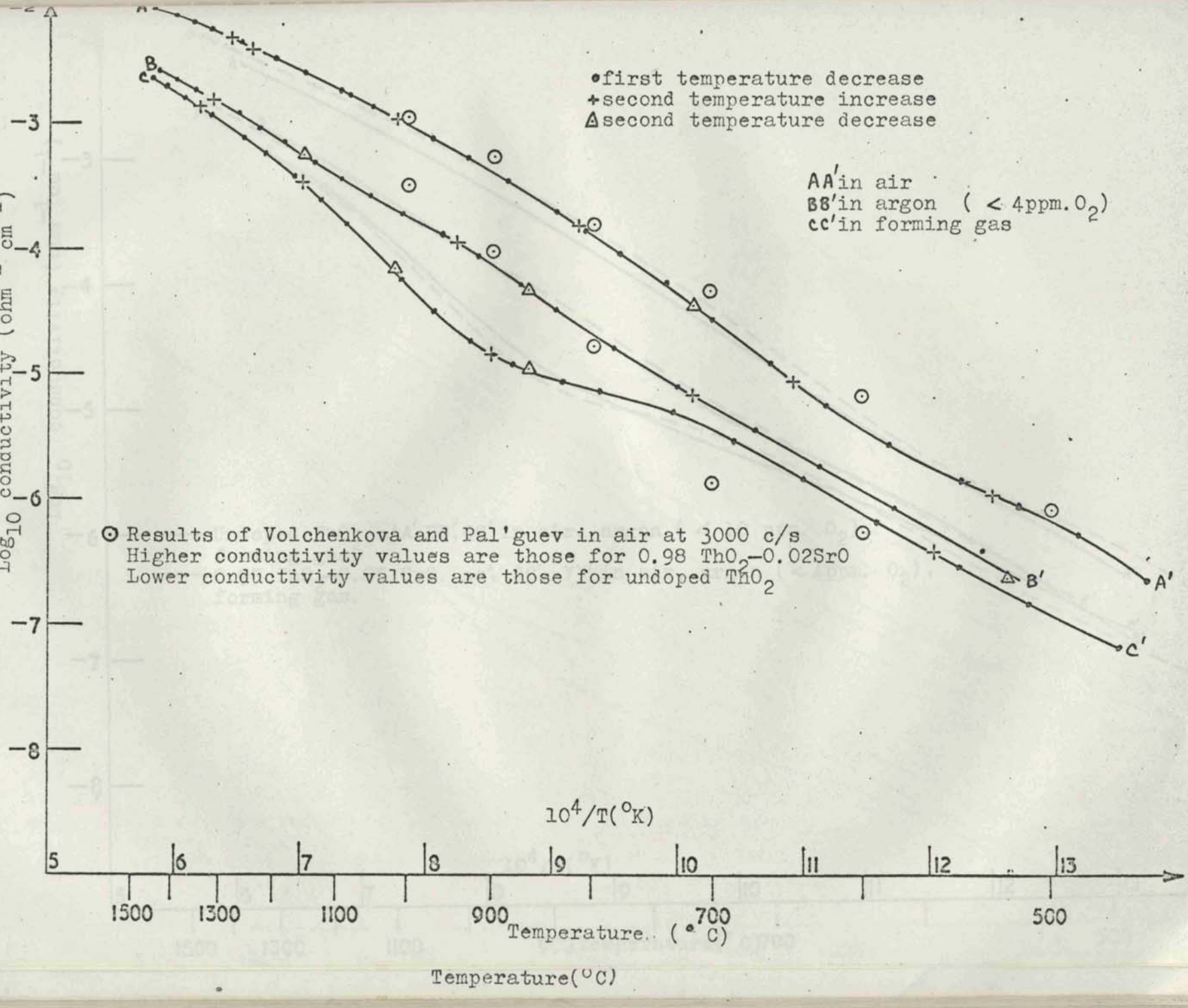

Fig. 30. Variation with temperature of the conductivity of 0.95 ThO_2—0.05 SrO at 1592 c/s

Fig. 31. Comparison of the conductivity of undoped ThO_2 and 0.95 ThO_2 —0.05 SrO at 1592 c/s.

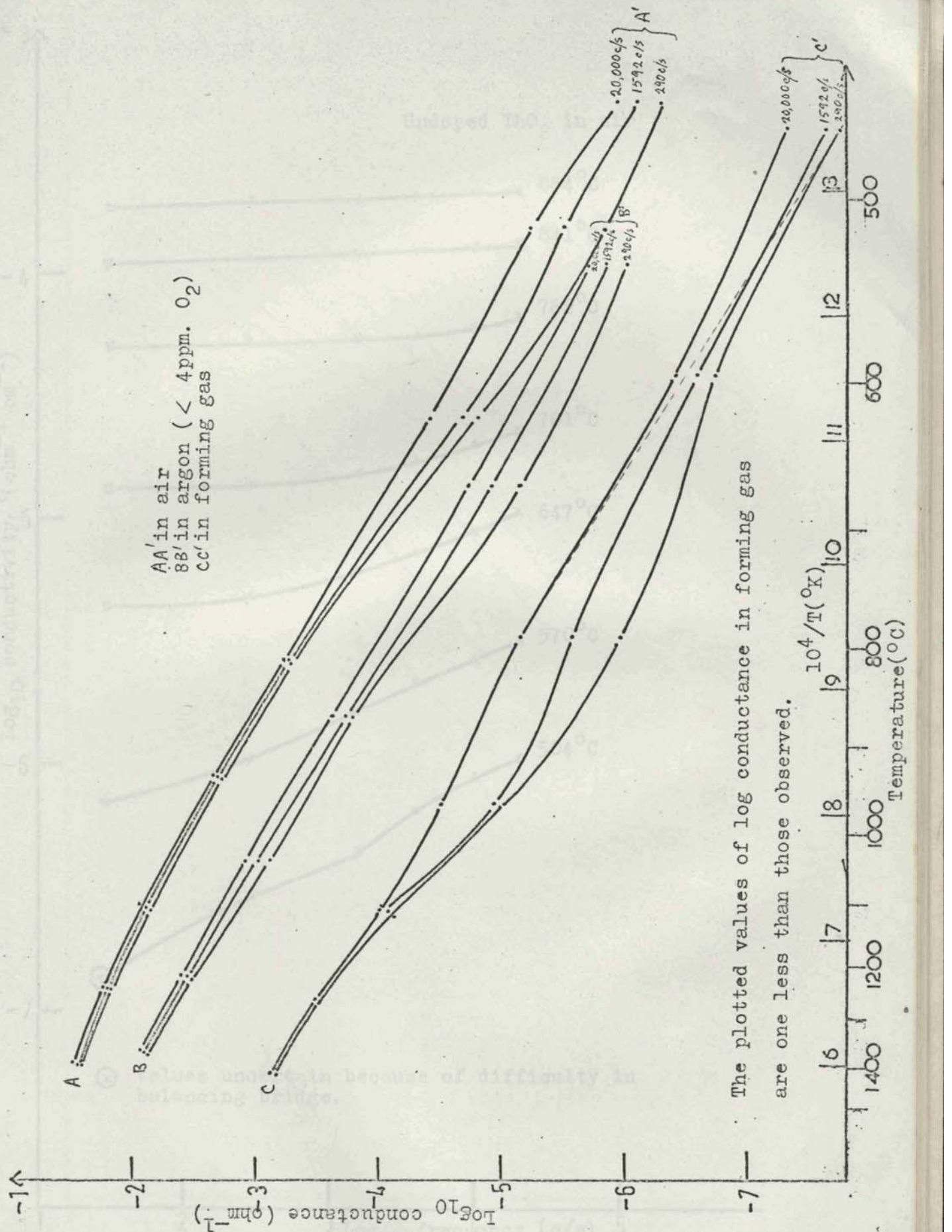

Fig. 32. The effect of different measuring frequencies on the variation of conductance with temperature for 0.95 ThO_2 —0.05 SrO.

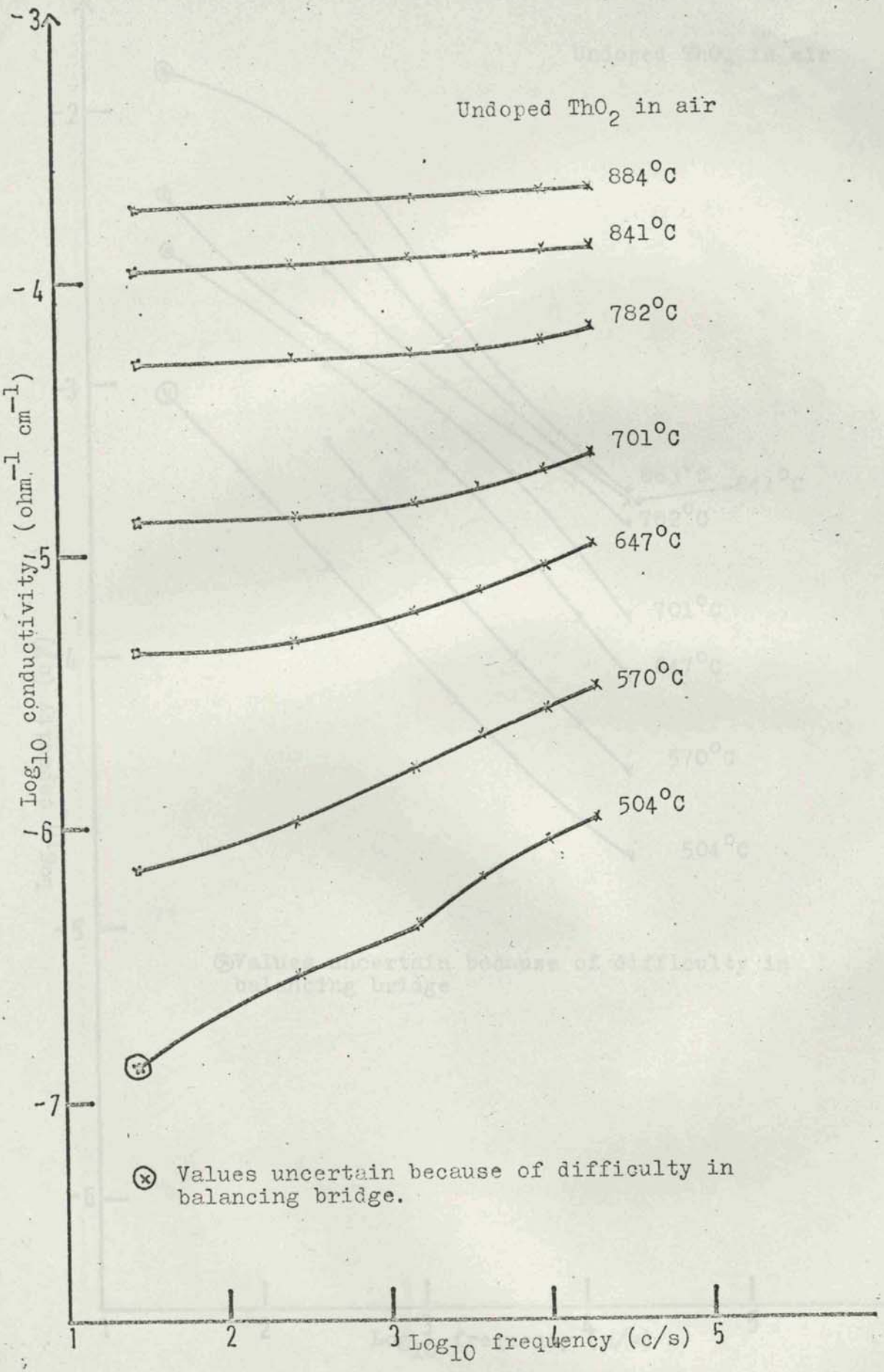

Fig. 33. Variation of conductivity with frequency for undoped ThO_2

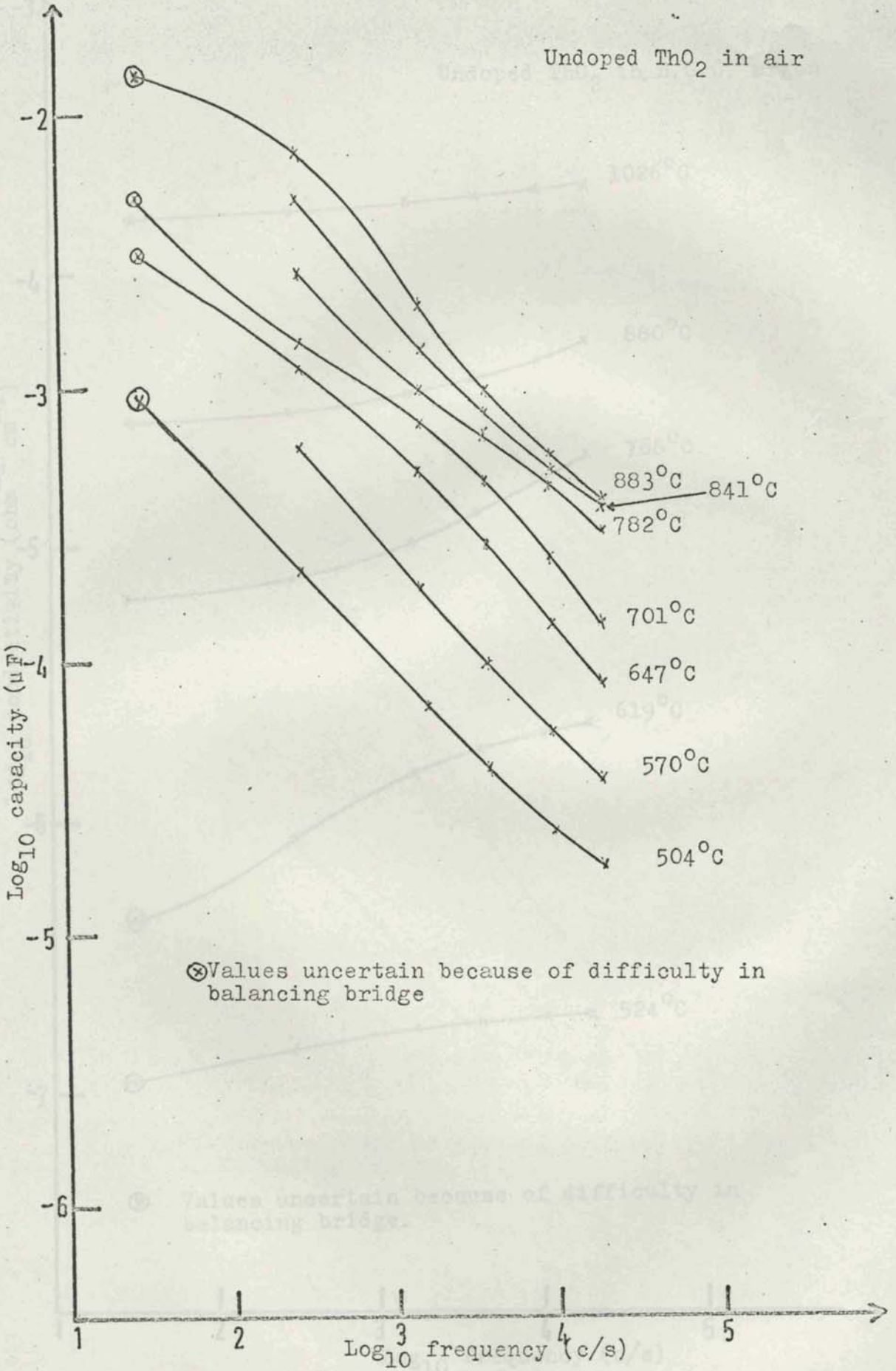

Fig. 34. Variation of capacity with frequency for undoped ThO_2

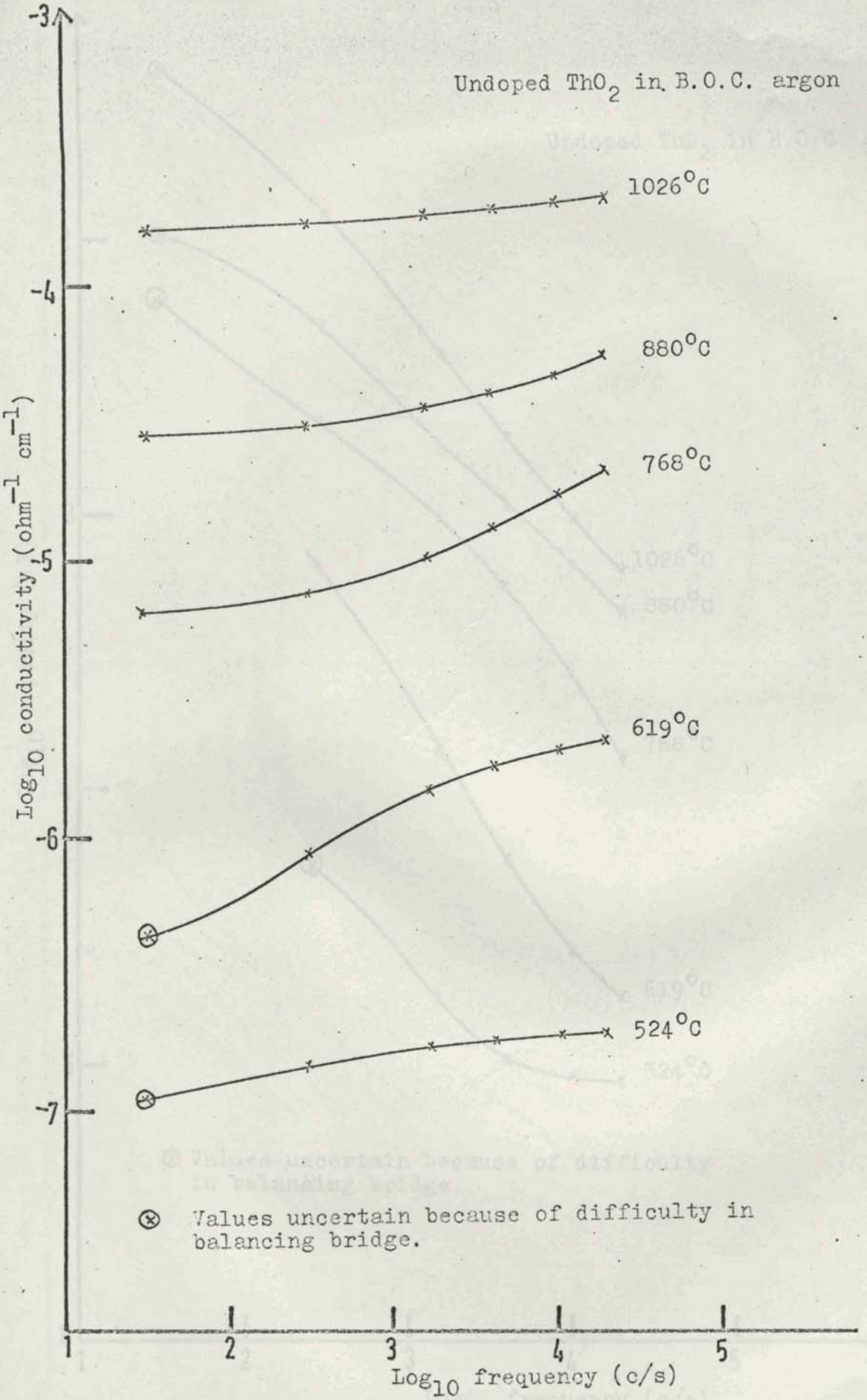

Fig. 35. Variation of conductivity with frequency for undoped ThO_2.

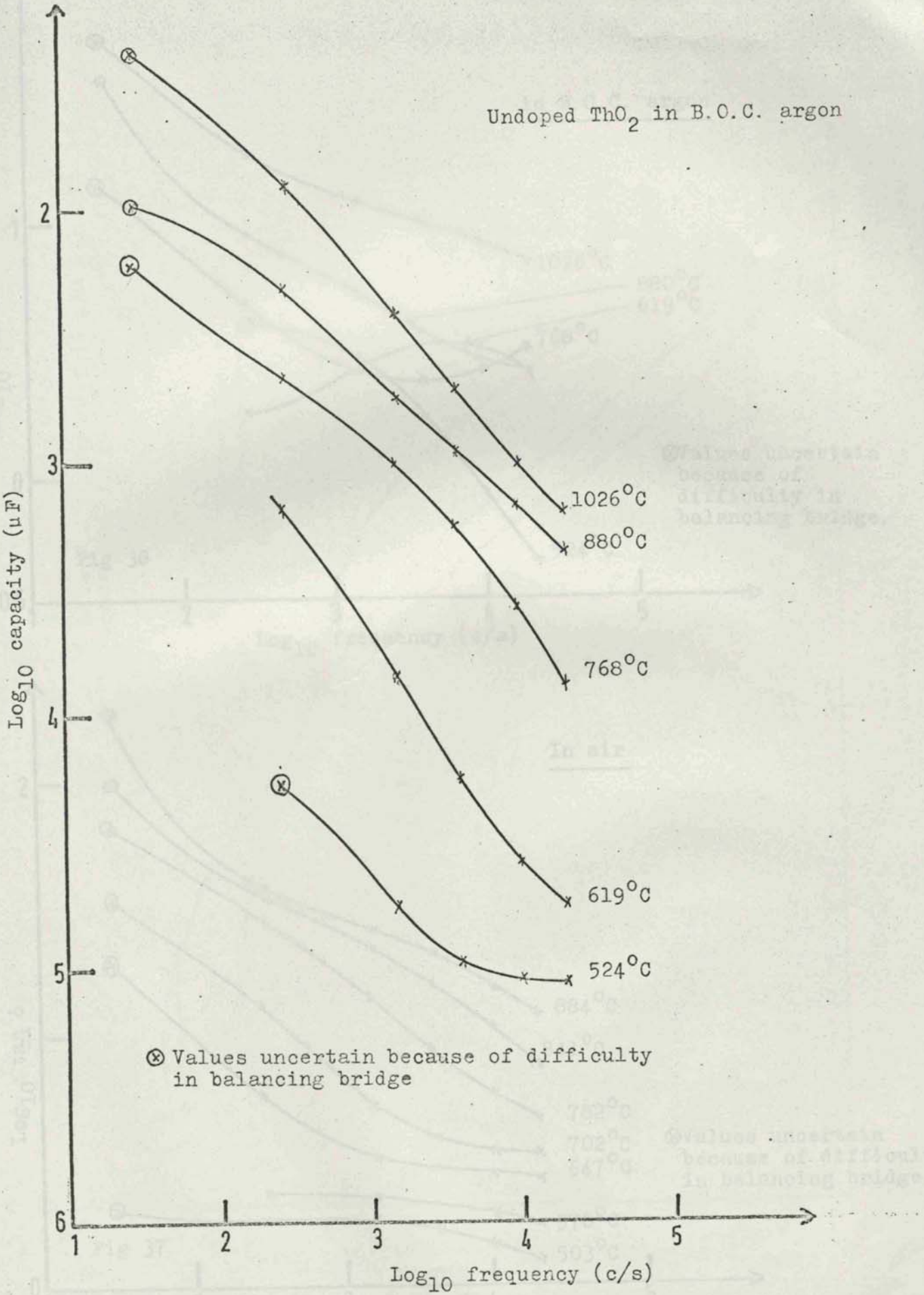

Fig. 36. Variation of capacity with frequency for undoped ThO_2

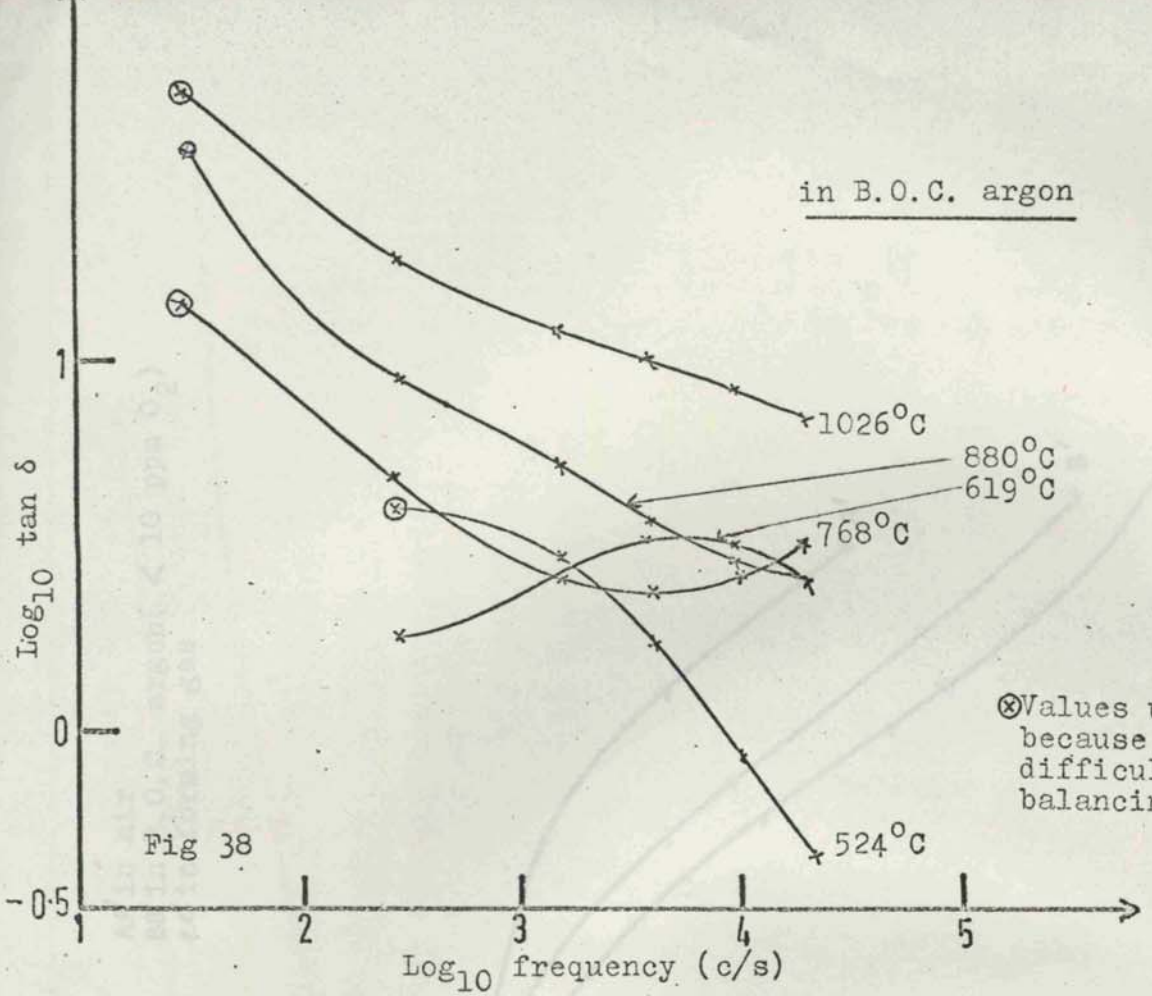

Fig 38

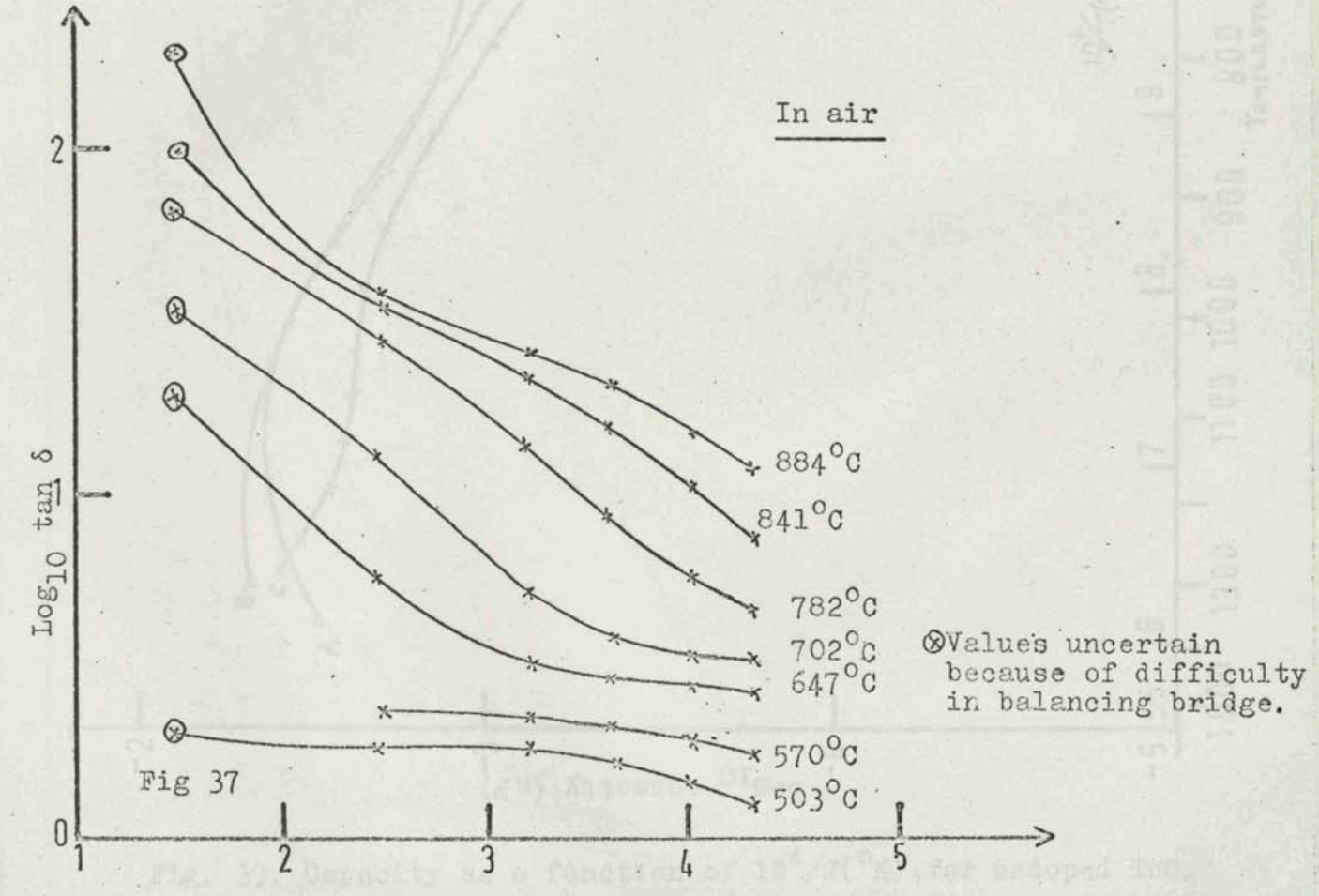

Fig 37

Figs. 37 and 38. Variation of tan δ with frequency for undoped ThO_2

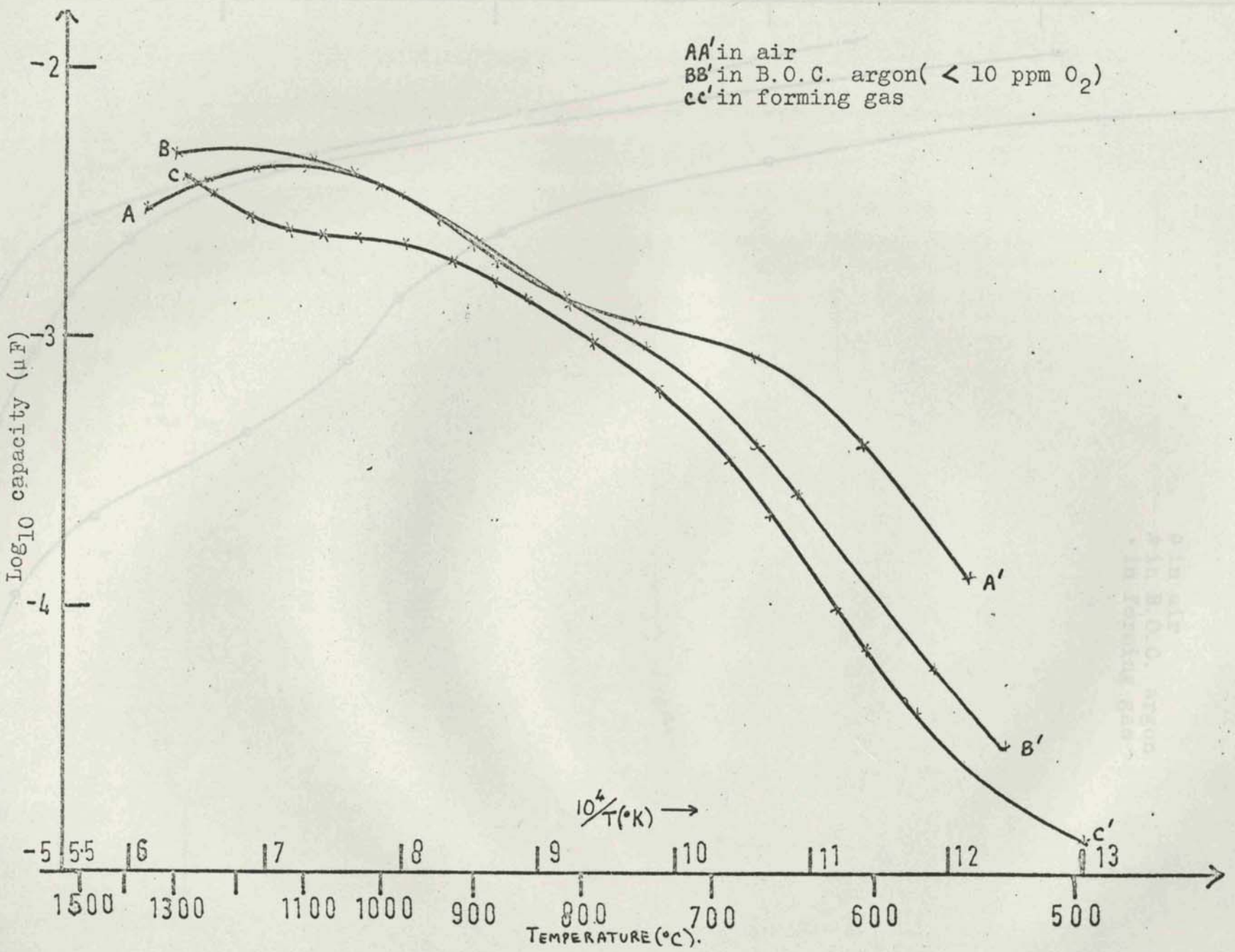

Fig. 39. Capacity as a function of $10^4/T(°K)$ for undoped ThO_2 at 1592 c/s.

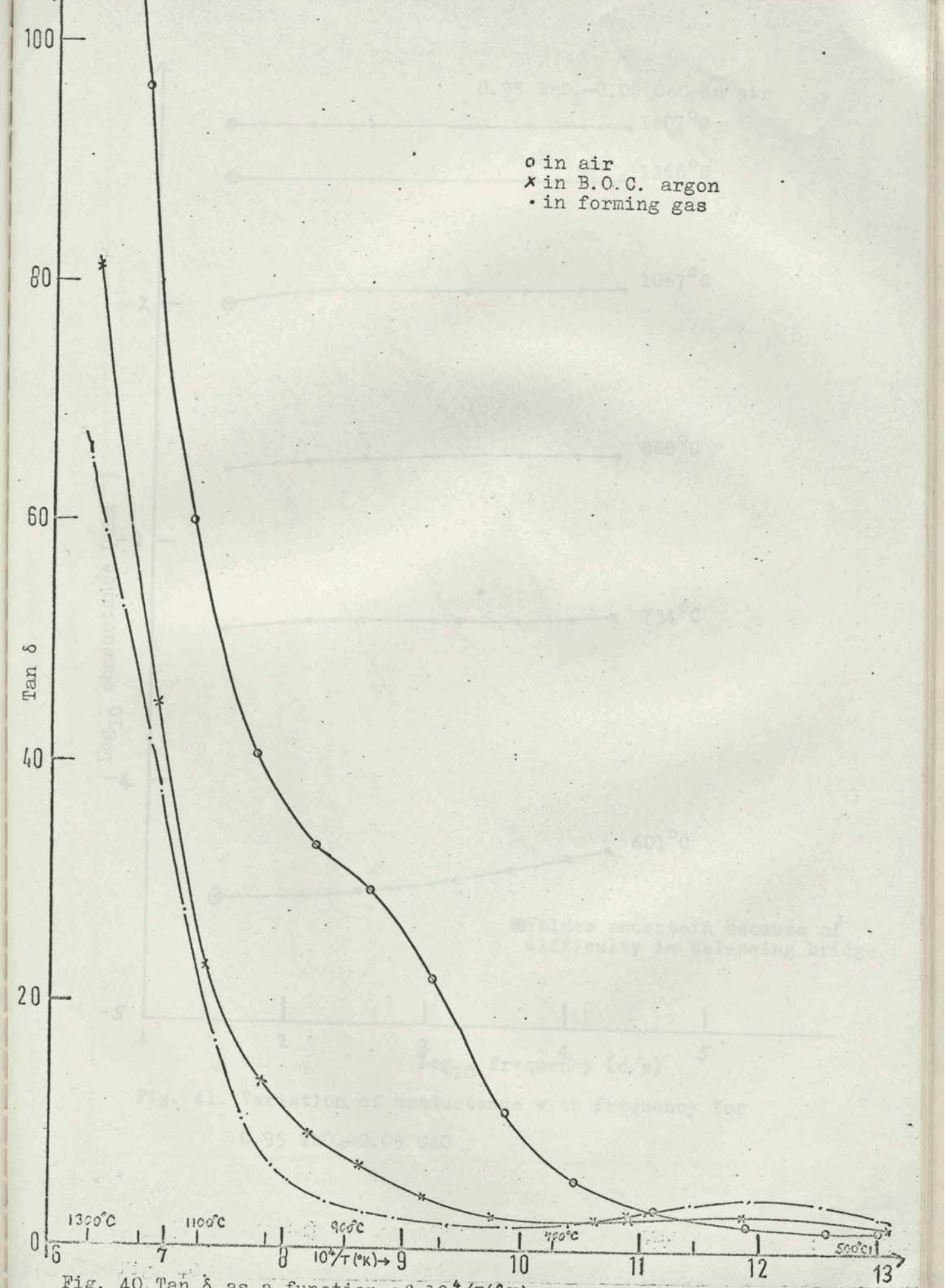

Fig. 40. Tan δ as a function of $10^4/T(°K)$ at 1592 c/s for undoped ThO_2.

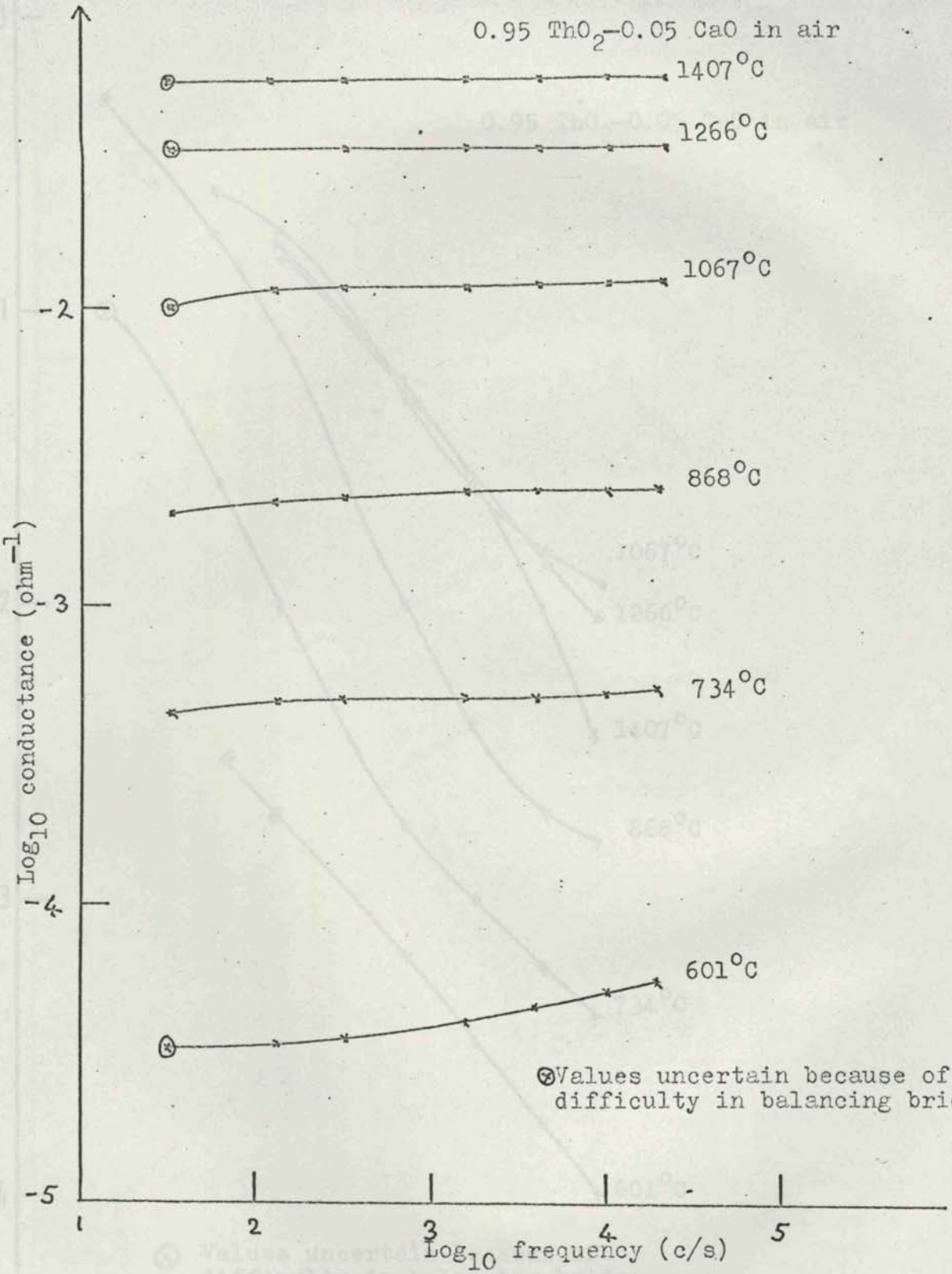

Fig. 41. Variation of conductance with frequency for 0.95 ThO_2–0.05 CaO

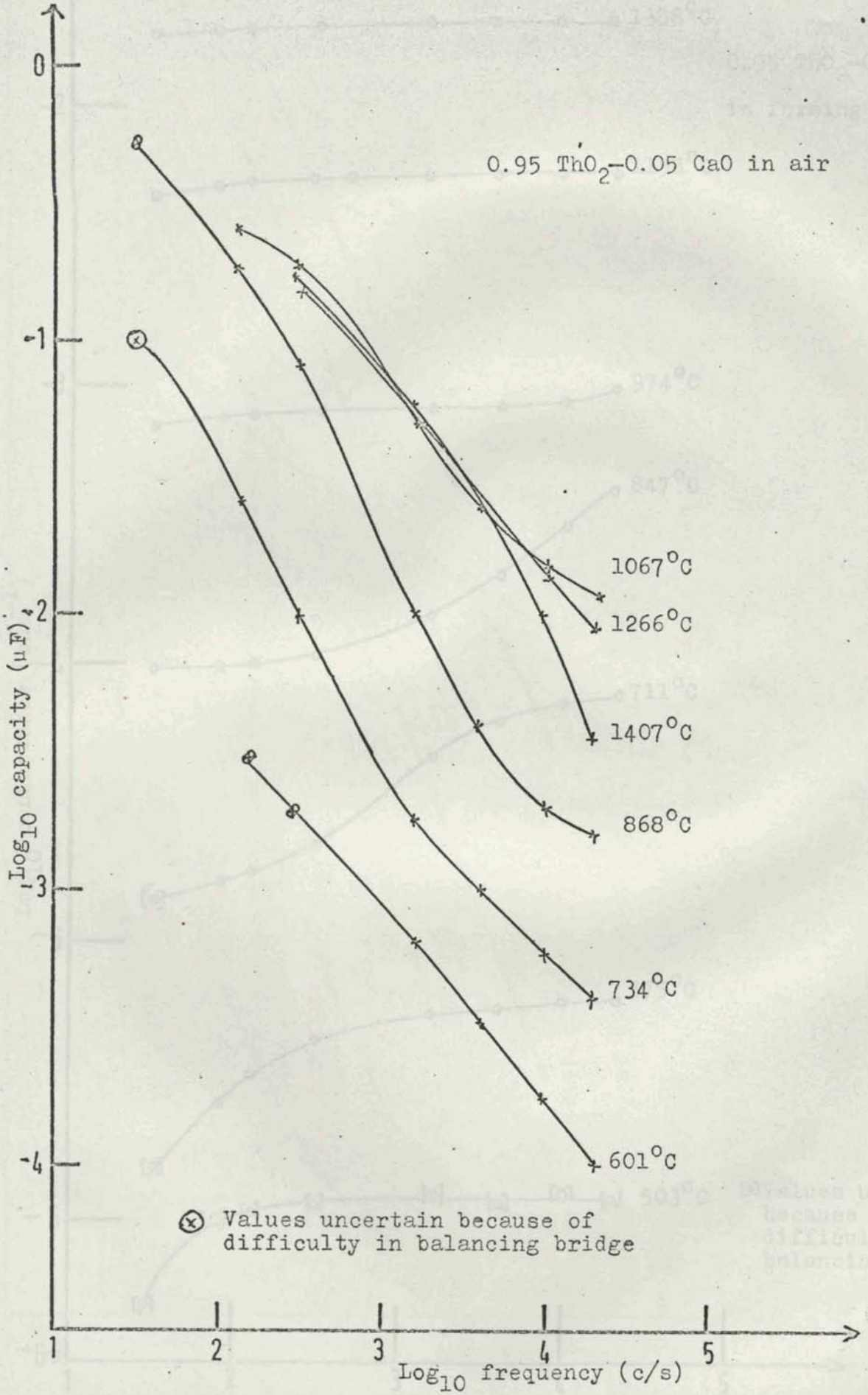

Fig. 42. Variation of capacity with frequency for 0.95 ThO_2 –0.05 CaO

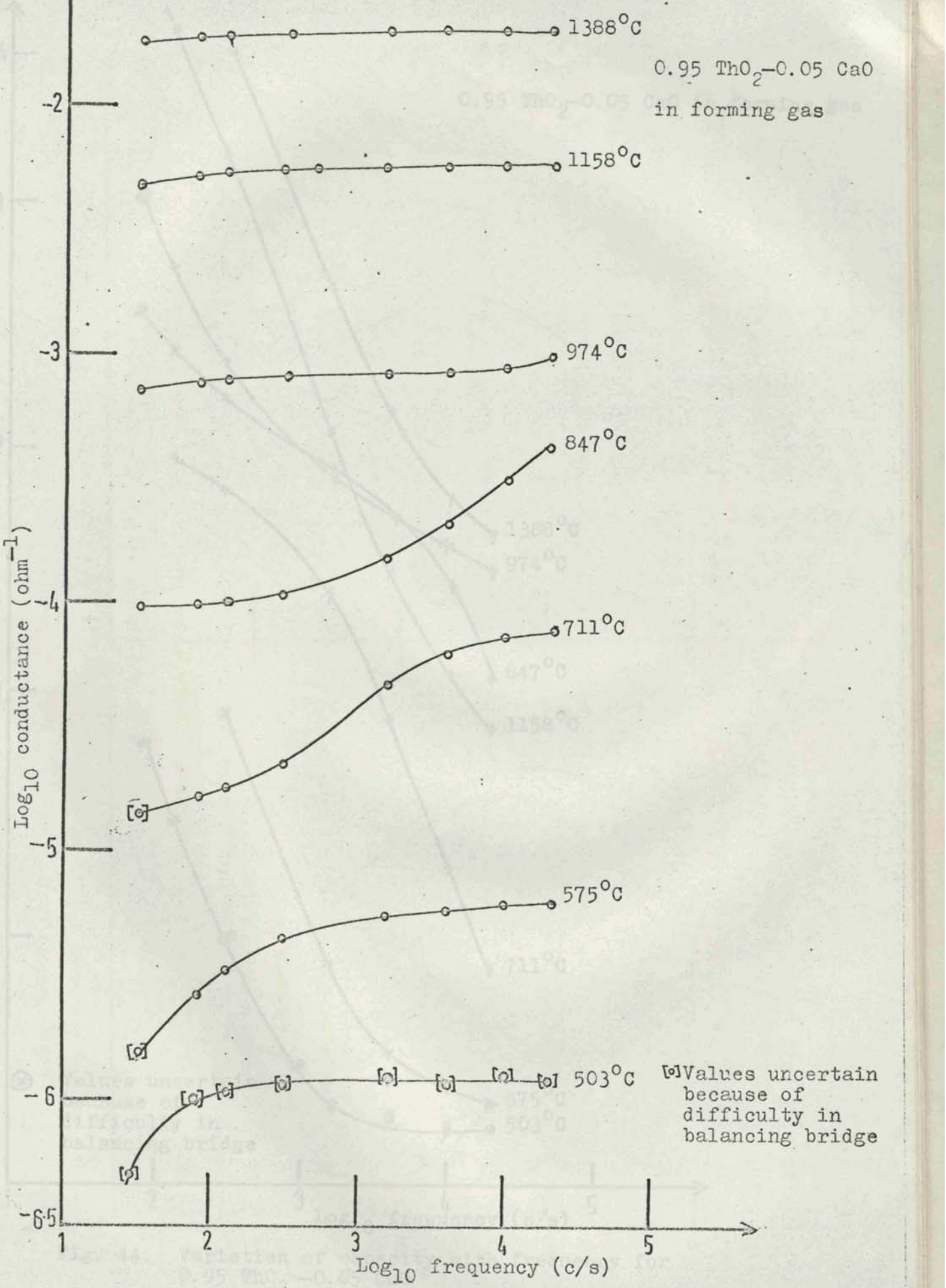

Fig. 43. Variation of conductance with frequency for 0.95 ThO_2 –0.05 CaO.

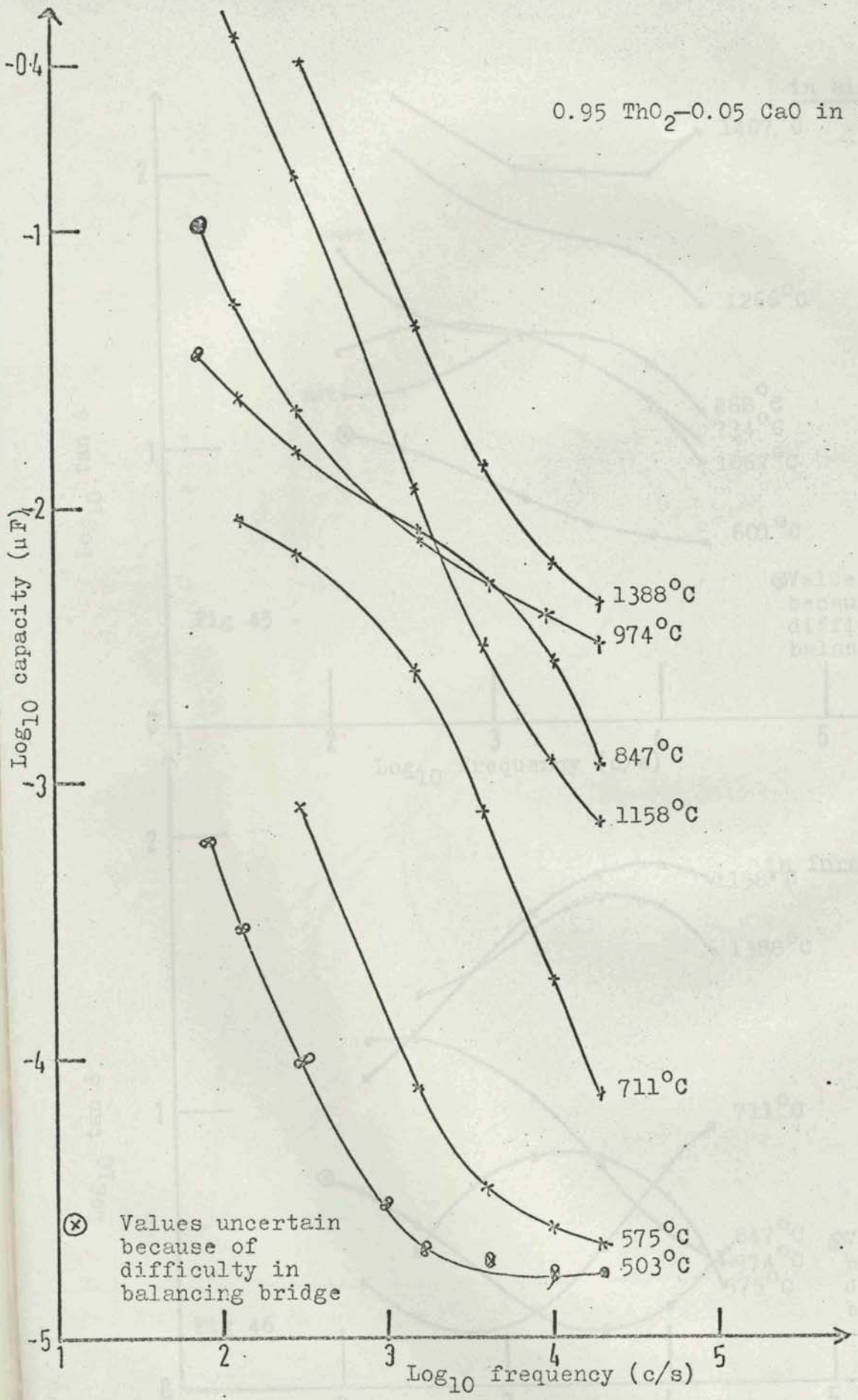

Fig. 44. Variation of capacity with frequency for
0.95 ThO_2 —0.05 CaO

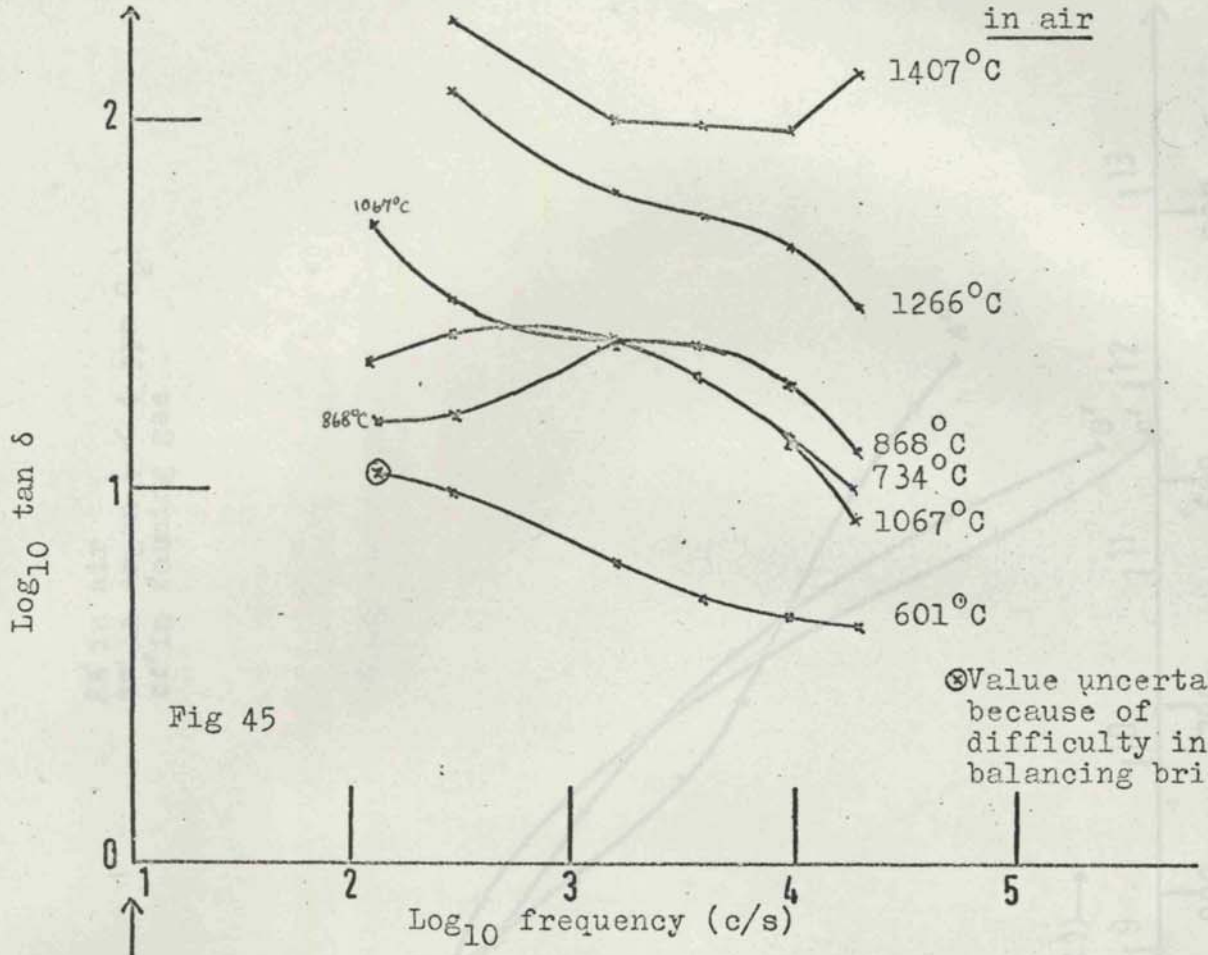

Fig 45

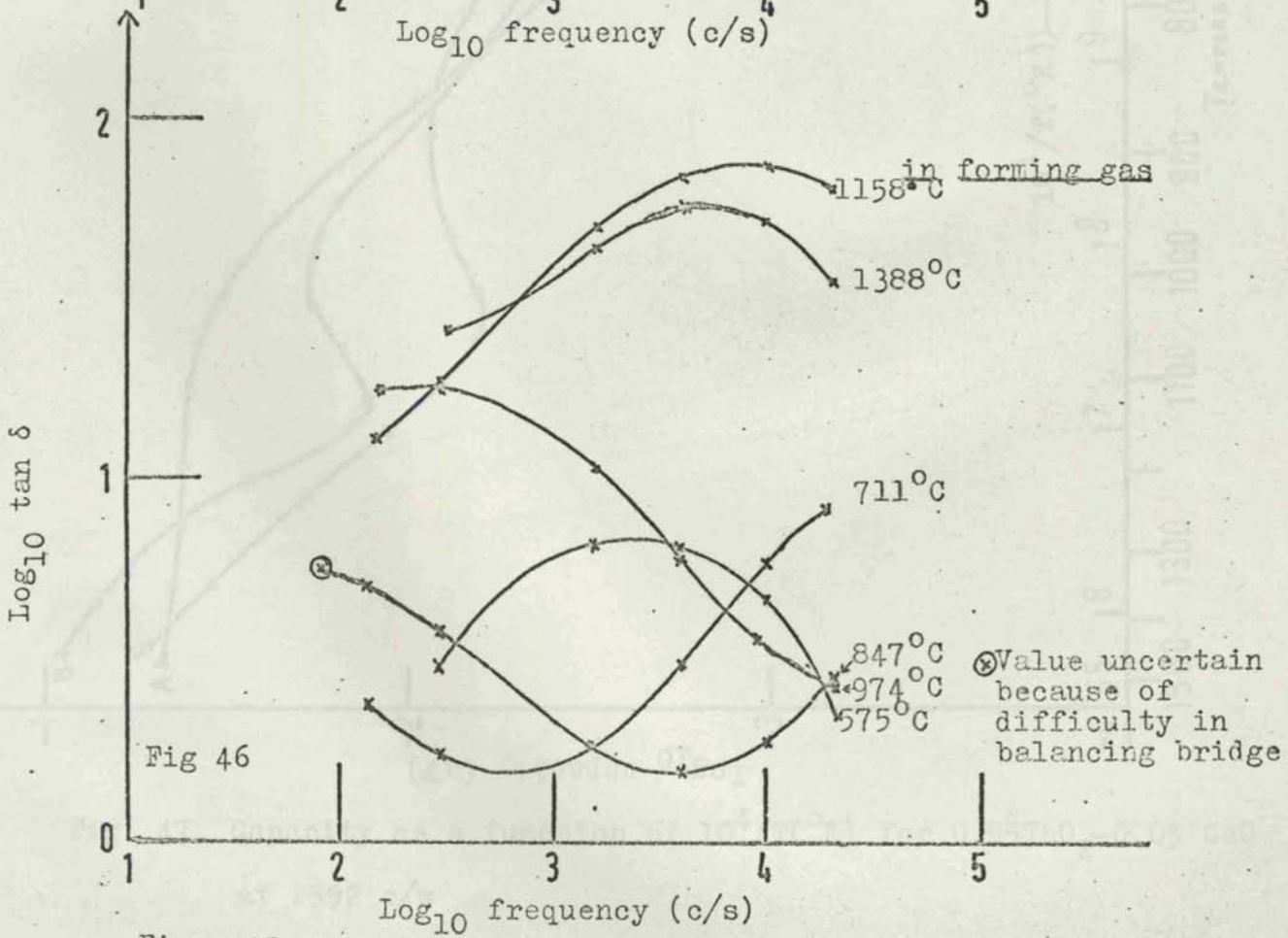

Fig 46

Figs. 45 and 46 Variation of tan δ with frequency for 0.95 ThO_2 – 0.05 CaO

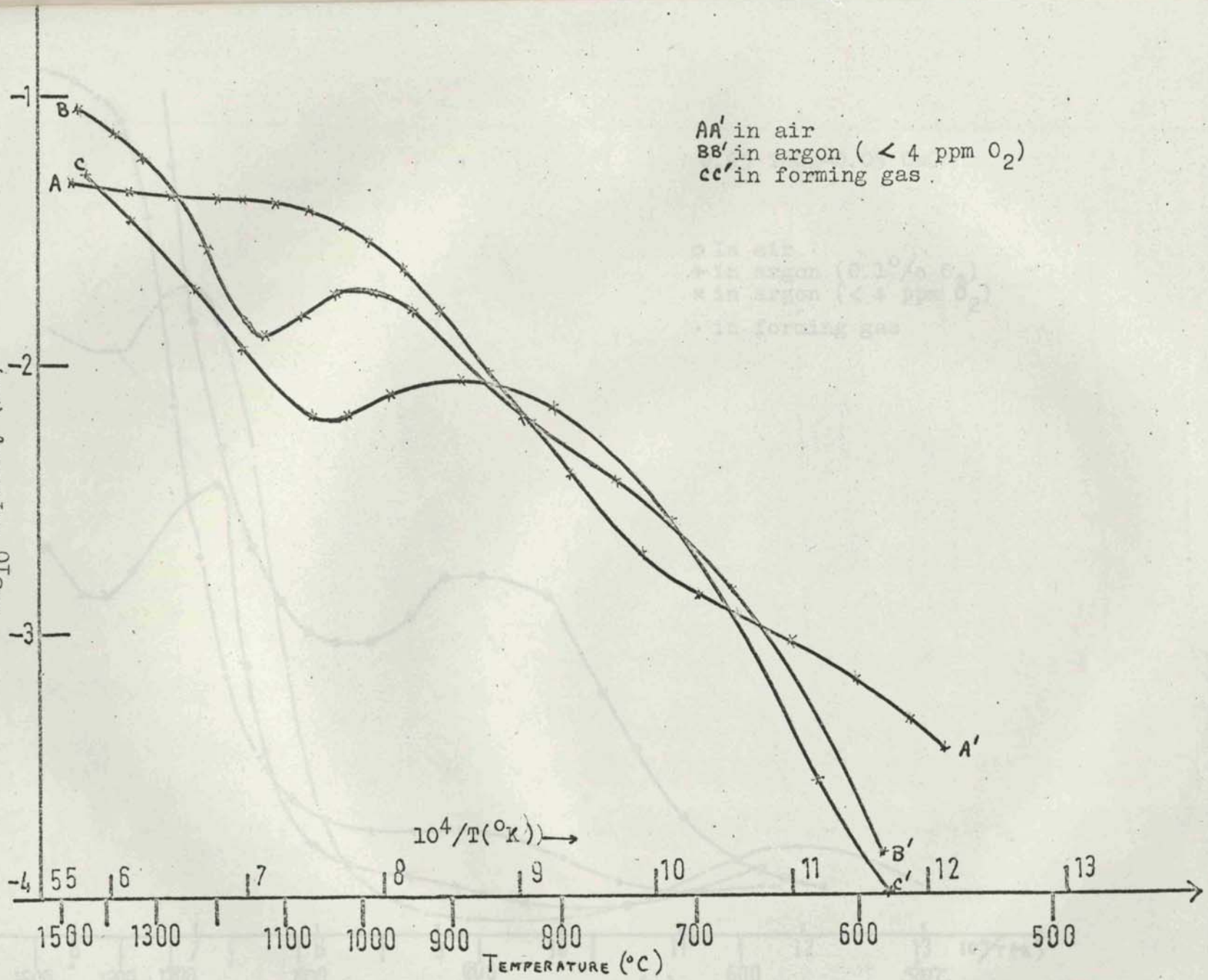

Fig. 47. Capacity as a function of $10^4/T(^oK)$ for $0.95ThO_2$–0.05 CaO at 1592 c/s

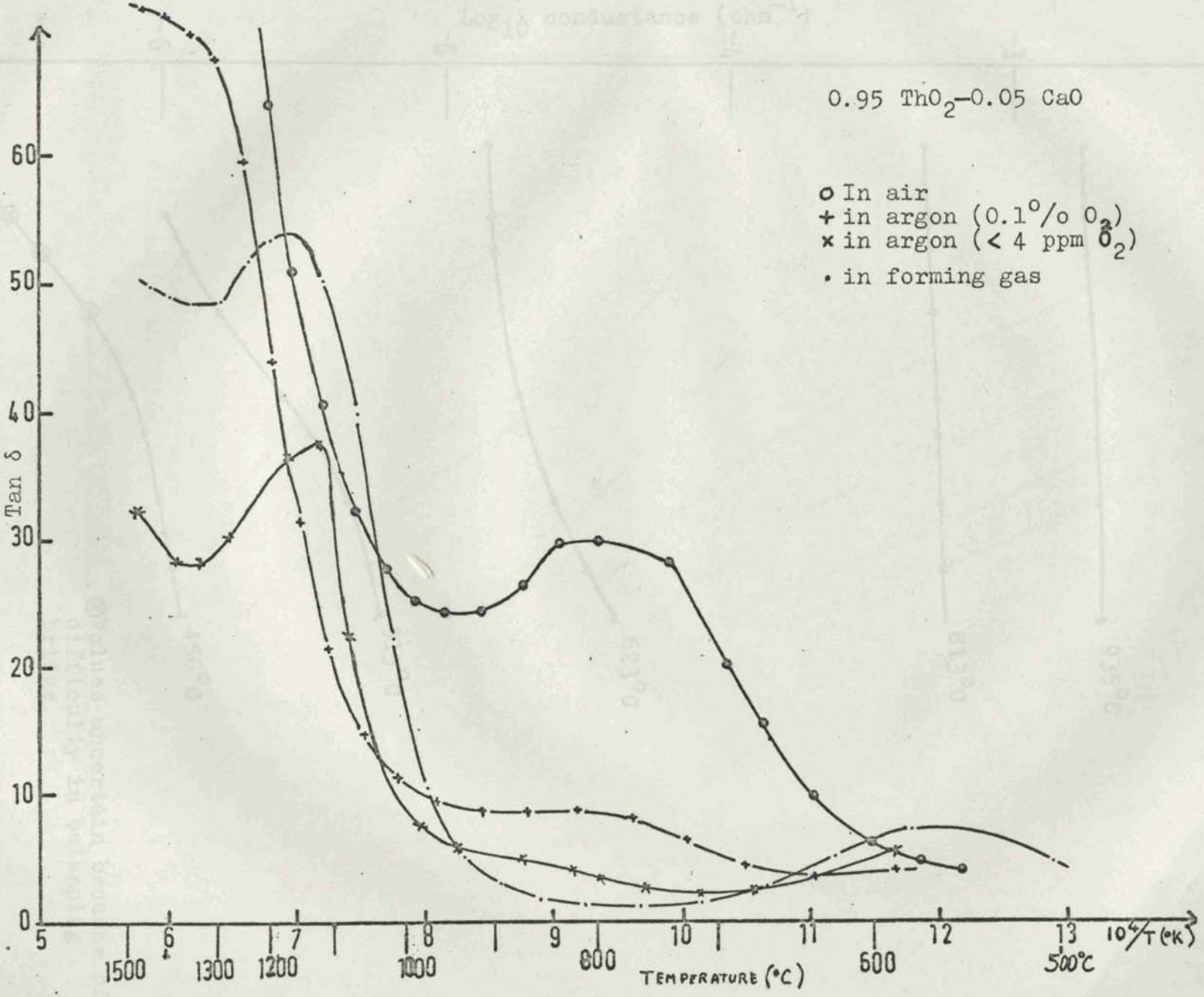

Fig 48. Tan δ as a function of $10^4/T(°K)$ at 1592 c/s for 0.95 ThO_2 – 0.05 CaO

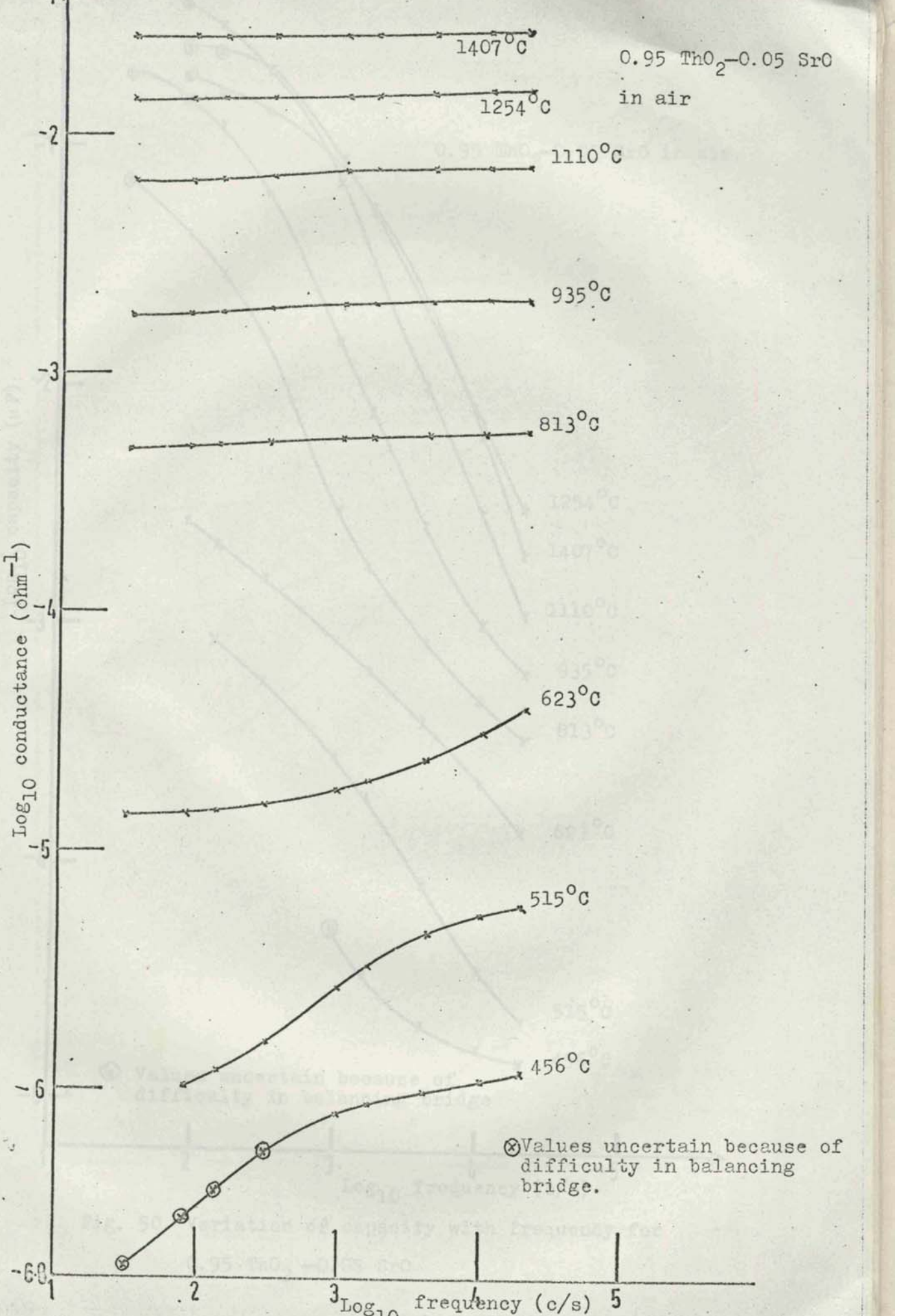

Fig. 49. Variation of conductance with frequency for $0.95ThO_2$-0.05SrO

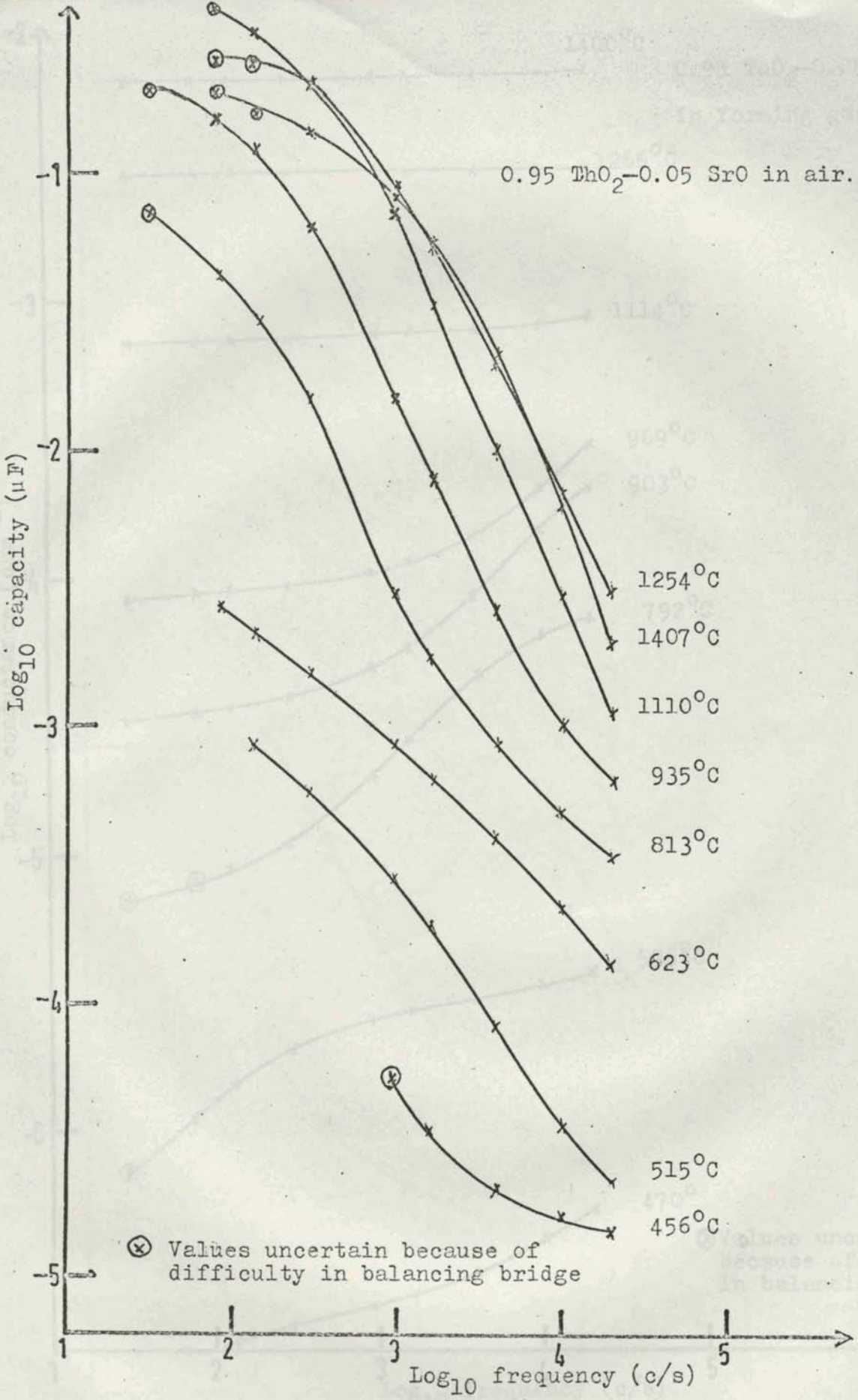

Fig. 50. Variation of capacity with frequency for 0.95 ThO_2 –0.05 SrO

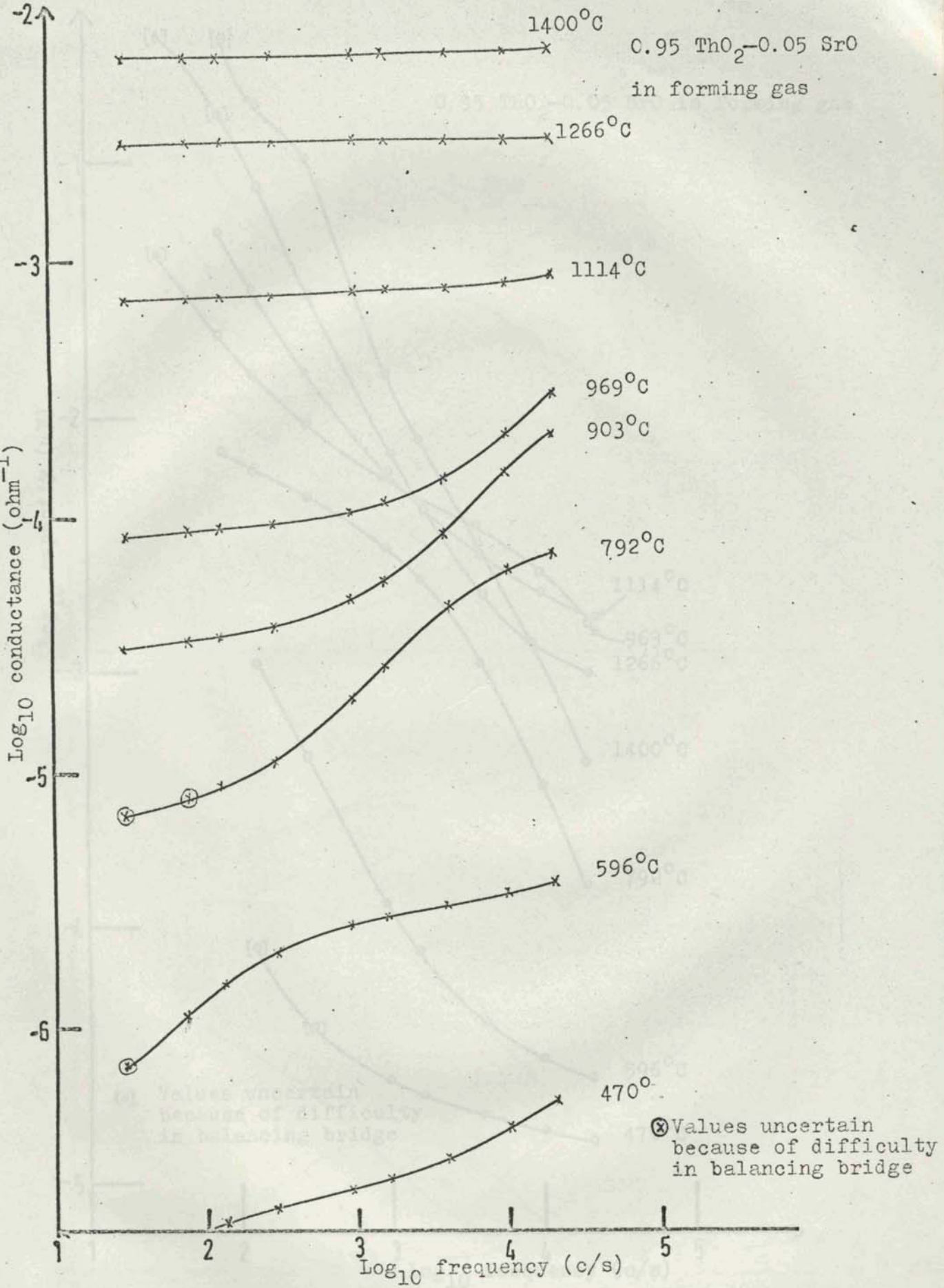

Fig. 51. Variation of conductance with frequency for 0.95 ThO_2 –0.05 SrO.

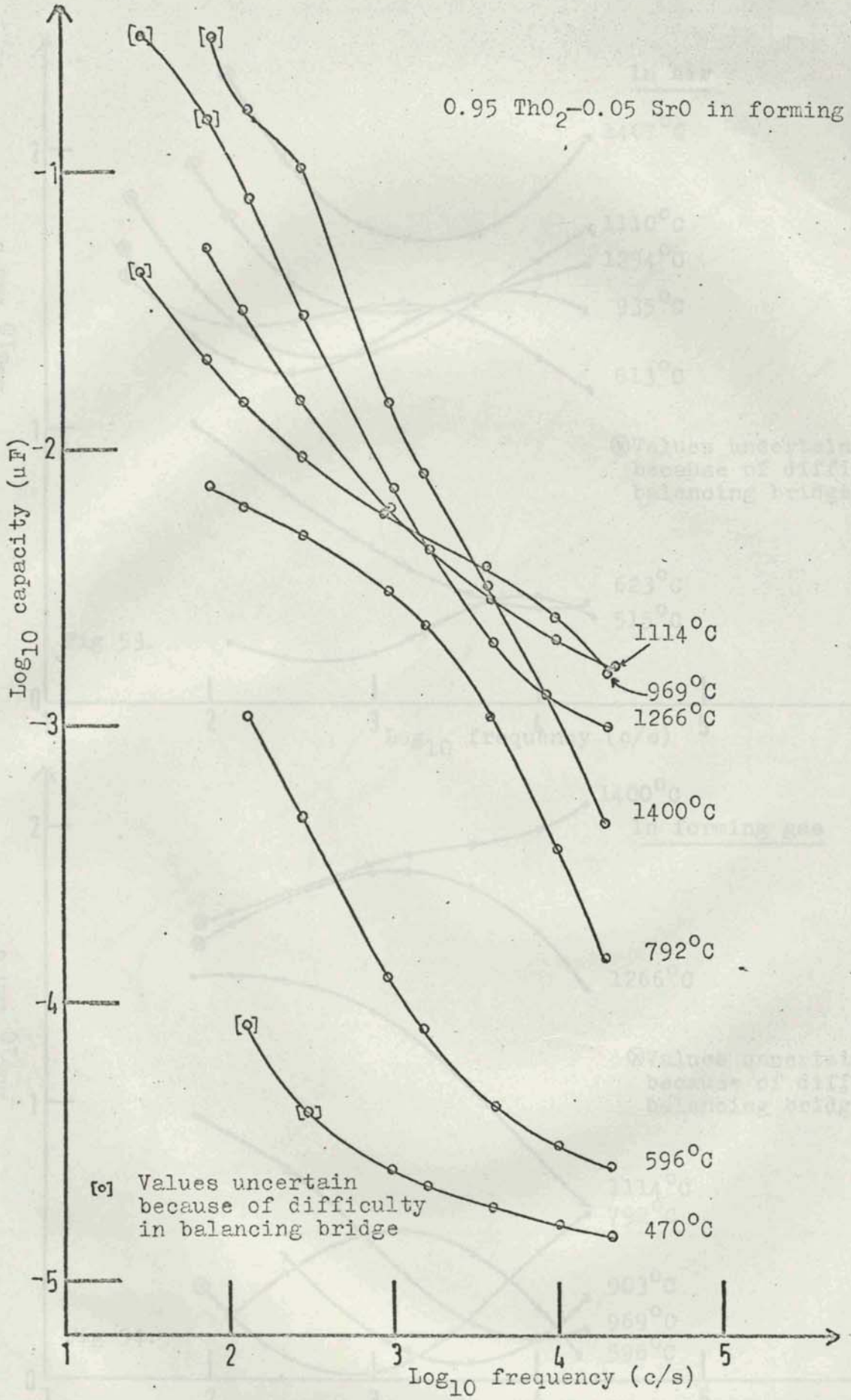

Fig. 52. Variation of capacity with frequency for 0.95 ThO_2 –0.05 SrO

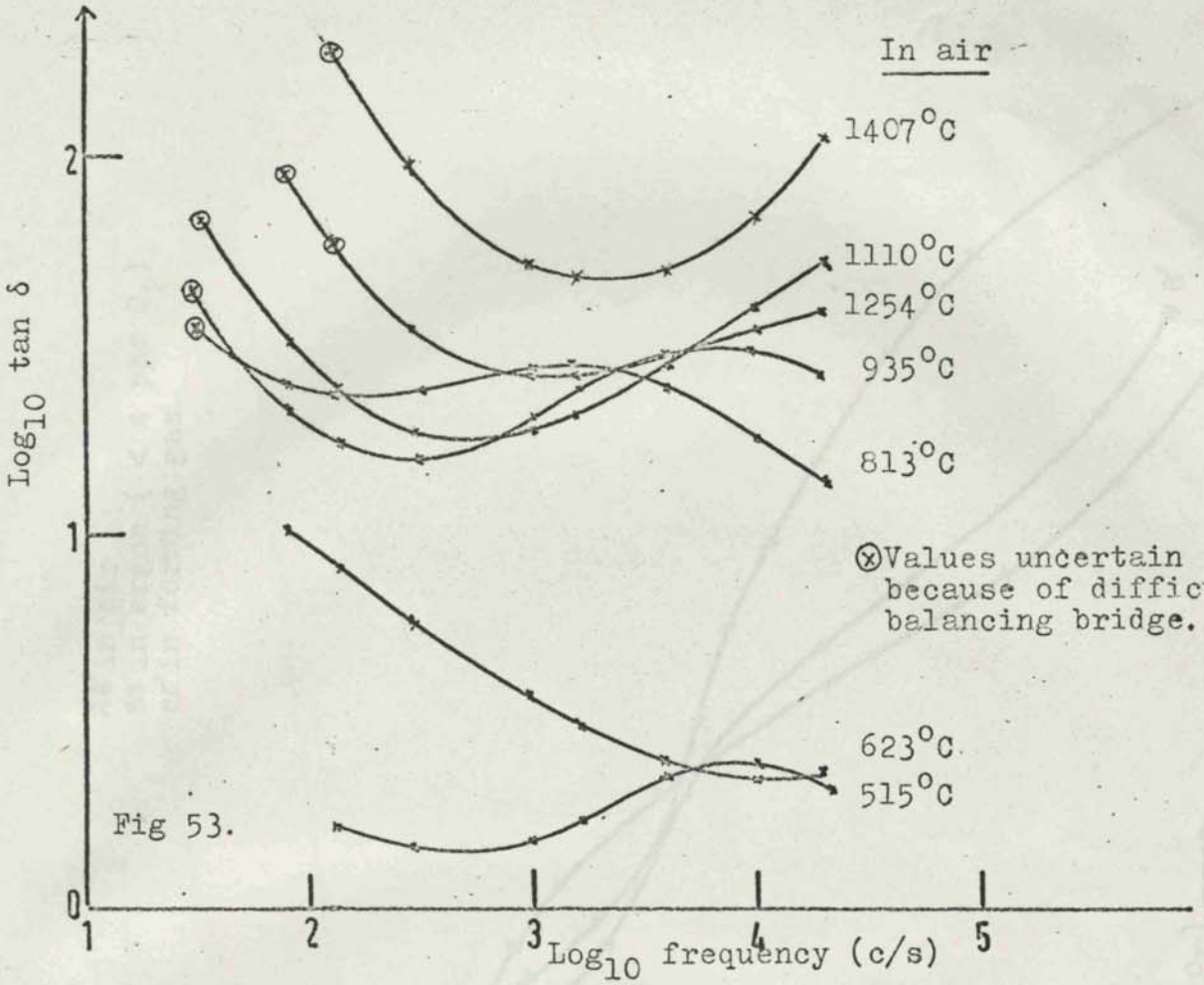

Fig 53.

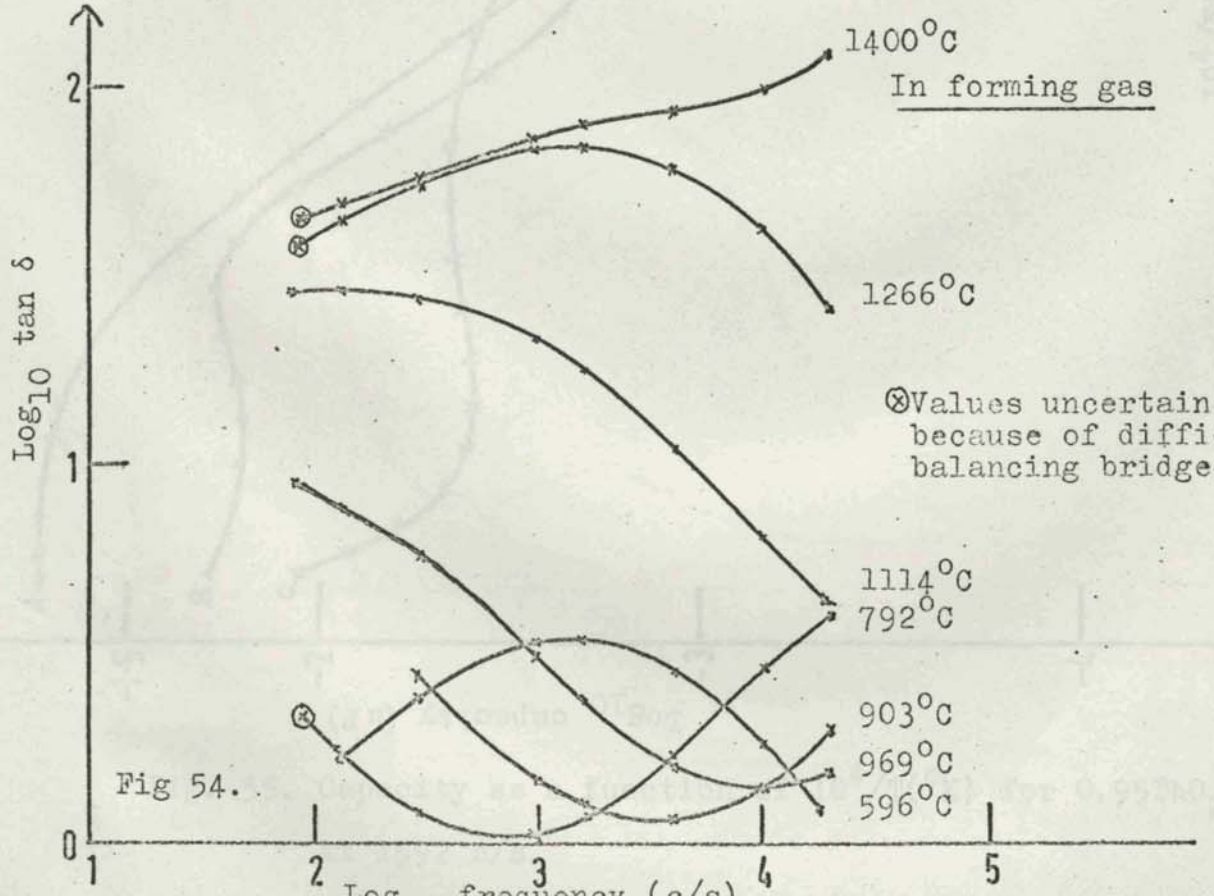

Fig 54.

Figs 53 and 54. Variation of tan δ with frequency for 0.95 ThO_2 – 0.05 SrO

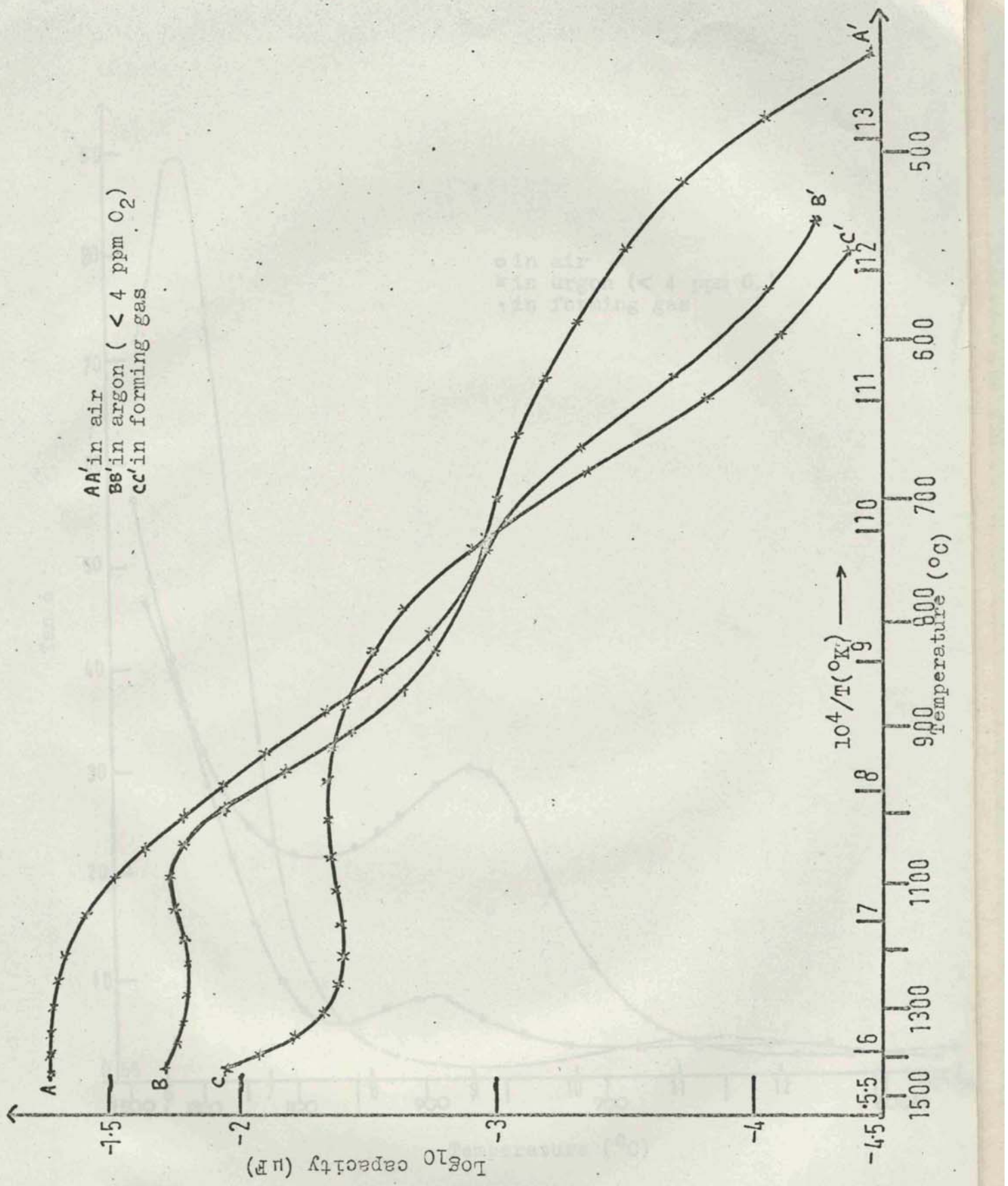

Fig. 55. Capacity as a function of $10^4/T(^oK)$ for $0.95ThO_2$–0.05SrO at 1592 c/s.

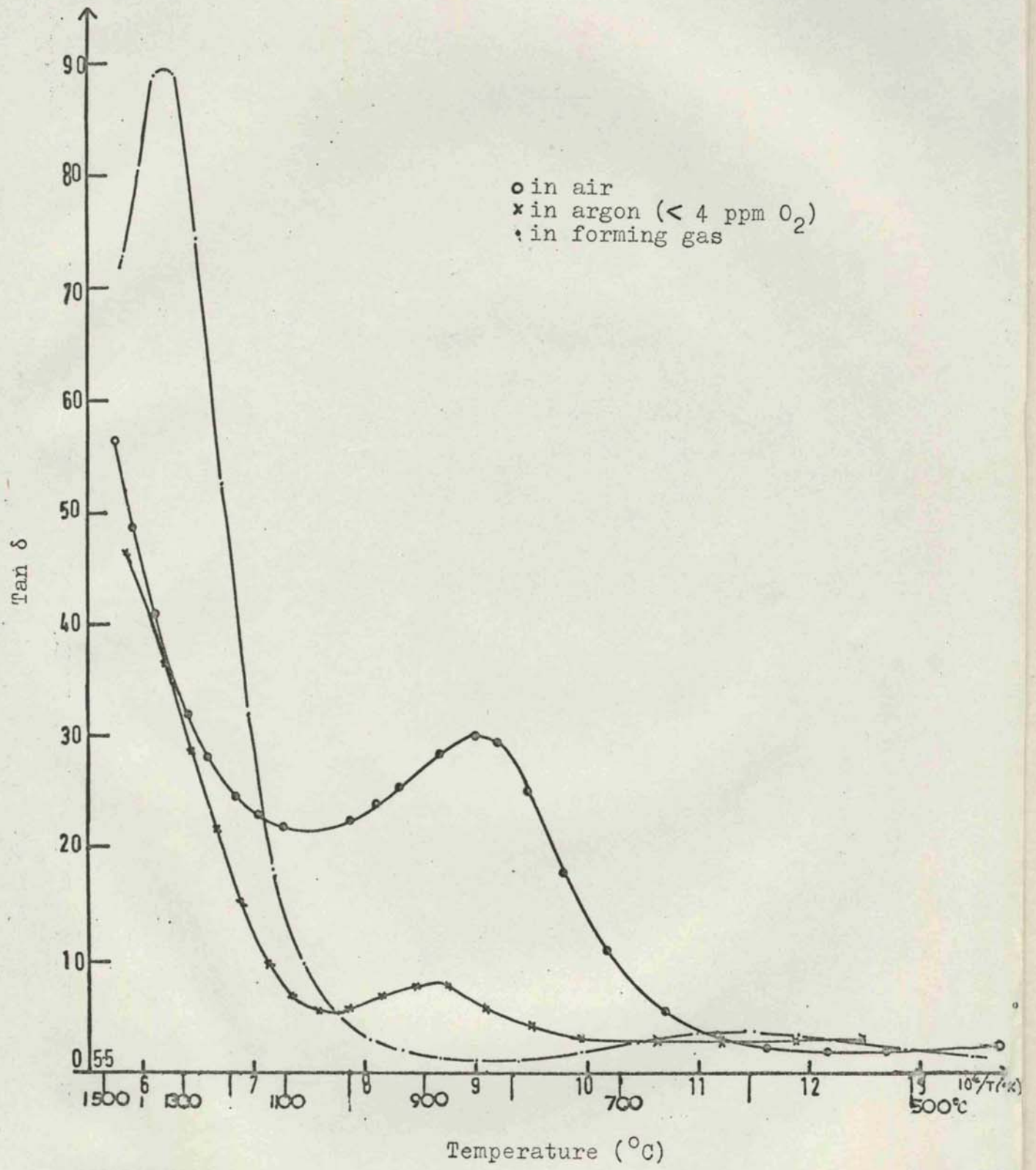

Fig. 56. Tan δ as a function of $10^4/T(^{\circ}K)$ at 1592 c/s for 0.95 ThO_2–0.05 SrO